Modeling cerebrocerebellar control in horizontal planar arm movements of humans and the monkey

by
Kazutaka Takahashi

Submitted to the Department of Aeronautics and Astronautics
in partial fulfillment of the requirements for the degree of
Doctor of Philosophy
at the
MASSACHUSETTS INSTITUTE OF TECHNOLOGY
February 2007

Author .....
Department of Aeronautics and Astronautics
October 6, 2006

Certified by .....
Steve G. Massaquoi
Associate Professor of Electrical Engineering and Computer Science
Thesis Supervisor

Certified by .....
Munther Dahleh
Professor of Electrical Engineering and Computer Science
Thesis Supervisor

Certified by .....
Timothy J. Ebner
Professor of Neuroscience, University of Minnesota
Thesis Supervisor

Certified by .....
Dava Newman
Professor of Aeronautics and Astronautics
Thesis Supervisor

Accepted by .....
Jaime Peraire
Professor of Aeronautics and Astronautics, Chairman,
Committee on Graduate Students

Modeling cerebrocerebellar control in horizontal planar arm movements of humans and the monkey

by

Kazutaka Takahashi

Submitted to the Department of Aeronautics and Astronautics
on September 25, 2006, in partial fulfillment of the
requirements for the degree of
Doctor of Philosophy

Abstract

In daily life, animals including humans make a wide repertoire of limb movements effortlessly without consciously thinking about joint trajectories or muscle contractions. These movements are the outcome of a series of processes and computations carried out by multiple subsystems within the central nervous system. In particular, the cerebrocerebellar system is central to motor control and has been modeled by many investigators. The bulk of cerebrocerebellar control involves both forward command and sensory feedback information inextricably combined. However, it is not yet clear how these types of signals are reflected in spiking activity in cerebellar cells in vivo. Segmentation of apparently continuous movements was first observed more than a century ago. Since then, submovements, which have been identified by non-smooth speed profiles, have been described in many types of movements. However, physiological origins of submovement have not been well understood.

This thesis demonstrates that a currently proposed recurrent integrator PID (RIPID) cerebellar limb control model (Massaquoi 2006a) is consistent with average neural activity recorded in a monkey by developing the Recurrent Integrator-based Cerebellar Simple Spike (RICSS) model. The RICSS formulation is consistent with known or plausible cerebrocerebellar and spinocerebellar neurocircuitry, including hypothetical classification of mossy fiber signals. The RICSS model accounts well for variety of cerebellar simple spike activity recorded from the monkey and outperforms any other existing models. The RIPID model is extended to include a simplified cortico-basal ganglionic loop to capture statistical characterization of intermittency observed in individual trials of the monkey. In order to extend the capability of the RIPID model to a larger workspace and faster movements, the model needs to be gainscheduled based on the local state information. A linear parameter varying (LPV) formulation, which shares a similar structure to that suggested by the RICSS model, is performed and its applicability was tested on human subjects performing double step tasks which requires rapid change in movement directions.

Thesis Supervisor: Steve G. Massaquoi
Title: Associate Professor of Electrical Engineering and Computer Science

Thesis Supervisor: Munther Dahleh
Title: Professor of Electrical Engineering and Computer Science

Thesis Supervisor: Timothy J. Ebner
Title: Professor of Neuroscience, University of Minnesota

Thesis Supervisor: Dava Newman
Title: Professor of Aeronautics and Astronautics

Acknowledgments

First, I would like to express my gratitude to my thesis supervisor, Prof. Steve Massaquoi for opening a door for me to an exciting field of neuroengineering. I will always remember the influence Steve has given me. I would sincerely like to thank Prof. Munther Dahleh for his most generous and timely offer of help as well as deep insights to control theory as well as biological system were extremely valuable resources for my development of how to view systems. I wish to deeply thank Prof. Tim Ebner from University of Minnesota. Thanks to the primate data by Tim and Dr. Roitman, now at UCSF, can Chapter 3 which lays out the basis of my thesis only exist. In addition, his acceptance of my late request to join my committee made my research as well as my thesis progress meaningful. His caring, insightful, detailed, and prompt feedback made him my role model not only as a neuroscientist but also as a professional. I would sincerely thank Prof. Dava Newman for kindly accepting my request to be in my thesis committee as a representative of my department. Dava's comments especially on my thesis draft and defense preparation were very helpful.

I would like to thank Prof. Zhi-Hong Mao at University of Pittsburgh and Dr. Max Berniker at Media lab. They kindly accepted my last minute invitations to be the readers for my defense committee to give me great feedback for thesis and defense preparation.

I want to thank Prof. Emery Brown at BCS/MGH and Dr. Hirofumi Aoki from MVL for their assistance with statistical analysis for RICSS chapter and the corresponding paper. Interaction with Emery at Neuroinformatics at MBL shed a different perspective on how to view neuro data as well.

My tie to Course 16 could not have been active without all the help from Marie Stuppard and Barbara Lechner. They had always been on my side to sustain my existence in the department as well as to put me through till the end of my graduate student life.

One of the best experience in my student life at MIT was to be surrounded by great friends. Without their presence, my life at MIT would not be so meaningful and enjoyable. I want to thank Prof. Zhi-Hong Mao again as we have been very good friends for most of my time at MIT since we were officemates in 35-223, Dr. Sungho Jo and Iahn Cajigas González

as good friends , officemates in Stata, and most accessible and demanding critics, Lily Kim as we spent a lot of time to talk about research and food in a windowless 7th floor office in Tech square, Ola Ayaso, Dr. Georgios Kotsalis, and Mario Valenti as not only did they share different perspectives on my research but also did they make life at MIT "life", and Eric Smith as I am indebted for his help on building the human experimental setup. I also would like to thank my friends in Steve's group, Munzer's group, EECS, CSAIL, LIDS, Course 16.

Since I started working with Steve, being a TA for a Course 6 class became a big part of my student life. It had been rewarding to work with distinguished faculty members in EECS department every term. First I would like to thank Prof. Grimson and Prof. Verghese. They have given me an opportunity to be a TA not only for the financial support needed but also for mental and spiritual support essential for me to remain as a graduate student over the years. Thanks to all the encouragements from Prof. Qing Hu, I decided to stay at MIT for a graduate degree. I sincerely appreciate all the care that Prof. Jae Lim has given me as if he had been my advisor, or even a mentor. Prof. Dennis Freeman has been in many way my advisor not only for the course we taught together, but to discuss research problems as well as some more serious problems that I had faced as a graduate student. Finally, but not least at all, I was truly lucky to work with Prof. Alan Willsky. He and his family are probably one of the most treasurable fruits from MIT professionally and intellectually. Through my teaching, I have met many other TA's that I can respect as friends and professionals: Stephen M. Hou, Alex S. Park, Keith R Santarelli, just to name a few.

I also would like to thank the administrative staff of LIDS, CSAIL, and EECS, in particular Fifa Monserate, Cindy LeBlanc, Victoria Palay, and Lisa Bella. Their very timely help made my life at MIT much smoother.

I am eternally grateful to my family in Japan for their support in every aspect from my day one on this earth. All the freedom they have given me has shaped who I am.

Finally, but not least, I would like to sincerely thank Yao Li. Without her unconditional support I have received over the past few years, I would not have completed my degree.

Contents

1 Introduction **25**

1.1 Motivation 25

1.2 Problem formulation 28

1.3 Approach 29

1.4 Thesis organization 30

2 Background **33**

2.1 Relevant anatomy and physiology 33

2.1.1 Cerebellum 33

2.1.2 Motor cortical areas 40

2.1.3 Parietal cortex 46

2.1.4 Somatosensory cortex 47

2.1.5 Basal Ganglia 47

2.2 Examples of current motor control models 49

2.2.1 Cerebrocerebellar communication system by Allen and Tsukahara (1974) 51

2.2.2 Inverse/Internal models 52

2.2.3 Smith predictor (Miall et al. 1993c) 54

2.2.4 Schweighofer et al. (1998a,b) models 56

2.2.5 Wolpert and Kawato (1998) models 57

2.2.6 Kettner et al. (1997) and Barto et al. (1999) models 59

2.2.7 RIPID model (Massaquoi 2006a) 61

2.3 Intermittency 62

3 Recurrent Integrator Cerebellar Simple Spike (RICSS) Model 65

3.1 Introduction 65

3.2 Methods 68

3.2.1 Purkinje cell simple spike data 68

3.2.2 Purkinje cell recording and properties 69

3.2.3 Synopsis of the RIPID two-joint arm control model 71

3.2.4 Cerebrocerebellar interconnectivity and the RICSS model 73

3.2.5 Alternative models 79

3.2.6 Simulations and data analysis 81

3.3 Results 83

3.3.1 Simulation results 83

3.3.2 AKc models 83

3.3.3 UPVSc and RICSS models 85

3.3.4 Unit activity characteristics 87

3.3.5 Joint coordinate models 90

3.4 Discussion 91

3.4.1 Suitability of regression models examined. 91

3.4.2 Higher order, nonsinusoidal, and nonlinear kinematic content of simple spike signals 92

3.4.3 Rationale for RICSS model structural details 95

3.4.4 Coordinate system in cerebellum 97

3.4.5 Model implications 98

4 Submovement analysis and modeling of non-human primate manual tracking 101

4.1 Introduction 102

4.2 Methods 106

4.2.1 Behavioral task . . . 106
4.2.2 Data acquisition . . . 107
4.2.3 Speed pulse analysis . . . 108
4.2.4 Control experiment (Roitman et al. 2004) . . . 109
4.2.5 BG-RIPID model . . . 109
4.3 Results . . . 111
4.3.1 General description of kinematics . . . 111
4.3.2 Speed pulse analysis . . . 113
4.3.3 BG-RIPID model with a cortico-basal ganglia system (Mao 2005) . . . 117
4.4 Discussion . . . 123
4.4.1 Existence and detection of submovements . . . 123
4.4.2 Scaling properties of submovements . . . 124
4.4.3 Underlying generation mechanism of submovements . . . 126

5 Linear parameter varying (LPV) formulation 131
5.1 Introduction . . . 131
5.2 Theoretical background . . . 135
5.3 Formulation for the two-link arm plant . . . 139
5.4 Simulation method . . . 144
5.5 Simulation results . . . 146
5.5.1 Circular tracking performance . . . 146
5.5.2 Single $\mathcal{H}_\infty$ controller . . . 147
5.5.3 LPV controllers . . . 148
5.6 Discussions . . . 154
5.6.1 Comparison of LPV with other control models . . . 157
5.6.2 Feasibility/rationale of LPV/gainscheduling models for cerebrocerebellar limb control system . . . 159
5.6.3 Reduction of the number of scheduling variables . . . 163
5.6.4 Cerebellum as a gain-scheduled controller . . . 165

6 Human double step experiment **169**

6.1 Introduction 169

6.2 Methods 170

6.2.1 Behavioral task 170

6.2.2 Data acquisition 173

6.2.3 Data analysis 173

6.3 Results 175

6.3.1 General description of kinematics 175

6.3.2 Kinematic Data Fit 177

6.3.3 LPV model fit 184

6.4 Discussion 187

6.4.1 On movement variability 187

6.4.2 Sequential command 192

6.4.3 LPV system to characterize a double-step movement 193

7 Conclusions and future extensions **199**

7.1 Conclusions 199

7.1.1 RIPID and RICSS models 200

7.1.2 Intermittency 202

7.1.3 Gainscheduling 204

7.2 Possible extensions 205

7.2.1 Further extensions of RIPID 205

7.2.2 Adaptive RIPID/RICSS 206

7.2.3 Classification of submovements 207

7.2.4 Application to neuroprostheses 208

A Tables **211**

A.1 The two-link arm plant dynamics and muscle model parameters used in Chapter 3 211

A.2 The two-link arm plant dynamics parameters used in Chapter 5 213

List of Figures

2-1 Zones of the cerebellum 35

2-2 Area 3a and surrounding cortical areas in a flattened left hemisphere. Adapted from 36

2-3 Cell types and layer structure in the cerebellar cortex. 37

2-4 Major cortical areas (adapted from http://cti.itc.virginia.edu/ psyc220/) . . 41

2-5 Locations of the motor areas of the medial wall of the hemispheres of the monkey. Adapted from Picard and Strick (1996). 44

2-6 Area 3a and surrounding cortical areas in a flattened left hemisphere. Adapted from Huffman and Krubitzer (2001a). 48

2-7 Feedforward/inverse control system 49

2-8 Feedback control system 50

2-9 Feedback learning inverse/internal dynamics system 50

2-10 Cerebrocerebellar communication system (Allen and Tsukahara 1974). See the text for details. 51

2-11 Smith predictor architecture (Miall et al. 1993c). Two internal predictive loops are indicated by dashed lines. Comparators are indicated by circles with one filled quadrant, and the empty circle is a positive feedback connection. . . . 55

2-12 Functional diagram of the model for on-line control of arm movements with the inferior olive (IO) which computes the feedback error for adaptation (Schweighofer et al. 1998b). See the text for more details. 57

2-13 Model architecture of multiple paired forward-inverse model including n modules that are shown as stacked sheets. The detail of the each module is shown in the first module. from Wolpert and Kawato (1998). 58

2-14 Block diagram of the model. Although the brain stem integrator and the eye plant are modeled by the same set of equations in the model, these 2 functions are distinguished in the diagram to emphasize their different neural substrates and the idea that both proprioceptive and efference copy signals may provide eye position and velocity information. All lines indicate the flow of multivariate information, with the heavier arrow indicating the wider bandwidth associated with the expansive recoding of mossy inputs. Smaller boxes: pure delays in the model. Open arrowhead: indirect action climbing fiber training signals have on information throughput by the alteration of network weights via the learning rule. Visual input to the system is assumed to take the form of retinal error signals that are obtained by a subtraction at the node labeled S of target and eye position signals (Kettner et al. 1997). . 60

2-15 Model architecture. PC, Purkinje cell; MFs, mossy fibers; PFs, parallel fibers; CF, climbing fiber; τ_i, $i = 1, \ldots, 5$ conduction delays. The labels A and B mark places in the system to which Barto et al. (1999) refer discussing the model's behavior. 61

2-16 One version of RIPID model. Colored circles designate functional subcategories of sensorimotor cortical groups. 62

3-1 Arm configuration relative to the workspace of the monkey. The origin of Cartesian hand coordinate is set at the center of the circle on which the target cursor travels. The hand location is defined relative to this origin. The shoulder and elbow angles are defined as shown in the figure. Three functional muscle groups: shoulder flexors/extensors, elbow flexors/extensors, and two-joint flexors/extensors as in Katayama and Kawato (1993) and Flash (1987) are modeled. 69

3-2 Recording sites are denoted with filled circles as shown in the lateral view of the cerebellum. The primary fissure is marked with the arrow labeled PF. Not all the recording sites for the cells used in the analysis are displayed and some recording sites correspond to several cells). Inset shows dorsal view of the cerebellum, with the ovals denoting the penetration regions. The figure is modified from Roitman et al. (2005). 70

3-3 RIPID Model. Colored circles designate functional subcategories of sensorimotor cortical (SMC) units. See text for details. 72

3-4 Cerebral cortical component of RICSS model from the perspective of a single cerebellar Purkinje cell. 8 cerebral cortical columns in Sensorimotor Cortical Area 3a (SMC-1, unit 1 in Fig.3-3) implementing a neural population-based representation, e.g. Georgopoulos et al. (1982a), of the tracking error-like vector (red arrow) and subsequent distribution after cerebellar processing (see text for details). 74

3-5 Cerebellar Architecture proposed to underlie PC SS activity, (see text for details). 76

3-6 Recorded and RIPID model-simulated hand motion. Left figure: Hand location. Right figure: Hand speed. In both figures, the solid red lines show averaged data over 10 trials with the target moving at 6.5 cm/s in a CW direction at the starting angle of 180 degrees, the dashed blue the Cartesian intended hand position and speed corresponding to $\boldsymbol{\theta}_{target}$ and the solid blue lines the tracking simulation. 84

3-7 Joint angles and their derivatives used in the regression. Left figure: Shoulder angle, θ_s and its derivatives. Right figure: Elbow angle, θ_e and its derivatives. Blue line denotes joint angle, green first derivative, red second derivative, and cyan third derivative respectively in each plot. The signals shown are for the target speed 8.3 cm/s in the CC direction. 85

3-8 (a) Histogram of adj-$R^2$of AK1c, AK2c, and AK3c. (b) Box plots for the adj-R^2 differences, AK2c-AK1c (left) and AK3c-AK2c (right). Each box indicates the lower quartile, median, and upper quartile values. The whiskers indicate the extent of the rest of the data, assuming that there is no outlier. The asterisks denote outliers which have values more than 1.5 times the interquartile range away from the top or bottom of the box. 86

3-9 Comparison of AKc models for Cell #49, the small circles represent the average firing rates over a ten degree interval. The blue line is for AK1c, the green line for AK2c, and the cyan for AK3c. adj-R^2 of each model is 0.62, 0.63, and 0.64 respectively. 87

3-10 (a) Histogram of adj- R^2 of AK3c, UPVSc, and RICSS. (b) Box plots for the adj- R^2 differences, RICSS-AK3c (left) and UPVSc-AK3c (right). 88

3-11 Comparison of unit firing with AK3c, UPVSc, and RICSS fits for Cell #50. Activity intensity is indicated by color, with red highest and indigo lowest. The radial coordinate in each annular figure denotes the target (intended hand) speed ranging from 3.1 to 8.3 cm/s from inside out and the angular coordinate relative to the origin denotes the hand position ϕ_h of the monkey during tracking. The upper row contains the firing rates for CC rotational direction and the lower row CW rotational direction. adj-R^2 are 0.05, 0.05, and 0.09 for AK3c, UPVSc, and RICSS respectively. 89

3-12 The furthest left column shows the averaged firing rate of simple spikes from Cell #22. This cell shows asymmetric firing patterns across the rotational directions, the maximum firing rate is attained at medium speed (around 5 o'clock direction) for CW, and multimodal distribution. AK3c and UPVSc models can capture only naively extremities for CC, while RICSS model captures all the three characteristics mentioned above for both CC and CW. adj-R^2 are 0.43, 0.43, and 0.75 for AK3c, UPVSc, and RICSS respectively. . 90

3-13 Comparison of Cartesian coordinate models and joint coordinate models for Cell #65. The small circles represent the average firing rates over a ten degree interval. The solid lines are the fits for AK3 and the dashdot lines for UPVSc. Green lines represent models in Cartesian coordinates and blue in joint coordinates. 91

3-14 $|\mathbf{e}_{cb}|$ and $\cos\phi_e$ as functions of intended hand speed varying from 3.1 cm/s to 8.3 cm/s and hand location angle ϕ_h. 96

4-1 Feedforward model to generate intermittency. The bidirectional arrow after $e(t)$ denotes a sample and hold mechanism. 103

4-2 Sampled feedback model to generate intermittency. 104

4-3 Possible strategies to generate submovements. 104

4-4 Experimental protocol. Adapted from Roitman et al. (2005). 107

4-5 Definition of the speed pulse used in this study. 109

4-6 The cortico-BG interaction embedded to the RIPID, BG-RIPID model. . . . 110

4-7 Averaged trajectories on the left column and speed profiles on the right column over 10 trials. Plotted are monkey hand data (solid blue) and target data (dashed red). Starting angle was at 90 degree, and direction of motion was CCW. Zero time corresponds to the onset of the Intercept period. 112

4-8 Individual trajectories on the left column and speed profiles on the right column from single trial movement trajectories. The color scheme, the starting angle, and the rotational direction are the same as that in Fig, 4-7. Speed overshoots and undershoots are prominent in both Intercept and Track periods. 114

4-9 Empirical probability distributions of speed pulse durations across the target speeds. 115

4-10 A - E: Amplitude–duration distributions at each target speed for the Intercept (red) and Track (blue) periods. F:Amplitude–duration regression slope dependence on the target speed. Shown are the amplitude–duration slopes at each target speed for the Intercept (red) and Track (blue) periods. 118

4-11 Position response of the BG-RIPID model. Position traces (blue) and the command (dashed red) at the five speeds simulated are shown. 119

4-12 Velocity response of the BG-RIPID model. Velocity traces (blue) and the command (dashed red) at the five speeds simulated are shown. 120

4-13 BG duration distributions 121

4-14 A-E: Amplitude-duration distributions at each target speed for the tracking period from the simulation of the extended RIPID model. 122

5-1 RIPID model simulated hand motion for the tracking speed 1.5 times faster than the fastest speed that the monkey performed in the experiment described in Chapter 3. In all four figures, the dashed blue lines show the Cartesian intended hand position and the solid blue lines the tracking simulation. A through D represent different launch angles, 0, 90, 180, and 270 degree respectively. 132

5-2 A realization of RIPID/RICSS structure as a gain-scheduling control system. 133

5-3 Polytope configuration. This example shows the case of 3 scheduling variables. 136

5-4 Formal LPV formulation 137

5-5 System diagram for loopshaping with two weighting transfer functions $\mathbf{W}_1$ and $\mathbf{W}_2$. Δ is a delay operator. 139

5-6 The arm configuration for the simulation. 145

5-7 LPV2 and $\mathcal{H}_\infty$ controller models simulated hand motion for the tracking speed at 150 deg/s. In all four figures, the solid blue lines show the Cartesian reference hand position, the green dash-dot lines the responses of $\mathcal{H}_\infty$ controller system, and the magenta dotted lines the responses of LPV2 controller system.A through D represent different launch angles, 0, 90, 180, and 270 respectively. 148

5-8 A simulation result on the $\mathcal{H}_\infty$ controller with the nonlinear plant and the linearized plant about the center of the workspace. Upper row: Hand Speeds. Lower row: Hand paths. Left column: Target sequence N-C-E and second movement initiated at 300 ms after the first. Right column: Target sequence E-C-N and second movement at 200 ms. 149

5-9 A simulation result on the $\mathcal{H}_\infty$ controller with the nonlinear plant and the linearized plant about the center of the workspace. Upper row: Hand Speeds. Lower row: Hand paths. Left column: Target sequence N-C-S and second movement initiated at 300 ms after the first. Right column: Target sequence W-C-E and second movement at 200 ms. 150

5-10 Simulation results on LPV2 controller and $\mathcal{H}_\infty$ controller. The second segment is initiated at 150 ms after the first is initiated. 151

5-11 Trajectories of scheduling parameters ρ_1 and ρ_2 and of the weights α_i, $i = 1, 2, 3, 4$ for the LPV2 controller 152

5-12 Singular values of the frequency responses of arm dynamics evaluated at each vertex. Solid lines denote the largest singular values, and the Dashed-dotted lines the smallest singular values. A pair of lines for each color denotes the same scheduling variable values. 153

5-13 Simulation results on LPV1 controller and LPV2 controller. The reference commands are the same as in Fig. 5-10 155

5-14 Trajectories of scheduling parameters ρ_3 and of the weights α_1 and α_2 for the LPV1 controller 156

5-15 Control system gainscheduled by both feedforward and feedback signals. . . 160

5-16 Simulation results of hand speeds and hand paths for LPV2 system with feedforward and feedback scheduling. The reference commands are the same as in Fig. 5-10. 161

5-17 Simulation results of the scheduling parameters and the corresponding weights for LPV2 system with feedforward and feedback scheduling. Solid:Feedback, Dashed:Feedforward. 162

6-1 Human double-step reaching protocol. 171

6-2 An example of hand path and speed for a movement from S to C to R. Only one distinct speed peak is prominent. Red circles:Initial and target locations, Solid blue:Data, Solid red:Overall fit, Dashed red:Individual segment fits . . 177

6-3 Another example of hand path and speed for a movement from N to C to R. There are two distinct speed peaks. Line types are the same as in Fig. 6-2 . 178

6-4 An example of hand kinematics with a terminal hook and corresponding fit for a movement from N to C to L. Line types are the same as in Fig. 6-2 . . 179

6-5 An example of hand kinematics with convexity change and corresponding fit for a movement from S to C to R. Line types are the same as in Fig. 6-2 . . 180

6-6 Summary of movement durations. 182

6-7 Summary of reaction times. 184

6-8 An example of kinematic fit resulted in negative reaction time to the second target for a movement from N to C to R. Line types are the same as in Fig. 6-2 185

6-9 An example of kinematic fit of the data with response of the LPV2 system. Data from subject B11 performing S-C-R task. Experimental data (blue), LPV fit (red), and Reference command for the LPV system (green dashed). Left: Hand path. Right: Hand speed. 186

6-10 An example of kinematic fit of the data with response of the LPV2 system. Data from subject B12 performing S-C-R task. Line types follow Fig.6-9. . 187

6-11 An example of kinematic fit of the data with response of the LPV2 system. Data from subject R12 performing S-C-R task. Line types follow Fig.6-9. . . 188

6-12 An example of kinematic fit of the data with response of the LPV2 system. Data from subject B12 performing S-C-L task. Line types follow Fig.6-9. . . 189

6-13 An example of kinematic fit of the data with response of the LPV2 system. Data from subject B12 performing S-C-L task. The data was not fit well purely kinematically by a sequence of the minimum jerk profiles. The hand path is fairly curved with varying convexity with terminal hook. Line types follow Fig.6-9. 194

6-14 Another example of kinematic fit of the data with response of the LPV2 system. Data from subject R12 performing S-C-L task. The data was not fit well purely kinematically by a sequence of the minimum jerk profiles. The hand path makes almost a right turn. Line types follow Fig.6-9. 195

6-15 Difference between the single $\mathcal{H}_\infty$ controller response and the LPV2 response. Data from subject RB11 performing S-C-L task. Experimental data (blue), LPV fit (red), and $\mathcal{H}_\infty$ fit (yellow). Left: Hand path. Right: Hand speed. . . 197

7-1 A network illustration of receptive field-weighted regression. Adapted from Figure 3 in Schaal and Atkeson (1998). 207

List of Tables

4.1 Regression coefficients vs. target speeds for Intercept periods 116

4.2 Regression coefficients vs. target speeds for Track periods 117

4.3 Regression coefficients vs. target speeds for the simulation data. 117

5.1 Achievable performance of the controllers. 146

5.2 Variations in the singular values of the arm plant as the scheduling variables change. $\overline{\sigma}$ and $\underline{\sigma}$ denote the largest and the smallest singular values respectively. 154

6.1 Number of trials used in the kinematic and reaction time analyses. 179

6.2 Summary of the distance parameters in Eq's 6.1 $\sim$ 6.4 characterizing the hand position and velocity profiles in each type of paths in each subject. Each of the data entry takes the form of mean $\pm$ std. Units are in cm. 181

A.1 Arm plant parameters used in Chapter 3 - m_i is mass, l_i is limb segment length, $\bar{l}_i$ is distance to segment center of mass from joint, and h_i is moment of inertia for i-th link 211

A.2 Moment arms - See the notation inKatayama and Kawato (1993) 211

A.3 Arm plant parameters used in Chapter 5- m_i is mass, l_i is limb segment length, $\bar{l}_i$ is distance to segment center of mass from joint, and h_i is moment of inertia for i-th link 213

Chapter 1

Introduction

1.1 Motivation

In daily life, animals including humans can make a wide repertoire of limb movements effortlessly without consciously thinking about joint trajectories or muscle contractions to bring about specific motions. These movements are the outcome of a series of processes and computations carried out by the central nervous system (CNS). Even to make a simple reaching movement, to a tea cup for example, a number of distinct neuroanatomical areas participate to complete the task, and each area consists of numerous neurons that are densely interacting to each other.

In the study of motor control, or brain functions in general, a major obstacle is the fact that the CNS is a densely interconnected large scale system. With a rapid growth in the field of neuroscience, knowledge of the CNS at all levels of granularity, from molecular biology to behavioral psychology, has been expanding literally on a daily basis. Each discipline contributes to characterizations of parts of the CNS at corresponding resolutions. However, there is need for more effort in attempting to explain how and why individual cells in a particular area fire as observed and the role of anatomical connections in determining neural firing patterns as well as behavioral outcome. In order to answer to these questions, we need to apply a systems approach to develop computational models that are neurophysio-

logically and neuroanatomically consistent. Such computational models can be a gateway for researchers from different disciplines to complement each other's view to enhance the understanding of motor control.

The cerebrocerebellar system is central to motor control (Allen and Tsukahara 1974; Brooks 1986; Kelly and Strick 2003) and has been characterized in terms of its anatomical connections among the areas in the system (Allen and Tsukahara 1974; Kelly and Strick 2003). Furthermore, the neurophysiology of each area or network of cerebral cortical areas has been characterized quite extensively (Georgopoulos et al. 1982b; Kalaska et al. 1990; Matsuzaka and Tanji 1996; Sergio and Kalaska 1998; Marconi et al. 2001; Hoshi and Tanji 2004a; Scherberger et al. 2005). The cerebellum is intimately connected to almost all major motor and sensory areas in the CNS, and to high level cognitive areas in primates as well. Furthermore, cerebellar pathology usually results in uncoordinated movements (Bastian et al. 1996) or errors of directions, force (Maschke et al. 2004), amplitudes and delayed movement initiations (Holmes 1939). Therefore, an importance of the cerebellum in motor control should be emphasized in the analysis and modeling of cerebrocerebellar system. Given these considerations, some notable cerebellar motor control models are introduced here. They represent mathematically well-accepted neuroanatomy and neurophysiology and can explain kinematic behaviors as well as some internal signals or adaptation. Massaquoi and Slotine (1996) incorporated a control theory to account for stability of cerebellar control in the presence of transmission delay and has reproduced some neural firing activities. Jo and Massaquoi (2004) used the idea related to Massaquoi and Slotine (1996) with a gain scheduled control scheme and more anatomical details to achieve upright postural stabilization in their human model. Contreras-Vidal et al. (1997), Kettner et al. (1997) and Schweighofer et al. (1998b) followed a similar path to include fairly detailed cerebrocerebellar anatomy and physiology, and not only did their models manage to reproduce kinematic features, but also learning ability attributed to the cerebellum. The models by Contreras-Vidal et al. (1997) and Kettner et al. (1997) did not attempt to directly reproduce any specific cerebellar activity recorded in vivo. Note, however, that Schweighofer et al. (1998b) showed cerebellar Purkinje

cell firing patterns which qualitatively reproduced the directional preference observed in Fortier et al. (1989). However, there has not been any anatomical model that directly included and modeled recorded firing activity of cerebellar neurons. Thus, in order to make a contribution to the motor control community, it is crucial to develop a cerebrocerebellar model that can model both kinematics and cellular activity at the same time.

Kinematic segmentation of apparently continuous limb movements was first observed by Woodworth (Woodworth 1899) in a speed-accuracy trade-off study. Since then, submovements, which have been identified by non-smooth multi-peaked speed profiles, have been described in many types of movements. It has been noted that movements can be decomposed into scaled and dilated unit velocity templates, or unit movements (Flash and Henis 1991; Milner 1992). However, kinematic characteristics and physiological origins of submovements have not been well understood. The cerebrocerebellar system has already been connected to the fronto-cortico basal ganglionic system (Houk and Wise 1995a; Brown et al. 2004; Mao 2005). In particular, Brown et al. (2004) focused on saccades and qualitatively captured firing activities of more than a dozen of cell types from different brain areas - frontal eye field, basal ganglia and superior colliculus. Mao (2005) formulated a function of the basal ganglia to be a general context dependent controller and accounted for arm kinematic patterns of a few cases of basal ganglionic pathology. However, no equivalent system to explain intermittency observed in normal limb movements has been formulated.

Taken together, it is critical to develop neurophysiologically and neuroanatomically accurate cerebrocerebellar control models. The recurrent integrator Proportional-Integral-Derivative (RIPID) model has been suggested as a characterization of the cerebrocerebellar interaction for the long loop control. It has been applied to postural balance (Jo and Massaquoi 2004) and point-to-point arm reaching movements (Massaquoi 2006a). One potential advantage of the RIPID model is that like the model by Schweighofer et al. (1998b) and unlike a number of other models is that it makes fairly specific predictions at the neuronal circuitry and the corresponding firing patterns. Thanks to our collaborators, Prof. Ebner and Dr. Roitman at University of Minnesota, I was fortunate to have an access to a sizable

cerebellar Purkinje cell recording while a monkey was performing a set of tasks. Therefore, the RIPID model can be specifically tested for its feasibility against the actual neuronal data. Although such a test should be performed during continuous movements, as it is not clear how each cell contributes to the overall cerebellar signal processing, it is logical to show that the averaged Purkinje cell data at least does not falsify the RIPID model.

Given the construction of the currently proposed RIPID model, the model cannot generate individual continuous trajectories without detailed knowledge of high level cognitive and motor commands. However, it is reasonable to assume that a RIPID type model could control a continuous movement in such a way that similar statistical characteristics of the intermittency observed in individual trials could emerge by supplementing additional components to the RIPID model.

If a RIPID type model could account for detailed neuroanatomy and neurophysiology as well as statistical characteristics of individual trajectories, then a natural extension would be to explore the capability of the RIPID model for more dynamically demanding tasks in an entire plane.

1.2 Problem formulation

There are three major goals in my thesis work.

(a) Demonstrate that a currently proposed modified recurrent integrator Proportional-Integral-Derivative (RIPID) cerebellar limb control model (Massaquoi 2006a) is consistent with neuronal activity recorded in an experimental primate by collaborators at the University of Minnesota (Roitman et al. 2004). Specifically, I will attempt to determine whether the RIPID control model when extended by modeling neuroanatomical circuits in greater detail can be used to reproduce signals in primate Purkinje cells during arm motion.

(b) Characterize the kinematic intermittency observed in individual trajectories of the non-human primate in terms of its statistics. Suggest and evaluate a plausible and simple mechanism possibly based on cerebrocortico-cerebello-basal ganglionic interaction that

is extended from the RIPID model and that is consistent with the statistical characterization of the monkey data. Specifically, I will attempt to extend the currently proposed RIPID model (Massaquoi 2006a) by including a cortico-basal ganglia model suggested by Mao (2005) to account for task parameter dependent and invariant statistical characterization of intermittencies in individual trajectories.

(c) Analyze the performance of a gain-scheduled control model which is inspired from the results in Objective (a) above to extend the size of the workspace and to account for more dynamically demanding movements. Assess its likely validity for biological control in general, and its possible utility for more general control problems. Specifically, I will attempt to extract a structural essence of the detailed model from Objective (a) and cast it into an existing engineering framework.

1.3 Approach

The following approaches have been taken to tackle the objectives in the previous section.

- Objective (a) is to be addressed by developing a neuroanatomically and neurophysiologically realistic cerebrocerebellar regression model based on the RIPID model to capture averaged simple spike activities of Purkinje cells recorded from the monkey performing visuomotor circular tracking tasks.

- Objective (b) is to be addressed by analyzing the non-smoothness of individual trials of the monkey kinematic data. The RIPID model is going to be modified to include a functional, but anatomically and physiologically feasible intermittent command generator.Furthermore, to investigate performance limit of the generator and possible coupling of the intermittent command and gain-scheduling scheme in Objective (c), more dynamically demanding tasks will be carried out to human subjects.

- Objective (c) is to be addressed by proposing a specific gain-scheduling or gain-modulating control scheme based on the results of Objective (a). Next, more dynamically de-

manding horizontal planar movements are to be carried out by human subjects in our movement laboratory. These experiments are designed to test the limits of control performance.

1.4 Thesis organization

The rest of this thesis is organized as follows: Chapter 2 presents background materials in neuroanatomy and neurophysiology that are relevant to the work presented here. In addition, the currently proposed motor control models, cerebellar models in particular, are introduced. In Chapter 3, the modified RIPID model is extended to include more anatomical details on cerebrocerebellar interactions to further investigate the feasibility of the RIPID model. In order to capture Purkinje cell (PC) simple spike activity, the Recurrent Integrator-based Cerebellar Simple Spike (RICSS) model is developed. The quality of fit provided by the RICSS model compares favorably with fits using hand kinematics signals alone and that its structure accounts for the system nonlinearity predicted recently by a simpler empirical model (Roitman et al. 2005). The sufficiency of the RICSS model in accounting for a large PC data set supports the plausibility of the RIPID model formulation and the proposed cerebrocerebellar connection architecture in particular. Chapter 4 describes the intermittency analysis on the end point kinematics of a non-human primate. In particular, two features are illustrated: linear scaling properties of speed pulses against target speeds and invariant distributions of speed pulse intervals over a range of speeds. In order to explain both features, a simple model that is a one-dimensional version of a reduced RIPID model is introduced. Motivated from the RICSS model in the previous chapter, Chapter 5 describes Linear Parameter Varying (LPV) control systems as a possible control engineering model to characterize gain scheduled nature of the cerebrocerebellar control system. In addition, relation between the existing cerebrocerebellar limb control systems and LPV is discussed to possibly complement the weakness of the existing models. Chapter 6 summarizes the result of a set of human experiments using a double-step tracking task to test if we need more than one controller to account for the behavioral data, when the task becomes dynamically

demanding. Finally Chapter 7 concludes the thesis and provides possible extensions of the current work.

Chapter 2

Background

In this thesis, there are several areas of the central nervous system (CNS) that are particularly emphasized to understand a gross sensorimotor control system for upper limb movements in a neurophysiological and neuroanatomical manner. The first part of this chapter introduces relevant neuroanatomy and neurophysiology of the major areas related to the motor control. The second part lists notable motor control models whose emphasis is placed on cerebellum or cerebellum and its connection to other brain areas. The last part gives brief introduction on movement intermittency.

2.1 Relevant anatomy and physiology

Even for a simple reaching movement, many parts of the CNS are involved in serial and parallel fashion. In this section, several important building blocks in CNS for motor control, particularly, upper limb control, are introduced.

2.1.1 Cerebellum

Cerebellum, or "little brain" in Latin, is the second largest structure, measured in volume, in the CNS next to the cerebral cortex, but is the most numerous in terms of the number of the neurons. The human cerebellum would extend about one meter if unfolded in its

anteroposterior direction (Ito 1984). The cerebellum has been known as one of the key components in motor control through its pathological studies (Holmes 1939).

The cerebellar cortex has a notable structural difference from the cerebral cortex. The cerebellar cortex is more uniform in its cytoarchitectonics. Thus, functional differentiation largely, if not exclusively, depends on differences in the afferent and efferent connections. Note, however, that underlying molecular heterogeneity has been found in the rat cerebellar cortex using monoclonal antibodies to position particular molecular makers (Gravel et al. 1987). Functional implication of such heterogeneity is yet unknown, but it may suggest an organizational difference among individuals or regional organizational differences reflecting particular input-output relations (Hawkes and Leclerc 1987).

Organization

The cerebellum can be divided into three parts each of which has its distinctive connections with the rest of the brain: The vestibulocerebellum, the spinocerebellum, and the cerebrocerebellum, which appears to correspond loosely to the evolutional progression (Ito 1984).

- The vestibulocerebellum, or flocculonodular lobe, is different from the other two parts in that it does not have any deep cerebellar nucleus (DCN). Although in many ways the vestibular nuclei play a corresponding role. It receives its primary input, via mossy fiber, directly from the vestibular nuclei. Its output from Purkinje cells (PC) is sent back to the vestibular nuclei. Its major function is to control eye movements relative to body position and movements (vestibular ocular reflexes), axial musculature, and balance (Ito 1984).

- The spinocerebellum owes its name because most of its input from spinal cord. It consists of vermis and intermediate parts of the cerebellum. It receives sensory information from the periphery and from the primary motor cortex as well as somatosensory cortex. The PC's in vermis project to the fastigial nucleus and those in the intermediate part to the interpositus nucleus. in the monkey, interposed nuclei, globose and emboliform,

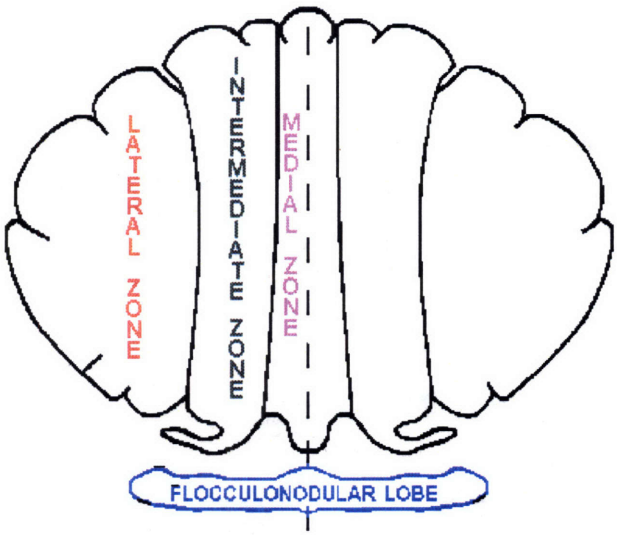

Figure 2-1: Zones of the cerebellum

in humans. The fastigial nucleus is concerned with posture and locomotion as well as gaze. The interpositus nucleus controls mainly distal muscle components in the execution of the movements. Both nuclei project to the motor cortex as well to form loops. Lesions of the intermediate cerebellum cause action tremor of the limb.

- The cerebrocerebellum, or lateral cerebellum, is the largest part of the three divisions. It receives its input from many parts of the cerebral cortex, including motor cortex, premotor cortex, parietal cortex, as well as sensorimotor cortex. Its output through PC's project to the dentate and thence to the premotor and other cortical areas via ventrolateral nucleus in the thalamus. The current hypotheses on the cerebrocerebellum functions include planning, initiation, timing of the movements, and mental process of motor actions, but also higher cognitive non-motor functions. The impairment of the lateral cerebellum consists principally of delays in movement initiation timing, decomposition of the multi-joint movements and even distal joints, as well as

some cognitive deficits.

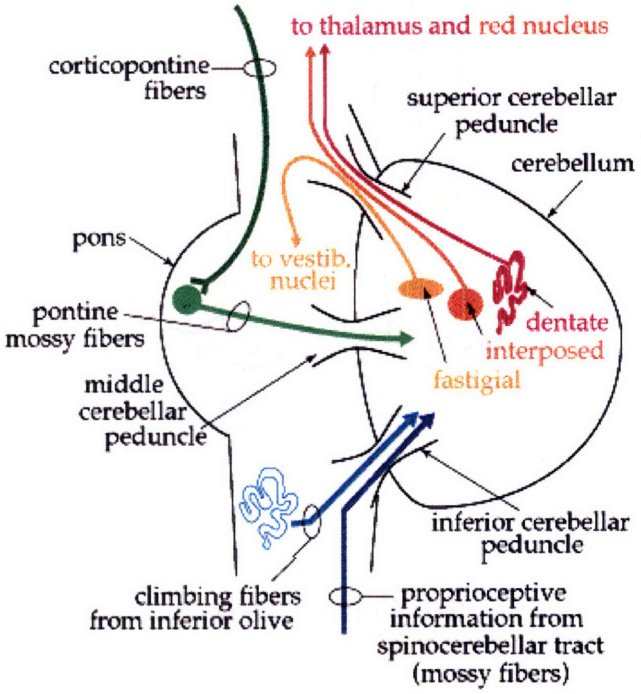

Figure 2-2: Area 3a and surrounding cortical areas in a flattened left hemisphere. Adapted from .

The cerebellar cortex can be divided into a number of sagittal zones, or microzones (Oscarsson 1979) each of which form, with its group of neurons, the operational unit of the cerebellum. This organization may be analogous to the modular columnar organization in the cerebral cortex (Mountcastle 1998). Ito (1984) extended this idea to a cerebellar microcomplex, consisting of a cerebellar microzone, projecting to a distinct group of nuclei, receiving two types of inputs, mossy fibers and climbing fibers, and sending the output through deep cerebellar nuclei. An estimate of such cerebellar modules in primates is yet unknown, but based on the mouse cerebellar cortex, there exist about 4000 modules or 40 Purkinje cells and their associated interneurons for each module (Hawkes and Eisenman 1997). An interesting suggestion by Hawkes and Eisenman (1997) is that the size, not the number, of modules would be expected to increase with increasing cerebellar surface area.

Cell types

There are three layers between the white matter and the surface of the cerebellar cortex as shown in Fig. 2.1.1 (adapted from http://www.tnb.ua.ac.be/models/models.shtml). The molecular layer is the most superficial in the cortex. The Purkinje cell layer is the middle layer containing cell bodies of Purkinje cells. The most inner layer is the granular layer on top of the white matter. Among these three layers, several types of cerebellar neurons reside. The input to the cortex is granule cell in granular layer. There are three types of interneurons: the Golgi cell in the granular layer and basket and stellate cells both in molecular layer. The sole output of the cerebellar cortex is Purkinje cell in Purkinje layer.

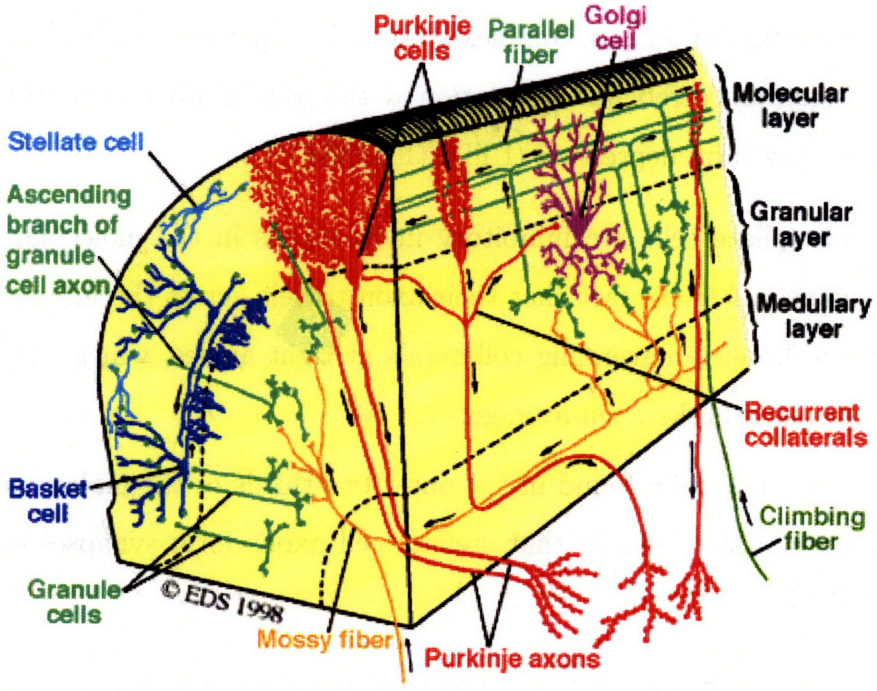

Figure 2-3: Cell types and layer structure in the cerebellar cortex.

- There are approximately 15 million Purkinje cells in human cerebellum. The cell bodies of the PC's are flask shaped and their axons go through the white matter to reach up to 30 or 40 DCN's or vestibular nuclei to provide the strong inhibitory sole output of the cerebellar cortex. The extensively, especially in primates, branched

dendrites form a coral-like structure into the molecular layer in a plane perpendicular to the longitudinal axis of the folium. PC's receive excitatory input from two distinct anatomical structures, the parallel fibers (PF) and the climbing fibers (CF). Each Purkinje cell is innervated by over 10^5 parallel fibers which synapse on its dendric arbor. Parallel fibers contain signals from mossy fibers and induce simple spike (SS) in PC's. SS activity is thought to encode sensory information or central commands depending on the origins of the mossy fibers. In contrast, only one climbing fiber makes strong synapses on to a PC and wraps around the proximal dendrites of the PC to make hundreds and thousands of synaptic connections. Climbing fiber originates from the inferior olivary nucleus, induces another type of very slow spiking activity of roughly one spike per second, complex spike in PC, and is thought to send an error, or teaching, signal for cerebellar adaptation at the parallel fiber - Purkinje cell synapses induced by long term depression (LTD) (Ito 1984).

- Basket and stellate cells are inhibitory interneurons in the molecular layer. Basket cells are named after the fact that their axon travels across the folium just above the Purkinje cell bodies, descending collaterals at right angles, which surround Purkinje cell somata like a basket. On average,

  Stellate cells are usually found in the outer two-thirds of the molecular layer and are different from basket cells in that stellate cell axons form synapses only on dendric shafts of PC's.

- Granule cells are the smallest and the most numerous cell type, about $10^{10} \sim 10^{11}$, in the cerebellar cortex. They relay mossy fiber afferents to the cerebellar cortex to excite all the other cell types in the cerebellar cortex. Each ascending granule cell axon has a T-shaped bifurcation in the molecular layer, giving rise to a pair of long thin fibers, parallel fibers. In general, the parallel fibers in the lower third of the molecular layer are myelinated and thicker than those in the upper thirds that are unmyelinated. These difference prompted a question regarding their functional difference (Ito 1984; Wyatt and Wang 2003; Ekerot 2005). The patches of PC responses may be attributed

to the patchy pattern of the underlying granule cells (Bower and Woolston 1983).

- Golgi cells in the granular layer receive excitatory inputs from mossy fibers as well as granule cells. Golgi cells inhibit granule cells in the glomeruli and its inhibition counteracts the excitatory effect of the mossy fiber synapses. In addition, Golgi cells inhibit also stellate and basket cells. Vos et al. (2000) suggested that Golgi cells in the network of mossy fiber, granule cell, and parallel fiber perform poorly as gain controllers at time scale of interest for cerebellar motor control, but also suggested that common parallel fiber inputs cause synchronization of beams of Golgi cells, which cause strong lateral inhibition to produce more regulated granule cell spiking activity for a relevant duration (Ito 1984) .

There are few other cell types found in the cerebellar cortex. The unipolar brush cells (UBC's) are identified in granular layer and are characterized by its dendric termination resembling a brush to receive mossy fiber terminals. UBC's are found in vestibulocerebellum and less often in spinocerebellum, but not in cerebrocerebellum. Their functions are yet to be determined, but appear to be involved in reflex mechanism through their excitatory to enhance the mossy fiber afferent to PC's with higher firing rates than Golgi cells (Simpson et al. 2005). Another class of cell type is Lugaro cell. It lies in the granular layer close to the Purkinje cell layer, but its physiological and functional characterizations have not been established (Ito 1984).

Learning/Adaptation

Based on the pioneering modeling work by Marr (1969) and Albus (1971), they proposed that the climbing fiber to PC's modified the response of the neurons to mossy fiber inputs and this change was sustained for a prolonged duration. This proposal was supported by a series of experiments on vestibulo-ocular reflex by Ito and his colleagues (Ito 1984, 2002). As introduced earlier, the climbing fiber weakens the parallel fiber-PC synapse by simultaneous stimulation of both climbing fiber and mossy fibers. This process is called long term depression (LTD). In this original formulation, climbing fibers detect discrepancies between

actual and expected sensory inputs, where the expected inputs are modified with successive movements by suppressing flawed activity patterns. Significant efforts have been made to study this type of cerebellar learning since 70's. There have been other suggestions, through physiology, genetics, and modeling, as to possible cites of such plasticity in the cerebellum as well as mechanism itself, depression alone or a combination of depression and potentiation. One standing question, however, is whether climbing fiber can produce the appropriate signals suggested by the proposals in vivo.

2.1.2 Motor cortical areas

The motor cortical areas are a heavily interconnected entity and include the primary motor cortex, premotor cortex, and supplementary motor cortex, and cingulate motor areas. The primary cortex and premotor areas receive input from the basal ganglia and the cerebellum via different set of thalamic nuclei. There appears to be segregated cortical-subcortical loops, and each loop makes different contribution to different aspect of motor and non-motor functions(Kelly and Strick 2003).

Primary motor cortex

The primary motor cortex (M1) owes its name to the fact that thresholds for evoking movement with electrical stimulation are lower here than in any other cortical regions (Dum and Strick 2005). M1, or cytoarchitectonically classified as area 4, is located in the anterior bank of the central sulcus and is usually identified by the presence of huge pyramidal output cells in cortical layer 5. Functionally, M1 has been considered as the executive locus of voluntary limb movements, although other cortical areas participate in these movements. The spiking activity of M1 has been shown to correlate with many aspects of the motor control and even cognitive functions.

Each individual neuron in M1 has a preferred direction (PD) for reaching or tracking movements (Georgopoulos et al. 1982b; Johnson et al. 1999). This typically refers to the direction of hand movement for which the neuron fires most intensely. When individual M1

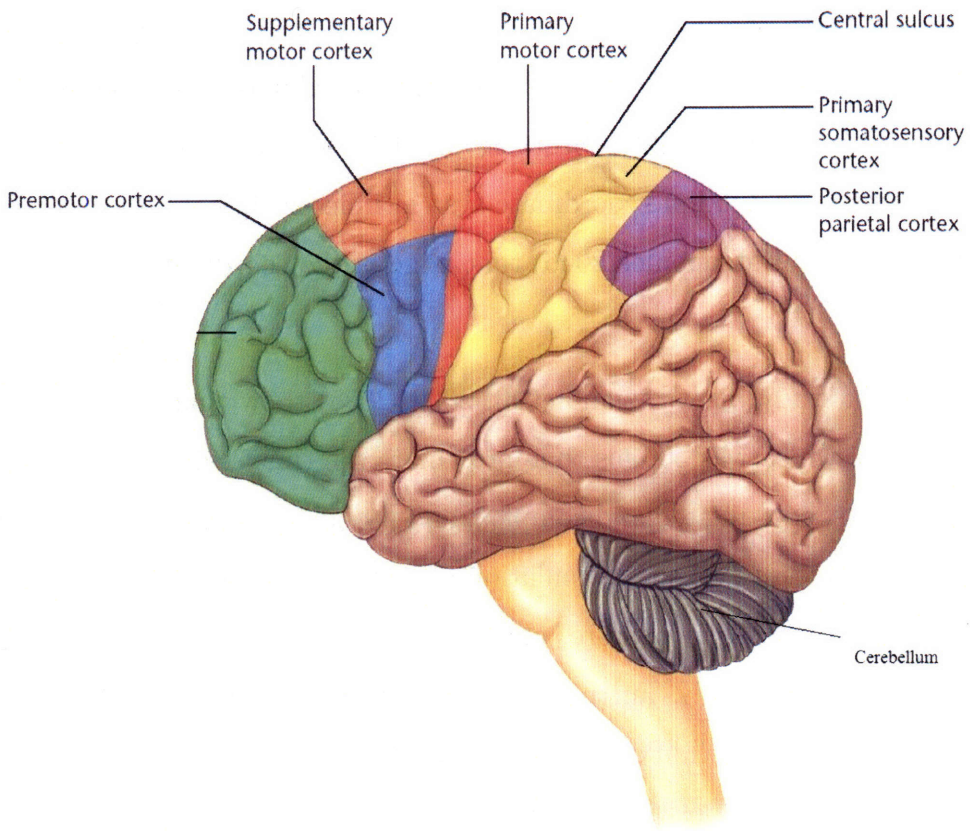

Figure 2-4: Major cortical areas (adapted from http://cti.itc.virginia.edu/ psyc220/)

neurons were represented as vectors that make weighted contributions along the axis of their PD (according to changes in their activity during the movement under consideration) the resulting vector sum of all cell vectors (population vector) was in a direction congruent with the direction of movement (Georgopoulos et al. 1988). In a recent study, Amirikian and Georgopoulos (2003) found that cells with similar PD's tended to segregate into vertically oriented minicolumns (50-100 μm wide and at least 500 μ m deep). Such minicolumns aggregated across the horizontal dimension in a secondary structure of higher order. In this structure, minicolumns with similar PDs were $\sim$ 200μm apart and were interleaved with minicolumns representing nearly orthogonal PD's. Furthermore, this directional preference does not change even when the origin of the movements are different (Kettner et al. 1988). The PD's characterized in the workspace coordinate may not be the most natural consequence of the fact that many layer 5 neurons in M1 have strong monosynaptic connections

to motoneurons. Thus, the population vector hypothesis has been tested against different coordinate systems, such as muscle coordinate, joint coordinate, body-centered coordinate, to name a few (Caminiti et al. 1990; Scott et al. 1997; Sergio and Kalaska 1997). However there is no consensus on a unique coordinate system inherent in M1. Recently study specifically showed (Wu and Hatsopoulos 2006) that none of the coordinate was dominant in M1 activities.

Recent series of study by (Graziano et al. 2002, 2005) show that, by applying electrical stimulation each of which was 500 ms to approximate the time scale of normal reaching and grasping movements, coordinated and complex, and probably more importantly behaviorally relevant, movements were evoked. Stimulation of one site, for example, caused a mouth to open, the hand to form a grip posture, and moved to the mouth, regardless of the initial configuration of the whole body. Furthermore, the evoked behaviors were found to be robust against reasonable load as well. Postures that involved the arm were arranged across cortex to form a map of hand end positions around the body. Thus, M1, and the premotor areas, appear to have somatopic map of the workspace around the body in terms of behavioral relevance. These results are still controversial in that there are no evidence of whether long sustained electrical stimulation train resembles actual cellular activity (Strick 2002).

Another series of focal and short intracortical stimulation evoked contractions of a single muscle at threshold (Asanuma and Rosen 1972). This observation could be explained by the limited branching patterns of some corticomotoneuronal neurons as well as the observation that small clusters of corticomotoneuronal neurons tend to innervate the same motoneuron pool (Shinoda et al. 1979). The motor system, or CNS for that matter, is a densely connected network system and the transsynaptic spread of signal through this network is a manifestation of the function of the network. Thus, to understand what the "natural" stimulus is an issue to be debated.

The presence of multiple representations of an individual movement/muscle in M1 has been proposed as an arrangement that allows a muscle to engage in multiple synergies with other muscles acting at the same or different joints (Schieber 2001). In addition, the so-

matotopic map in M1 is overlapping, intermingled, and fractured as observed by cortical stimulation and imaging (Donoghue et al. 1992; Sanes and Schieber 2001)

Rathelot and Strick (2006) used retrograde transneuronal transport rabies virus injected to digital muscles of macaques. In M1, the cortico-motoneuronal (CM) cells that make monosynaptic connections with the motoneurons of the injected muscles are found to be restricted to the caudal portion of M1 buried in the central sulcus. The CM cells are found to be widely distributed and even overlapping with the known-to-be shoulder regions. Furthermore, there are no focal representation of single muscles in M1.

Premotor areas

Premotor areas, or cytoarchitectonically classified as area 6, can also elicit movements by electrical stimulation, but the intensity threshold necessary to evoke movement is greater than that of M1. Area 6 lies anterior to the precentral gyrus, on the lateral and medial surfaces of the cerebral cortex. Pyramidal cells in the layer 5 are found in the premotor areas and do project to M1 and the spinal cord, but they tend to be smaller and fewer than that of M1. PD representations as well as hand end position map centered around the body as discussed above are still in tact in the lateral premotor areas. However, the premotor areas in the medial wall of the hemisphere do not appear to show such organization. The origins of corticospinal and cortico-cortical projections to M1 do not show somatotopic organization. This hypothesis is made based on the fact that the origin of corticospinal neurons in the premotor areas that projected to cervical or to lumbar segments of the spinal cord corresponded remarkably well to the origin of neurons in the premotor areas that projected directly to the M1 arm or to the M1 leg representations, respectively. The inputs to the premotor areas are quite different from those to M1. Damage to premotor areas cause more complex motor impairments than the case of M1. In particular, an animal with such damage cannot incorporate visuospatial information about the target into a kinematic plan (Kandel et al. 2000).

There are at least four anatomical divisions in the premotor areas in primates. Two on

the lateral convexity are the (lateral) ventral, PMv, and (lateral) dorsal, PMd. The other two in the medial wall of the hemisphere are the supplementary motor area, SMA (SMA proper and preSMA) and the cingulate motor areas, CMA, which are buried in the cingulate sulcus. In the motor planning hierarchy,Movement initiated and guided by internal cues appears to involve SMA. Movement initiated and guided by external cues appears to involve lateral PM.

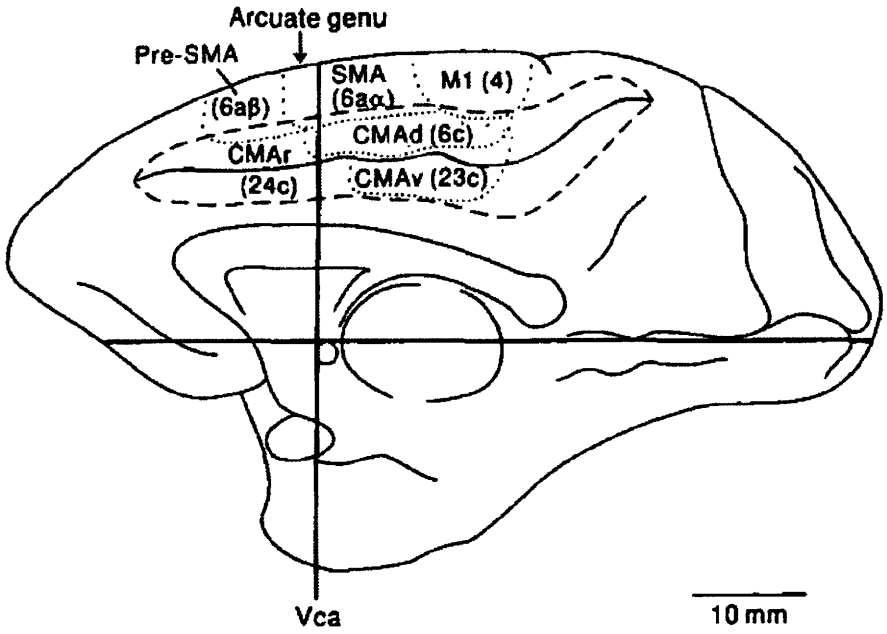

Figure 2-5: Locations of the motor areas of the medial wall of the hemispheres of the monkey. Adapted from Picard and Strick (1996).

SMA or preSMA itself could evoke movements, but movements elicited in the preSMA were typically slow, involved multiple joints, and resembled natural postural movements. PreSMA neurons often responded to visual but not to somatosensory stimuli, whereas SMA neurons had the opposite characteristics, responding to somatosensory but not visual stimuli (Matsuzaka et al. 1992; Inase et al. 1999). SMA and preSMA are attributed to the internal representation of sequence of movements, and their neurons primarily fire only to the memorized sequences. Hoshi and Tanji (2004b) found functional specialization between these

two areas as follows: 1) neuronal activity preceding the appearance of visual cues was more frequent in the pre-SMA; 2) a majority of pre-SMA neurons, but much fewer SMA neurons, responded to what was shown or instructed; 3) in addition, pre-SMA neurons often reflected information combining the instructions in the first and second cues; 4) during the motor-set period, pre-SMA neurons preferentially reflected the location of the target, while SMA neurons mainly reflected which arm to use; and 5) when executing the movement, a majority of SMA neurons increased their activity and were largely selective for the use of either the ipsilateral or contralateral arm. In contrast, the activity of pre-SMA neurons tended to be suppressed. Thus, these two structures have fairly distinct functional specialization with respect to receiving associative cues, information processing, motor behavior planning, movement execution, and motor learning.

Within the lateral premotor areas, PMd and PMv differ in many aspects. First, PMd receives inputs from the medial dorsal parietal (MDP) and medial intraparietal (MIP) areas in parietal cortex. This connection is responsible for integration of visuomotor transformation of the object to be reached and information about which arm to use. On the other hand, PMv receives parietal input from anterior intraparietal area (AIP) and mostly reflects properties of an objet to be reached (Hoshi and Tanji 2006).

Very little is known about the functional role of the cingulate motor area in arm movements compared to other motor areas. The rostral CMA played a part in processing the reward information for motor selection when there were many possible choices to choose from (Shima and Tanji 1998). Wang et al. (2004) found that the cells in CMA that project to frontal eye field and M1 scarcely overlapped, and that each of the two areas receive different sets of information from the cingulate cortex for possible integration of multimodal signals for high level motor functions. For visually guided reaching movements, CMA appeared to context-dependent movement related activity such as movement direction and target locations (Crutcher et al. 2004).

2.1.3 Parietal cortex

Parietal lobe contains many parietal association areas, but in this section only area 5 in posterior parietal cortex that is relevant to the work in this thesis is reviewed.

Arm related area 5 neurons showed graded changes in spiking activity in different directions which are similar to what's observed in M1. One critical difference was that activity of the area 5 neurons were insensitive to the load while M1 cells showed significant sensitivity to the force (Kalaska et al. 1990). In addition, populations of neurons in area 5 coded either the starting point, the final point, or the combination of the two in the body centered coordinate and each coordinate axis was coded in different subpopulations Lacquaniti et al. (1995). Further, the cells in the area 5 appeared to code spatial attributes of the hand trajectory that was influenced by arm geometry (Scott et al. 1997). Desmurget et al. (1999) suggested that area 5 neurons, or more extended posterior parietal network, computed ongoing error signal used by other motor areas to make corrections to the ongoing trajectory. The origin of the error signal was not clearly stated, but the above studies showed that area 5 neurons represent kinematic trajectory of the arm, not the hand alone, and ongoing error signals.

Another interest feature of the area 5 neurons was demonstrated to explain how the timing of action were coded with respect to external cue or internal cue (self-timed). Neurons in cortical area 5 exhibited phasic discharge modulations that were generally comparable for both modes of action, with some neurons increasing and others decreasing their firing rates with movement. For self-timed movements, however, there was an additional, slow ramp-up or ramp-down of activity in the few hundred milliseconds before the phasic discharge. These ramping modulations occurred well before any detectable changes in arm-muscle activity and their time course bore a striking resemblance to activity in the putamen preceding self-timed movements, observed previously. Together, the results suggest a possible mechanism for the internal timing of action within the motor system. In this model, reverberant activity in cortico-basal ganglia circuits reaches a threshold level resulting in much larger perimovement discharges within the same network, consequently driving the initiation of action(Maimon and Assad 2006).

2.1.4 Somatosensory cortex

The anatomical organization of anterior parietal somatosensory cortical areas such as 1, 2, and 3b has been well documented (Pons and Kaas 1985). However, the somatosensory system must be tightly linked with the motor system to generate discrete, coordinated movements necessary for fine tactile discrimination, hand/mouth coordination, and goal-directed reaching. Area 3a, which receives most of its afferent input from muscle spindles (Hore et al. 1976).

Area 3a

The cortical connections of area 3a are distinct from other somatosensory areas in that area 3a receives its densest input from cortical areas associated with the motor system, including M1, SMA, and premotor areas. Area 3a is also densely interconnected with areas in the posterior parietal cortex (Huffman and Krubitzer 2001a,b).

A surprising result from Rathelot and Strick (2006) is that about 15% of the cortico-motoneuronal cells originate from area 3a, which supports the finding of Wu et al. (2000) that the electrical stimulation to area 3a evoked hand movements of prosimian primates.

In terms of the sensory response, Carolyn W.-H. Wu (2003) found that the neurons in area 3a were typically unresponsive to light touch and the movement of hairs, but they often could be activated by tapping and manipulating body parts, suggesting the activation of deep receptors in muscles and joints. Occasionally, neurons could be activated by moderately intense pressure, especially on the digits of the hand. Area 3a was also distinguished by larger layer V pyramidal cells and was responsive to muscle spindle receptor activation and cutaneous receptors in monkeys (Krubitzer and Kaas 1990).

2.1.5 Basal Ganglia

Basal ganglia (BG) have been known as major components of the motor system (Kandel et al. 2000). The BG consist of four major nuclei: the striatum, the globus pallidus (GP), the substantia nigra, and the subthalamic nucleus. Almost all the cerebral cortical areas

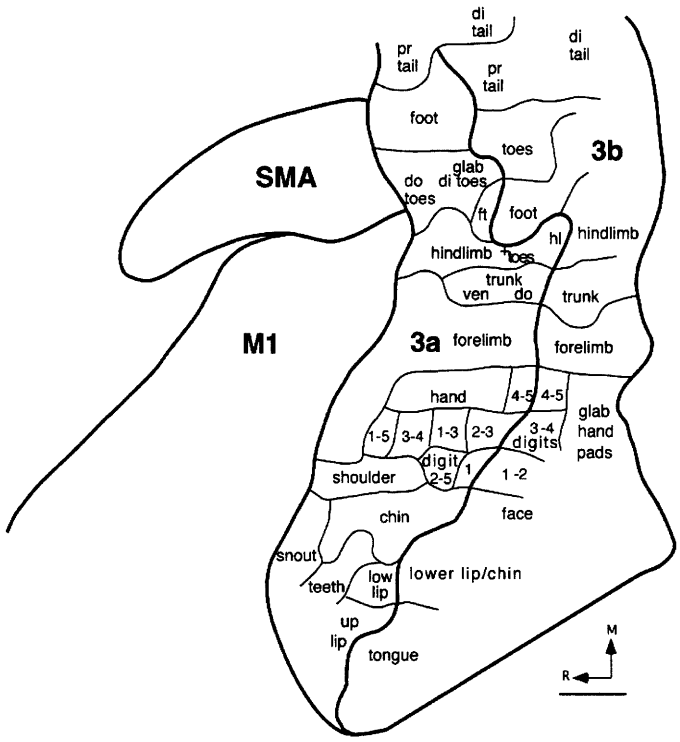

Figure 2-6: Area 3a and surrounding cortical areas in a flattened left hemisphere. Adapted from Huffman and Krubitzer (2001a).

send excitatory projections to the striatum. The striatum also receives dense excitatory inputs from the thalamus. Within the striatum, the caudate receives inputs mainly from the prefrontal cortex and this connection is sometimes attributed to motor planning. The putamen is mostly connected to the cortical motor areas and its connection is thought to regulate the level of the motor execution.

This group of nuclei are involved in many neural pathways implicating not only motor functions, but also wider cognitive functions (Brown et al. 1997) such as learning, working memory (Levy et al. 1997), and attention. In addition to its multi functionality in normal behavior, dysfunction of the BG has been related to brain disorders including Parkinson's disease, Huntington's disease, and schizophrenia. For this reason, the BG has attracted a very intense clinical interests which have suggested numerous functions of the BG. An interesting point is that the basal ganglia is not directly connected to the spinal cord unlike most other motor systems. Therefore, its motor function is attributed via other systems,

especially, motor areas of the cerebral cortex (Kandel et al. 2000)). The basal ganglionic neural circuit seems to do discrete operation of context-to-control mapping (Mao 2005).

2.2 Examples of current motor control models

Because of the its uniform structure and the relevance to its function in motor control, the cerebellum has attracted many theorists and modelers over the years. A significant number of models have been suggested to account for functions of the cerebellum (for a survey on a variety of cerebellar models, see Barlow (2002)), but in this section a few configurations of control models are shown first, then a several models that have relevance to the work in this thesis are presented.

One of the reasons why there is a long-standing controversy in motor control modeling is the presence of an afferent delay in the biological systems (Contreras-Vidal et al. 1997; Kawato 1999). Especially for limb movements, afferent delays in proprioceptive and visual feedback can be fairly significant.

In the three figures below, P is a plant to be controlled, G is a controller, $x(t)$ is the input to the controller, $y(t)$ is the output from the plant, $d(t)$ is a disturbance signal, $\hat{P}^{-1}$ is an approximation of the inverse of the plant (if exists), Δ is a delay operator such that its input-output relation is characterized by the following: $l(t) = m(t - \Delta)$ where $l(t)$ is the output of the operator and $m(t)$ is the input to the operator.

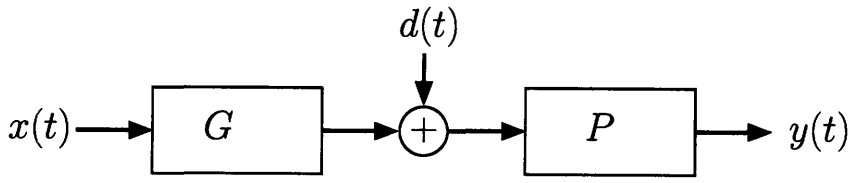

Figure 2-7: Feedforward/inverse control system

Fig. 2-7 shows a feedforward/inverse dynamics configuration. The plant output $y(t)$ will be identical to the input $x(t)$ if $G = P^{-1}$ and $d(t) = 0$. Suppose P is an unstable system. If $d(t) \neq 0$, then $y(t)$ is divergent unless the unstable part of P is canceled by $d(t)$. Even without

the presence of the disturbance, in order to achieve a perfect tracking of the input to the output, the controller needs to be a perfect inversion of the plant. Such a perfect inversion is extremely difficult to achieve, especially given the variability of neuronal activities. However, the controller in this scheme was suggested to be a function of cerebellum by Shidara et al. (1993).

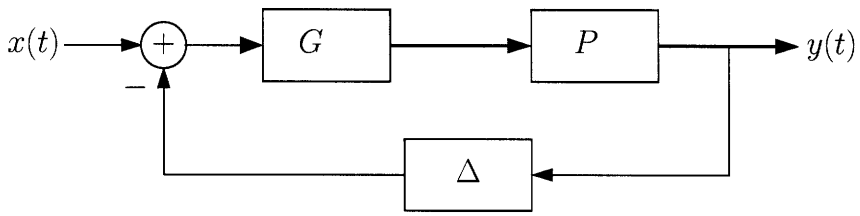

Figure 2-8: Feedback control system

Another configuration is a feedback control system as shown in Fig. 2-8. Anatomically it has been known that transcortical feedback loop exists (Brooks 1986) and is involved in motor control. Stabilization in this case is achieved by feedback induced changes in the closed loop dynamics that are more robust against the parameter variation as well as disturbances than explicit cancelation of the plant modes as in the feedforward scheme in Fig. 2-7. The models by Kettner et al. (1997), Barto et al. (1999), and Massaquoi (2006a) explicitly use this type of formulation and the cerebellum is posited as part of the controller.

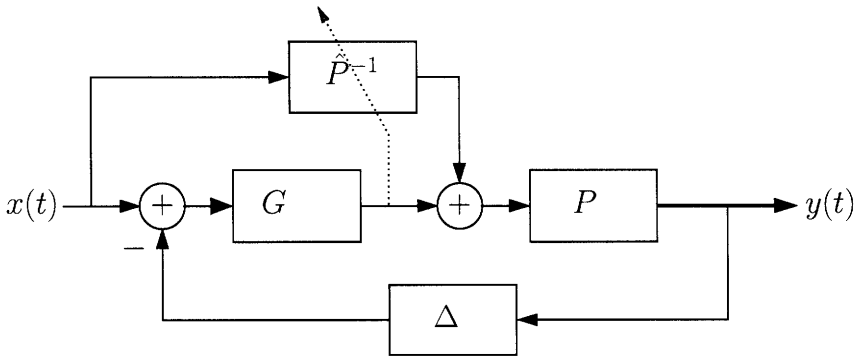

Figure 2-9: Feedback learning inverse/internal dynamics system

The last configuration is a combination of the feedforward and feedback configurations.

Many models which claim this type are learning models. The controller G is crude and as the system learns an accurate estimate of an inverse of the plant, $\hat{P}^{-1}$, the real time execution depends more on the feedforward path, through $\hat{P}^{-1}$ and P, than the feedback (Gomi and Kawato 1992a; Kawato and Gomi 1992b). It has been proposed that the cerebellum is a locus of the approximation of the plant inverse (Kawato and Gomi 1992b; Gomi and Kawato 1992a; Miall et al. 1993c; Wolpert and Kawato 1998; Schweighofer et al. 1998b).

2.2.1 Cerebrocerebellar communication system by Allen and Tsukahara (1974)

Allen and Tsukahara (1974) suggested a functional two-stage, planning and execution system involving the interaction between cerebral cortex and cerebellum. Fig. 2-10 shows a schematic connection of the suggested system.

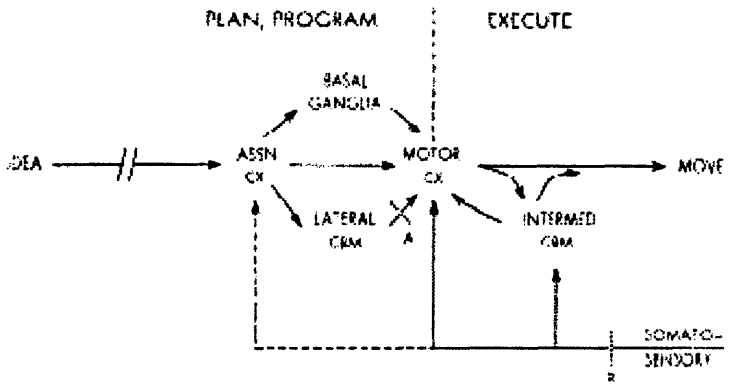

Figure 2-10: Cerebrocerebellar communication system (Allen and Tsukahara 1974). See the text for details.

A thin dashed line connecting the somatosensory feedback to association cortex (ASSN CX) represents a pathway whose function/importance was unknown at the time of the formulation. The dense dashed lines noted with A and B represent cooling of cerebellar dentate and sectioning of the dorsal columns, respectively. In the formulation, it was proposed that the lateral cerebellum and the basal ganglia were involved with ASSN CX in planning and

programming an appropriate patterned of certain motor cortical columns and their corresponding movements (Asanuma and Rosen 1972). Once the movement was planned within the planning center, the motor cortex issued a descending command to execute a movement. The intermediate cerebellum updated the ongoing movement based on the motor command from the motor cortex and somatosensory information of the limb's state. The lower execution loop did not participate in a long term planning, but only in a short term planning and follow-up corrections.

In order to test this two-stage classification, two pathological studies were performed. First, upon cooling of the cerebellar dentate of a monkey, a few behavioral changes were observed: Movement became slower, auditory and visual cues were used to locate the targets, and errors were developed in rate and range in attempting the movements. Thus, the authors concluded that these observations were consistent with the notion that the movement was primarily preprogrammed. Second, sectioning of the dorsal columns did not cause performance deterioration. That supported the idea that ASSN CX and lateral cerebellum were involved in preprogramming of movements.

2.2.2 Inverse/Internal models

One standing issue on computational neuroscience, motor control in particular, is whether internal models (Shidara et al. 1993; Gomi et al. 1998) exist in the brain or not, and if so, where they are located. Although a few researchers have tried to straighten confusions among neuroscientists as to what feedforward, inverse, or internal model means (Karniel 2002), there still has fair amount of confusion on what it means possibly due to its sources.

A series of studies (Kawato and Gomi 1992b; Gomi and Kawato 1992a) have suggested that the cerebellum is a locus of the plant inverse in relation to the adaptive feedback learning models. In the formulation by Gomi and Kawato (1992a), the proposed adaptive feedback control model is developed in detail as a specific neural circuit model for three different regions of the cerebellum and the learning of the corresponding representative movements: (i) the flocculus and adaptive modification of the vestibulo-ocular reflex and optokinetic eye-

movement responses, (ii) the vermis and adaptive posture control, and (iii) the intermediate zones of the hemisphere and adaptive control of locomotion.

Biological plausibility of the internal model being implemented in cerebellum was first suggested by Shidara et al. (1993) using kinematics of eye movements for a step-tracking task and simultaneously recorded Purkinje cells' simple spike firing activities. The authors showed that simple spike activities of majority of the task-relevant Purkinje cells, 19 out of 23, in the ventral paraflocculus (VPFL) of the cerebellum were accounted well for by the inverse-dynamics representation as below:

$$f(t-\Delta) = a\ddot{e}(t) + b\dot{e}(t) + ce(t) + d, \tag{2.1}$$

where $f(t)$, $\ddot{e}(t)$, $\dot{e}(t)$, $e(t)$, and Δ are the firing frequency at time t, the eye acceleration, velocity, and position at time t, and the time delay between firing frequency and movement, respectively. Therefore, they assumed that the forward dynamics of the eye movement could be derived as below:

$$M\ddot{e}(t) + B\dot{e}(t) + Ke(t) = m(t-\Delta_m) = \sum_{i=1}^{N} w_i f_i(t-\Delta_i) + \sum_{j=1}^{L} p_j g_j(t-\Delta_j), \tag{2.2}$$

where M, B, and K are the acceleration, velocity, and position coefficients, $m(t)$, the final motor command to be the weighted sum of the firing $f_i(t)$ of the $i-$th PC weighted by w_i, and the firing (rate) $g_j(t)$ of the $j-$th neuron weighted by p_j in *another brain region.*

However, in this analysis, Eqn's 2.1 and 2.2 merely show that the firing rates of the Purkinje cells is a linear summation of kinematic variables. Thus, it should not be concluded that the cerebellum is a site of the inverse dynamics of the plant.

Gomi et al. (1998) followed a similar manner by studying ocular following response (OFR) and found that 86% of the well-modulated temporal firing patterns taken from those 30 Purkinje cells from the VPFL were reconstructed successfully from eye movement. Further, the estimated coefficients of the regression model were larger (statistically significant) for slow

stimuli than for fast stimuli, suggesting changes in sensitivities under different conditions. However, firing patterns of each cell under several different conditions were frequently well reconstructed by an inverse dynamics representation with a single set of coefficients, which, as the authors claimed, possibly implied that within the stimulus range tested the relation between the eye movement response and VPFL PC simple spike firing patterns was roughly linear. An interesting observation was that without positional component, remarkable differences between observed and reconstructed firing patterns were noted especially in the initial phase of the movements, indicating that the negative positional component was not negligible during OFR. Therefore, individual PC's was not capable to generate final motor position command to the OFR system.

One of the issues in the above two studies is their logical construct to conclude that the cerebellum implements inverse dynamics simply because the firing rates of Purkinje cells can be approximated by kinematic signals. Furthermore, in order to check if the cerebellum receives feedback signals, there should have been an application of disturbances.

There has never been any electrophysiological studies to show that this inverse dynamics argument holds for multi-joint arm movements, where the arm dynamics is more complicated. Yet, there has been a significant amount of literatures arguing, based on the two studies above, that the cerebellum is a site of inverse dynamics implementation to mimic a map from position motor command to force/torque output. The following three models are just examples of such an argument.

2.2.3 Smith predictor (Miall et al. 1993c)

One of the most critical issues of the biological feedback control system is how to account for various types of delays present in the neural system. Smith predictor is a particular controller structure for systems with long loop delay by having a model of the plant and the delay. As long as the predictive plant and the delay models are accurate, then the delays are effectively moved outside of the feedback loop, as the actual and predicted feedback signals cancel each other out. One specific implementation of Smith predictor is shown below.

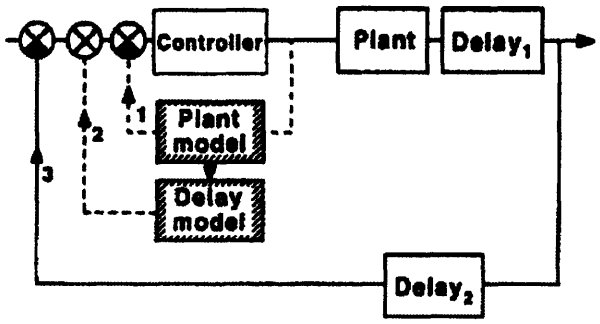

Figure 2-11: Smith predictor architecture (Miall et al. 1993c). Two internal predictive loops are indicated by dashed lines. Comparators are indicated by circles with one filled quadrant, and the empty circle is a positive feedback connection.

Miall et al. (1993c) suggested that the cerebellum formed two types of internal model. One was a forward predictive model of the motor apparatus, limb and muscle for arm movement, to provide rapid prediction of the sensory consequences of movement. The second model was of the time delays in the control loop to account for receptor and effector delays, axonal conductances, and cognitive processing delays. The reasons why the cerebellum was an obvious candidate was that a number of constraints posed on the Smith predictor structure fit with cerebellar anatomy and physiology. In particular, although there was no modeling or simulation was performed, the authors suggested that the comparison between expected, or reafference, and actual sensory signals, from which a teaching signal was provided for the cerebellum, was carried out by the inferior olive. One key weakness of Smith predictor formulation, at least based on a series simulations shown in the paper, was that both the delay model and the plant model had to be perfect. It is not clear how robust the Smith predictor formulation is against disturbances and parametric uncertainty in the plant and the delay models, especially with high dimensional nonlinear systems.

Miall and Jackson (2006) reported a study on adaptation to delayed visual feedback during a manual tracking task, testing the nature of the adapted responses with frequency analysis. Introduction of the visual feedback delay significantly disrupted tracking performance, with an increase in errors and a reduction in frequency of corrective movements.

Subjects showed clear evidence of adaptation during the 5 day experiment, decreasing tracking error and decreasing the mean power of intermittent corrections. However, there was no evidence of a return towards the initial high frequency intermittent tracking. The authors suggest that the adaptation observed in this study reflects the modification of predictive feedforward actions, but that these data do not support control based on Smith Prediction due to the fact that the Smith predictor uses a single adaptive forward model both for predicting the consequences of actions and for control at the same time.

2.2.4 Schweighofer et al. (1998a,b) models

Another model which incorporates basic components of CNS, cerebellum in particular, is suggested by Schweighofer et al. (1998a,b). As the virtual trajectory model (Bizzi et al. 1984; McIntyre and Bizzi 1993) was not successfully extended to account for rapid reaching movements in the order of 0.5 second because the controllers operating at each joint were not coupled, Schweighofer et al. (1998a) proposed a distributed functional model in which the CNS acquired a crude inverse dynamics of the arm in the motor cortex and spinal cord, Then, the model was complemented with the cerebellum for the interaction torques among the limb segments by learning a portion of the inverse dynamics model. Therefore, there are at least two sites distributed over the motor cortex and the cerebellum where the inverse dynamics are implemented.

In Schweighofer et al. (1998b), this model was modified into a more biologically feasible model with additions of inferior olive and specific cell types of the cerebellum as well as afferent and efferent delays present in the neural pathways. the inferior olive made the model adaptable. The updated model learned the part of inverse dynamics of the arm not provided by explicit feedback/feedforward controller. The authors found that only long parallel fibers allowed the proper learning of appropriate coordination of movement at two joints. If the parallel fibers were too short, then the PC's inputs originated mostly from the same joint so that proper associations between the joints were not learned. One interesting feature after learning was that the modeled PC's exhibited directional tuning (compare with

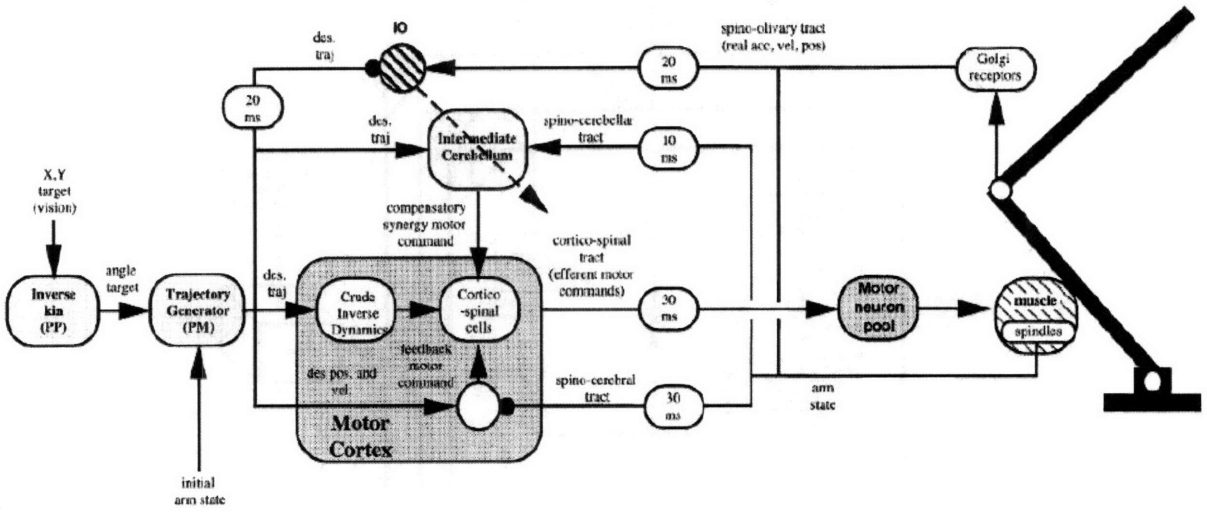

Figure 2-12: Functional diagram of the model for on-line control of arm movements with the inferior olive (IO) which computes the feedback error for adaptation (Schweighofer et al. 1998b). See the text for more details.

physiological results from Coltz et al. (1999)). Another interesting finding was that during learning, two peaks of inferior olive activity occurred at the beginning and the end of the movement, but after learning only the early peak that was locked with movement onset was present.

2.2.5 Wolpert and Kawato (1998) models

Wolpert and Kawato (1998) extended the hypothesis, that the CNS learned and maintained internal models of sensorimotor system and of objects in the external environment, by incorporating an idea that specific sensorimotor transformations must have been employed that were tailored to particular context or environment in order to deal with a variety of behavioral paradigms associated with different objects and environments. It is proposed that a new computationally intensive and anatomically reasonable model in which each inverse controller was augmented with a corresponding forward predictive model, the pair being tightly coupled during acquisition, motor learning, and use, through gating dependent on

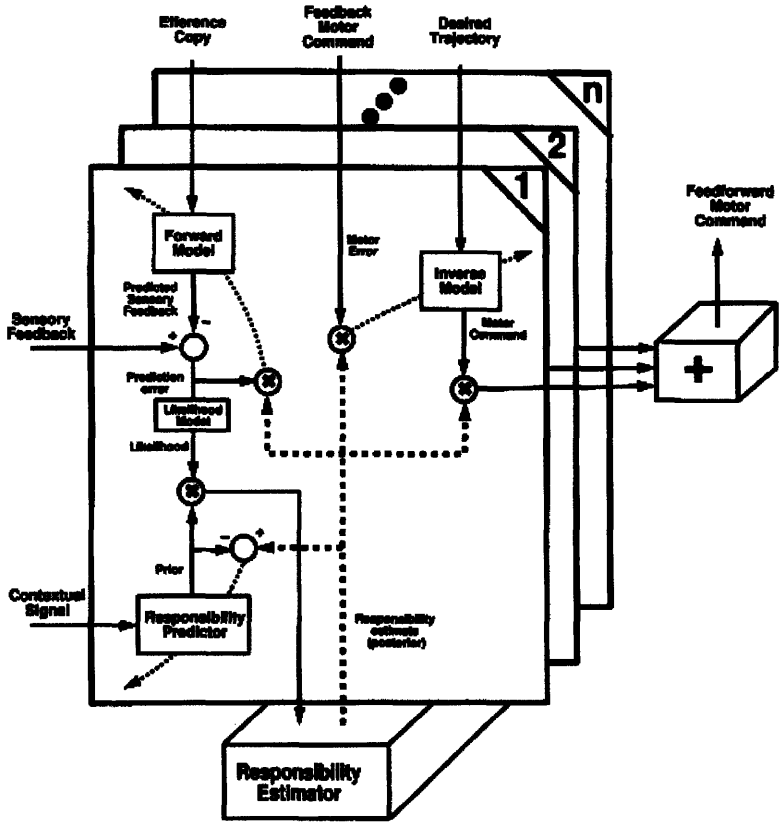

Figure 2-13: Model architecture of multiple paired forward-inverse model including n modules that are shown as stacked sheets. The detail of the each module is shown in the first module. from Wolpert and Kawato (1998).

the behavioral context. Ensembles of such pairs were called multiple forward inverse model as shown in Fig. 2-13. Each module consisted of three interacting parts. The first two, the forward model and the responsibility predictor, were used to determine the responsibility, or extent of participation, of the module. This responsibility signal reflected the degree to which the module captured the current context and hence should participate in control. The aim was that the multiple forward models learned to divide experience so that at least one forward model was active to predict the consequence of performed actions at any moment. It was assumed that the cerebellum was the most logical site for the location of the forward and inverse models and that a pair were localized within microzone or possibly larger functional unit in the cerebellar cortex. It was also assumed that both forward and inverse models were used in mental simulation of movement to account for a series of fMRI studies. One

issue that was not addressed in this formulation, unlike Miall et al. (1993c) and Schweighofer et al. (1998b), was the generality of the formulation against neural delays and its robustness against disturbance.

2.2.6 Kettner et al. (1997) and Barto et al. (1999) models

Kettner et al. (1997) suggested a neural network model of pursuit movement based on the anatomy and physiology of the cerebellum without having any explicit implementation of inverse dynamics unlike the few models introduced earlier. The model allowed the prediction of complex movements by adding a feature that an array of inputs were distributed over a range of physiologically justified delays and over different parts of state space, i.e., position and velocity space. It was confirmed against a primate experiment that both the model and the eye make short-term predictions about future events to compensate for visual feedback delays in receiving information about the direction of a target moving along a changing trajectory. In addition, both the eye and the model could adjust to abrupt changes in target direction on the basis of visual feedback, but did so after significant processing delays.

In a similar spirit to that of Kettner et al. (1997), Barto et al. (1999) developed a cerebellar model that was much simpler than that of Kettner et al. (1997), but for a single degree of freedom limb with a muscle which had the nonlinear velocity dependence of the stretch reflex. The model explored its potential for adaptive, predictive control based on delayed feedback information as in Kettner et al. (1997). An abstract representation of a single Purkinje cell with multi-stable properties was interfaced, using a formalized premotor network. The input command was chosen to be series of pulses, non-smooth transitions, of equilibrium points. By including realistic mossy fiber signals, a sparse expansive encoding of MF signals, as well as realistic conduction delays in afferent and efferent pathways, the model allowed the investigation of timing and predictive processes relevant to cerebellar involvement in the control of movement. (Fig. 2-15). This idea was motivated by the activity of the discharge patterns of MF's involving a diverse combinations of tonic and phasic components as well as the firing onset variability relative to the movement onset (van Kan et al. 1993). The model

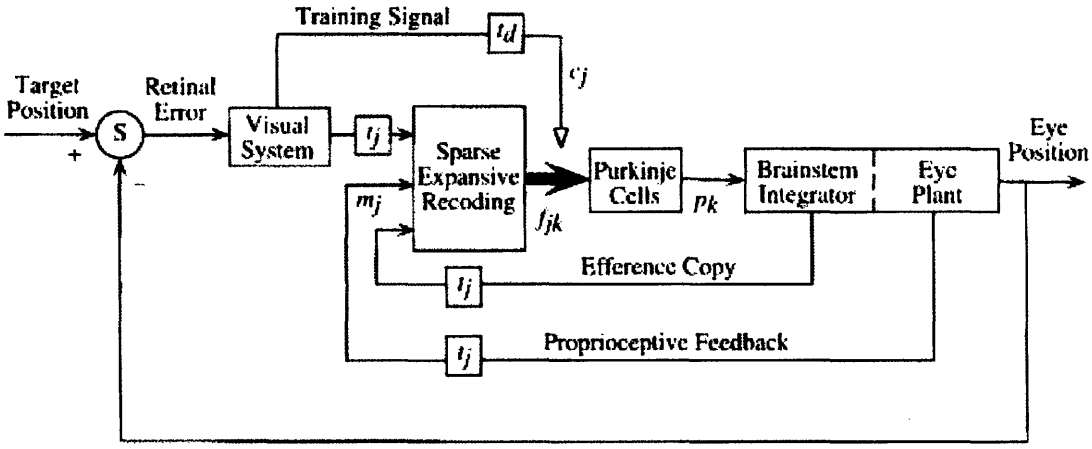

Figure 2-14: Block diagram of the model. Although the brain stem integrator and the eye plant are modeled by the same set of equations in the model, these 2 functions are distinguished in the diagram to emphasize their different neural substrates and the idea that both proprioceptive and efference copy signals may provide eye position and velocity information. All lines indicate the flow of multivariate information, with the heavier arrow indicating the wider bandwidth associated with the expansive recoding of mossy inputs. Smaller boxes: pure delays in the model. Open arrowhead: indirect action climbing fiber training signals have on information throughput by the alteration of network weights via the learning rule. Visual input to the system is assumed to take the form of retinal error signals that are obtained by a subtraction at the node labeled S of target and eye position signals (Kettner et al. 1997).

regulates movement by learning to react in an anticipatory fashion to sensory feedback. Learning depends on training information generated from corrective movements and uses a temporally asymmetric form of plasticity for the parallel .ber synapses on Purkinje cells.

These two models suggested that, although the arm model was of single degree of freedom and the eve model was an uncoupled two dimensional plant, in order to account for realistic kinematics as well as to achieve biologically feasible adaptation mechanism, realistic biological implementations were sufficient and strong notion such as internal model was not necessary.

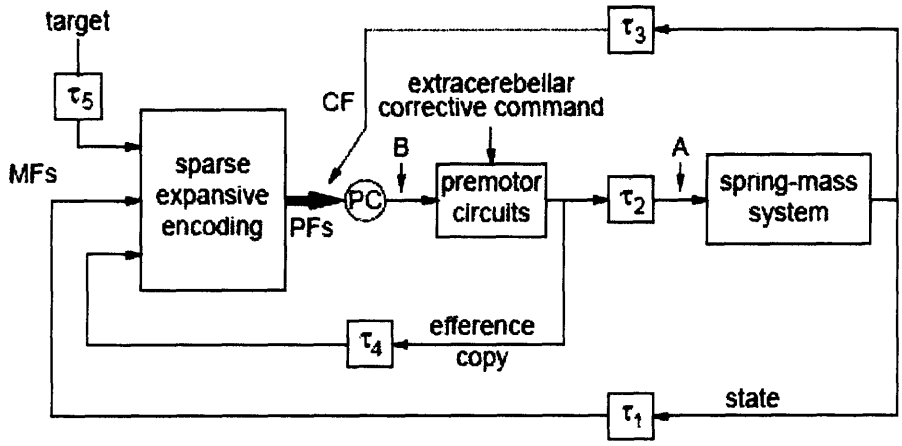

Figure 2-15: Model architecture. PC, Purkinje cell; MFs, mossy fibers; PFs, parallel fibers; CF, climbing fiber; τ_i, $i = 1, \ldots, 5$ conduction delays. The labels A and B mark places in the system to which Barto et al. (1999) refer discussing the model's behavior.

2.2.7 RIPID model (Massaquoi 2006a)

Many of the motor control models, the ones based on cerebellar functions in particular, focused more on achieving biologically feasible learning, but not much on cerebrocerebellar long loop compensation that the CNS is capable of. Thus in order to tackle this issue, Massaquoi (2006a) formulated a recurrent integrator proportional-integral-derivative, RIPID, control system that was based on anatomically feasible cerebrocerebellar communication.

This system appear to characterize a dominant role of cerebrocerebellar long-loop system in postural stabilization and two-joint arm and three-link leg (Jo and Massaquoi 2004) control without explicit dynamic inversion or internal forward predictive models. In addition, several signals from the model that have anatomical correspondence resembled various cell types recorded from M1 and area 5, which support biological feasibility of the model over the other existing models. At this point, however, the adaptation mechanism of this model is not clear.

This particular cerebrocerebellar long loop formulation is a basis of the modeling work shown in Chapters 3 and 4.

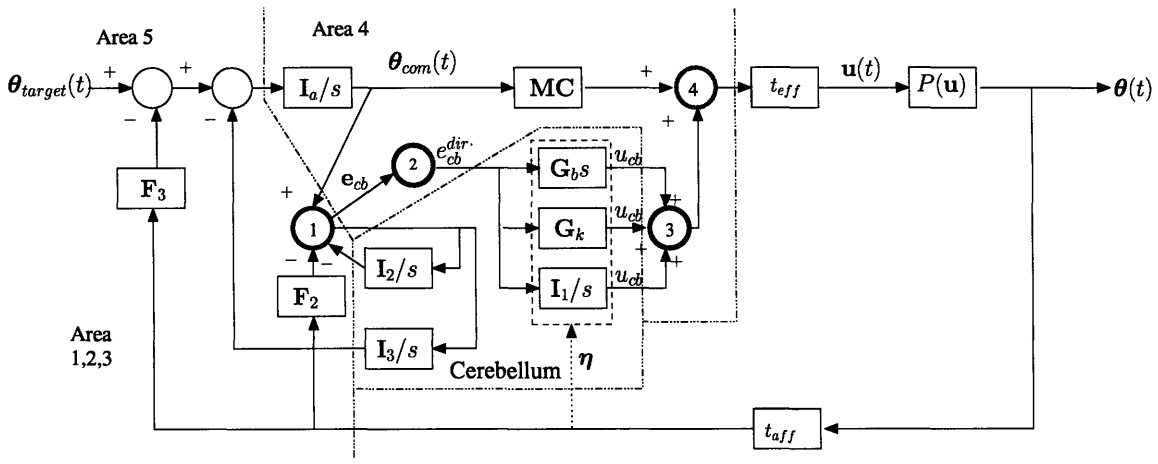

Figure 2-16: One version of RIPID model. Colored circles designate functional subcategories of sensorimotor cortical groups.

2.3 Intermittency

Movement 'intermittency' or 'segmentation' refers to the commonly observed characteristic of continuous movements to have brief intermittent reductions in speed without full stops. Between the local speed minima, the speed profile is typically a smooth roughly bell-shaped curve. Physically, this corresponds to the appearance that continuous movements are generated as segments that are blended together. Segmentation of apparently continuous movements was first observed by Woodworth (1899) in a speed-accuracy trade-off study. Since then, submovements, which have been identified by non-smooth speed profiles, have been described in many types of movements: pursuit tracking (Miall et al. 1986, 1988), reaching (Meyer et al. 1982) with or without visual feedback (Doeringer and Hogan 1998), interception of moving targets (Lee et al. 1997), cursor movement during isometric force task (Massey et al. 1992), and rapid hand movements (Novak et al. 2000, 2002). Submovements characterize both human and non-human primate limb movements (Miall et al. 1986). Emergence of intermittency is not only limited to end effectors of interest, but also to EMG. Segmentations were found in the EMG activity during slow finger movements (Vallbo and Wessberg 1993) and during point-to-point reaching movement with a wide range of speeds (Dipirtro et al. 2005), demonstrating that the descending command can also be inherently

intermittent. Furthermore, motor disorders, including Parkinson's disease, often increase segmentation (Flash et al. 1992; Hocherman and Aharon-Peretz 1994). The kinematic study of stroke patients, with different brain lesions, demonstrated that severely irregular intermittency during a continuous arm motion, but the speed profile of each submovement was verified to be invariant with speed (Krebs et al. 1999) and the severeness of the intermittency improved to decrease numbers of the submovements in a given movement and to increase peak speed as well as duration during recovery (Rohrer et al. 2004). These pathological cases indicate that some component of the CNS is responsible for integrating unit movements to make smooth movements.

Many researchers have noted the invariance of the velocity template, mainly in point-to-point movements. This invariance led to the hypothesis that a series of stereotypical submovements were used to make one composite movement (Milner 1992) and a few speed profile templates have been suggested such as minimum jerk criterion (Flash 1987) or individually fitted prototypes (Milner 1992). An example in (Milner 1992) as well as numerous point-to-point reaching studies showed that velocity profiles of accurate movements were asymmetric. Woodworth (1899) noticed this and suggested that accurate movements consisted of two phases: An initial phase in which the limb was brought near the target, and the current control phase make corrections to reduce terminal accuracy. Even with this classification, the initial phase of movements were still highly invariant (Milner and Ijaz 1990)

However, based on the observations of tracing of various geometric figures, Todorov and Jordan (1998) suggested that correlation between speed and curvature might be a consequence of an underlying motor strategy to produce smooth movements by maximizing smoothness along a predefined path, and the resultant intermittency is a byproduct of such an optimization principle. This correlation was stronger for movement with shorter durations and was not affected by the spatial scale or speed. Thus, even to maximize smoothness, existence of discrete and highly invariant unit movement emerged.

There are many suspects of possible causes of intermittency. One might wonder if the

intermittency is a manifestation of anisotropic neuromuscular dynamics. Massey et al. (1992) suggested that arm dynamics played no major role in the temporal correlation between tangential velocity minima and curvature maxima. The neuromuscular dynamics might not be a major player in the intermittency, but might be a minor contributor to intermittency. Neural noise could be another source of intermittency, but regardless of the templates used to decompose speed profiles into submovements, the high invariance of the speed profile implies that the intermittency is not a consequence of neural noise alone. Visual feedback delay could be another source of intermittency because in pursuit tasks with visual feedback, the speed profiles contained frequency content concentrated between $1 \sim 2$ Hz (Miall et al. 1993a). However, as Doeringer and Hogan (1998) showed that intermittency in that frequency still persisted after removing visual feedback, and further showed that the intermittency was not the result of a feedback delay alone whether the system was linear or nonlinear. A recent imaging study by Vaillancourt et al. (2006) showed that intermittency in visually guided force control task was a function of frequency of visual feedback and different brain regions were involved depending on the feedback frequency. Infrequent (0.4 Hz) visual feedback did not result in visuomotor activation in lateral cerebellum (lobule VI/Crus I), whereas frequent (25 Hz) intermittent visual feedback did. This is in contrast to the anterior intermediate cerebellum (lobule V/VI), which was consistently active across all force conditions compared with rest. Second, confirming previous observations, the parietal and premotor cortices were active during grip force with frequent visual feedback. The novel finding was that the parietal and premotor cortex were also active during grip force with infrequent visual feedback. Third, right inferior parietal lobule, dorsal premotor cortex, and ventral premotor cortex had greater activation in the frequent compared with the infrequent grip force condition. Therefore, in order to understand the underlying mechanism of intermittency generation, it is critical to look into actual neural implementations.

Chapter 3

Recurrent Integrator Cerebellar Simple Spike (RICSS) Model

3.1 Introduction

A number of studies have examined simple spike firing in cerebellar Purkinje cells (Bauswein et al. 1984; Fu et al. 1997; Gilbert and Thach 1977; Gomi et al. 1998; Ojakangas and Ebner 1992). Those analyzing the firing patterns in anterior intermediate and lateral cerebellum (motor cerebellum) have generally found correlations between Purkinje cell (PC) simple spike frequency and position and/or velocity. However, a functional model that accounts for the temporal details of these signals during arm movement control is still lacking.

In regard to modeling, it is important to note that typically PCs have been found to fire in relation to both passive and active motion of the body part under study, though perhaps not as vigorously in the former condition with respect to the latter (Bauswein et al. 1983; MacKay and Murphy 1974). This suggests that these cells may be involved in both monitoring and controlling body parts. Because the cerebellum is a site of considerable convergence of both peripheral sensory information via the spinocerebellar tracts and brainstem counterparts, and copies of motor outflow via pontine nuclei (Kakei et al. 1995) and spinocerebellar tracts (Bosco and Poppele 2001) it is natural to consider that PC activity may be a function of both

sensory information and motor outflow. This would be consistent with the observation that interpositus and dentate firing activity modulates during point-to-point movement control (Fortier et al. 1989; MacKay 1988; Thach 1975), passive body movement (MacKay and Murphy 1974) and postural maintenance (Horak and Diener 1994).

The preceding observation is not of trivial consequence because important motor control models emphasizing feedforward control based on desired, rather than sensed, movement trajectories (e.g., Contreras-Vidal et al. (1997); Gomi et al. (1998); Houk and Wise (1995b); Keifer and Houk (1994)) do not necessarily predict that sensory information would be prominent in cerebellar movement control signals. Other formulations (Massaquoi and Slotine 1996; Miall et al. 1993c; Paulin 1993; Wolpert and Kawato 1998) in principle include the possibility or prediction that sensory signals are prominently represented in at least some Purkinje cells. A minority of investigators have, in fact, promoted the view that the cerebellum is principally an organ that processes sensory signals and that motor function is secondary (Bower 1997). Massaquoi and Slotine (1996) showed an anatomically feasible feedback formulation that predicted interpositus nucleus firing activity. However, the model did not specifically show how PC simple spike activity could be accounted for. Gomi et al. (1998) showed that ventral paraflocculus PC simple spike firing activity can be fit by a linear combination of signals needed for dynamic control of the eyes. Although presented in support of a feedforward model, the data do not specifically indicate as to whether the PC signal is or is not dependent upon sensory information.

More recently, a model of cerebellar control based upon the processing of error-type signals has been proposed (Jo and Massaquoi 2004). The Recurrent Integrator PID (RIPID) cerebrocerebellar control model that evolved from a wave variable model (Massaquoi and Slotine 1996) posits that certain recurrent signals from cerebellum stabilize long-loop proprioceptive responses so that they may participate strongly in both postural maintenance (Jo and Massaquoi 2004) and point-to-point movement control (Massaquoi 2006a). From the perspective of these models, the bulk of cerebrocerebellar control involves both forward command and sensory feedback information inextricably combined. This view has poten-

tially significant practical implications. For example, it predicts that forward commands may be fairly simple or crude and still be highly effective because refinement will occur due to feedback. This would imply in turn that cerebral cortical command generation circuitry may be simpler than might otherwise be surmised. The view also predicts that fundamentally most motor cortical and cerebellar signals recorded in intact animals will not be entirely representative of the signals recorded in deafferented animals. If true, this fact could be relevant to optimizing the design of decoding algorithms for neuroprostheses (Donoghue 2002; Shenoy et al. 2003) to be used when afferent pathways have been compromised. Conceivably, if the role of sensory input is correctly understood, appropriate adjustments can be made to signals recorded in their absence.

Thus, it is potentially valuable to have an accurate representation of cerebellar waveforms in terms of the control signals that are processed there. The situation with two degree-of-freedom nonlinear arm control is more complicated than with single degree-of-freedom eye movements. Control is presumably implemented by a distributed population of units and the biomechanics of the arm about which the cerebellum is very likely concerned, are more complex. Moreover a full quantitative accounting for the role of a given set of experimentally recorded PCs in arm control is in principle difficult to achieve. First, the dataset must include a substantial fraction of the PCs involved in the control, and the relative degree to which each contributes to the total cerebellar output must be determined. To date, such data are not available. However, it is both possible and important to at least check whether a functional formulation such as the RIPID control model could account for observed PC activity waveforms while it controls motion of the arm.

Here it is demonstrated that a basic RIPID cerebrocerebellar control model can be elaborated to include plausible representations of cerebral, cerebellar and spinocerebellar circuitry in a manner such that a large number of waveforms recorded experimentally in primates during circular arm movement can be explained in terms of arm control signals. The resulting model will be referred to here as the Recurrent Integrator-based Cerebellar Simple Spike (RICSS) signal model. It is shown that the quality of fit provided by the RICSS model com-

pares favorably with fits using hand kinematics signals alone and that its structure accounts for the system nonlinearity predicted recently by a simpler empirical model (Roitman et al. 2005). The sufficiency of the RICSS model in accounting for a large PC dataset supports the plausibility of the RIPID model formulation in general, and the proposed cerebrocerebellar connection architecture in particular.

3.2 Methods

3.2.1 Purkinje cell simple spike data

The experimental setup is described in detail elsewhere (Roitman et al. 2004, 2005) and Chapter ?? in this thesis. Briefly, a right-handed female monkey (Macaca mulatta, Monkey M in Roitman et al. (2005)) was trained to use a two-joint manipulandum to make visually guided horizontal planar multi-joint arm movements. Targets and hand cursor were displayed on a vertically placed LCD monitor in front of monkeys. This investigation used the data from more than 25000 movement trials. Each trial consisted of four phases: Hold, Cue, Intercept, and Tracking. The monkey initially held the cursor at the centrally located hold target for a random duration between 1 and 2 seconds. Next, a cue target appeared at one of four angles (0, 90, 180, and 270 degrees) on an (invisible) 5 cm radius circle centered on the hold target, and began clockwise (CW) or counterclockwise (CC) circular motion while the monkey held the cursor at the hold target. After the target moved 180 degrees, its color changed to signal the onset of the Interception phase. The monkey was trained to intercept the target before the target moved 65 degrees farther. Once the target was acquired, the monkey was to track the target for 360 degrees. For the earlier experiments, the four target speeds ranged from 3.1 cm/s to 8.3 cm/s by 1.7 cm/s increments. For later experiments, five target speeds were used over the same range, differing by 1.3 cm/s. In contrast to the data used for analysis in Chapter 4, both speed increments are used in this chapter. Target speeds, initial launch angles, and rotational directions were varied randomly such that 10 trials were given for each target speed, initial angle, and rotational direction.

Target locations and hand locations in terms of x- and y- coordinate relative to the center of the workspace were recorded at 200 Hz.

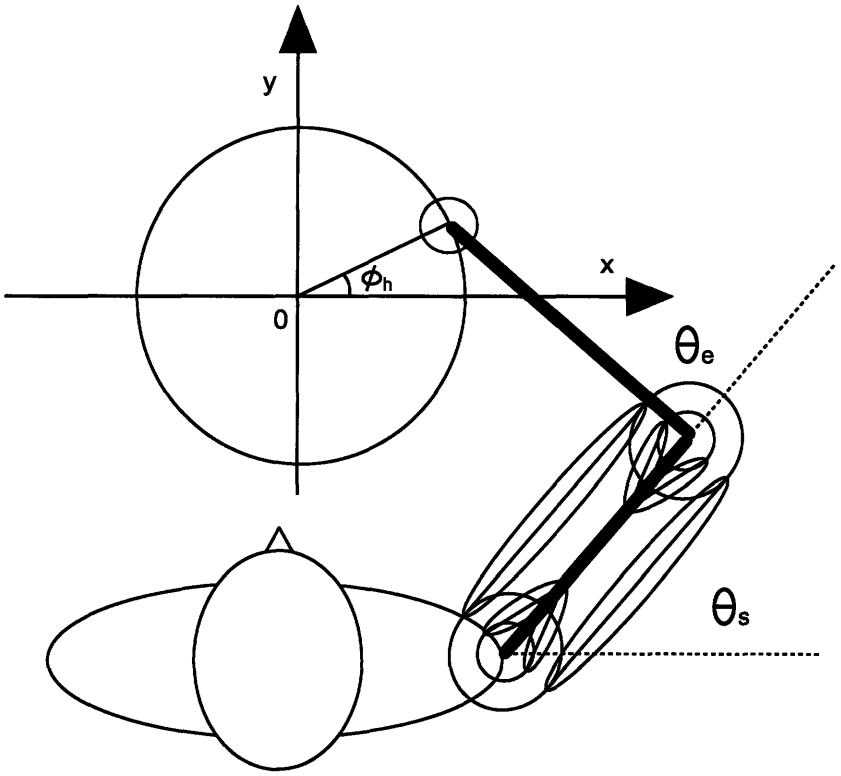

Figure 3-1: Arm configuration relative to the workspace of the monkey. The origin of Cartesian hand coordinate is set at the center of the circle on which the target cursor travels. The hand location is defined relative to this origin. The shoulder and elbow angles are defined as shown in the figure. Three functional muscle groups: shoulder flexors/extensors, elbow flexors/extensors, and two-joint flexors/extensors as in Katayama and Kawato (1993) and Flash (1987) are modeled.

3.2.2 Purkinje cell recording and properties

The recording chamber was placed over the parietal cortex ipsilateral to the tracking arm and was stereotactically positioned to target the electrode recordings in the intermediate and lateral zones of cerebellar lobules V-VI where arm related PCs have been described (Ojakangas and Ebner 1992; Fu et al. 1997). Simple spike data was sampled at 1 kHz and was examined qualitatively to test the responsiveness of individual PCs to passive manipulation of the shoulder, elbow, and wrist joints.

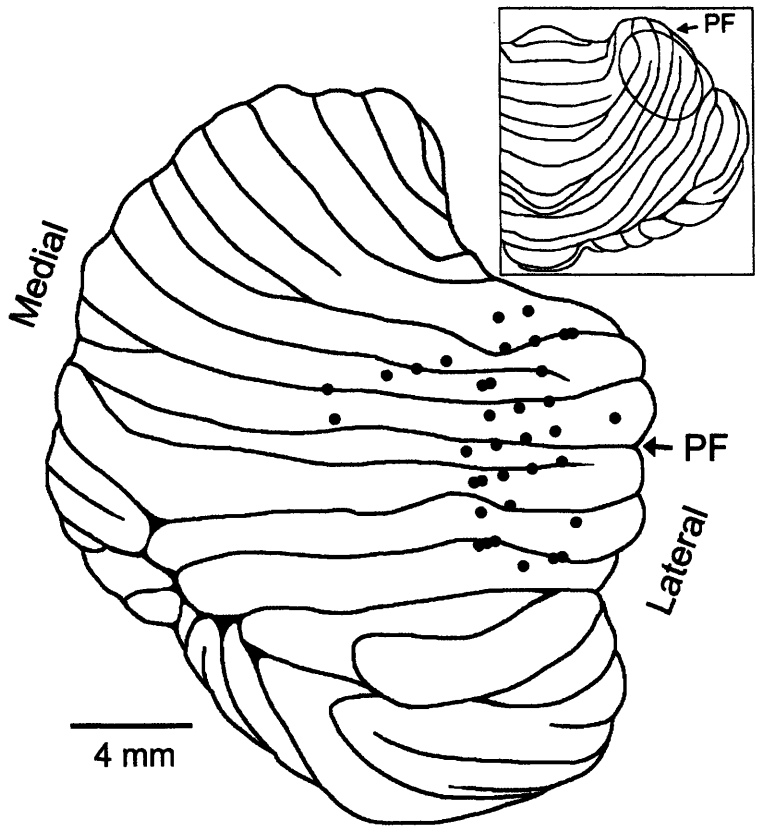

Figure 3-2: Recording sites are denoted with filled circles as shown in the lateral view of the cerebellum. The primary fissure is marked with the arrow labeled PF. Not all the recording sites for the cells used in the analysis are displayed and some recording sites correspond to several cells). Inset shows dorsal view of the cerebellum, with the ovals denoting the penetration regions. The figure is modified from Roitman et al. (2005).

Sixty-nine Purkinje cells were used for this study. Twenty-six cells were recorded with four target speeds and 43 cells with five target speeds. It was found that the majority of the tested PCs were modulated by passive arm movements (Roitman et al. 2005). The histological study showed that the locations of the recordings are consistent with previous studies that Purkinje cell activities were involving visually guided arm movements, but hardly, if any, related to eye movements (Coltz et al. 1999; Fu et al. 1997; Roitman et al. 2005).

3.2.3 Synopsis of the RIPID two-joint arm control model

The PC signal model is based on an elaboration and refinement of the RIPID two-joint arm control model (Fig. 3-3) that is presented in detail elsewhere (Massaquoi 2006a).

The model is seen to contain a nonlinear plant P that represents the two-joint, six-muscle group, arm musculoskeletal system with equations of motion given by Eq. (3.1) , see Katayama and Kawato (1993), together with its segmental spinal reflex control. For this study, spinal reflexes were subsumed within the stiffness of the muscular system Eq. (3.2):

$$\boldsymbol{\tau} = \mathbf{H}(\boldsymbol{\theta})\ddot{\boldsymbol{\theta}} + \mathbf{C}(\boldsymbol{\theta}, \dot{\boldsymbol{\theta}})\dot{\boldsymbol{\theta}} \tag{3.1}$$

$$\boldsymbol{\tau} = -\mathbf{A}^T \left[\mathbf{K}_m \left[-\mathbf{A}\left(\mathbf{l}_e(\mathbf{u}) - \mathbf{l}\right)\right]_+ - \mathbf{B}_m \left(-\mathbf{A}(-\mathbf{l})\right)\right]_+ \tag{3.2}$$

where $\boldsymbol{\theta} = [\theta_s, \theta_e]^T$ are joint angles as defined in Fig. (3-1), $\mathbf{H}(\boldsymbol{\theta})$ is the 2×2 configuration dependent inertia matrix, $\mathbf{C}(\boldsymbol{\theta}, \dot{\boldsymbol{\theta}})$ is the 2×2 configuration and velocity dependent matrix of velocity cross terms, $\boldsymbol{\tau}$ is vector of joint torques, $\mathbf{A}$ is a 2×6 moment arm matrix, $\mathbf{K}_m$ is a 6×6 stiffness matrix, $\mathbf{B}_m$ is a 6×6 viscosity matrix, $\mathbf{l}$ is a 6 dimensional vector of muscle lengths, $\mathbf{l}_e(\mathbf{u}) = \mathbf{A}^T\mathbf{u}$ is a vector of equilibrium muscle lengths controlled by a 2×1 vector of joint signals $\mathbf{u}$, and $[x]_+ = max(x, 0)$. The structure and parameters for this model were adapted from Katayama and Kawato (1993) to be appropriate for the monkey and are given in the appendices.

The neural control is represented by lumped parameters describing the scaling afforded by various components of the cerebro-cerebellar system driven by the intended motion reference command $\boldsymbol{\theta}_{target}(t)$, in contrast to the static reference position command $\boldsymbol{\theta}_{ref}(t)$ in Jo and Massaquoi (2004). The dynamics of individual neurons are not modeled explicitly. Values for the 2×2 cerebral gain matrices $\mathbf{I}_a$ and $\mathbf{MC}$, the cerebellar gain matrices $\mathbf{G}_k$, $\mathbf{G}_b$, $\mathbf{I}_1$, $\mathbf{I}_2$ and $\mathbf{I}_3$ and feedback gain matrices $\mathbf{F}_2$ and $\mathbf{F}_3$ were selected empirically to afford nearly circular hand motions while exhibiting physiologically low stiffness values with respect to peripheral disturbances. Physiological neural signal transmission delay values were used. These values are given in the appendices.

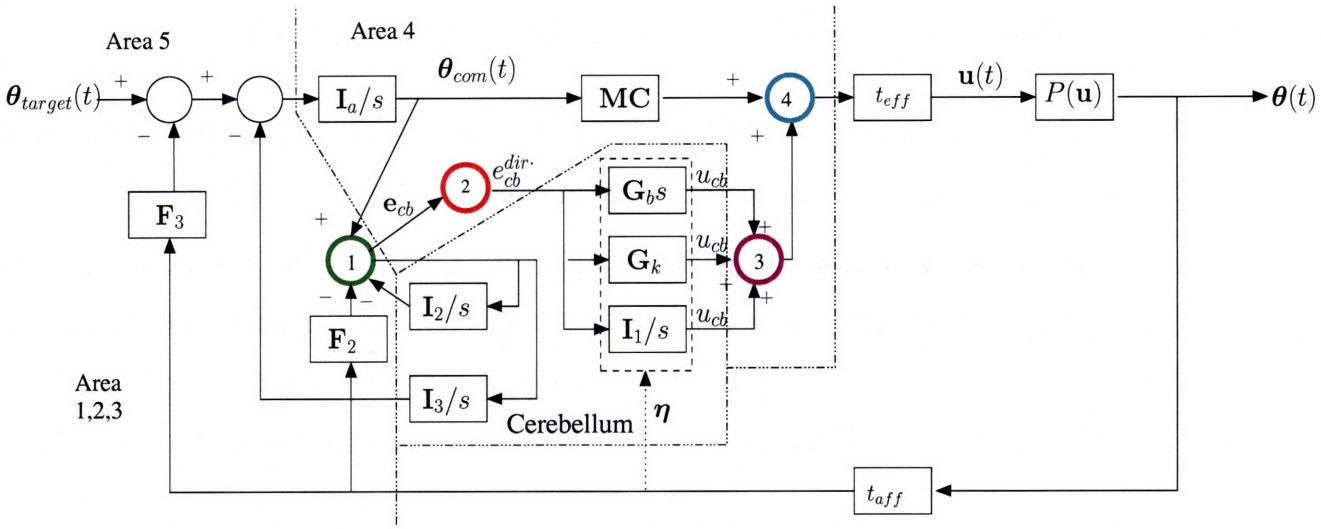

Figure 3-3: RIPID Model. Colored circles designate functional subcategories of sensorimotor cortical (SMC) units. See text for details.

Prominently rendered in Fig.3-3 are long-loop pathways to areas 3a and 5 and motor command paths direct through motor cortex (via **MC**) to spinal cord with efferent delay t_{eff}, and indirectly through cerebrocerebellar connections. Fundamentally, the signals that percolate through the control system are posited to be functions of a principal tracking error formed in parietal area 5, $\boldsymbol{\theta}_{target}(t) - \mathbf{F}_3\boldsymbol{\theta}(t - t_{aff})$ where t_{aff} is a sum of the spinal and peripheral delay, and more direct afferent information received via Area 3a (via $\mathbf{F}_2$ and category 1 sensorimotor cortical units (SMC-1) in Fig.3-3). The nature of the inputs to cerebellum depends upon the source. The signal from area 3a is proposed to travel to intermediate cerebellum and that from area 4 (SMC-2 units in Fig.3-3) to intermediate and lateral cerebellum. These are considered the principal signals that in the cerebellum and precerebellar nuclei undergo scaling, delay, recombination and reverberation to affect proportional, derivative and integral processing ($\mathbf{G}_b s$, $\mathbf{G}_k$, and $\mathbf{I}_1/s$, $\mathbf{I}_2/s$, and $\mathbf{I}_3/s$, respectively, where s denotes Laplace variable). These actions contribute to phase advancement (due to $\mathbf{I}_2/s$ feedback loop) for long-loop stabilization and sculpting forward control signals ($\mathbf{G}_b s$, $\mathbf{G}_k$, $\mathbf{I}_1/s$ path) that return to motor cortex where they are collected and redistributed via SMC-3 and SMC-4 units before descending through the spinal cord as motor command $\mathbf{u}$. A second important set of inputs is posited to consist of modulating signals from spinocere-

bellar tracts ($\boldsymbol{\eta}$, dashed arrow, see below). These signals effectively modify the values of $\mathbf{G}_b$, $\mathbf{G}_k$, $\mathbf{I}_1$ according to limb configuration and velocity as detailed below. In addition to the principal transcerebellar pathways there is additional internal feedback to the parietal lobe and/or motor cortex via $\mathbf{I}_3/s$ that contributes to loop stability.

The key prediction of the model is that many Purkinje cells in intermediate and lateral cerebellum that are involved in arm control will receive the signals $\mathbf{e}_{cb}(t)$ that can be seen to be a function of the error-like vector signal $\mathbf{e}_{f_2}(t) = \boldsymbol{\theta}_{com}(t) - \mathbf{F}_2\boldsymbol{\theta}(t - t_{aff})$. In particular, $\mathbf{e}_{cb}(t)$ is approximately equal to the scaled and filtered derivative of $\mathbf{e}_{f_2}(t)$ (see Eq. (3.4) below) that is generated by the recurrent integrator circuit.

3.2.4 Cerebrocerebellar interconnectivity and the RICSS model

Combining the studies of intra-cortical connectivity (Asanuma and Rosen 1972; Kaneko et al. 1994) with recent data on cerebrocerebellar connectivity (Kelly and Strick 2003), and established concept of distributed representation of signals in terms of population vectors (Georgopoulos et al. 1982a), a slightly more detailed but still simple picture of the cerebrocerebellar connection architecture can be proposed as shown in Fig. 3-4. The cortical component of the RICSS model is organized in terms of proposed functional groups or categories of cortical columns (Asanuma and Rosen 1972) that would be simultaneously consistent with known cerebrocerebellar connectivity and the RIPID control model. Here, it is assumed that $\mathbf{e}_{cb}$ in area 3a is represented as a population vector and then distributed to different PCs via SMC-2 columns (Figs. 3-3, 3-4). It is also considered that the particular SMC-1 column projecting to a given PC could vary according to cursor tracking direction. Hence, from the perspective of each PC, $\mathbf{e}_{cb}$ it is represented more specifically as the scalars $e_{cb}^{dir\cdot}(t)$, where $dir = cw$ (clockwise) or cc (counterclockwise) and $\cdot = +$ or $-$ as will be shown below. Thus, we associate with each column r a *nominal tuning direction* ϕ_r that would be the direction, in joint coordinates, in which a unit magnitude error would maximally activate the column (the "*preferred direction*" for a unit amplitude signal). It is assumed therefore that the major component of firing activity in column r is then determined by the projection of the vector

signal being represented onto the unit vector along ϕ_r.

It was seen empirically that a second activity component in these units is a tonic background signal that scales with the square root of the intended (constant) hand speed, v_h(see Eq.(3.3) for the detailed expression). The neurophysiological source of this signal is not specified in the model. However, some models of muscle spindle function (Hasan 1983; Houk et al. 1981) include a forward bias signal and a subunity exponent for the speed dependence of spindle output that appear to be consistent with this feature.

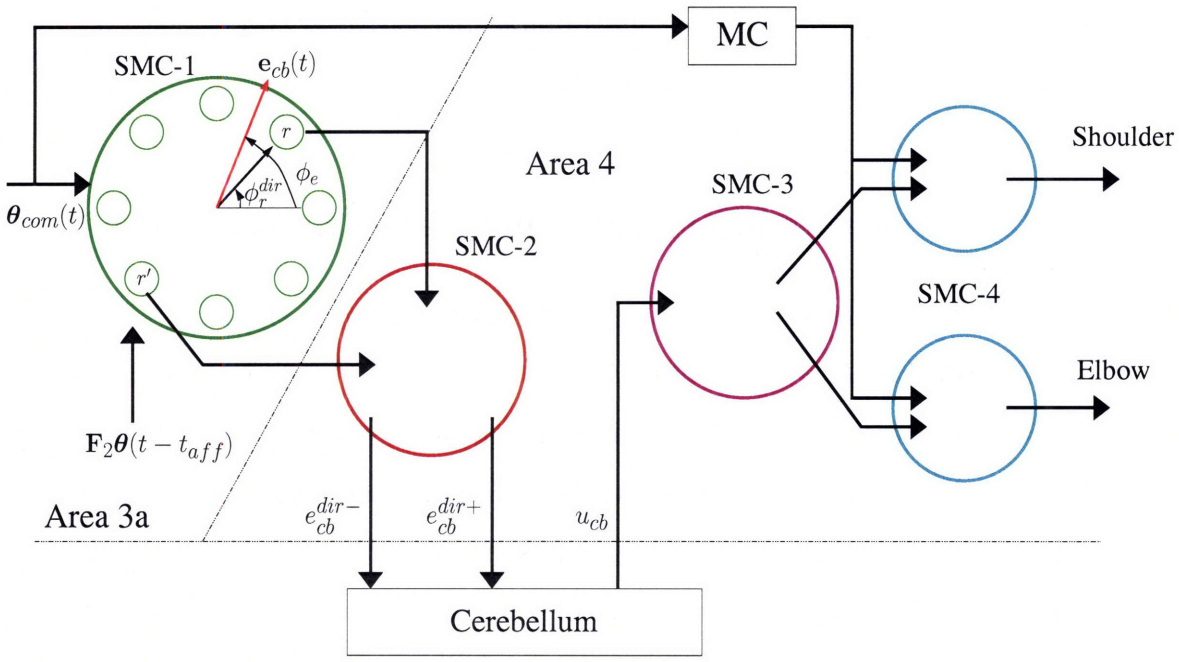

Figure 3-4: Cerebral cortical component of RICSS model from the perspective of a single cerebellar Purkinje cell. 8 cerebral cortical columns in Sensorimotor Cortical Area 3a (SMC-1, unit 1 in Fig.3-3) implementing a neural population-based representation, e.g. Georgopoulos et al. (1982a), of the tracking error-like vector (red arrow) and subsequent distribution after cerebellar processing (see text for details).

Activity is then transmitted to other sensorimotor cortical columns (SMC-2) and thence to the cerebellum. Fortier et al. (1989), Coltz et al. (1999) and others have pointed out that cerebellar PCs exhibit population vector-like tuning curves as do those in motor cortex. However, there are some characteristic differences from the latter. A number of cells, around 15 % in Coltz et al. (1999), have more bimodal curves with activity peaks that occur at two angles separated roughly by π instead of a single peak. In the current scheme, this could be

accounted for by assuming that occasionally columns with oppositely-directed ϕ_r^{dir} (Asanuma and Rosen 1972) project to the same PCs. Both unimodal and bimodal firing patterns in cerebellar PCs are represented in the model depending upon the relative dominance of parameters β^{dir+} or β^{dir-} in Eq. (3.3) below. The RICSS model also assumes that the columnar source of cerebellar input can differ according to intended cursor tracking direction. Thus it allows $\phi_r^{cw} \neq \phi_r^{cc}$

The return signals from cerebellum u_{cb} are afforded by cerebellar dentate (DN) and interposed nuclei, relayed via the VLc subnucleus of the thalamus (Asanuma et al. 1983) and distributed to selected motor cortical neuronal groups (SMC-3 and 4, in Figs. 2,3).

Fig.3-5 depicts the cerebellar component of the RICSS model. Here an array of Purkinje cells as would lie within a microzone (Oscarsson 1979) projects to a single group of deep cerebellar nuclear cells to form a functional corticonuclear microcomplex (Ito 1984). PCs are assumed to receive two types of parallel fiber input. Descending signals $e_{cb}^{dir}(t)$ from area 3a or 4 travel by mossy fibers designated here as signal mossy fibers (sigMF) to reach signal parallel fibers (sigPF) that are considered here to be those whose ascending axons synapse multiply on proximal PC dendrites to afford a strong excitatory connection (Bower 2002; Santamaria et al. 2002). A given set of sigPF inputs is presumed to synapse upon many PCs within the microzone and upon the associated deep nuclear cell. On the other hand, the distal dendrites of each PC are influenced more subtly by passing parallel fibers (Bower 2002; Santamaria et al. 2002). These are termed here selector parallel fibers (selPFs). The principal action of these fibers in the present model is to inhibit laterally adjacent PCs via basket cells (shown in red in Fig. 3-5). Thus, each PC is potentially suppressible by 'beams' of active parallel fibers to either side. Conversely, PC activity along an active beam of selPFs is comparatively preserved. This mechanism is consistent with the experimental observations of active centers and inhibitory surrounds within the cerebellar cortex (Cohen and Yarom 2000; Dunbar et al. 2004). The quantitative formulation is very similar to that described in Jo and Massaquoi (2004) but updated to be more consistent with the work of Bower (2002) and Santamaria et al. (2002). Selector parallel fibers are assumed to be supplied

by spinocerebellar tracts among other input pathways and thus to carry information about body state (Poppele et al. 2002) and other context variables.

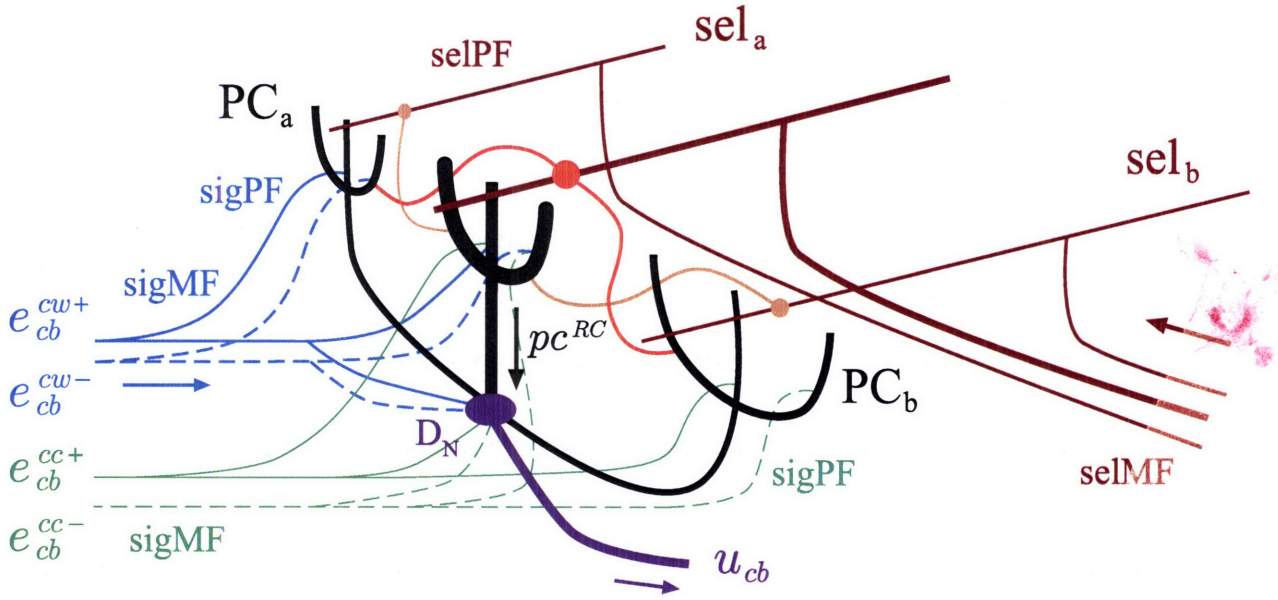

Figure 3-5: Cerebellar Architecture proposed to underlie PC SS activity, (see text for details).

Based on the architecture outlined above, PC simple spike firing depends upon both descending signal parallel fiber inputs and modulation by coincident selector fiber activity. It is assumed that in general that the descending cortical inputs may come from different SMC-2 units depending upon behavioral intent (roughly "motor set" by Brooks (1986)). In the current experiment it is assumed in particular that sigPF signals (as opposed to the selPF activity) differ for the two directions of cursor tracking. This assumption is reasonable based on a study of M1 cells for spiral drawing (Schwartz and Moran 1999) and on a study of parietal cells for movement intention (Scherberger et al. 2005). In these studies it was found that motor cortical cells fire differently depending on the rotational direction of spirals to be traced and cells in parietal reach region appear to encode the direction of currently planned arm movement.

Thus, for the RICSS (RC) model we represent the tracking direction dependent activity

of a Purkinje cell

$$pc^{RC}(\phi_h) = \alpha_{bg} + [1 - sel_a - sel_b]_+ \cdot (\beta^{dir+} e_{cb}^{dir+} + \beta^{dir-} e_{cb}^{dir-})$$

where α_{bg} is a constant level of background firing in the PCs, β^{dir+} and β^{dir-} are connection weights of the sigPFs onto the PC, and sel_a, sel_b represent the inhibitory effects of adjacent selector parallel fibers. For simplicity we assume that $\phi_{r'}^{dir} = \phi_r^{dir} + \pi$ and that the connection strengths of both inputs from SMC-1 to SMC-2 columns is equal so that $e_{cb,r}^{cw} = -e_{cb,r'}^{cw}$. In this case, the descending signals are defined as

$$\begin{aligned} e_{cb}^{dir+} &= \left[\alpha_{v_h} v_h^{0.5} + \delta_{cw}^{dir} e_{cb,r}^{cw} + \delta_{cc}^{dir} e_{cb,r}^{cc}\right]_+ \\ e_{cb}^{dir-} &= \left[-\alpha_{v_h} v_h^{0.5} + \delta_{cw}^{dir} e_{cb,r'}^{cw} + \delta_{cc}^{dir} e_{cb,r'}^{cc}\right]_+ \end{aligned} \tag{3.3}$$

where

$$\begin{aligned} e_{cb,r}^{cw} &= |\mathbf{e}_{cb}| \cos(\phi_e - \phi_r^{cw}) \\ e_{cb,r'}^{cw} &= |\mathbf{e}_{cb}| \cos(\phi_e - \phi_{r'}^{cw}) \\ e_{cb,r}^{cc} &= |\mathbf{e}_{cb}| \cos(\phi_e - \phi_r^{cc}) \\ e_{cb,r'}^{cc} &= |\mathbf{e}_{cb}| \cos(\phi_e - \phi_{r'}^{cc}) \end{aligned}$$

$$\mathbf{e}_{cb} = (s\mathbf{I} + \mathbf{I}_2)^{-1} s\mathbf{I}\mathbf{e}_{f_2} \approx \mathbf{I}_2^{-1} \frac{d\mathbf{e}_{f_2}}{dt}, \tag{3.4}$$

if $\mathbf{I}_2$ is a diagonal matrix and each element is large

where $|\mathbf{e}_{cb}|$ and ϕ_e are the magnitude and angle, respectively, of the filtered derivative (Eq. (3.4)) of the error vector signal, $\mathbf{e}_{cb}$ described above, $\mathbf{I}$ is an identity matrix whose dimension is compatible with $\mathbf{I}_2$, ϕ_r^{dir} designates an arbitrary nominal direction, and in Eq.(3.4), s is the Laplace variable. $\delta_{dir'}^{dir}$ are simple binary switch variables such that $\delta_{dir'}^{dir} = 1$ if $dir = dir'$,

and 0 otherwise. This corresponds to the switch in cortical column according to rotational tracking direction.

The modulatory effect of selPFs is represented by Eq. (3.5):

$$sel_i = \mu_i \left[\boldsymbol{\eta}_{i+} \cdot \mathbf{qq}(t - t_{aff})\right]_+ + (1 - \mu_i) \left[\boldsymbol{\eta}_{i-} \cdot \mathbf{qq}(t - t_{aff})\right]_+, \; i = a, b$$

where

$$\begin{aligned} \boldsymbol{\eta}_{i+} &= [-\eta_{i0+}, \eta_{i1}, \eta_{i2}, \eta_{i3}, \eta_{i4}]^T, \\ \boldsymbol{\eta}_{i-} &= -[\eta_{i0-}, \eta_{i1}, \eta_{i2}, \eta_{i3}, \eta_{i4}]^T, \\ \mathbf{qq} &= [1, \theta_s, \theta_e, \dot{\theta}_e, \dot{\theta}_s]^T. \end{aligned}$$

Evidently, when either bracketed term representing the activity of a particular group of selPFs in Eq. (3.5) is nonzero, the sum of sel_i $(i = a, b)$ is nonzero and therefore PC activity is suppressed. These terms consist of the (nonnegative, delayed) projections of the sensed limb location in state space $[\theta_s, \theta_e, \dot{\theta}_e, \dot{\theta}_s]^T$, onto nominal directions $\pm[\eta_{i1}, \eta_{i2}, \eta_{i3}, \eta_{i4}]^T$, that are then thresholded by η_{i0+} or η_{i0-}. As a result, selPFs cooperatively select, by jointly failing to suppress, PCs only when the limb state lies within certain regions of state space that are bounded by the planes defined by $\boldsymbol{\eta}_{i+}$ and $\boldsymbol{\eta}_{i-}$ (Jo and Massaquoi 2004). The parameter μ_i affects the strength of the two selPF groups' contributions and thus the relative importance of the two boundary planes. This PC modulation is hypothesized to implement switching or scheduling of cerebellar gains to enable cerebellar dynamics to vary according to body state (Jo and Massaquoi 2004) . This particular representation of selPF signal content used here appears to be grossly consistent with that of spinocerebellar tract neurons (Bosco and Poppele 2001). Similar, but not identical, formulations have been used previously in cerebellar modeling (e.g. Kettner et al. (1997)). The 23 parameters $\alpha_{v_h}^{cw}$, $\alpha_{v_h}^{cc}$, ϕ_r^{cw}, ϕ_r^{cc}, μ_i, η_{i0+}, η_{i0-}, η_{ij} $(i = a, b; j = 1, 2, 3, 4)$, α_{bg}, β^{cw+}, β^{cw-}, β^{cc+}, β^{cc-} are therefore free and available for fitting. It may be noted that 9 are specific for tracking direction, while 14 are related to arm state independent of direction.

3.2.5 Alternative models

The RIPID Cerebellar Simple Spike signal (RICSS) model was evaluated alongside several models that include arm kinematic variables more simply. We chose to examine a range of empirical models of the type that have been proposed previously (Coltz et al. 1999; Roitman et al. 2005) that include arm kinematic variables linearly or in a simple nonlinear manner. These models provide benchmarks with regard to model fitting performance and potentially indicate the type of information and its complexity of representation in the PC single spike data.

The first Arm Kinematics model AK1c (Eq.(3.5)) is based upon the initial linear model developed by Roitman et al. (2005) and represents arm kinematics in Cartesian coordinates. This model intends to capture a significant fraction of the signal complexity and may have particular functional relevance if the recorded Purkinje cells are involved primarily in monitoring hand or limb position in a simple way. The AK1c model for the activity of a PC response is

$$pc^{AK1c}(\phi_h) = b_0 + b_1 x(\phi_h) + b_2 y(\phi_h) + b_3 \frac{\dot{x}(\phi_h)}{v_h} + b_4 \frac{\dot{y}(\phi_h)}{v_h} + b_5 v_h, \tag{3.5}$$

where θ_h is the angular location of the monkey's hand on the circle, and $x(\theta_h)$ and $y(\theta_h)$ are and coordinates of the hand relative to the center of the workspace. $\dot{x}(\phi_h)$ and $\dot{y}(\phi_h)$ are, respectively, the x and y components of the hand's velocity, and v_h is the hand's intended speed. It was confirmed that for these very well trained monkeys, the target speed represented the intended hand speed, and that it also very closely approximated the average hand speed. The latter was confirmed in Roitman et al. (2004). For this reason, target speed was used for v_h and was constant for any individual movement trial. The b_i are free parameters. The normalization of velocity components is undertaken to dissociate movement direction from hand speed. Thus, AK1c is a linear sum of the target position, target movement direction, and the intended speed of the hand.

The AK2c model (Eq.(3.6)) is very similar in form to that of AK1c, but it includes

two more terms to account for hand acceleration. Assuming that the actual motion is quite similar to the intended motion, AK2c could have particular relevance if Purkinje cells processed a feedforward signal based on the intended hand movement to approximate an inverse dynamics model as proposed by several investigators (Gomi and Kawato 1992b; Kawato and Gomi 1992a; Schweighofer et al. 1998a). Although Eq. (3.6) includes a velocity normalization factor and a tonic bias term, for any individual movement trial, its structure is otherwise that of a linear inverse dynamics model. This is especially so for the joint coordinate version (see below). To be sure, feedforward arm control need not consist of the simple combination of variables represented here. This model therefore represents only one possible form of a feedforward control signal.

$$pc^{AK2c}(\phi_h) = b_0 + b_1 x(\phi_h) + b_2 y(\phi_h) + b_3 \frac{\dot{x}(\phi_h)}{v_h} + b_4 \frac{\dot{y}(\phi_h)}{v_h} + b_5 \ddot{x}(\phi_h) + b_6 \ddot{y}(\phi_h) + b_7 v_h. \quad (3.6)$$

Adding terms that represent jerk yields the AK3c model (Eq. (3.7)). Current models of cerebellar function do not contain jerk processing. However, it has been argued that jerk (Hogan 1985) or torque-change (related to jerk) (Uno et al. 1989) cost may be assessed in optimizing motor performance and that cerebellar signals use higher derivatives in Taylor expansions to reconstruct kinematic variables (Pellionisz and Llinas 1982). It is conceivable, therefore that cerebellar signals could contain this higher derivative information.

$$\begin{aligned} pc^{AK3c}(\phi_h) &= b_0 + b_1 x(\phi_h) + b_2 y(\phi_h) + b_3 \frac{\dot{x}(\phi_h)}{v_h} \\ &+ b_4 \frac{\dot{y}(\phi_h)}{v_h} + b_5 \ddot{x}(\phi_h) + b_6 \ddot{y}(\phi_h) + b_7 \dddot{x}(\phi_h) + b_8 \dddot{y}(\phi_h) + b_9 v_h. \end{aligned} \quad (3.7)$$

Recently Roitman et al. (2005) have refined their initial kinematic model to better address the speed dependent changes in PC signal modulation depth. The resulting UPVSc (unit position, velocity and speed) model (Eq.(3.8)) is nonlinear but retains the underlying direct dependence on arm kinematics in Cartesian coordinates.

$$pc^{UPVSc}(\phi_h) = b_0(1 + b_1 v_h) + (1 + b_6 v_h) \cdot \left(b_2 x(\phi_h) + b_3 y(\phi_h) + b_4 \frac{\dot{x}(\phi_h)}{v_h} + b_5 \frac{\dot{y}(\phi_h)}{v_h} \right). \quad (3.8)$$

It was noted that the activity of some PCs is distinctly non-sinusoidal (Roitman et al. 2005). To possibly account for these more efficiently, joint-coordinate based models were tested. Specifically, for the AKc and UPVSc (originally introduced as UPVS in Roitman et al. (2005)) models which are all in Cartesian coodiantes denoted by the subscript, c, the following substitutions were made: $x(\phi_h) \Rightarrow \theta_s(\phi_h)$, $y(\phi_h) \Rightarrow \theta_e(\phi_h)$ and $v_h \Rightarrow v_j(\phi_h)$ where θ_s and θ_e are shoulder and elbow angles as defined in Fig. 1 and v_j is (non-constant) intended joint speed, analogue of intended hand speed. In the following, the joint coordinate counterpart models are designated by the subscript, j.

3.2.6 Simulations and data analysis

The RIPID control model was first tuned to reproduce arm movement kinematics reflecting the tasks of the experiments. This was done before evaluation of fit to PC data. After the model produced realistic motions, $\mathbf{e}_{f_2}(t)$ was computed and used in Eq. (3.4) above.

Because it is not necessary that the neural control of the intercept and tracking phases are managed by the same neuronal populations, for simplicity we chose to restrict analysis of all models to the steady state tracking phase. Accordingly, to minimize any residual effects from the intercept phase, the first 150 degrees of both PC and simulation tracking phase data were discarded. Then, PC simple spike counts were collected within 36 bins, each representing 10 degrees of hand motion relative to the center of the circle. Counts from the 10 trials having 4 different launch angles but the same rotational direction and the same speed were pooled. Then, these PC firing data were stacked to create a single 36 $\times$ 2 $\times$ (4 or 5) element total data vector that was to be fit by the various models. To obtain the corresponding input (regressor) signal vectors, three methods were used. For the AKc and UPVSc models, cursor motion data was differentiated sufficiently and then averaged within each 10 degree interval of hand motion This yielded 36 element signal vectors: $x(\phi_h)$, $y(\phi_h)$, $\dot{x}(\phi_h)$, $\dot{y}(\phi_h)$, $\ddot{x}(\phi_h)$, $\ddot{y}(\phi_h)$, $\dddot{x}(\phi_h)$, $\dddot{y}(\phi_h)$, for each tracking direction and movement speed.For fitting the AKj and UPVScj models, 36 element joint angular motion signal vectors were estimated from the cursor motion (and motion derivative) data trigonometrically using

primate limb dimensions and the assumption that wrist motion was not marked. The latter was reasonable based on the typical posture of the primates. For fitting the RICSS model, kinematic signals $\theta_s(\phi_h)$, $\theta_e(\phi_h)$, $\dot{\theta}_s(\phi_h)$, $\dot{\theta}_e(\phi_h)$, and $\mathbf{e}_{cb}(\phi_h)$ were derived from RIPID model-simulated tracking motions in four launch directions, two rotational directions and all (4 or 5, depending on the trial) intended hand speeds. The simulation-derived data were averaged within each 10 degree interval of hand motion and across the four different launch directions to again yield a 36 element signal vector for each tracking direction and movement speed. For each model, the 36 element input signal vectors were stacked to yield 36 $\times$ 2 $\times$ (4 or 5) input signal vectors commensurate with the total firing data vector. A single set of parameters was then identified for each model to address both movement directions and all movement speeds. For the AK and UPVSc models the parameter set was found using least-squares linear regression, the RICSS model was fit using the method as described below.

The coefficients for RICSS were found using a nonlinear optimization routine in MATLAB starting with randomly chosen initial conditions within a certain range. The following was performed to find the range of initial conditions. First, approximately 20 to 30 sets of initial conditions were found by inspecting fits visually while manually changing parameters for firing frequency of several cells. Second, for each initial condition a nonlinear optimization was performed to minimize the sum of squares of the difference between the actual firing and the fit. If some conditions did not perform well in terms of R^2, those conditions were discarded. Third, a superset of the initial conditions for all cells was obtained. Fourth, because exhaustive exploration of a fine grid of parameter values was computationally prohibitive, for each cell, 5000 or 10000 initial conditions were randomly chosen uniformly for each cell from the superset defined previously. A second series of nonlinear optimizations was then run starting from each of these initial conditions to find the best parameters, except for the background firing rates, α_{bg}, of each cell which were always chosen from the range of $(1 \pm 0.2)\times$ mean firing rates across all the speeds and both rotational directions. For some cells, it was tested with 100000 initial conditions to see if there was any significant effect of a small number of initial conditions. However, there was no significant effect in terms of R^2

achieved through the optimization routine for the cells tested.

In order to assess the efficiency of the models in terms of their abilities to account for data variance relative to their number of free parameters, the following formula is used for adj-R^2 :

$$\text{adj-}R^2 = 1 - (1 - R^2)\frac{n-1}{n-k-1},$$

where n is the number of data points used in the fit and k is the number of model parameters.

Fourier analysis was used to assess the sinusoidality of the firing activity in terms of average fractional power of the fundamental (AFPF). At each speed and rotational direction, the DC component of the firing signal was removed. Then the power due to the first frequency mode of the residual signal was computed and divided by the total power over all frequencies. This ratio was averaged across all hand speeds for each rotation direction.

3.3 Results

3.3.1 Simulation results

Arm control simulations using RIPID model are shown in Fig. 3-6 to demonstrate the quality of fit to hand kinematics. The averaged hand path of the primate is slightly non-circular, but is otherwise closely approximated by the RIPID model when it is driven as here with a circular intended motion input command (corresponding to the joint coordinate command, $\boldsymbol{\theta}_{target}$) with constant tracking phase speed. Primate cursor tracking motion typically shows minor speed fluctuations (Roitman et al. 2004) that are not captured by this RIPID model simulation. In Fig. 3-7, the joint angles and especially their derivatives exhibit considerable nonsinusoidal individuality.

3.3.2 AKc models

The performance of the AK1c model applied to four or five target speeds and both rotational directions was reported previously (Roitman et al. 2005). The quality of fit using

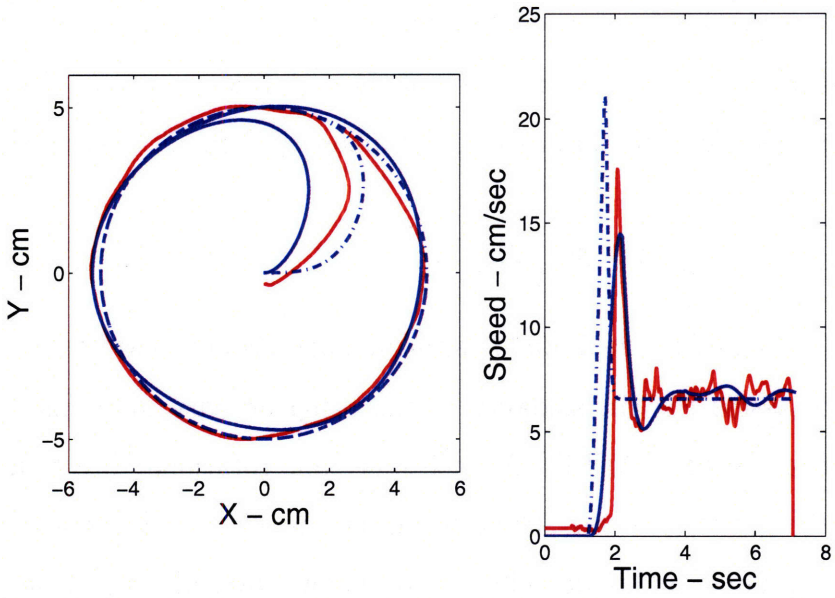

Figure 3-6: Recorded and RIPID model-simulated hand motion. Left figure: Hand location. Right figure: Hand speed. In both figures, the solid red lines show averaged data over 10 trials with the target moving at 6.5 cm/s in a CW direction at the starting angle of 180 degrees, the dashed blue the Cartesian intended hand position and speed corresponding to $\boldsymbol{\theta}_{target}$ and the solid blue lines the tracking simulation.

the higher order models though similar overall is slightly improved. Specifically, the mean adj-$R^2$are 0.34 ± 0.21(mean$\pm$SD),0.35 ± 0.21 and 0.35 ± 0.21 for AK1c, AK2c, and AK3c respectively. The average improvement from AK1c to AK2c or AK3c can not considered to be null (Wilcoxon paired signed rank test, $\alpha = 0.05$) because 22% (15/69) and 30% (21/69) of the cells appreciated the addition of higher derivative terms (F-test, $\alpha < 0.05$) from AK1c to AK2c or AK3c respectively. However, the performance of AK2c and AK3c are statistically not distinguishable (Wilcoxon paired signed rank test, $\alpha = 0.05$) because none of the cells appreciated the addition of acceleration terms to AK2c (F-test, $\alpha < 0.05$). The overall distributions for all the three AKc models and the box plots for the differences of adj-R^2, AK2c-AK1c and AK3c-AK2c are shown in Fig. 3-8.

Approximately 26 % (18/69), 28% (19/69), and 28% (19/69) of the cells are fit with adj-$R^2 > 0.5$ using AK1c, AK2c, and AK3c respectively, while 42% (29/69), 41% (28/69), and 41% (28/69) of the cells are fit with adj-$R^2 < 0.3$ using AK1c, AK2c, and AK3c respectively.

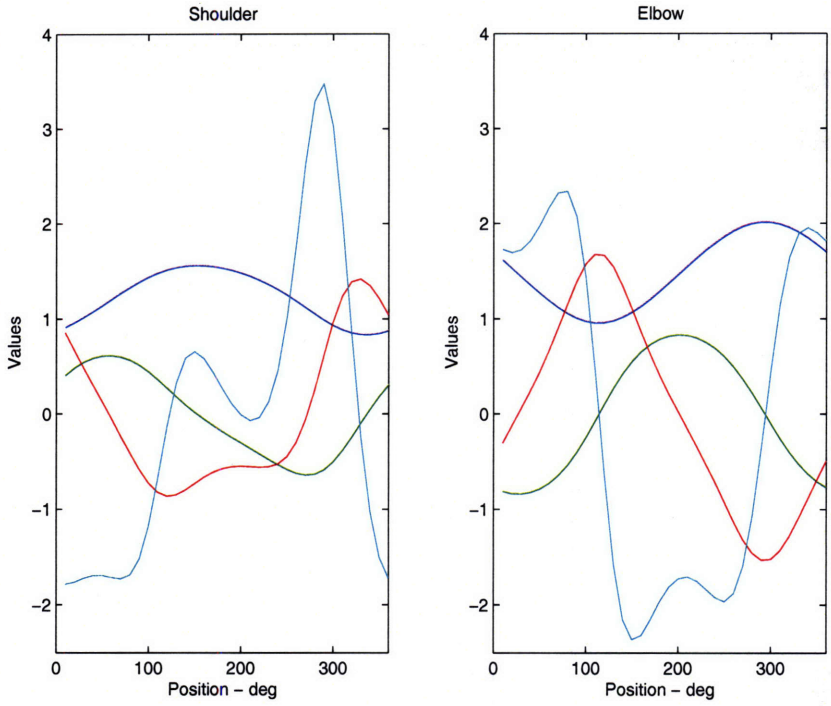

Figure 3-7: Joint angles and their derivatives used in the regression. Left figure: Shoulder angle, θ_s and its derivatives. Right figure: Elbow angle, θ_e and its derivatives. Blue line denotes joint angle, green first derivative, red second derivative, and cyan third derivative respectively in each plot. The signals shown are for the target speed 8.3 cm/s in the CC direction.

Cells in the former group, such as Cell #49 shown in Fig. 3-9, tend to have substantially sinusoidal activity patterns and to be reasonably well fit by all the AKc models. The AFPF of this cell is 77% for CC and 52% for CW direction on average over intended speeds.

3.3.3 UPVSc and RICSS models

For the UPVSc, the mean adj-R^2 is 0.36 ± 0.22. The RICSS achieved 0.44 ± 0.23 for its mean adj-R^2 . UPVSc and RICSS are statistically progressively better in terms of adj-R^2 than all the AKc models (Wilcoxon paired signed rank test, $\alpha = 0.05$). The overall adj-R^2 distributions of UPVSc and RICSS, along with that of AK3c and the boxplot for the differences of adj-R^2 , RICSS-AK3c and UPVSc-AK3c are shown in Fig. 3-10.

Approximately 29 % (20/69) and 42% (29/69) of the cells are fit with adj-$R^2 > 0.5$ using

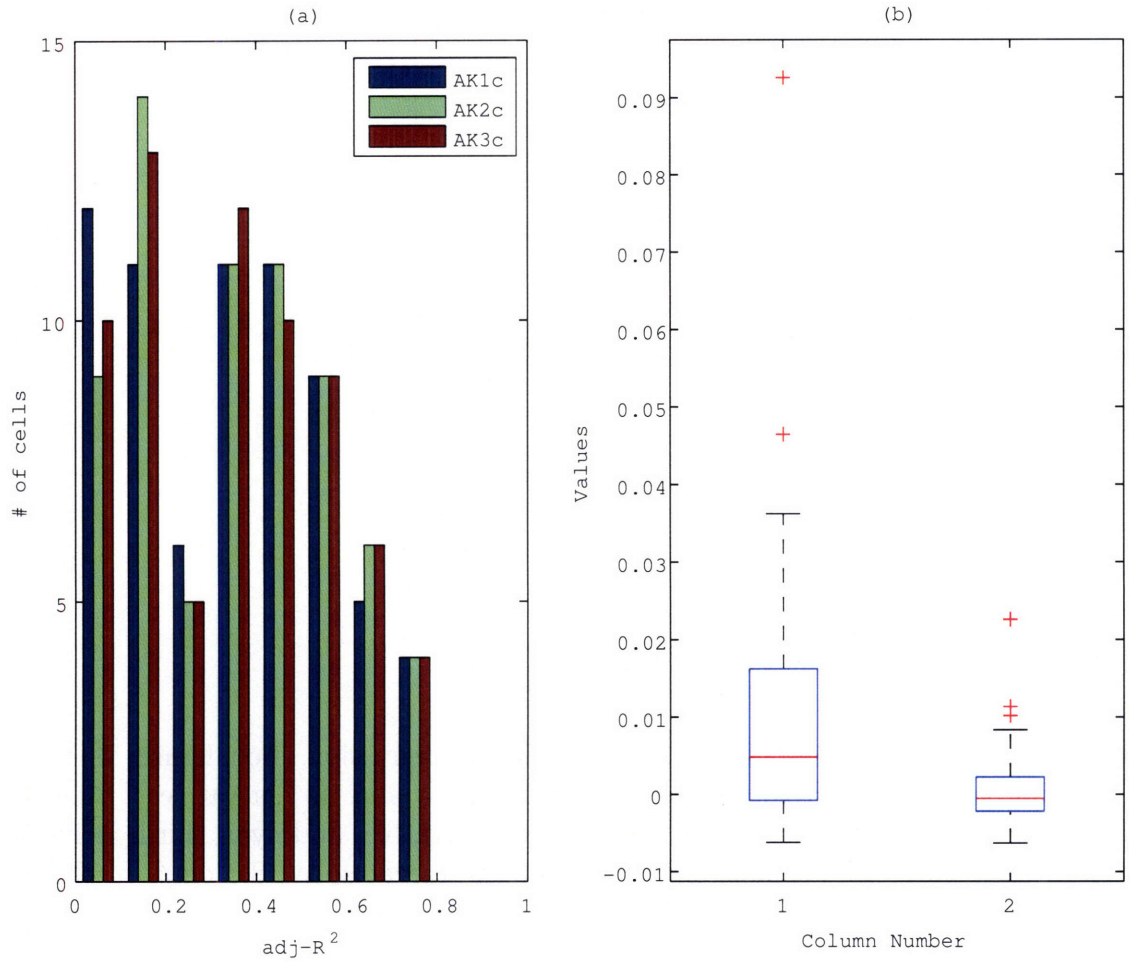

Figure 3-8: (a) Histogram of adj-$R^2$of AK1c, AK2c, and AK3c. (b) Box plots for the adj-R^2 differences, AK2c-AK1c (left) and AK3c-AK2c (right). Each box indicates the lower quartile, median, and upper quartile values. The whiskers indicate the extent of the rest of the data, assuming that there is no outlier. The asterisks denote outliers which have values more than 1.5 times the interquartile range away from the top or bottom of the box.

UPVSc and RICSS respectively, while 38 % (26/69) and 33% (23/69) of the cells are fit with adj-R^2 <0.3 using UPVSc and RICSS respectively. In a cell-by-cell adj-R^2 analysis, AK3c fits better than RICSS for only 6 % (4/69) of the cells while UPVSc better than RICSS for only 13 % (9/69) of the cells. In terms of median, UPVSc outperforms AK3c statistically as shown above, however its margin is much smaller compared to that of RICSS.

Among all the models tested, RICSS yields the highest mean (and median) adj-R^2 and only RICSS has adj-R^2 values that can be considered from a normal distribution (Lillifors

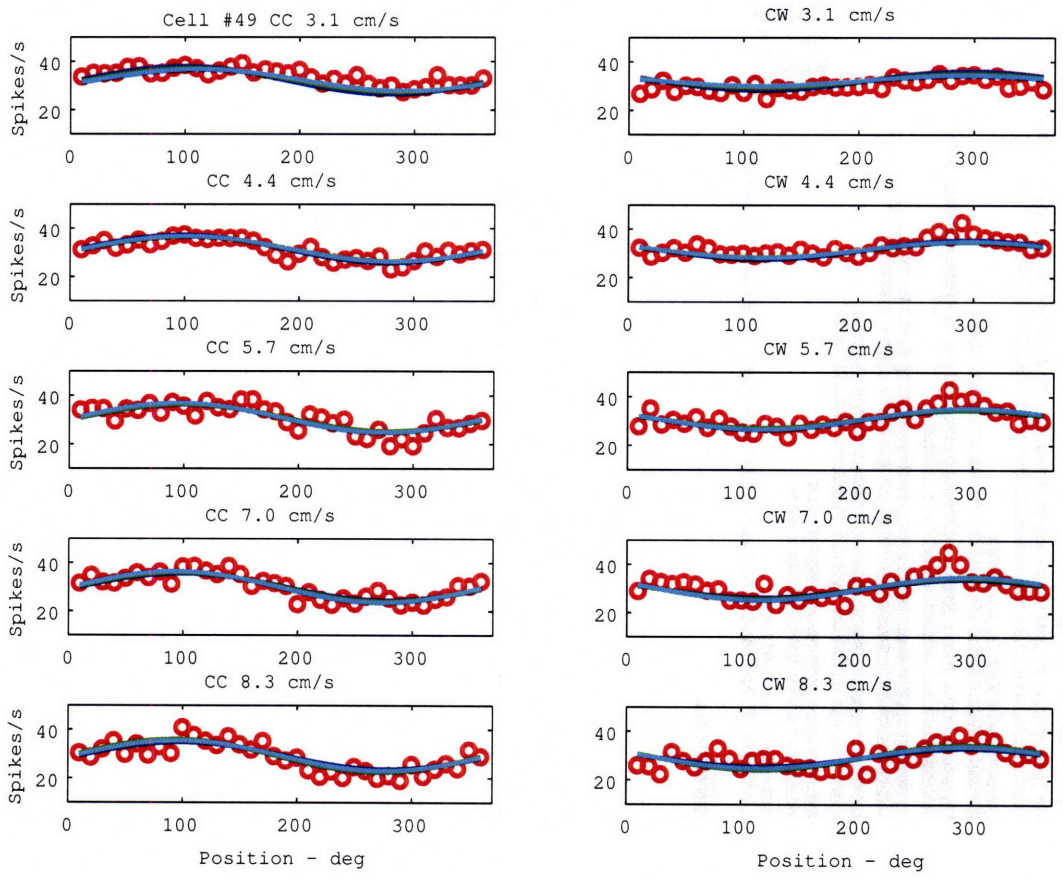

Figure 3-9: Comparison of AKc models for Cell #49, the small circles represent the average firing rates over a ten degree interval. The blue line is for AK1c, the green line for AK2c, and the cyan for AK3c. adj-R^2 of each model is 0.62, 0.63, and 0.64 respectively.

test, $\alpha = 0.05$).

3.3.4 Unit activity characteristics

Based on the Fourier analysis, 35% (24/69) of the cells have less than 20% of AFPF in CC direction and 38% (26/69) have such low fundamental frequency power in CW direction. In 15 cells, AFPF is less than 20%. The firing activity of 14 cells among those 15 cells is fit poorly (adj-$R^2 < 0.2$) by all the kinematic models. On the other hand, 16% (11/69) of the cells have more than 50% of AFPF, i.e., are quite sinusoidal, in both rotational directions. The adj-R^2 for these 11 cells are above 0.56 with all the models. Therefore, there is a clear

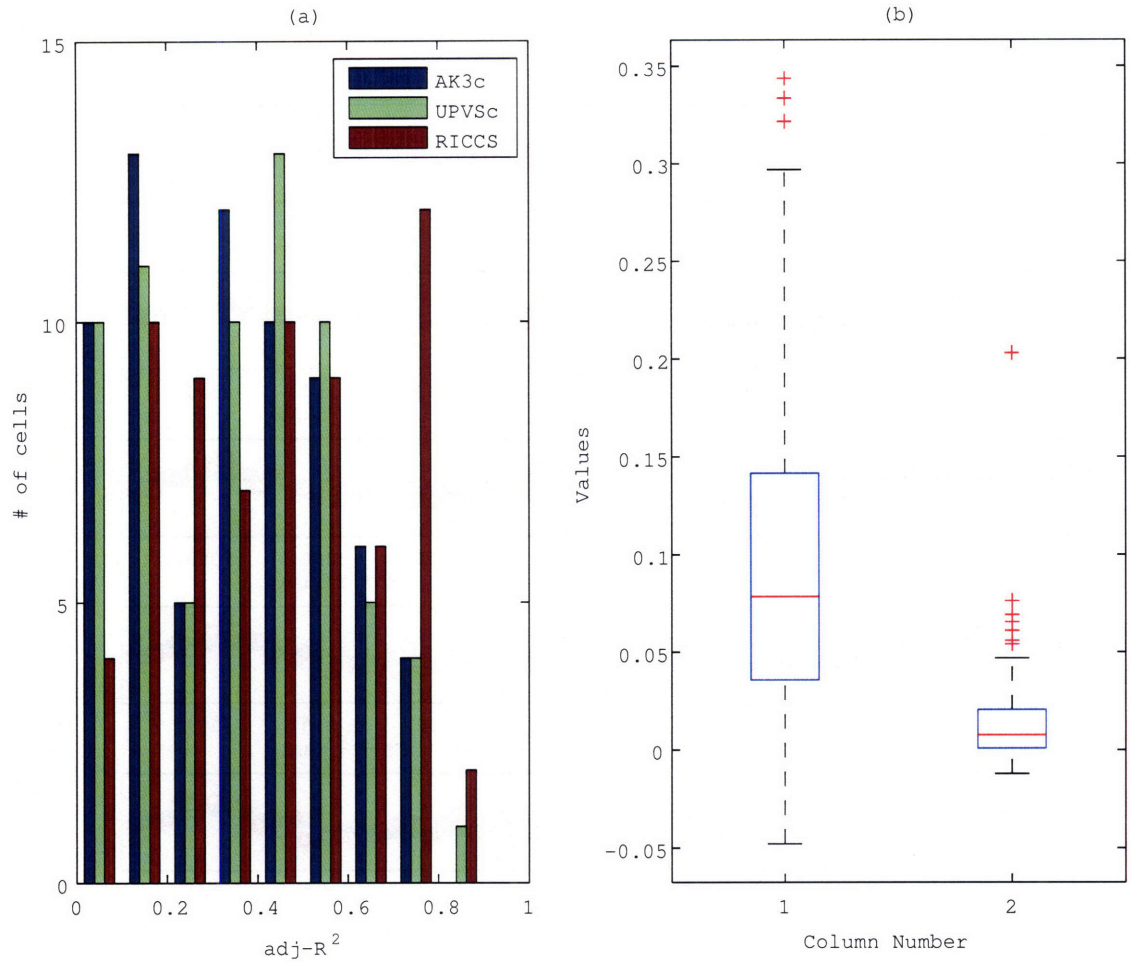

Figure 3-10: (a) Histogram of adj- R^2 of AK3c, UPVSc, and RICSS. (b) Box plots for the adj- R^2 differences, RICSS-AK3c (left) and UPVSc-AK3c (right).

correlation between the frequency content of the signals and the quality achievable by the kinematic models on a cell-by-cell basis.

In Fig.3-11 an example of fits with AK3c, UPVSc, and RICSS models are shown for Cell #50 which is one of the few that were poorly fit by all the models tested. Based on the Fourier analysis, the signal appears to show little power due to the fundamental frequency, 18% for CC and 10% for CW directions respectively.

Some other qualitative features of the PC simple spike activity aside from sinusoidality appeared to be related to model fit. The activity of Cell #22 (Fig.3-12) shows asymmetric AFPF (65% for CC, 5% for CW) across rotation direction. It also shows consistent, but

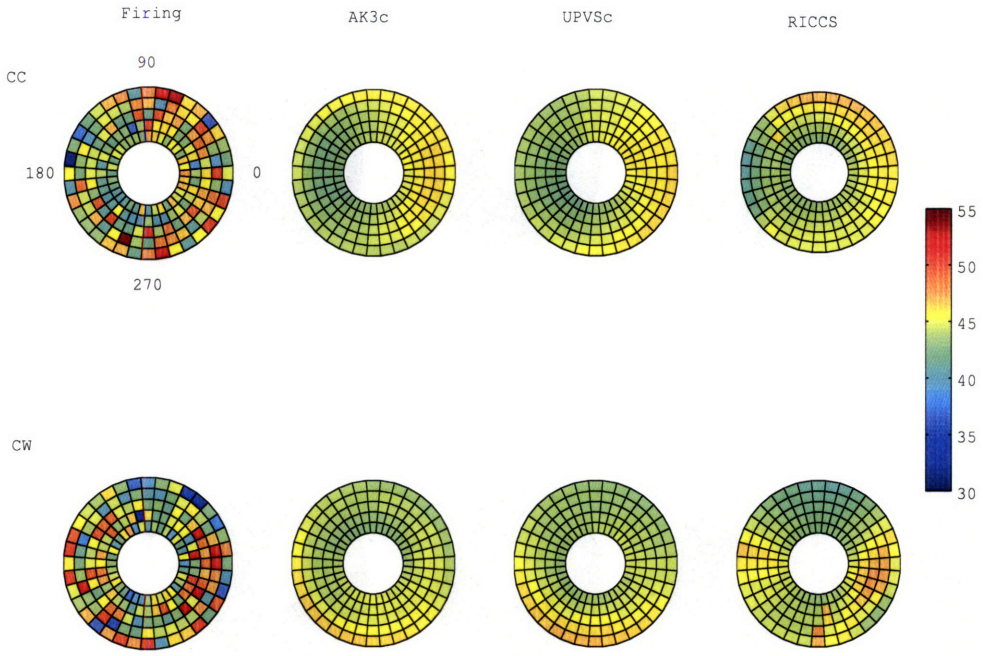

Figure 3-11: Comparison of unit firing with AK3c, UPVSc, and RICSS fits for Cell #50. Activity intensity is indicated by color, with red highest and indigo lowest. The radial coordinate in each annular figure denotes the target (intended hand) speed ranging from 3.1 to 8.3 cm/s from inside out and the angular coordinate relative to the origin denotes the hand position ϕ_h of the monkey during tracking. The upper row contains the firing rates for CC rotational direction and the lower row CW rotational direction. adj-R^2 are 0.05, 0.05, and 0.09 for AK3c, UPVSc, and RICSS respectively.

different, locations of "hot" and "cold" regions across speeds for each rotation direction. AK3c and UPVSc have similar adj-R^2, 0.43 and 0.43 respectively. On the other hand, RICSS has an adj-R^2 of 0.75 due to its capability to account for depth of firing rates as well as angular width of variability of firing intensity. AK3c and UPVSc account fairly well for a "warm" range around 10 to 30 degrees in the CC rotational direction. However, it is the RICSS model that captures firing intensity patterns on both CC and CW simultaneously.

Near 300 degrees hand location during CW tracking, and near 45 and 270 degrees during CC hand motion, Cell #22 shows first an increase then a decrease in firing intensity with increasing hand speed (Fig.3-12). Such sometimes subtle non-monotonic dependence of simple spiking on hand speed was noted in approximately 10% (7/69) units. Only the RICSS model could reproduce this feature.

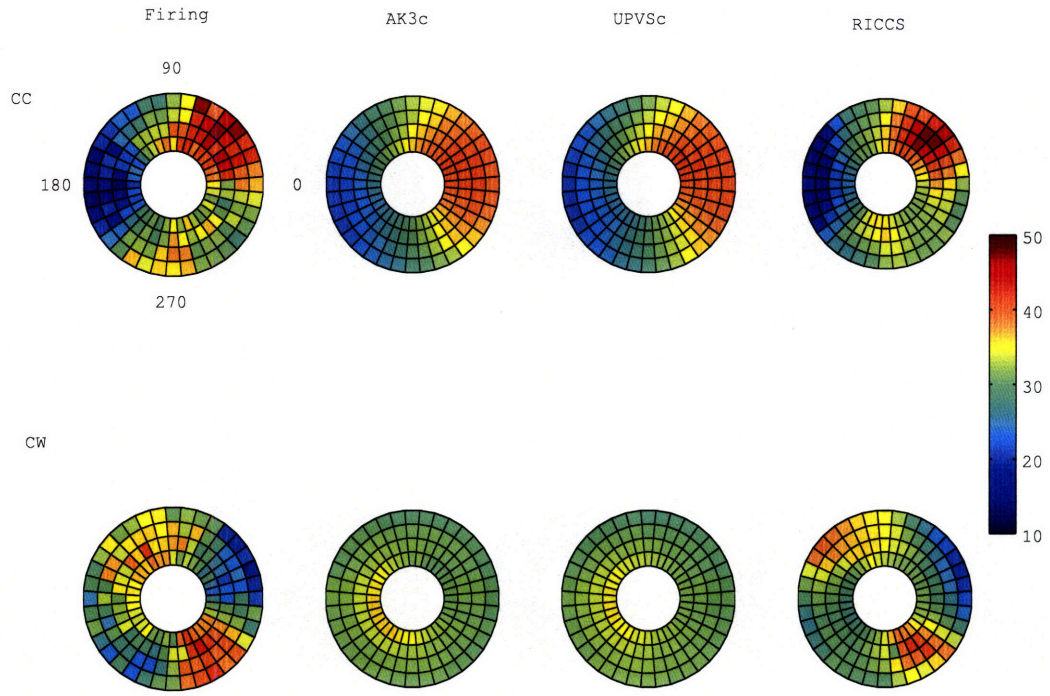

Figure 3-12: The furthest left column shows the averaged firing rate of simple spikes from Cell #22. This cell shows asymmetric firing patterns across the rotational directions, the maximum firing rate is attained at medium speed (around 5 o'clock direction) for CW, and multimodal distribution. AK3c and UPVSc models can capture only naively extremities for CC, while RICSS model captures all the three characteristics mentioned above for both CC and CW. adj-R^2 are 0.43, 0.43, and 0.75 for AK3c, UPVSc, and RICSS respectively.

3.3.5 Joint coordinate models

As a whole, all models expressed in joint coordinates underperformed their Cartesian counterparts in terms of adj-R^2. However, some cells were fit better with the former, especially 41 % (28/69) and 52% (36/69) of the cells were fit better with AK3j and UPVScj respectively. The activity of these cells (e.g., Cell #65, Fig. 3-13) was characteristically nonsinusoidal and/or contained higher frequency components more similar to the joint kinematic signals presented in Fig. 3-7. While, AK3c and UPVSc can capture the underlying sinusoidal waveform, their joint counterparts capture more local details, especially in the clockwise direction where there are local minima around 100 and 300 degrees. The adj-R^2 of fits are 0.37 and 0.38 for AK3c and UPVSc while 0.47 and 0.62 for AK3j and UPVScj respectively.

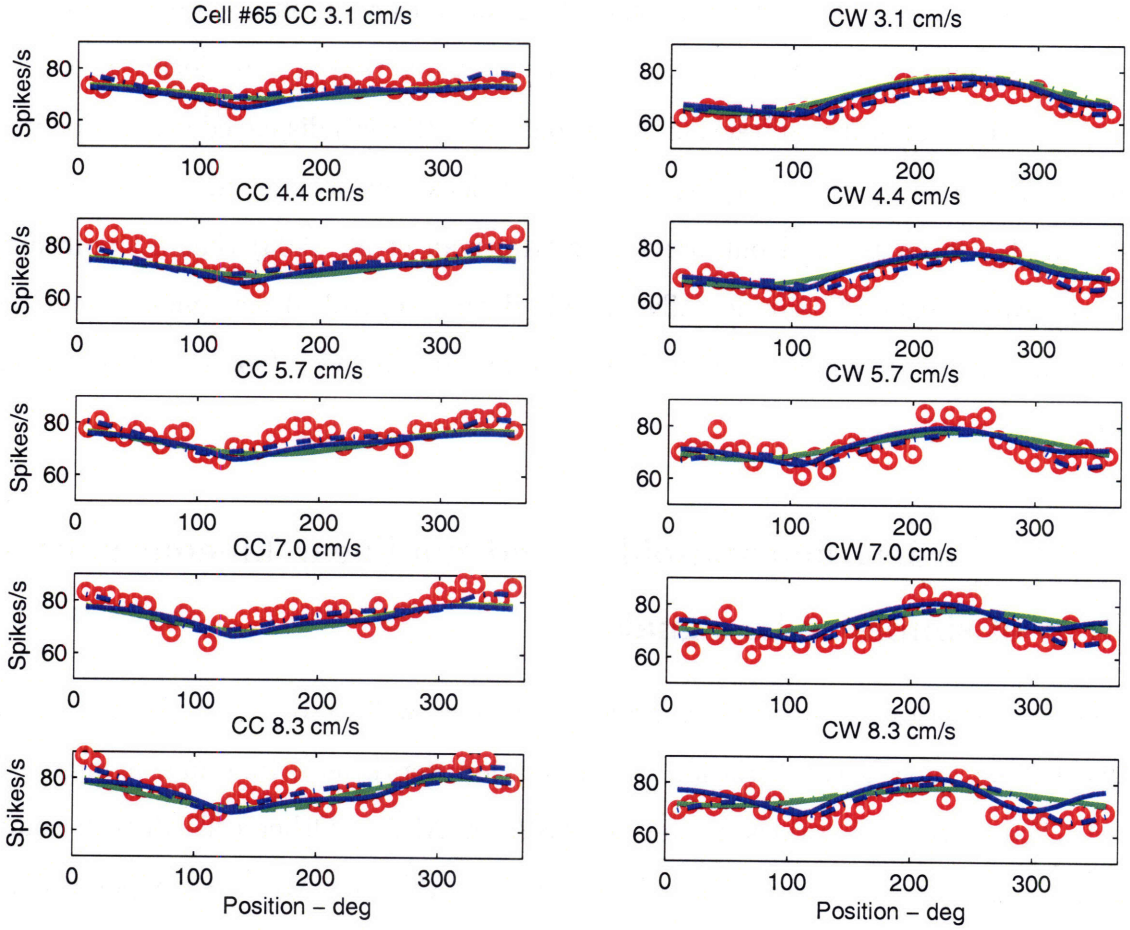

Figure 3-13: Comparison of Cartesian coordinate models and joint coordinate models for Cell #65. The small circles represent the average firing rates over a ten degree interval. The solid lines are the fits for AK3 and the dashdot lines for UPVSc. Green lines represent models in Cartesian coordinates and blue in joint coordinates.

3.4 Discussion

3.4.1 Suitability of regression models examined.

Approximately 33% (23/69) of PC simple-spike activity profiles were poorly fit (adj-$R^2 < 0.3$) by all the models. These units, such as Cell #50, typically exhibited firing activity that did not have a simple speed dependency at a given hand location and/or did not have smooth intensity variation with hand position at a given hand speed. In particular, the activity of those cells, in general, had fairly low power content due to the first frequency mode.

Meanwhile, all the models considered have smooth, if not linear, amplitude dependence on hand speed v_h and have locally smooth firing activity as a function of hand location ϕ_h.

On the other hand, a nontrivial fraction of neurons, 42% (29/69) displayed simple spiking activity that was reasonably well fit $adj - R^2 > 0.5$ by at least one of the models. The results reemphasize, as has been pointed out previously (Roitman et al. 2005) that a significant amount of the variance in PC simple spike signals during controlled arm motion can be accounted for by kinematic signals that include position and velocity (speed and direction information).

3.4.2 Higher order, nonsinusoidal, and nonlinear kinematic content of simple spike signals

The cells whose activities are strongly sinusoidal and were well fit by all of the Cartesian AK models did not show great variation in modulation depth as a function of intended hand speed. For these, AK1c does as well as AK2c or AK3c. Other cells display some amplitude increase with higher hand speed. For these, AK2c or AK3c could potentially improve fit significantly because they include terms that increase in amplitude as a function of, respectively, the square or cube of the rotational frequency, and hence of v_h. However, such faster-than-linear speed dependencies are empirically too strong. Therefore, the additional terms of AK2c and AK3c cannot be weighted strongly and these models in practice do not provide much better performance.

In contrast to Cartesian kinematics models, higher derivative components in joint coordinate models contribute significant change in waveform shape in addition to speed dependence of amplitude. Thus, for cells such as Cell #65 that exhibit less sinusoidal waveforms, higher order joint kinematic models typically performed better than the Cartesian counterparts. However, the degree of sinusoidality observed varied considerably and therefore the kinematic models did not consistently support one coordinate frame over the other.

The distribution of adj-R^2 values indicates that AK3c, UPVSc and RICSS models improve progressively with differences that are statistically significant. The particularly good

performance of the UPVSc and RICSS models with respect to AK3c appears to derive from their inherent nonlinearity, especially given that the effective numbers of the regression coefficients for AK3c and UPVSc are the same. Specifically, Roitman et al. (2005) have pointed out that signal modulation depth changes in a manner that is reasonably described by a model that includes a product relationship between speed and a linear combination of hand location and direction of hand velocity. Although the UPVSc is cast in Cartesian coordinates and the RICSS is expressed in joint coordinates, the underlying similarity between the UPVSc and RICSS models can be demonstrated readily. To simplify the analysis, consider movement in only one rotational direction so that the direction superscripts can be ignored. Assume also that one selector PF in Eq. (3.3) is active (e.g., let $sel_b = 0$). In addition, assume that

$$\begin{aligned} \eta_{0+} &\leq \eta_1\theta_s + \eta_2\theta_e + \eta_3\dot{\theta}_s + \eta_4\dot{\theta}_e, \\ -\eta_{0-} &\leq \eta_1\theta_s + \eta_2\theta_e + \eta_3\dot{\theta}_s + \eta_4\dot{\theta}_e, \\ 1 + \mu\eta_{0+} &\geq \eta_1\theta_s + \eta_2\theta_e + \eta_3\dot{\theta}_s + \eta_4\dot{\theta}_e, \end{aligned}$$

and

$$\alpha_{v_h} v_h^{0.5} + |\mathbf{e}_{cb}| \cos(\phi_e - \phi_r) \geq 0,$$

throughout motion. This corresponds to active contribution from all model components (except one selector PF). In this case,

$$\begin{aligned} pc^{RC} &= \alpha_{bg} + (1 + \mu\eta_{0+} - \mu(\eta_1\theta_s + \eta_2\theta_e + \eta_3\dot{\theta}_s + \eta_4\dot{\theta}_e)) \\ &\quad \cdot\beta^{+}(\alpha_{v_h} v_h^{0.5} + |\mathbf{e}_{cb}| \cos(\phi_e - \phi_r)), \end{aligned}$$

and then expanding, we obtain

$$\begin{aligned} pc^{RC} &= \alpha_{bg} + (1+\mu\eta_{0+})\beta^{+}\alpha_{v_h} v_h^{0.5} \\ &\quad -\mu\beta^{+}\alpha_{v_h} v_h^{0.5}(\eta_1\theta_s + \eta_2\theta_e + \eta_3\dot{\theta}_s + \eta_4\dot{\theta}_e) \\ &\quad +(1+\mu\eta_{0+} - \mu(\eta_1\theta_s + \eta_2\theta_e + \eta_3\dot{\theta}_s + \eta_4\dot{\theta}_e)) \\ &\quad \cdot\beta^{+}|\dot{e}_{cb}|\cos(\phi_e - \phi_r). \end{aligned} \tag{3.9}$$

It can be seen that Eqs. (??) and (3.9) contain two terms that are structurally similar: A baseline term (the sum of the first two terms in Eq. (3.9)) consisting of the sum of one constant and another modulated by (a function of) the intended hand speed v_h, and a kinematics cross term (the third term of Eq. (3.9)) consisting of an interaction between v_h and joint angles and velocities. These features common to the UPVSc and RICSS models appear to better capture the variation of simple spike intensity with intended movement speed than do the higher order AKc models.

Several other nonlinearities appear to contribute to its the particularly greater accuracy of the RICSS model. First, v_h occurs with a subunity exponent that appears to represent the speed dependence of waveform modulation especially well. Second, it includes a threshold effect caused by the assumed constraint that firing rate never becomes negative. This affords more marked transitions in firing intensity with changes in limb configuration and speed yielding narrower local "hot" and "cold" regions as in Fig. 3-12.

A third feature is the variable product of $|\mathbf{e}_{cb}|\cos(\phi_e - \phi_r)$ and a linear combination of joint kinematics (the fourth term in Eq. (3.9)). When the selector PF mechanism is not active, i.e., $[1 - sel_a - sel_b]$ in Eq. (3.3) is unity, then the PC SS activity is predicted to be simpler and more sinusoidal. This would be particularly true if $|\mathbf{e}_{cb}|$ were in Cartesian coordinates (see below). However, when sel_a and/or sel_b is nonzero, as in the analysis above, then interaction between joint coordinate signals affords much less sinusoidal signals. This appears to account for the qualitative variation in degree of sinusoidality in different PCs within a single model.

A fourth nonlinear effect is more subtle, but still noteworthy. Several units (7/69) display modulation depth that is not monotonic with tracking speed. Instead, they appear to show a 'preferred' speed at which they best respond and become less active otherwise. This type of firing behavior has been noted previously (Coltz et al. 1999). To a certain degree, the RICSS can capture such non-monotonic speed dependence as in Fig. 3-12. This effect appears to be partially attributable to speed dependence of the phase angle of the filtered error-like vector, $\phi_e = \phi_e(v_h, \phi_h)$ in Eq. (3.3). Thus, while the magnitude $|\mathbf{e}_{cb}|$ increases monotonically as a function of at any given hand location, the values of $\cos\phi_e$(and hence of $\cos(\phi_r^{dir})$ and $\cos(\phi_{r'}^{dir})$) at certain positions decrease with v_h (e.g., at ϕ_h between 100 and 150 degrees) as shown in Fig. 3-14. For this reason, if the latter effect dominates at some hand positions, unit activity may be predicted to decline locally as speed increases even though the inherent sensitivity of the transmitting neuron is not reduced at higher speeds. Thus, at least some apparent "speed tuning" might be artifactual. Still, we note that the current experiment does not involve fast arm movements. Dynamic demands on movement controllers change dramatically with large accelerations and speeds. Therefore, it would not be surprising if the cerebrocerebellar system was in fact scheduled according to speed or velocity. In any case, the RICSS supports, extends and refines the principle of important nonlinearity put forth in the UPVSc model.

3.4.3 Rationale for RICSS model structural details

The basic structure of the RICSS arose from neurophysiological and neuroanatomical considerations. However, two principal features were developed more empirically. The first is the dependence of cortical background firing rate on the square-root of movement speed. The precise origin of cortical background activity is unknown. However, it is noteworthy that some models of muscle spindle function (Hasan 1983; Houk et al. 1981) have used a similar subunity exponent for the velocity dependence of stretch responses that include a static bias offset. The latter is generally considered related to efferent static gamma action that could well vary in intensity with intended movement speed. The signal could in turn

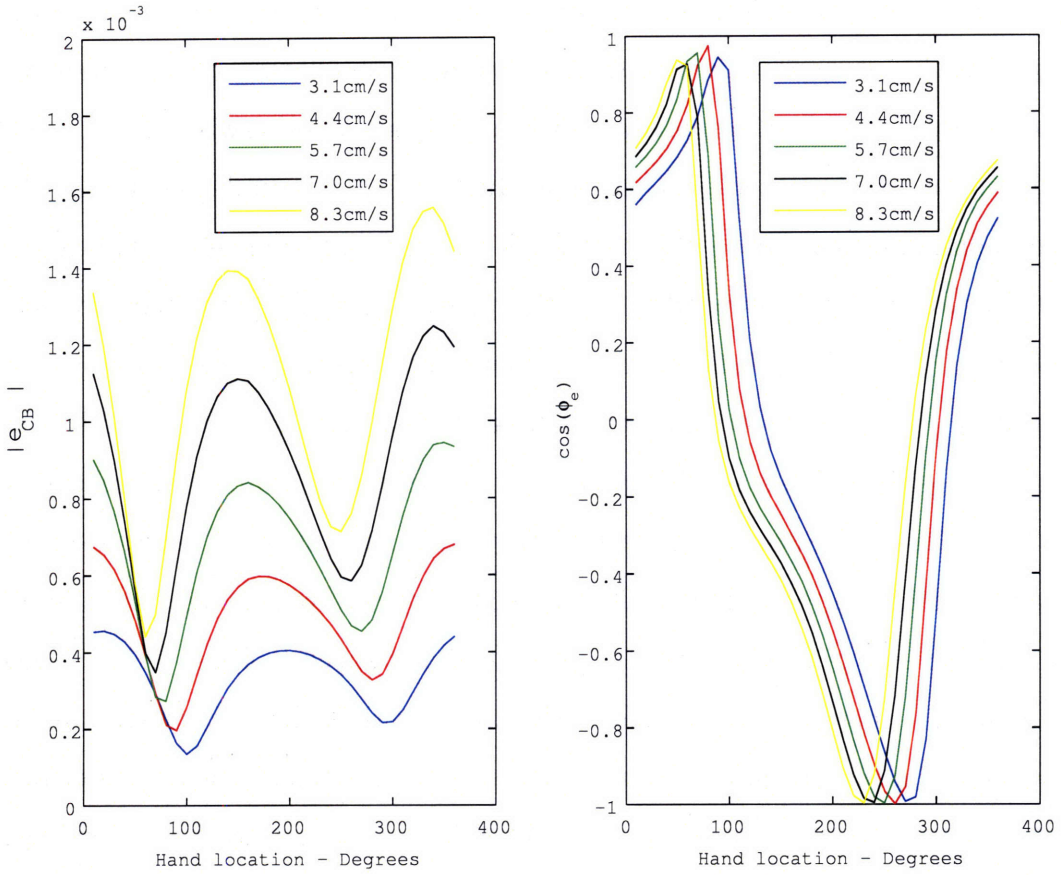

Figure 3-14: $|\mathbf{e}_{cb}|$ and $\cos\phi_e$ as functions of intended hand speed varying from 3.1 cm/s to 8.3 cm/s and hand location angle ϕ_h.

bias the activity of cortical targets of spindle afferents.

The second empirically useful proposition is the simple nonlinear action of the hypothetical selector PF's. Ongoing studies of the cerebellar cortex reveal increasing complexities in its circuitry (e.g., Simpson et al. (2005)). It is conceivable that therefore Eq. (3.3) represents an undue oversimplification. Especially given the large number of selPFs and interneurons that potentially influence a given PC, it is arguable that the model should have greater complexity. Although the incorporation of these elements could improve the fit, it would not alter the overall implications of the model. The fact that the current model is effective in describing the SS activity of most PCs, may indicate that it includes a good functional description of selPF activity notwithstanding its relative simplicity.

The Lillifors normality test indicates that the simpler regression models are not able to

treat all of the PC firing activity as being derived from a single population of similar neurons. Although this may indicate physiological inhomogeneity of the PC population, the effect may instead primarily reflect structural limitations in these simpler models. The normality of the adj-R^2 distribution of RICSS model fits is consistent with the latter possibility. A clear example of the value of the RICSS model's increased complexity is its unique ability among the models of RICSS to account for firing activity that is highly asymmetric with respect to rotational tracking direction.

3.4.4 Coordinate system in cerebellum

The often better performance of the AKc models than the AKj models suggests that Cartesian or possibly other workspace coordinate information may be present in PC signals. On the other hand, the generally better performance of UPVSc and RICSS indicates that coordinate frame is not the overriding factor in model performance. Still, these observations suggest that the inclusion of more Cartesian information in the RICSS might provide even more realistic modeling. The RICSS is based on a RIPID model that largely for convenience, as with most other control models (e.g., Bhushan and Shadmehr (1999); Schweighofer et al. (1998b)), are formulated entirely in terms of joint coordinate signals.

Many areas in cerebral cortex appear to conform different or mixed coordinate systems depending on their functions. A number of studies suggest that motor cortex contain much information in joint coordinates (Ajemian et al. 2001; Scott and Kalaska 1997), Cartesian coordinates (Georgopoulos et al. 1982b), or muscle groups (Asanuma and Rosen 1972).

and motor cerebellum contain much information in joint coordinates (Ajemian et al. 2001; Poppele et al. 2002; Scott and Kalaska 1997) . However, other physiological studies are consistent with the possibility that especially parietal signals and perhaps some motor cortical signals are in Cartesian (Kalaska et al. 1997) or body-centered (Graziano 2001), shoulder-centered (Ferraina and Bianchi 1994; Soechting and Flanders 1989) workspace coordinates, or a mixture of those (Reina et al. 2001). Moreover, simulation studies have demonstrated that workspace to joint coordinate conversion can occur readily within a servo control loop

(Ayaso et al. 2002; Micci Barreca and Guenther 2001). Thus, it is plausible that a modified RICSS model that included an interaction between Cartesian or other coordinate signals from the cerebral cortex, and joint coordinate state feedback information on selector parallel fibers, might provide further improvement in modeling.

3.4.5 Model implications

The central implication of the UPVSc (Roitman et al. 2005) and RICSS models is that the PC simple spike activity patterns in a behaving monkey can be described by relatively simple nonlinear models. The RICSS appears to provide an explanation for the effectiveness of UPVSc in a manner that is consistent with known or plausible cerebrocerebellar and spinocerebellar neurocircuitry as well as physical control of a primate limb using long-loop servo control. In particular, the activity might be based upon processing of the filtered error-like signal proposed by the RIPID cerebrocerebellar control model (Massaquoi 2006a). Moreover, the nonlinearity that appears to be fundamentally important derives in part from the multiplicative interaction between error-like signal transmitted by signal parallel fibers, and state feedback information carried hypothetically by selector parallel fibers. This feature is consistent with the hypothesized mechanism of cerebellar gainscheduling that is posited to enable the cerebellum to adjust its feedback control according to body motion and configuration (Jo and Massaquoi 2004). Taken together, the findings herein support the validity of RIPID control model.

Unfortunately, because the net cerebellar control signal is presumably related to the output of the entire PC population as well as direct transnuclear signals from precerebellar nuclei to deep cerebellar neurons, which are unknown to us, we cannot directly relate the PC signals seen here to the motor command to the arm. In addition, the RIPID control model also suggests that other extra-cerebellar pathways contribute significantly to arm control which further reduces the likelihood of interpreting limb control directly in terms of the recorded PC activity. Still, although the RIPID and RICSS models contain a number of free parameters, their structures are specific and explicit. They therefore constrain internal

signal behavior and afford specific, quantitative predictions for future studies.

The regression findings do not in themselves exclude other models that have been proposed for cerebellar function. However, taken together with other accumulating evidence, the results highlight contrast to alternative formulations. The observation by the investigators here that most units responded to passive manipulation argues strongly for the presence of feedback signals in PC firing activity, as used by the RICSS model, and against purely feedforward cerebellar control models (Contreras-Vidal et al. 1997; Kawato et al. 1987). The nonlinearity in the relationship between kinematics and cerebellar signals confirmed here had not been emphasized before the UPVSc model, although purely linear formulations such as in Pellionisz and Llinas (1982) and Gomi et al. (1998), do not appear to consider linearity as a fundamental requirement. Other proposals (Kawato 1999; Kettner et al. 1997; Schweighofer et al. 1998b) are already sufficiently general to be potentially consistent with PC data used here. However, these models have not yet been explicitly reconciled with cerebrocebellar circuitry and cerebellar signals recorded during arm movement.

Chapter 4

Submovement analysis and modeling of non-human primate manual tracking

This chapter describes the analysis and modeling of submovements during manual tracking in non-human primate. Segmentation of the speed profiles into the submovements has been observed in various limb movements that include reaching, tracking, and isometric tasks. The task in the experiment consisted of the interception and visually guided tracking of a target moving along a circle. The submovements were characterized based on their durations, each of which was defined by two consecutive local minima, and amplitudes being the maximum speed within the duration. Speed intermittency was apparent both in the interception and tracking phases. The distributions of durations across the speed tested were found to be invariant. Amplitude of submovements had an affine relation to the duration, and the slope was also an affine function of the target speeds in tracking condition. In order to capture those observed features, the RIPID model was extended to include a cortico-basal ganglia loop by Mao (2005),Mao and Massaquoi (2005), and Massaquoi (2006b) . The modeling effort was limited to a pseudo one dimensional angular tracking task, but the model qualitatively reproduced the invariant distributions of durations across a range of speeds while receiving a

smooth reference signal as well as the two affine relations: 1) between the durations and the amplitudes of the submovements and 2) the slope of the first affine relation and the target speeds.

4.1 Introduction

Most studies have emphasized submovements' role in feedback error corrections with a refractory period of 170 - 250 ms (Miall et al. 1993a), feedforward control (Miall et al. 1986), or both (Novak et al. 2000, 2002). It is also possible that the submovements are themselves movement errors, i.e., the uncorrected consequences of musculoskeletal dynamics. Authors of the early pursuit tracking studies argued that reversals of the velocity profile were dependent on past visual input (Hartman and Fitts 1955). However, movement segmentation persists in the absence of visual feedback (Doeringer and Hogan 1998). Very slow reaching movements or those requiring extreme accuracy are also characterized by submovements (Milner and Ijaz 1990), suggesting that submovements are corrective actions by which the hand eventually achieves the target with a prescribed accuracy constraint (Milner 1992). This led to a hypothesis that a series of stereotypical submovements are used to make one composite movement (Milner 1992). Stereotypy is an appealing concept in that it reduces the trajectory planning problem to manipulating scaled versions of a single prototype velocity template. Based on this concept, submovements during reaching (Milner 1992) and interception (Lee et al. 1997) tasks have been modeled based on velocity templates such as minimum jerk criterion (Flash 1987) or individually fitted templates (Milner 1992). Thus it is important to test if the stereotypy is a result of specific motor planning or if the kinematic stereotypy is a result of an inherent neural mechanism that segments a continuous reference signal.

The four figures below, Fig.4-1, through 4-3 briefly explain the structures of each type of suggested intermittency generation mechanisms. In each figure, $x(t)$, $y(t)$ and $e(t)$ denote the reference command, the output, and the error signal respectively, P the plant, G a system which may be a controller, Δ a delay operator such that its input-output relation is

characterized by the following: $l(t) = m(t - \Delta)$ where $l(t)$ is the output of the operator and $m(t)$ is the input to the operator.Finally, the box with a Gaussian-like curve is a template-based command generator that can scale and dilate a given template.

The first class is a purely feedforward model suggested by Miall et al. (1986) where the continuous reference command $x(t)$ is fed to a system G which is a linear feedforward model consisting of a lowpass filter with a delay. This model was suggested to explain a small variation in magnitude and delay observed in a sinusoidal manual tracing task performed by monkeys. As it can be seen that this model does not contain any active mechanism to generate intermittency, the model could explain only overall frequency response of the kinematics.

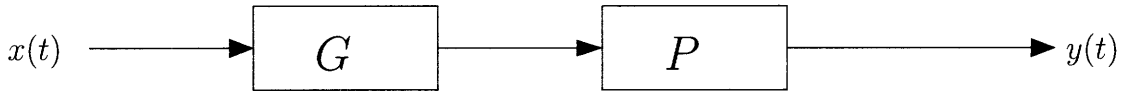

Figure 4-1: Feedforward model to generate intermittency. The bidirectional arrow after $e(t)$ denotes a sample and hold mechanism.

In order to account for intermittency seen in individual trials, Miall et al. (1986) and Miall et al. (1993b) used the idea by Craik (1947) that human manually tracking a visual target behaved like an intermittent servo-controller and suggested a sampled feedback model with a loop delay of 250-280 ms. Intermittency allows the monkeys to achieve a good frequency response and maintain tracking stability despite an irreducible visuomotor loop delay of 250-300 ms. The sampling frequency was fixed to be approximately 250 ms regardless of the reference signal to be tracked. Another class of a sampled feedback system was suggested by Navas and Stark (1968). In the latter scheme, the sampling was not performed based on the timing, or clock-synchronized sampling, but rather on the input, or error induced by the input. The actual implementation does not include sampling in proprioceptive loop, but only in visual loop. An interesting feature suggested by Navas and Stark (1968), Miall et al. (1986) and Miall et al. (1993b) is that there is a dead-zone to the error signal so that if the error is smaller than a threshold of the dead-zone, then the effective signal sent to

the sampler becomes 0. Another important feature of this model is that there is no velocity template embedded in the formulation.

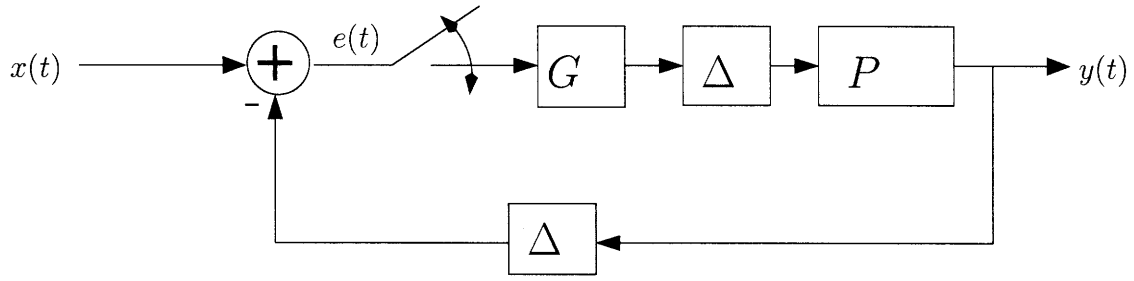

Figure 4-2: Sampled feedback model to generate intermittency.

The model assumes that when a submovement is present, its onset is associated with a change in the direction of the hand path and/or a zero crossing or inflection in at least one of the components of the velocity vector. The model is consistent with a strategy in which precision is achieved by periodic discrete actions which redirect the moving arm in order to bring the hand closer to the target. Since submovements were also observed in slow movements where accuracy constraints had been relaxed, we hypothesize that the strategy of superimposing a series of submovements to make one composite movement may be a general one. We suggest that it would be particularly appropriate for the process of learning a new motor skill.

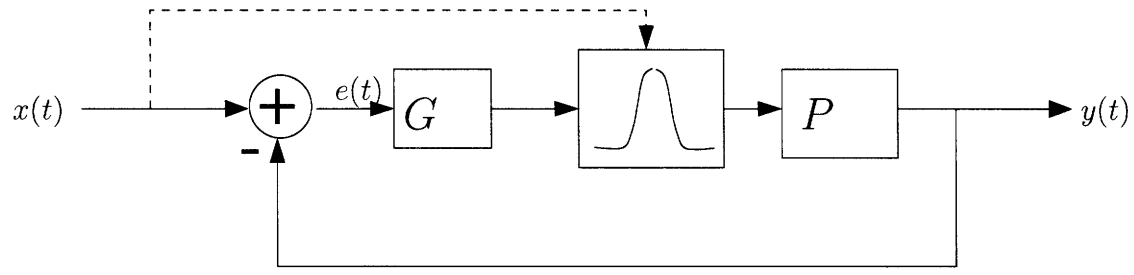

Figure 4-3: Possible strategies to generate submovements.

Given the above stereotypy concept, the nature of the scaling properties remains unknown. Understanding submovement scaling is important to independently examine the

stereotypy hypothesis. The duration of a submovement is monotonically related to both the distance it covers (Miall et al. 1986) and its velocity amplitude (Milner 1992).

It is important to note that the observation of stereotypy does not imply that scaled and dilated template movement commands are submitted to the motor control system in a feedforward manner as in Fig. 4-2. It is also possible, with the previously proposed notion of intermittent feedback control with refractory period (Fig. 4-2), that movement trajectories can display a segmented appearance. The latter possibility would be relevant to the RIPID mode which places emphasis on the processing of error type signals rather than feedforward signals.

However, the detailed properties of the scaling across a wide range of movement parameters have not been studied. Therefore the first aim of this study was to characterize the amplitude–duration scaling properties of submovements across different speeds of circular manual tracking in the monkey. These scaling properties were examined to identify the concept of intermittency in the monkey's movements. The results demonstrate that submovement amplitude scaled affinely with duration, and that this scaling was a function of the tracking speed. Additional property found in this study during the tracking phase was the invariant distributions of durations of submovements over the speeds tested.

If the submovements are an essential part of primate limb movements, then it is reasonable to argue that the intermittency is a manifestation of the motor system. The RIPID formulation was supported further by the RICSS formulation in Chapter 3 while accounting for average behavior. Thus, the RIPID formulation was extended by including a cortico-basal ganglia loop model recently developed by Mao (2005) to account for intermittency observed in individual trials. The extended model was preliminarily aimed to qualitatively reproduce statistical features observed in the monkey's individual trial data. The extended model managed to qualitatively capture those two features in pseudo one dimensional tracking task. This suggests that intermittency can be seen as a result of internal segmentation mechanism.

4.2 Methods

4.2.1 Behavioral task

Experimentation was conducted according to the Guiding Principles in the Care and Use of Animals as endorsed by the American Physiological Society and was approved by the Institutional Animal Care and Use Committee of the University of Minnesota. One female right-handed monkey was trained to use multi-joint arm movements in the horizontal plane (Fu et al. 1993; Johnson et al. 1999) to move a cursor on a monitor vertically placed in front of the monkey. The task included an initial interception of a circularly moving target from a centrally located hold target and a subsequent visually guided pursuit of the target for one rotation.

The trial sequence which is shown in Fig. 4-4 was initiated when the monkey held the cursor (1-cm black cross-hair) on the hold target (1.8-cm-diam red circle) for a time period randomly generated between 1 and 2 seconds (Hold period). A cue target (2.5-cm-diameter yellow circle) then appeared at a radius of 5 cm and moved around a circle centered on the hold target while the monkey maintained the cursor in the hold target (Cue period). After 180 degrees of circular travel, the target changed color (red) signaling the onset of interception. The monkey had 65 degrees of target travel to intercept the circularly moving target (Intercept period). After intercepting the target, the monkey continued to track the target for another 360 degrees (Track period). Target speed, starting angle, and direction were varied in a randomized and blocked fashion. The five target speeds ranged from 3.1 to 8.3 cm/s, in 1.3-cm/s increments, or equivalently, from 35 deg/s to 95 deg/s in 15 deg/s increments. The starting angle of the Cue period varied from 0 degree to 270 degrees in 90 degree increments. Target travel was also randomized between clockwise (CW) and counter clockwise (CCW) directions. For each trial type, 5–10 repetitions were obtained for a total of 200–400 trials per experiment. At any point in the trial sequence, deviation of the cursor from the hold or moving target would abort the trial. The monkeys could see their hands and manipulundum, but the task was set up such that the animal was only able to view the

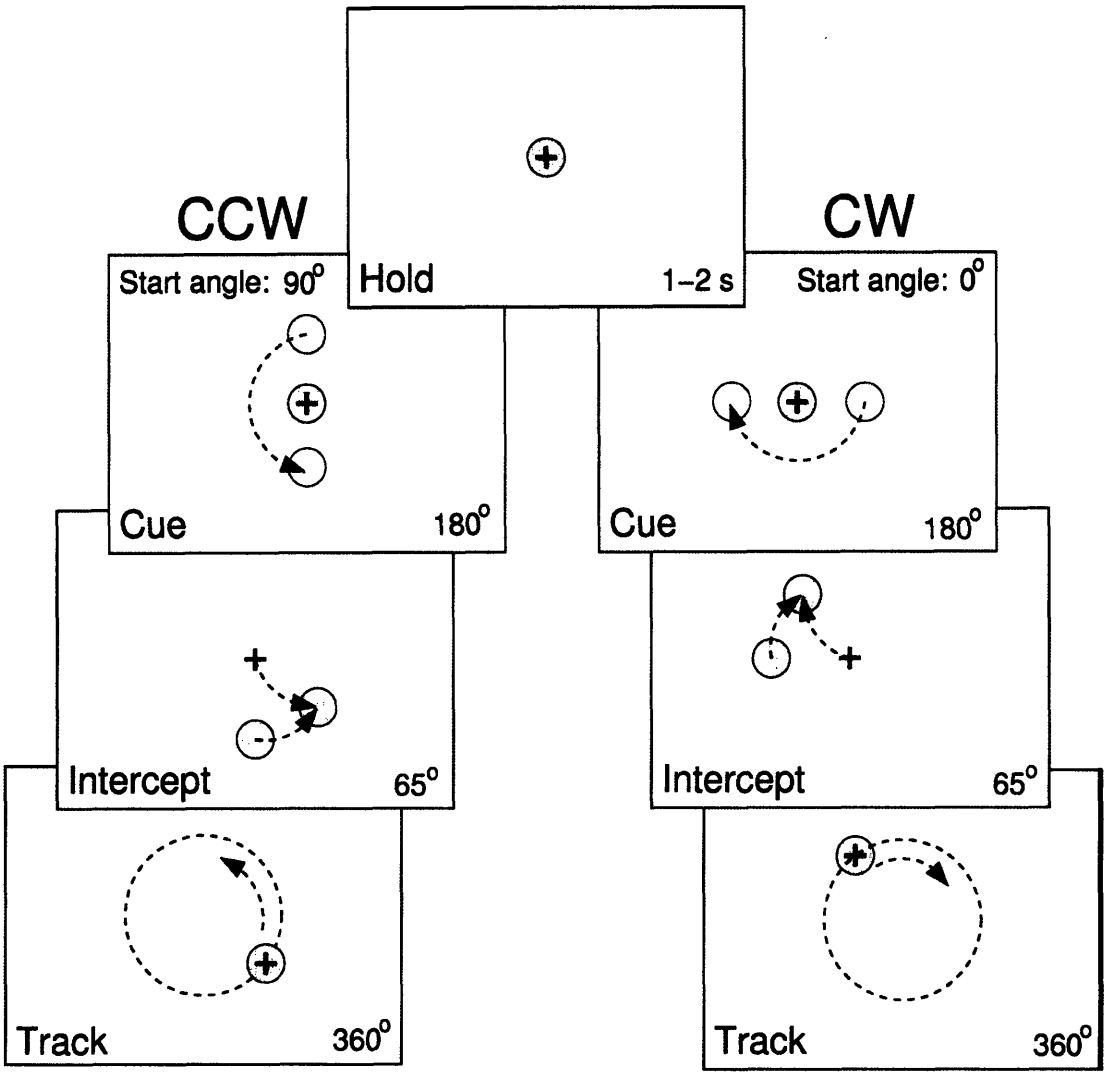

Figure 4-4: Experimental protocol. Adapted from Roitman et al. (2005).

vertically positioned monitor.

4.2.2 Data acquisition

Hand trajectory was digitized using two potentiometers in the joints of the manipulundum. The position data was sampled at 200 Hz and used to drive the cursor position on the monitor. Both the mechanical manipulundum system and electrical data acquisition system will be referred to as instrumentation. Velocity was calculated by numerical differentiation of the position data and was filtered using a low-pass 12th-order Butterworth filter with 6

Hz cutoff frequency. The filter was applied successively in forward and reverse directions to preserve the phase of the signal. The cutoff frequency of filtering was selected based on a qualitative speed pulse analysis detailed in section 4.2.3, using 6 and 12 Hz low-pass filter. The 6 Hz filter was selected because it kept the majority of the large speed pulses were kept while attenuating high frequency noise effectively.

4.2.3 Speed pulse analysis

The analysis of the submovements in this study is based on the peaks in the hand speed profile, which we will refer to as speed pulses. The bell-shaped profiles of the speed pulses were identified by finding the local minima in the speed profiles (see Fig. 4-5). Each $i-$th pulse in a given trial is characterized by the duration ΔT_i and the amplitude $\overline{U}_i$. Two measurements, duration and amplitude, were recorded for each pulse. The duration, ΔT_i, of the $i-$th pulse was defined as the time interval between successive speed minima $\underline{U}_{i-1}$ and $\underline{U}_i$, $T_i - T_{i-1}$. The amplitude, $\overline{U}_i$, of the i-th pulse was the peak speed within ΔT_i. First, the empirical distributions of the pulse durations were obtained to investigate the relation between the duration distributions and the target speeds. Second, the linear regression model

$$\overline{U}_i = a_0 + a_1 \Delta T_i + \epsilon, \tag{4.1}$$

where a_0 and a_1 were constants to be determined and ϵ the error term, was employed to determine the relation between the duration and amplitude of the pulses.

The regression analysis was carried out for both Intercept and Track periods separately at all experimental conditions. For consistency, all analyses were limited to 13 data sets. Each data set consisted of 400 trials (2 directions, 4 starting angles, 5 speeds, 10 repetitions for each condition) so that the results from 10 trials of each type could be averaged.

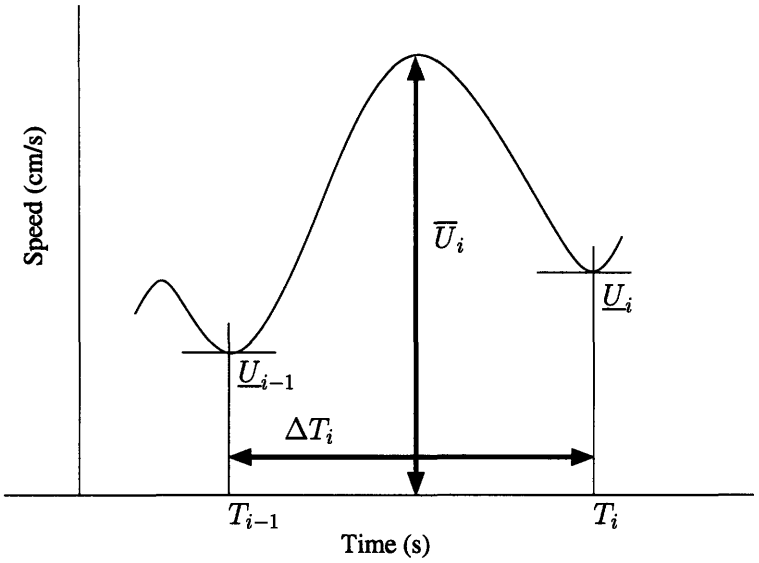

Figure 4-5: Definition of the speed pulse used in this study.

4.2.4 Control experiment (Roitman et al. 2004)

A simple control experiment was designed to ensure that the submovements analyzed were generated by the monkey and not by instrumentation artifacts. This control experiment consisted of a balanced rotational setup (Rotational Inertial Accessory, PASCO Scientific ME-8953, mounted on a Rotating Platform, PASCO Scientific ME-8951) connected to the manipulundum via a low-friction pin coupling. Position data were recorded from the manipulundum during free rotation at speeds comparable to those used in the tracking task. The acquired control data were analyzed in the same manner as the primate tracking data. This control experiment measured the instrumentation noise. A threshold of 3 cm/s was chosen based on the results of this control experiment and on those obtained from the animals during non-movement periods.

4.2.5 BG-RIPID model

In order to test if the intermittency can be a result of an internal neural mechanism, the RIPID model was extended by including a cortico-basal ganglia loop model suggested by Mao (2005). The basal ganglia is suggested to be a context dependent switching controller

which monitors the context, the magnitude of the error signals in this study, and regulates the amount of the error signal to be integrated to generate a command-like signal for the motor execution. The particular part of the RIPID model, enclosed in the blue box in the upper figure in Fig. 4-6 is enhanced with the cortico-BG interaction as shown in the lower figure. In this schematic, the error signal generated at SUM 1, i.e., the difference between

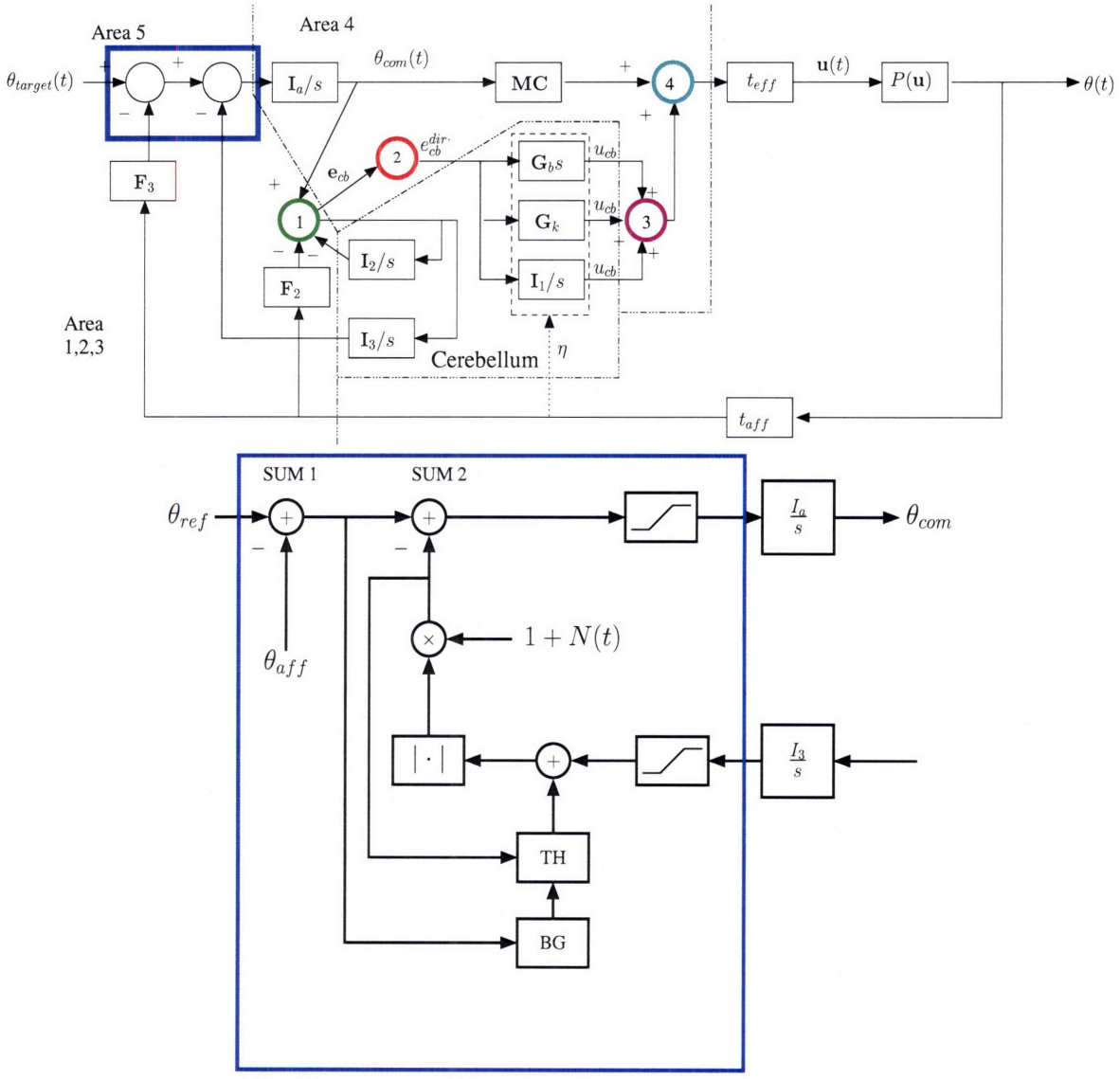

Figure 4-6: The cortico-BG interaction embedded to the RIPID, BG-RIPID model.

θ_{ref} and θ_{aff} is monitored by the basal ganglia, BG. BG, then compares the error signal

against a threshold value. If the error is larger than the threshold, then the BG outputs 1, otherwise 0. This pair of binary BG output regulate the activity of the thalamus (TH). If the BG output is 1, then TH puts through its input signal, otherwise outs a constant background activity. The output of TH and the output from the cerebellar integrator $\frac{I_3}{s}$ are summed and the magnitude of the sum is multiplied by a noise which consists of band-limited white noise. Almost identical implementation was done to the error signal generated at SUM 2. For this case, the signal coming into the saturation block is replaced with the error signal coming out of SUM 2. Then, both error signals are monitored by BG. This multiplicative noise is a model fluctuation of activity in a population of neurons and this type of multiplicative model has been suggested (Grossberg and Kuperstein 1989) and for noise in particular by Harris and Wolpert (1998) to affect motor planning and command generation.

Although the task that the monkey performed was a two-dimensional tracking task, the extended model was designed to represent a pseudo-one degree of freedom arm movements. In order to compare statistical similarities between the features found in the monkey data and that from the simulation of the extended model, the tracking in one dimension was simulated for over a range of speeds. Therefore, the aim of this part was to investigate a possibility of the mechanism to reproduce kinematic variability seen in individual trials. In order to collect substantial amount of submovements, 100 simulations were performed at five different speeds during which the band-limited white noise was multiplicatively applied so that each simulation showed difference in the kinematic output. The submovement extraction procedure is the same as that used for the monkey data.

4.3 Results

4.3.1 General description of kinematics

Data from 69 data sets recorded from the monkey were used in this study, and only 13 data sets, each consisted of 400 trials total, 10 trials for each type described in Section 4.2.3 were analyzed. The monkey successfully intercepted and tracked the target with her right hand in

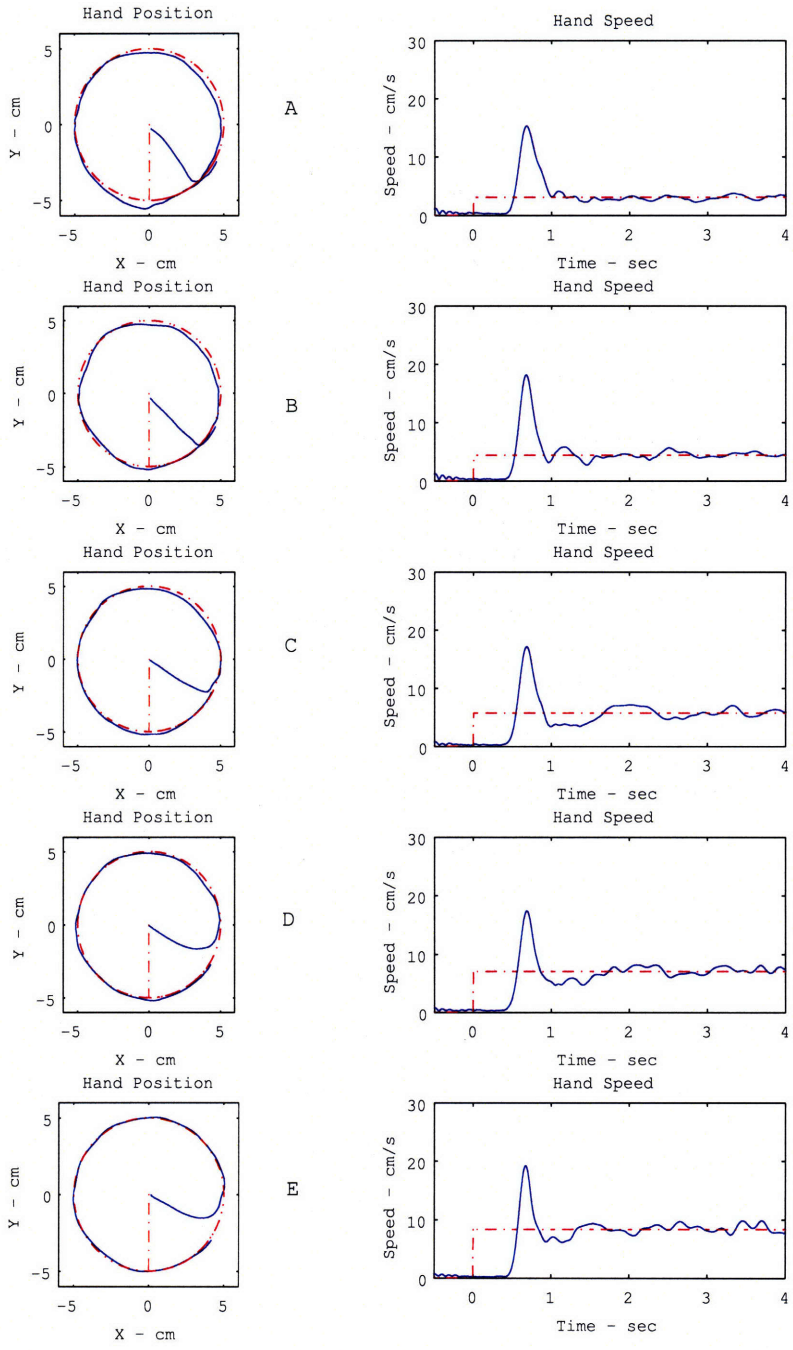

Figure 4-7: Averaged trajectories on the left column and speed profiles on the right column over 10 trials. Plotted are monkey hand data (solid blue) and target data (dashed red). Starting angle was at 90 degree, and direction of motion was CCW. Zero time corresponds to the onset of the Intercept period.

this error-constrained task. Fig. 4-7 shows averaged movement trajectories and speed profiles of the hand and target at the five target speeds. The position trajectories followed the target reasonably well. The speed profiles are notable for an initial bell-shaped peak during the Intercept period. This initial peak, usually the maximum, was followed by subsequent local minima and maxima in amplitude of the hand speed. Single trial trajectories and speed profiles demonstrated a significantly more noticeable variability compared with the averaged traces during the Track period. The differences in the kinematics of the movement could be appreciated by comparing the averaged (Fig. 4-7) versus single trial trajectories and speed profiles (Fig.4-8). The single trial speed profiles were most notable for the prominent peaks during tracking. Qualitatively these peaks have bell-shaped profiles similar to those occurring during the Interception period. The spatial locations of the peaks did not exhibit any patterns.

4.3.2 Speed pulse analysis

The results of the control experiment using the balanced rotational setup demonstrated that the primate tracking speed irregularities are not due to the instrumentation noise during movement of the manipulundum . The speed pulse amplitudes during passive movement were comparable to those observed in the Hold and Cue periods. Furthermore, it was shown in Roitman et al. (2004) that the speed pulse during movement in Intercept and Track periods reflected the properties of the monkey's movements, but not the artifacts caused by the experimental setup. First, the relation between the pulse durations and the target speeds was sought. During tracking phase at a given target speed, the durations of pulses took a wide range of values. Fig 4-9 shows a set of empirical normalized distributions of the unit movement intervals for the five target speeds. One striking feature is that although target speeds varied considerably, almost threefold, the interval distributions remained similar across the speeds. Statistically, however, only three pairs are considered to have the same medians; 95 deg/s and 80 deg/s, 95 deg/s and 65 deg/s, and 80 deg/s and 65 deg/s (rank sum test, $P > 0.05$). The same finding was reported by Pasalar et al. (2005) in a human

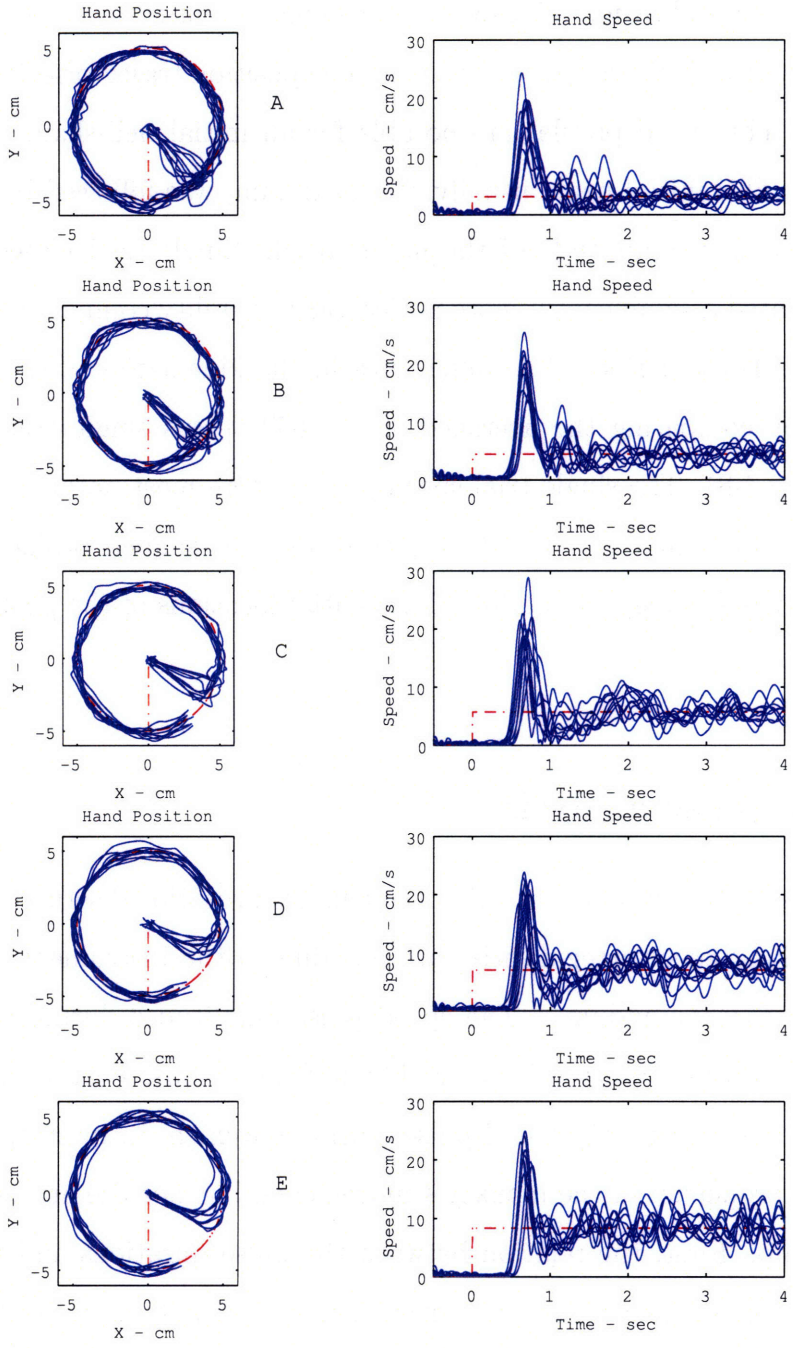

Figure 4-8: Individual trajectories on the left column and speed profiles on the right column from single trial movement trajectories. The color scheme, the starting angle, and the rotational direction are the same as that in Fig, 4-7. Speed overshoots and undershoots are prominent in both Intercept and Track periods.

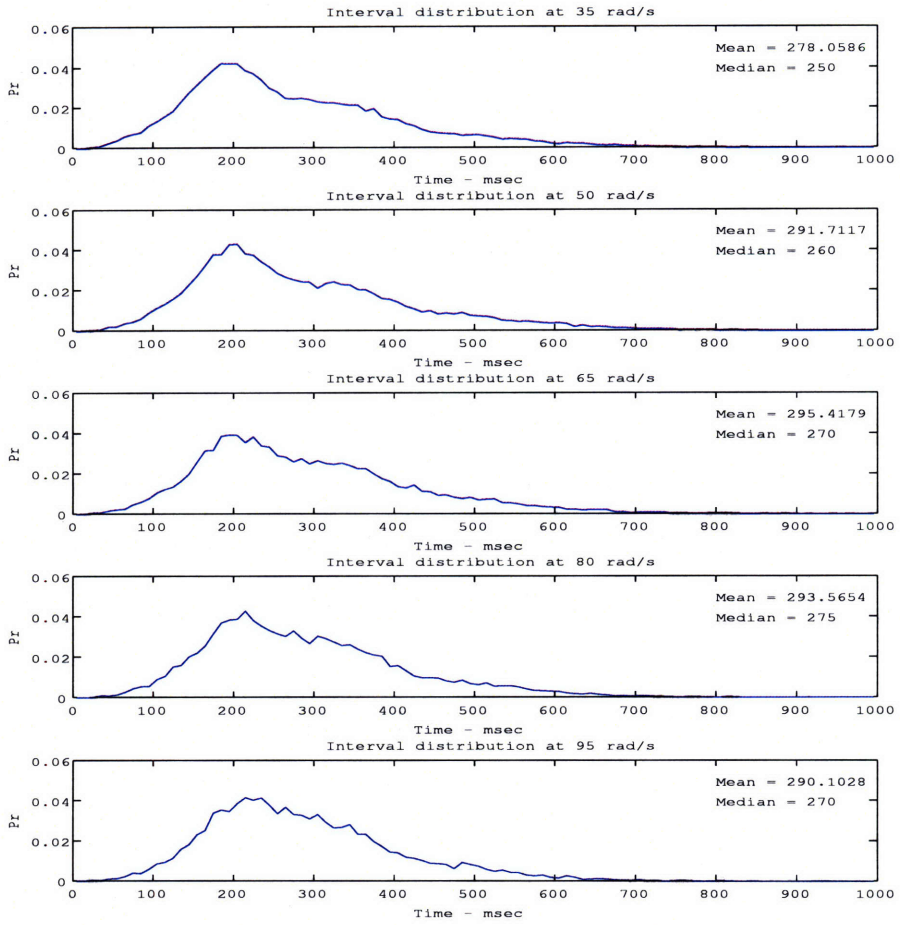

Figure 4-9: Empirical probability distributions of speed pulse durations across the target speeds.

study where the subjects performed the identical tasks with a different speed range.

The second goal for the speed pulse analysis was to seek the relationship between speed pulse amplitude and duration. In Fig. 4-10, cluster plots of the $\overline{U}_i$ against ΔT_i of the speed pulses reveal an affine relation for both the Intercept and Track periods. The slope, a_1 in Eq. (4.1), of the Intercept period differed significantly across speeds ($P < 0.05$). There were no significant difference ($P > 0.05$) in the slope of the Intercept period between CW and CCW directions, but there was a significant difference in the slope of the Intercept period across the four starting angles ($P < 0.05$). Roitman et al. (2004) showed in a smaller data set that only the two starting angles of 180 degrees and 270 degrees produced significantly different

slopes. The slope of the Track period showed significant difference across speeds ($P < 0.05$), but there was no significant difference ($P > 0.05$) in the slope of the Track period either between CW and CCW directions or across four starting angles of tracking. Based on these observations, tracking speed was determined to be the only significant factor consistently affecting the slope. Thus for further analysis, the slope values for both Intercept and Track periods were averaged across both directions and all starting angles of tracking.

Simple regression analysis between $\overline{U}_i$ and ΔT_i (Eq. 4.1) confirmed the affine dependency in the tracking condition. The regression coefficients (across starting angles and rotational directions) for the regressions for the Intercept and Track periods, respectively, are summarized below (Tables 4.1 and 4.2). The quadratic model was tested as well, but the coefficients for the quadratic terms were non-significant for all speeds (sequential F-test, $P > 0.005$). One difference between the result presented here and that in (Roitman et al. 2004) is that the affine relation of the slope does not hold for Intercept phase in the current study. This difference may be due to the fact that more data points were included in the analysis in this study. Then, relatively less data points were added for smaller values of ΔT_i as the target speed increased. Thus, the bias term in the regression became dominant and the linear slope became less prominent to account for this effect in Intercept phase. It is unclear whether this discrepancy becomes apparent purely due to sizes of the data sets used or not. However, it can still be concluded that speed pulse amplitude and duration are affinely related for at least tracking condition.

coefficients \ speed (rad/s)	35	50	65	80	95
a_0	2.1406	3.2133	6.1778	10.1961	13.8768
a_1	29.3125	30.1105	21.6624	21.6624	16.9991

Table 4.1: Regression coefficients vs. target speeds for Intercept periods

It is reported (Roitman et al. 2004) that a similar target speed dependency on the slope as shown above was found for another monkey performed the same task except at a higher speed range. Therefore, this affine scaling property is not limited to a particular monkey's strategy, but presumably is applicable as a general principle.

coefficients \ speed (rad/s)	35	50	65	80	95
a_0	2.2674	3.3687	4.4417	5.6602	7.0827
a_1	5.7499	7.0322	8.5950	9.9362	10.9439

Table 4.2: Regression coefficients vs. target speeds for Track periods

4.3.3 BG-RIPID model with a cortico-basal ganglia system (Mao 2005)

The extended RIPID model was simulated over a range of speeds. The seed of the bandlimited noise was varied in each trial to produce trial-by-trial variability. At each speed, 100 simulations were performed. To extract the submovements, the same detection method was used as that in the monkey data except that only the tracking phase data was used in the analysis. A tracking phase was defined to be after the temporarily second local minima. Fig's 4-11 and 4-12 show an example of position traces and seed profiles at each speed.

The duration distributions are shown in Fig. 4-13 against the target speeds, the slowest (top) to the fastest (bottom). Qualitatively, the ranges of the durations are similar as well as the tapering of the both edges. These features were observed in the monkey data as well. However, the unimodal nature of the distributions is violated in the simulated distributions, especially when the target speed increased. The exact origin of emergence of bimodal distributions as a function of target speeds is now known at this point.

In Fig. 4-14, cluster plots of the $\overline{U}_i$ against ΔT_i of the speed pulses reveal an affine relation between the two variables. The affine relation between the slope, a_1 in Eq. (4.1) and the target speeds is shown in the lower right plot and the coefficients a_0 and a_1 as functions of the target speeds are summarized in Table 4.3.

coefficients \ speed	1	1.5	2	2.5	3
a_0	7.836e-4	11.9493e-4	16.0524e-4	20.0213e-4	24.2759e-4
a_1	3.0136e-4	3.9785e-4	4.8867e-4	6.1619e-4	6.7182e-4

Table 4.3: Regression coefficients vs. target speeds for the simulation data.

One significant difference in the cluster plots between that for the simulation and that

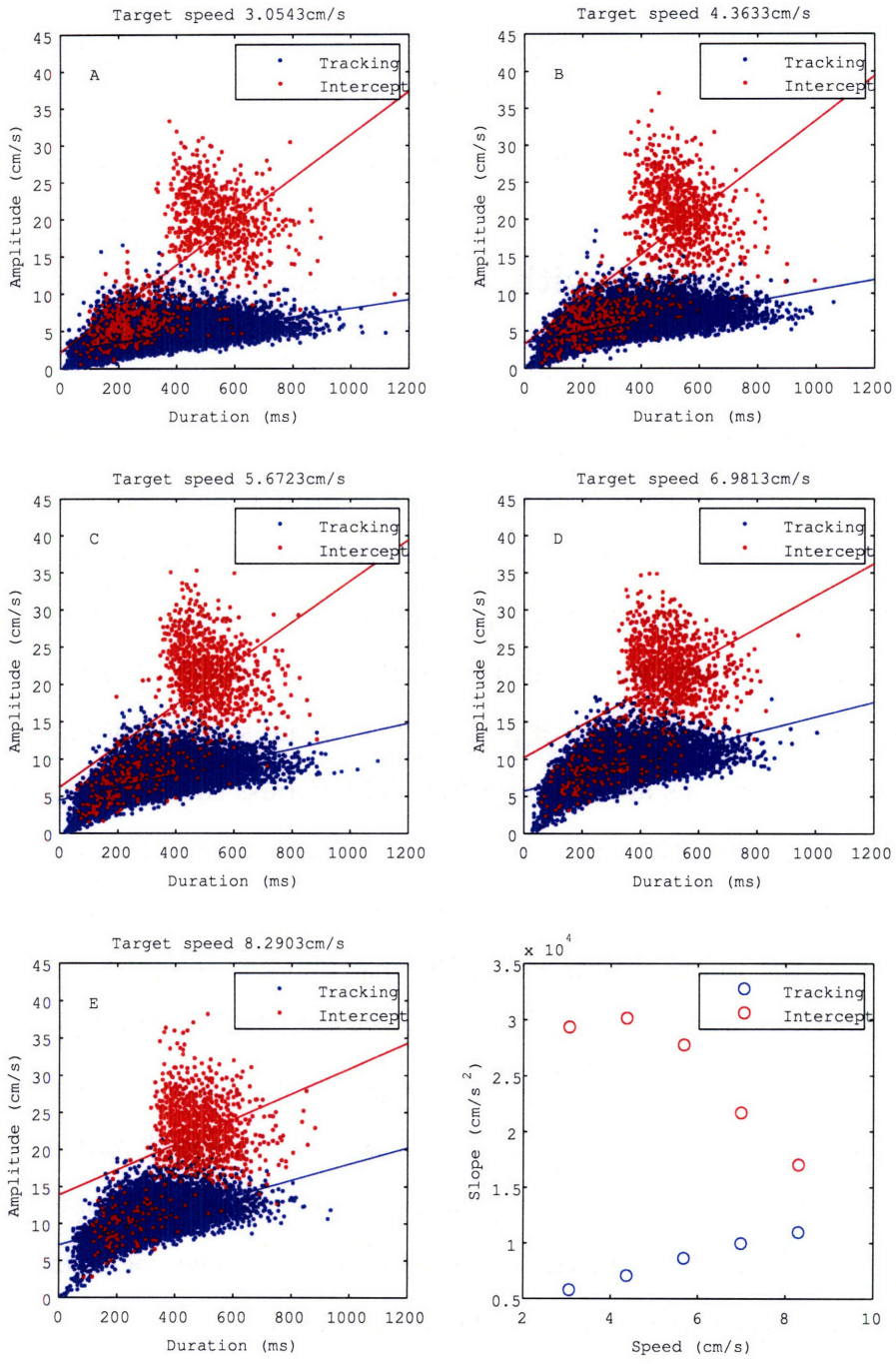

Figure 4-10: A - E: Amplitude–duration distributions at each target speed for the Intercept (red) and Track (blue) periods. F:Amplitude–duration regression slope dependence on the target speed. Shown are the amplitude–duration slopes at each target speed for the Intercept (red) and Track (blue) periods.

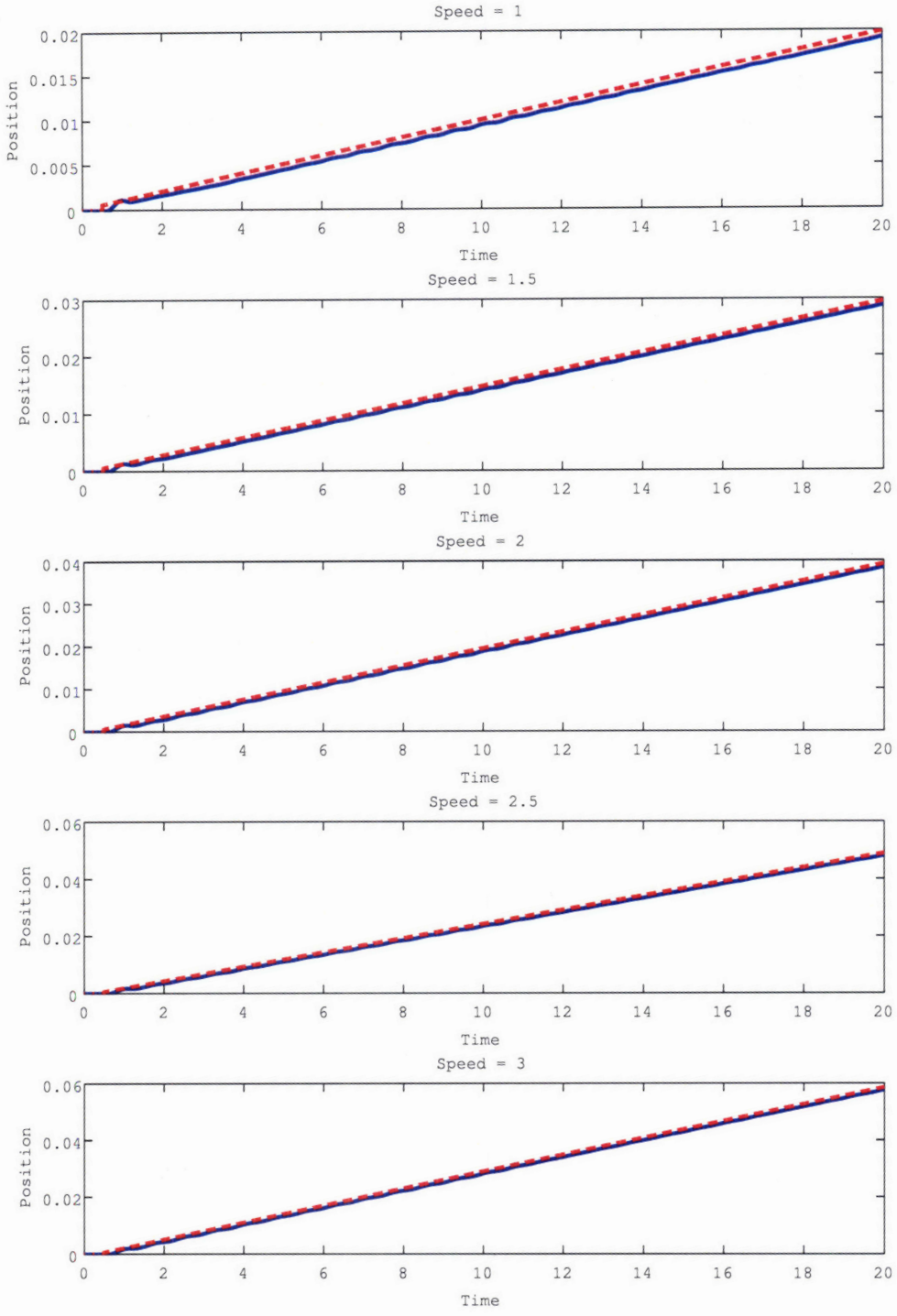

Figure 4-11: Position response of the BG-RIPID model. Position traces (blue) and the command (dashed red) at the five speeds simulated are shown.

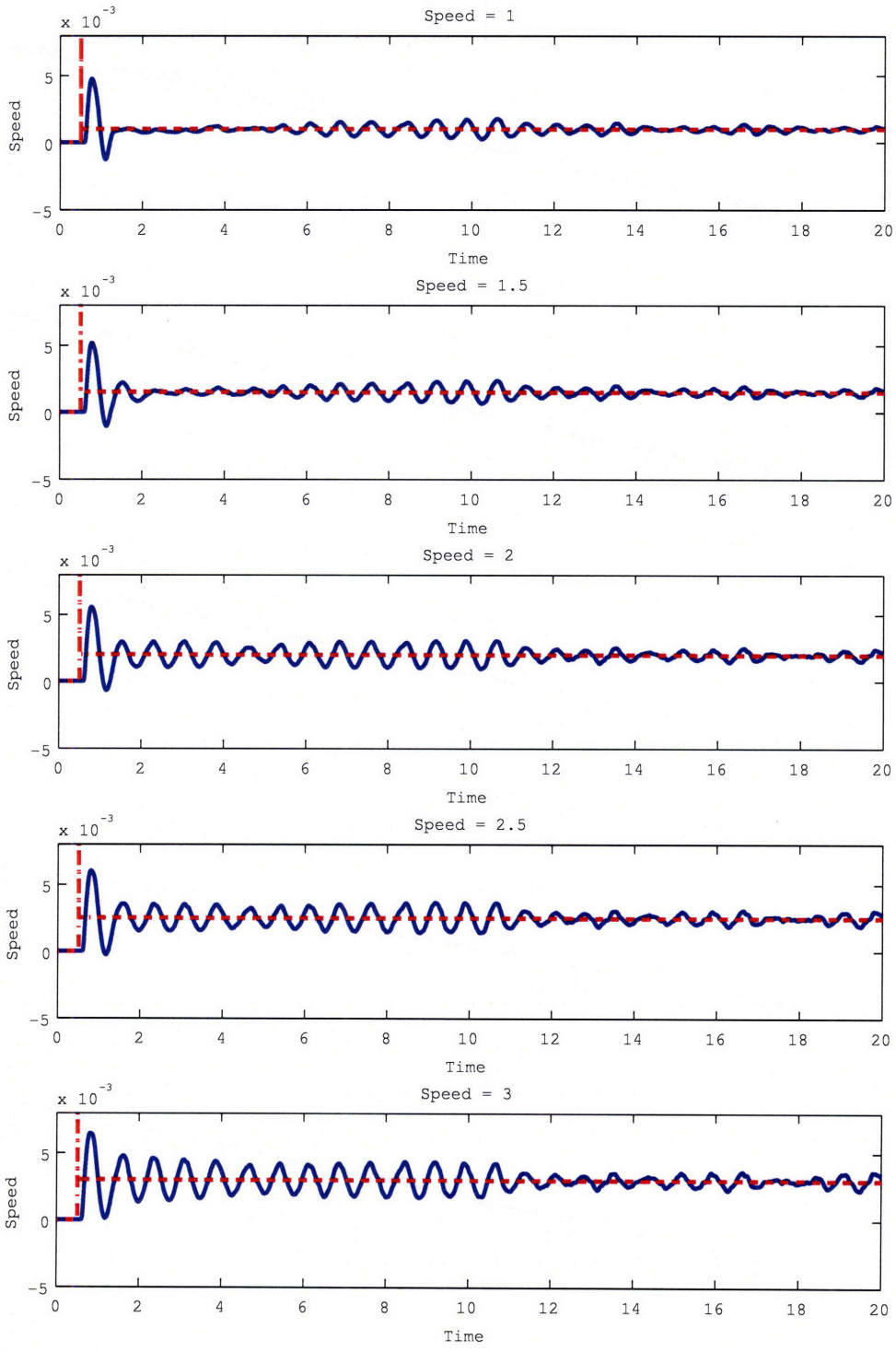

Figure 4-12: Velocity response of the BG-RIPID model. Velocity traces (blue) and the command (dashed red) at the five speeds simulated are shown.

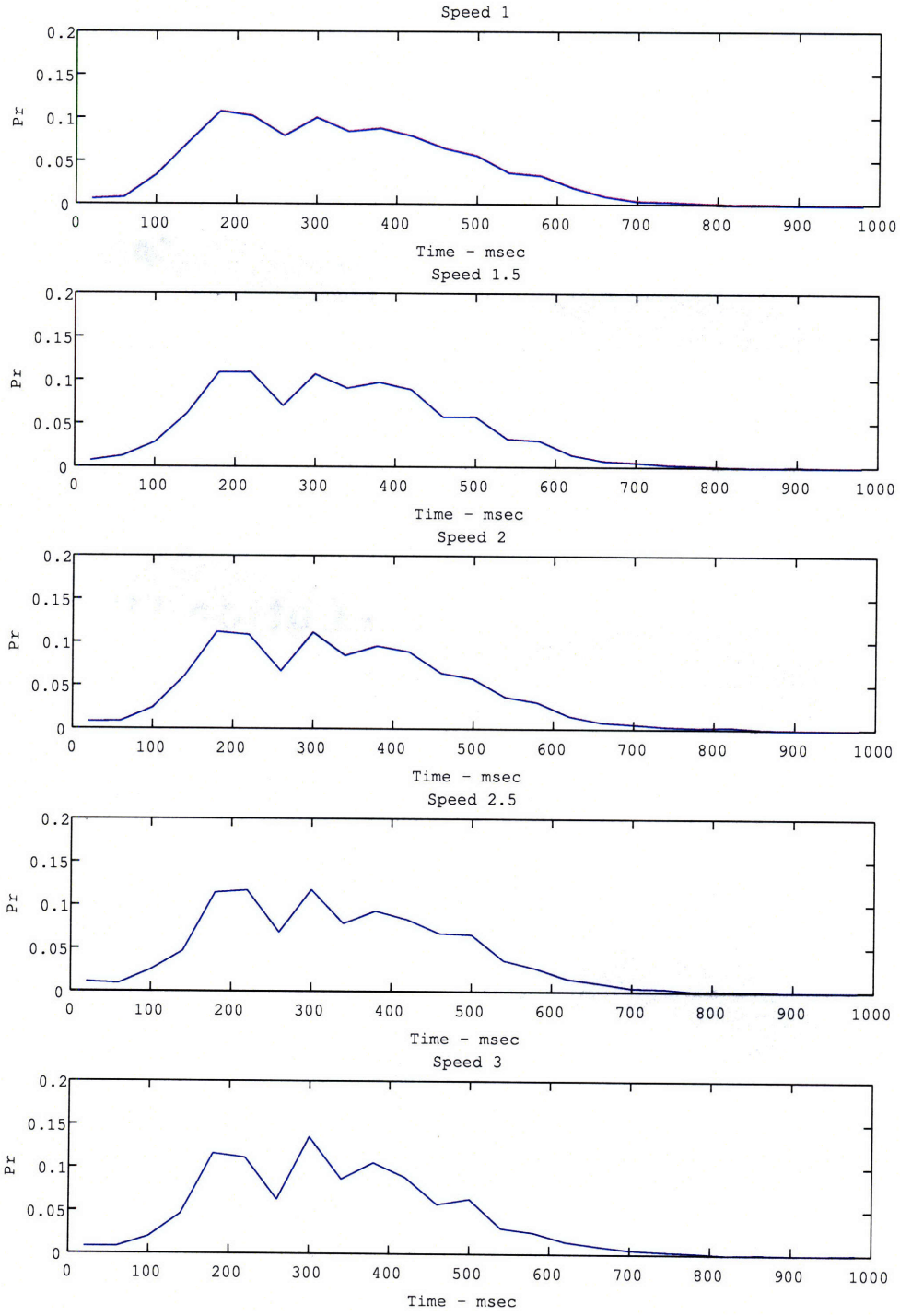

Figure 4-13: BG duration distributions

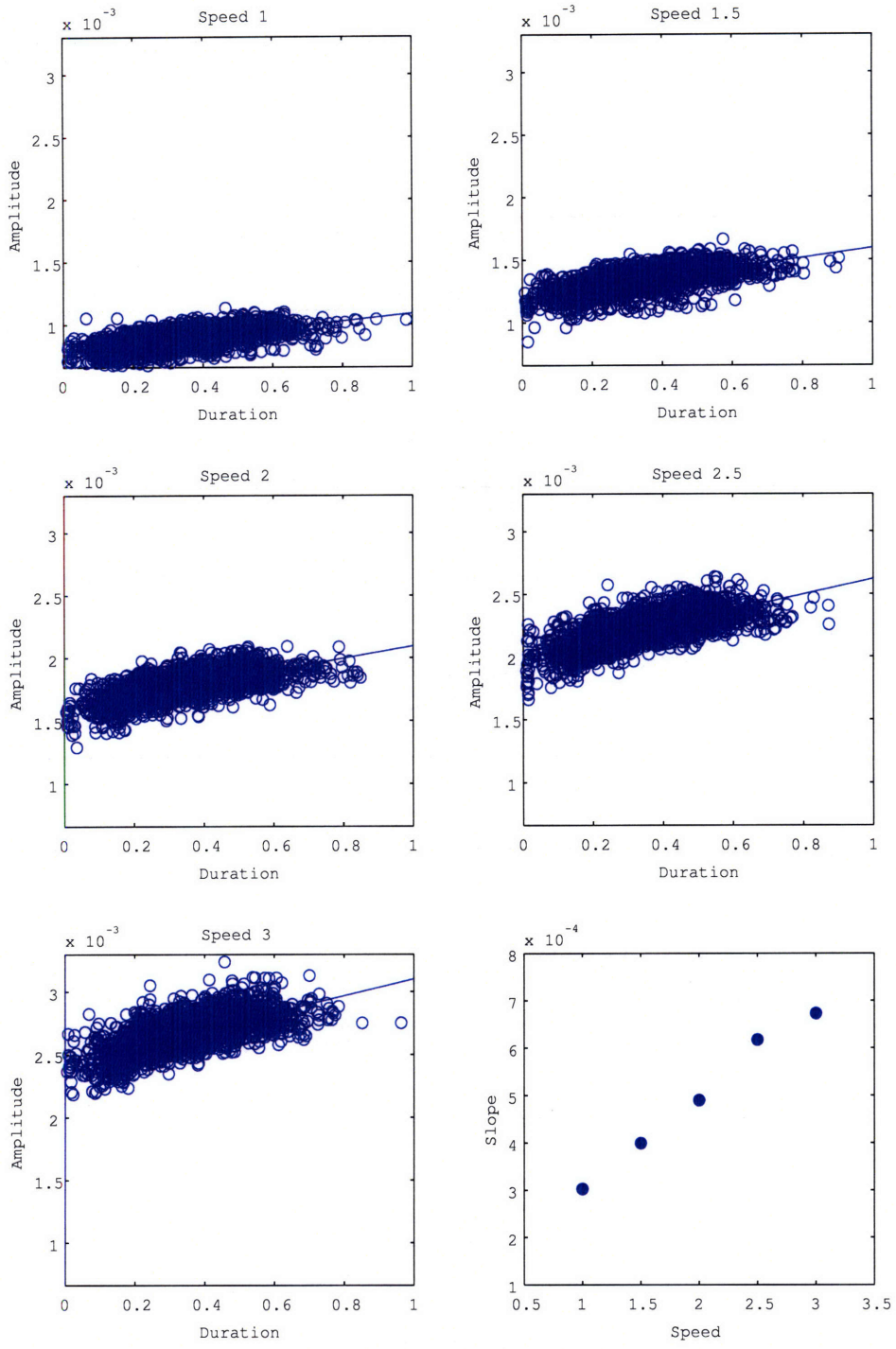

Figure 4-14: A-E: Amplitude-duration distributions at each target speed for the tracking period from the simulation of the extended RIPID model.

for the monkey data is the spread of the data points at a given pulse duration. In particular, there are much less data points of short durations with high amplitudes in the simulation data. It is possible that such a type of pulses in the monkey data may reflect "catch-up" movements where the monkey detected a large error and made a cognitive correction to reach to the moving target.

4.4 Discussion

4.4.1 Existence and detection of submovements

The results demonstrated that arm movements during manual visual pursuit tracking in the monkey were not continuous, but instead, consist of submovements. These results confirmed previous findings that the speed traces of virtually all human and non-human primate movements are not smooth (Doeringer and Hogan 1998; Lee et al. 1997; Massey et al. 1992; Meyer et al. 1982; Miall et al. 1986, 1988; Milner and Ijaz 1990; Novak et al. 2000).

The amplitude of submovements and their other properties were clearly distinguishable from any noise introduced by the acquisition system and were not present in passive movement. The amplitude and duration of submovements were not constant but rather spanned wide ranges with speed scaling properties, but submovements themselves were not fixed in time or space.

The submovement detection method used in this study by definition did not allow for the speed pulses to overlap. This method was chosen for its simplicity to enable us to deal with a large data set of more than 5000 trials. There exist more elaborate submovement detection algorithms available. Rohrer and Hogan (2003) introduced a branch-and-bound algorithm for submovement extraction which can avoid spurious decompositions given a profile of the unit movement and an error bound. However, the algorithm is computationally too expensive ($\approx$ 30 hours for one trial in Fig. 4 in the paper). Lee et al. (1997) assumed that the unit profile took the form of minimum jerk (Flash 1987), then guessed a set of initial conditions to be used for nonlinear optimization to minimize the error between the data and the fit.

This approach is only useful when there is only a small number of the speed pulses in a trial and a small number of the trials to be analyzed. For the submovements that overlap with the speed minimum in between, this method will detect two speed pulses with amplitudes and durations smaller than those of the overlapping submovements. For the submovements that overlap without the speed minimum in between, this method will detect one speed pulse with the larger amplitude and combined duration of the overlapping submovements. The distortion produced by each type varies depending on the size of the submovements and extent of overlap. Therefore when analyzing large numbers of speed pulses (more than 100,000 in this study), the two types of distortions should approximately compensate for each other and average out.

4.4.2 Scaling properties of submovements

Analysis of the speed pulses revealed three properties of the submovements. The first property is the invariant duration distributions over the speeds. This finding is not consistent with a few previous findings (Milner 1992). One potential reason for this discrepancy is the submovement decomposition methods. In Milner (1992), an empirical speed template was obtained. If a movement consists of a series of overlapping speed templates, then depending on the pulse magnitude scaling again speed as well as how consecutive submovements are overlapped, it is possible to have a similar duration invariance.

The second property is the linear relation between the amplitude and the duration of speed pulses at a fixed target speed. Since the target speed and the average speed of tracking are nearly identical, this linear relation also holds true at a given tracking speed. The third property is the linear relation between the scaling factor a_1 and the target speed in tracking phase.

The third property suggests that the mean acceleration and deceleration during a submovement in the tracking phase remain constant across the wide range of submovement amplitudes and durations. From Eq. (4.1) one can infer the approximate mean acceleration from the regression slope. For a given target speed, the mean acceleration is constant and

can be related to a constant average force. Therefore the three scaling properties can be restated as follows. For a given speed of tracking, the submovements are generated by a constant average force applied to the hand/manipulundum. Similarly, the average amount of force in a submovement increases linearly with tracking speed.

The acceleration/force arguments represent only a first approximation and could be challenged. First, it can be argued that the relationship between speed change and average acceleration in two dimensions is more complex than proportionality because of their vector nature. However, because the speed pulses are relatively short and the corresponding path segments are relatively straight, the average scaling properties can be well described by proportionality. Second, the speed pulses are not necessarily symmetric. However, Roitman et al. (2004) evaluated the average acceleration and deceleration for the pulses as a measure of symmetry. The evaluation yielded absolute value differences not exceeding 2.3% across all experimental conditions (average difference was $1.4 \pm 0.7\%$). Therefore as a first approximation, interpreting the amplitude-duration scaling properties in acceleration/force terms is justified.

The scaling properties of the speed pulses are consistent with the notion of stereotypy (Milner 1992), which states that a complex movement is composed of scaled versions of a prototype velocity profile. Although submovements have been extracted based on minimum jerk criteria (Flash 1987; Lee et al. 1997) or individually fitted velocity prototypes (Milner 1992), these approaches cannot verify the concept since they assume stereotypy. Without making any assumptions, the results show that the amplitude of the speed pulses scales with their duration; this is an independent confirmation of stereotypy at least in terms of amplitude and duration, though not necessarily shape.

The second and third properties of submovement scaling further extend the stereotypy concept (Milner 1992). The linear dependence on movement speed reflects the adjustment of the prototype. Controlling faster movements may be achieved simply by scaling the amplitude of a prototype submovement. On the musculoskeletal level, this can be performed by increasing the average force applied to generate a submovement (Roitman et al. 2004).

This is similar to the proposed pulse-height regulator that sets pulse size and thus the overall speed of movements (Vallbo and Wessberg 1993). In addition, the validity of the trends in slopes for both Intercept and Tracking phases supports the idea that underline control or planning strategies for reaching and tracking are the same, as argued by Flash and Henis (1991).

4.4.3 Underlying generation mechanism of submovements

A large body of literature exists on how to extract submovements (Rohrer and Hogan 2006, 2003; Krebs et al. 1999; Milner 1992) from speed profiles of the end effector which is usually a hand. The "Unit" movement in each extraction algorithm differs from each other, but needs to have a temporal template, whether it is defined in terms of symmetric functions such as minimum jerk and gaussian, or asymmetric functions such as support-bounded lognormal (Rohrer and Hogan 2003; Krebs et al. 1999). Although this type of submovement decomposition may give a useful metric in terms of degree of blending of submovements to measure smoothness of the movement, in practice it is computationally very expensive (Rohrer and Hogan 2003), even after a significant improvement of the existing algorithm (Rohrer and Hogan 2006), without explaining any underlying neural structure of intermittency generation. Psychophysically, both the direction and speed of the finger's motion are coordinated in such a manner that the time to intercept, or possibly the distance the target travels before interception, is held constant (Engel and Soechting 2000). Todorov and Jordan (1998) suggested that by maximizing the smoothness of the movements along a predefined path, a continuous fluctuation of the tempo of discrete movements may appear as segmentation. However, there has not been much research as to how intermittency is generated and which neural circuitry is involved for such segmentation. It is still not even clear if the intermittency of limb kinematics is a correction mechanism as suggested by Roitman et al. (2004) or inherent manifestation of the motor system.

What central processes might be responsible for initiating and regulating these discrete, corrective submovements? It is possible that spinal dynamics may contribute to movement

segmentation. However, our hypothesis is that the brain detects the need for and generates the commands required to produce the intermittent commands. Although a specific implementation was not performed, Novak et al. (2002) suggested a gross anatomical model that might be responsible for initiating and regulating intermittency (see Fig. 9 in (Novak et al. 2002)). A similarity between the BG-RIPID model and the one suggested by Novak et al. (2002) is that the specific channel through the basal ganglia is thought to be particularly important in the initiation or crafting of the motor command. The pulse-like command in their model may play the same role at the activation state of the basal ganglia in the BG-RIPID model. This type is consistent with observations from patients with basal ganglia deficits. In Parkinson disease, when the inhibitory output of the basal ganglia is hyperactive, patients have trouble initiating movements (Flash et al. 1992). In contrast, in Huntington disease, when inhibitory basal ganglia output is decreased, subjects tend to produce many more unnecessary corrective submovements (Smith et al. 2000). While the basal ganglia may be important for regulating the initiation of the commands for primary movements and corrective submovements in motor cortex, the cerebellum is believed to regulate the dynamics of the commands. This role of cerebellum is also consistent with the RIPID, hence the BG-RIPID formulation as well.

Thus it is important to investigate what neural system may be responsible for the generation of intermittency. The RIPID formulation obtained further support from the RIPID formulation and accounted for averaged movements. In order to explain intermittency in individual trials, the basal ganglia (BG) model developed by Mao (2005) was added to the RIPID model. The BG acts as a context-based switch regulator. In the RIPID, the BG controls the signal flow of thalamus so that the output of the thalamus can be turned on or off. By this switching action, the process of integrating error signal to generate the command becomes intermittent. The extended model was applied to create a pseudo one dimensional system to mimic the system which takes the location of the targeting moving along a circle to control the hand always on the circle so that its dynamics can be described as a function of the angular angle. The simulation showed that the extended model qualitatively cap-

tured invariant duration distributions across the target speeds and achieved relatively good tracking performance of the speed when the input position command was a smooth ramp. Thus, although it is preliminary, the extended RIPID formulation has a potential to explain gross anatomy and physiology of cerebrocerebellar system coupled with cortico-basal ganglia system that can explain not only the average behavior but also intermittency observed in individual trials.

Roitman et al. (2004) suggested, based on the cross correlation of various error signals and the speed profiles, that two types of errors may trigger a submovement. The first type is the directional error (DE), which is the difference between the present direction and the desired direction of the motion. The second type is modified speed error (MSE) which is defined to be a linear sum of the difference between the present and desired position and the difference between the present and desired velocity multiplied by a time constant, τ. In both error signals, τ represents the interval for which the simple linear prediction about the target behavior is made by the control system (Engel and Soechting 2000). The temporal profiles of the correlograms between MSE and DE and tracking speed are consistent with these signals participating in intermittent error correction mechanism.

Since the BG-RIPID model is only for one dimensional, it is not possible to test if the DE can be a key factor to trigger a submovement. The MSE can be written as

$$\begin{aligned} MSE(t) &\approx x_{target}(t) - x(t) + \tau(\dot{x}_{target}(t) - \dot{x}(t)) \\ MSE(s) &\approx (1 + \tau s)\left(X_{target}(s) - X(s)\right), \end{aligned} \tag{4.2}$$

where the second equation is in Laplace domain. Thus, the MSE can be seen as a first order linear predictor of the error. In the RIPID model, the error signal fed to the BG, $e_a(t)$ can be expressed, with an abuse of notations, as below:

$$
\begin{aligned}
e_a(t) &= x_{target}(t) - F_2 x(t-\tau_{aff}) - \frac{I_3}{s+I_2}\left(\frac{I_a}{s}e_a(t) - F_3 x(t-\tau_{aff})\right) \\
e_a(t) &= \frac{s(s+I_2)}{s(s+I_2)+I_3 I_a}\left(x_{target} - x(t-\tau_{aff})\right) \\
&\quad + \frac{s((I-F_2)(s+I_2)+I_3 I_a)}{s(s+I_2)+I_3 I_a} x(t-\tau_{aff}) \\
e_a(t) &= \left(1 - \frac{I_3 I_a}{s(s+I_2)+I_3 I_a}\right)\left(x_{target} - x(t-\tau_{aff})\right) \\
&\quad + \left((I-F_2) + \frac{sI_3F_3 - (I-F_2)I_3 I_a}{s(s+I_2)+I_3 I_a}\right) x(t-\tau_{aff}).
\end{aligned} \tag{4.3}
$$

So when the value of $e_a(t)$ reaches zero the motor command ends. $e_a(t)$ can be seen as a predicted tracking error because it goes to zero more quickly than the true error because of the pure derivative acting on the pure error signal $x_{target} - x(t-\tau_{aff})$ as in the first term of Eq. (4.3). In addition, an integral of $e_a(t)$ can potentially become $x_{target}(t)$ so that by choosing I_a and F_3 properly, then $\left(\frac{I_a}{s}e_a(t) - F_3 x(t-\tau_{aff})\right)$ could participate to partially cancel an error $x_{target}(t) - F_2 x(t-\tau_{aff})$. Thus based on this mechanism, movement ceases when predicted error goes to zero. This mechanism is at least consistent with the mechanism of neurosurgical ablation of tremor (Massaquoi 2006b). At this point, it is not clear about the connection between two types of the errors defined by Eq. (4.2) and (4.3) each of which is used in different model to characterize potential sources of submovement initiations. The two mechanisms potentially function in a very similar way. Both formulations use the error signals instead of position or velocity alone. In fact, in the BG-RIPID the integrator doesn't get turned on again unless the error gets larger than a threshold. One possible difference in the models is that the MSE based model may cause the motor command generation mechanism to have to wait until the error is fairly large before initiating a submovement. The BG-RIPID would start rapidly then turn off when caught up. Furthermore, One potentially a huge difference between the two approaches is that the BG-RIPID model does not assume any submovement template and performs scaling of submovements automatically according to the reference command as in a model in Fig. 4-2, while the MSE model may require

a template and corresponding scaling of such a template based on the reference command as in a model in Fig 4-3. Thus, these possible similarity and difference should be explored further.

Although the nature of the task is different from that used in this chapter, Vaillancourt et al. (2003) used a visually guided force task with different frequency of visual feedback to show three findings. First, force variability was reduced with more frequent visual feedback and that infrequent visual feedback did not result in activation in lateral cerebellum whereas frequent visual feedback did. On the other hand, anterior intermediate cerebellum was consistently active. Second, the parietal and premotor cortex were also active during grip force with infrequent visual feedback. Third, right inferior parietal lobule, dorsal premotor cortex, and ventral premotor cortex had greater activation in the frequent compared with the infrequent grip force condition. Thus, the frequency of the visual feedback can be used to differentially modulate the neural activation related to visuomotor processing in the key motor areas such as cerebellum, parietal and premotor cortices. Further study of this type needs to be carried out in order to accumulate anatomical and physiological evidence to understand the generation of intermittency from the neural circuitry.

Chapter 5

Linear parameter varying (LPV) formulation

5.1 Introduction

So far in the previous chapters, the feasibility of the RIPID formulation was supported by developing an anatomical and physiological regression model, the RICSS model. The RICSS model included anatomical specificity of the cerebrocerebellar system and was capable to grossly reproduce the averaged simple spike firing patterns of a pool of the individual Purkinje cells using the signals used to control the arm movements in the RIPID. Then, in order to explain some features of the intermittency observed in the monkey data, an anatomically and physiologically feasible intermittent command generator, based on a model of cortico-basal ganglia loop suggested by Mao (2005), was integrated into the RIPID formulation. This extended model, the BG-RIPID model, managed to, preliminarily in one dimension, qualitatively account for the invariant distributions of the pulse durations across the target speeds as well as the affine relation between the amplitudes and durations of the speed pulses while the command to be traced was a smooth ramp position. Thus, now the next question is: Is the RIPID formulation capable to account for a larger workspace and faster movements, in particular, if the direction of a movement changes rapidly ? In Chapter 3, one set of

controller gains in the RIPID was tuned to cover the speed range tested in the experiment. However, if the gain set used can't achieve the same level of the tracking performance as that of the speed range in the experiment, then it may be necessary to extend the control structure. Fig. 5-1 below shows the kinematic performance for the tracking speed 1.5 times faster than the fastest speed that the monkey performed in the experiment. The controller gains used in the simulation are the same as those used in Chapter 3.

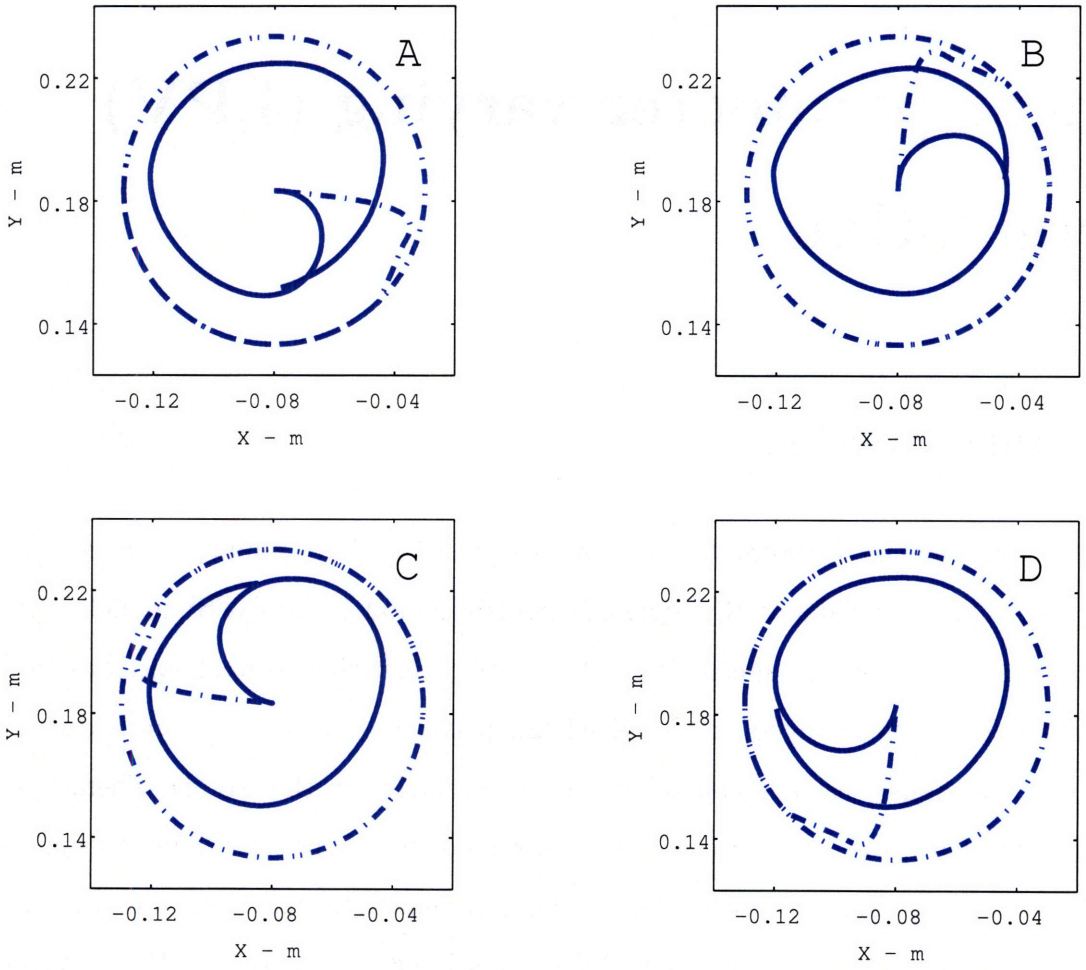

Figure 5-1: RIPID model simulated hand motion for the tracking speed 1.5 times faster than the fastest speed that the monkey performed in the experiment described in Chapter 3. In all four figures, the dashed blue lines show the Cartesian intended hand position and the solid blue lines the tracking simulation. A through D represent different launch angles, 0, 90, 180, and 270 degree respectively.

There are two distinct features in the response of the RIPID model. First, the scaling

is inappropriate (see Fig. 3-6 for comparison). Second, the path is eccentric. In particular, regardless of the launch angles, the paths are further away from the reference path along 2 o'clock through 8 o'clock. It is clear that the gain set that was appropriate for the low speed range used in the primate experiment could not handle the more dynamically demanding situation.

In the case of the RICSS model, it suggests that cerebellar PCs receive cortically-processed signals that are modulated by the state information conveyed through DSCT as shown with a dashed line with η in Fig. 3-3. More abstractly, such a scheme can be shown as below:

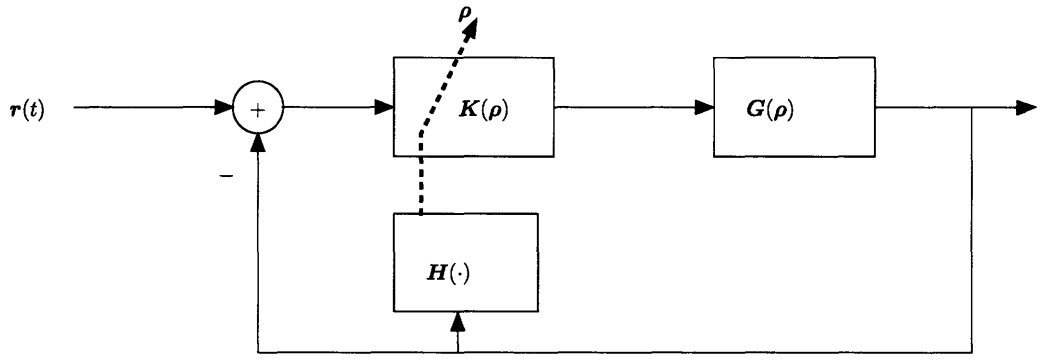

Figure 5-2: A realization of RIPID/RICSS structure as a gain-scheduling control system.

where $\boldsymbol{\rho}$ is a scheduling variable that may be a function ($\mathbf{H}(\cdot)$) of the state of the plant, $\mathbf{G}(\boldsymbol{\rho})$, $\mathbf{K}(\boldsymbol{\rho})$ is a set of controllers modulated, and $\mathbf{r}(t)$ is an exogenous input, for example, a reference signal.

There are many ways to design gainscheduling controllers. Classical gain scheduling scheme is typically based on a set of linear time invariant (LTI) controllers designed on a set of equilibrium points of a plant. At each equilibrium point, optimal and robust control synthesis for LTI systems can be applied to meet robustness and performance criteria locally. Often, a transition among the resulting LTI controllers is made by interpolating them based on the evolution of the scheduling variables. However, this method can be problematic especially when the scheduling variables have fast dynamics and usually requires extensive simulations to ensure the stability and performance because the synthesis cannot account

for either stability or performance (Shamma and Athans 1990; Lawrence and Rugh 1995).

Kajiwara et al. (1999) presented a comprehensive application of linear fractional transformation and polytopic control techniques for linear parameter varying (LPV) systems to the control of an arm-driven inverted pendulum. The authors showed that when the controllers were implementable, it has been observed that LPV controllers outperform fixed μ controllers both in robustness and performance. These observations were further confirmed by simulations but more importantly by a number of records on the physical experiment. Thus, in conjunction with the proposed structure of the RICSS model, it is reasonable to use the LPV formulation as a first step feasibility test for the RIPID model.

Furthermore, an amount of theoretical progress and practical applications of gain scheduling control has significantly increased in the past few decades, but applications of such control scheme to physiological systems have not been performed until recently. Hunt et al. (1998) applied a linear quadratic Gaussian (LQG) controller design procedure to control an ankle joint of paraplegic patients by applying electrical stimulation. The authors were interested in functional electrical stimulation (FES) in which the aim was to restore paralyzed muscles to some normal motor activities. This idea was extended by an introduction of gain scheduled controllers. The scheduling variable was a knee joint position. Six local controllers were designed and each controller was a state-feedback linear quadratic controller designed around an operation point. The proposed controller showed good tracking and robustness properties on the full range of extension on the knee joint angle of a physiological model simulator representing the knee joint dynamics. Furthermore, the authors showed that single linear controller was not suitable for the considered application since its performance was not satisfactory in the global operating range.

Taken together, it is important to develop a gain scheduling control synthesis to test the extendability of the RIPID model. Based on the theoretical tractability as well as a structural similarity to the RIPID model, an LPV formulation was used.

5.2 Theoretical background

Basic background on LPV synthesis is briefly introduced in this section. For more thorough materials, the readers should refer to Boyd et al. (1994); Apkarian and Gahinet (1995), and Apkarian et al. (1995).

The synthesis procedure discussed here applied to affine parameter-dependent plants described below:

$$\mathbf{P}(\cdot,\boldsymbol{\rho}) = \begin{cases} \dot{\mathbf{x}} &= \mathbf{A}(\boldsymbol{\rho})\mathbf{x} + \mathbf{B}_1(\boldsymbol{\rho})\mathbf{w} + \mathbf{B}_2\mathbf{u} \\ \mathbf{y} &= \mathbf{C}_1(\boldsymbol{\rho})\mathbf{x} + \mathbf{D}_{11}(\boldsymbol{\rho})\mathbf{w} + \mathbf{D}_{12}\mathbf{u} \\ \mathbf{z} &= \mathbf{C}_2\mathbf{x} + \mathbf{D}_{21}\mathbf{w} + \mathbf{D}_{22}\mathbf{u} \end{cases} \tag{5.1}$$

where

$$\boldsymbol{\rho}(t) = [\rho_1(t), \ldots, \rho_n(t)], \quad \underline{\rho}_i \leq \rho_i(t) \leq \overline{\rho}_i \tag{5.2}$$

is a time-varying vector of scheduling variables each component of which is bounded by its minimum and maximum values $\underline{\rho}_i$ and $\overline{\rho}_i$ respectively, n is the number of the scheduling variables, $\mathbf{A}(\cdot)$, $\mathbf{B_1}(\cdot)$, $\mathbf{C_1}(\cdot)$, and $\mathbf{D_{11}}(\cdot)$, are affine functions of $\boldsymbol{\rho}(t)$. Note that $\boldsymbol{\rho}(t)$ may contain part of the state vector itself , assuming that the corresponding states are accessible to measurement.

If the scheduling parameter vector $\boldsymbol{\rho}(t)$ takes values in a box of $\mathbb{R}^n$ with corners $\{\boldsymbol{\Pi}_i\}$, $i = 1, \ldots, N = 2^n$, the plant $\mathbf{P}(\cdot,\boldsymbol{\rho})$ ranges in a matrix polytope with vertices $\mathbf{V}(\boldsymbol{\Pi}_i)$. Namely, given any convex decomposition

$$\boldsymbol{\rho}(t) = \sum_{i=1}^{N} \alpha_i \boldsymbol{\Pi}_i, \quad \alpha_i \geq 0, \quad \sum_{i=1}^{N} \alpha_i = 1 \tag{5.3}$$

of $\boldsymbol{\rho}$ over the corners of the parameter box, then the parameter dependent system is given by

$$\mathbf{P}(\cdot,\boldsymbol{\rho}) = \sum_{i=1}^{N} \alpha_i \mathbf{V}(\boldsymbol{\Pi}_i). \tag{5.4}$$

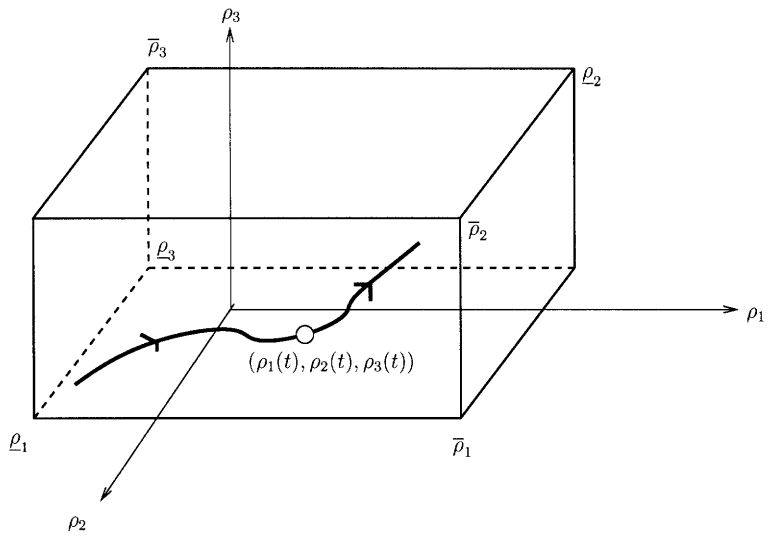

Figure 5-3: Polytope configuration. This example shows the case of 3 scheduling variables.

Thus, we would like to find a set of parameter dependent controllers taking the following form:

$$\mathbf{K}(\cdot,\rho) = \begin{cases} \dot{\boldsymbol{\xi}} & = \mathbf{A}_K(\boldsymbol{\rho})\boldsymbol{\xi} + \mathbf{B}_K(\boldsymbol{\rho})\mathbf{y} \\ \mathbf{u} & = \mathbf{C}_K(\boldsymbol{\rho})\boldsymbol{\xi} + \mathbf{D}_K(\boldsymbol{\rho})\mathbf{y} \end{cases}, \tag{5.5}$$

with the following vertex property:

Given the convex decomposition $\boldsymbol{\rho}(t) = \sum_{i=1}^{N} \alpha_i \boldsymbol{\Pi}_i$ of the current parameter value $\boldsymbol{\rho}(t)$, the values of $\mathbf{A}_K(\boldsymbol{\rho})$, $\mathbf{B}_K(\boldsymbol{\rho})$, $\mathbf{C}_K(\boldsymbol{\rho})$, and $\mathbf{D}_K(\boldsymbol{\rho})$ are expressed as a linear combination of $\mathbf{A}_K(\boldsymbol{\Pi}_i)$, $\mathbf{B}_K(\boldsymbol{\Pi}_i)$, $\mathbf{C}_K(\boldsymbol{\Pi}_i)$, and $\mathbf{D}_K(\boldsymbol{\Pi}_i)$, $i = 1, \cdots, N$ at the corners of the parameter box by

$$\begin{pmatrix} \mathbf{A}_K(\boldsymbol{\rho}) & \mathbf{B}_K(\boldsymbol{\rho}) \\ \mathbf{C}_K(\boldsymbol{\rho}) & \mathbf{D}_K(\boldsymbol{\rho}) \end{pmatrix} = \sum_{i=1}^{N} \alpha_i \begin{pmatrix} \mathbf{A}_K(\boldsymbol{\Pi}_i) & \mathbf{B}_K(\boldsymbol{\Pi}_i) \\ \mathbf{C}_K(\boldsymbol{\Pi}_i) & \mathbf{D}_K(\boldsymbol{\Pi}_i) \end{pmatrix}. \tag{5.6}$$

For this class of controllers, we would like to consider the gain-scheduled $\mathcal{H}_\infty$ problem for the interconnection shown in Fig. 5-4.

The objective is to design a gain-scheduled controller $\mathbf{K}(\cdot, \boldsymbol{\rho})$ that satisfies:

- the vertex property (Eq.(5.6))

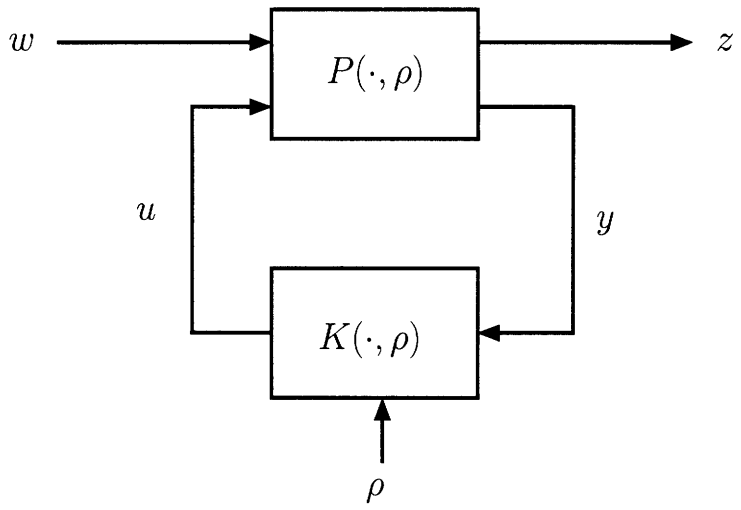

Figure 5-4: Formal LPV formulation

- the closed-loop system is stable for all admissible parameter trajectories $\boldsymbol{\rho}(t)$

- a guaranteed L_2-gain bound $\gamma > 0$ for the closed loop system from the generalized disturbance signal $\mathbf{w}$ to the error signal $\mathbf{z}$, i.e.,

$$\int_0^T \mathbf{z}^T \mathbf{z}\, dt \leq \gamma^2 \int_0^T \mathbf{w}^T \mathbf{w}\, dt,\ \forall T \geq 0 \tag{5.7}$$

  and all the admissible trajectories $\boldsymbol{\rho}$.

Theorem (Apkarian and Gahinet 1995)

Suboptimal scaled $\mathcal{H}_\infty$ problem is solvable if and only if there exist pairs of symmetric

matrices $\mathbf{R} \in \mathbb{R}^{n\times n}$ and $\mathbf{Q} \in \mathbb{R}^{n\times n}$ such that

$$\begin{pmatrix} \mathcal{N}_{12} & \mathbf{0} \\ \mathbf{0} & \mathbf{I} \end{pmatrix}^T \begin{pmatrix} \mathbf{A}_i\mathbf{R} + \mathbf{R}\mathbf{A}_i^T & \mathbf{R}\mathbf{C}_{1i}^T & \mathbf{B}_{1i} \\ \mathbf{C}_{1i}\mathbf{R} & -\gamma\mathbf{I} & \mathbf{D}_{11i} \\ \mathbf{B}_1^T & \mathbf{D}_{11i}^T & -\gamma\mathbf{I} \end{pmatrix} \begin{pmatrix} \mathcal{N}_{12} & \mathbf{0} \\ \mathbf{0} & \mathbf{I} \end{pmatrix} < \mathbf{0}, \tag{5.8}$$

$$\begin{pmatrix} \mathcal{N}_{21} & \mathbf{0} \\ \mathbf{0} & \mathbf{I} \end{pmatrix}^T \begin{pmatrix} \mathbf{A}_i^T\mathbf{Q} + \mathbf{Q}\mathbf{A}_i & \mathbf{Q}\mathbf{B}_{1i} & \mathbf{C}_{1i}^T \\ \mathbf{B}_{1i}^T\mathbf{Q} & -\gamma\mathbf{I} & \mathbf{D}_{11i}^T \\ \mathbf{C}_{1i} & \mathbf{D}_{11i} & -\gamma\mathbf{I} \end{pmatrix} \begin{pmatrix} \mathcal{N}_{21} & \mathbf{0} \\ \mathbf{0} & \mathbf{I} \end{pmatrix} < \mathbf{0}, \tag{5.9}$$

$$\begin{pmatrix} \mathbf{R} & \mathbf{I} \\ \mathbf{I} & \mathbf{Q} \end{pmatrix} \geq \mathbf{0}, \tag{5.10}$$

where

$$\begin{pmatrix} \mathbf{A}_i & \mathbf{B}_{1i} \\ \mathbf{C}_{1i} & \mathbf{D}_{11i} \end{pmatrix} = \begin{pmatrix} \mathbf{A}(\mathbf{\Pi}_i) & \mathbf{B}(\mathbf{\Pi}_i) \\ \mathbf{C}_1(\mathbf{\Pi}_i) & \mathbf{D}_{11}(\mathbf{\Pi}_i) \end{pmatrix}$$

for $i = 1, \ldots, N$ and $\mathcal{N}_{12}$ and $\mathcal{N}_{21}$ are bases of the null spaces of $(\mathbf{B}_2^T, \mathbf{D}_{12}^T)$ and $(\mathbf{C}_2, \mathbf{D}_{21})$, respectively. Recall that $N = 2^n$ where n is the number of the scheduling parameter. Thus, there will be $2^n + 1$ linear matrix inequalities (LMI) such as ones in Eqn's 5.8 $\sim$ 5.10. In this formulation, it is assumed $\mathbf{B}_2, \mathbf{C}_2, \mathbf{D}_{12}$, and $\mathbf{D}_{21}$ to be independent of the scheduling parameter vector $\boldsymbol{\rho}(t)$. This assumption (Apkarian et al. 1995) will be satisfied below by placing a lowpass filter, an excitation-contraction coupling filter in the arm formulation, so that the overall plant is realized as shown in Eq (5.1). To enforce the performance and robustness requirements, we can use the loop shaping criterion summarizing RMS gain constraint

$$\left\| \begin{matrix} \mathbf{W}_1\mathbf{S} \\ \mathbf{W}_2\mathbf{T} \end{matrix} \right\|_\infty < 1, \tag{5.11}$$

where $\mathbf{S}$ and $\mathbf{T}$ are a sensitivity function and a complementary sensitivity function defined

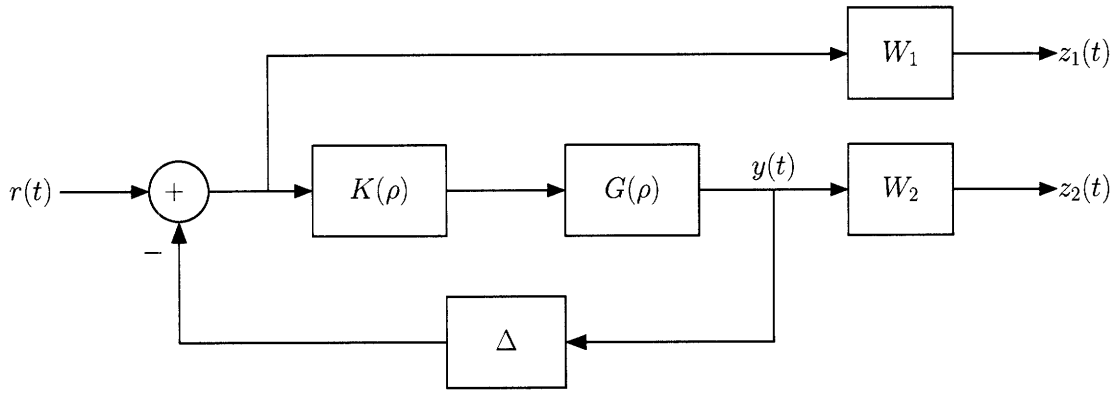

Figure 5-5: System diagram for loopshaping with two weighting transfer functions $\mathbf{W}_1$ and $\mathbf{W}_2$. Δ is a delay operator.

as

$$\begin{aligned} \mathbf{S} &= (\mathbf{I} + \mathbf{G}(\boldsymbol{\rho})\mathbf{K}(\boldsymbol{\rho}))^{-1} \\ \mathbf{T} &= \mathbf{G}(\boldsymbol{\rho})\mathbf{K}(\boldsymbol{\rho})\,(\mathbf{I} + \mathbf{G}(\boldsymbol{\rho})\mathbf{K}(\boldsymbol{\rho}))^{-1}. \end{aligned}$$

5.3 Formulation for the two-link arm plant

In this formulation, we consider the nonlinearity only due to inertia and viscosity terms, i.e., Eq. (3.1) is simplified to have a linear muscle model:

$$\boldsymbol{\tau}(t) = \mathbf{H}(\boldsymbol{\theta}(t))\ddot{\boldsymbol{\theta}}(t) + \mathbf{C}(\boldsymbol{\theta}(t), \dot{\boldsymbol{\theta}}(t))\dot{\boldsymbol{\theta}}(t) \tag{5.12}$$

$$\boldsymbol{\tau}(t) = \mathbf{K}\mathbf{u}(t) \tag{5.13}$$

$$\mathbf{u}(t) = \mathbf{EC}\,(\mathbf{r}(t) - \boldsymbol{\theta}(t - t_{aff})) \tag{5.14}$$

where $\mathbf{H}(\boldsymbol{\theta})$ and $\mathbf{C}(\boldsymbol{\theta}, \dot{\boldsymbol{\theta}})$ are the inertia and viscosity matrices respectively, and $\mathbf{K}$ is a muscle stiffness matrix, and the torque $\boldsymbol{\tau}$ is a linear function of the input signal $\mathbf{u}$ which is the output of the EC filter as in Chapter 3. Eq. (5.14), should be interpreted as a mapping of the difference between the reference signal $\mathbf{r}(t)$ and the delayed afferent joint

angles $\boldsymbol{\theta}(t - t_{aff})$, where t_{aff} is the afferent delay amount, and the output of the EC filter, $\mathbf{u}$ through the LTI system $\mathbf{EC}$. The inertia matrix can be seen as an affine function of the elbow angle θ_e:

$$\mathbf{H}(\boldsymbol{\theta}) = \mathbf{H}_0 + \cos\theta_e \mathbf{H}_1, \tag{5.15}$$

where

$$\mathbf{H}_0 = \begin{bmatrix} h_1 + h_2 + m_2 l_1^2 & h_2 \\ h_2 & h_2 \end{bmatrix}, \quad \mathbf{H}_1 = m_2 l_1 \bar{l}_2 \begin{bmatrix} 2 & 1 \\ 1 & 0 \end{bmatrix}. \tag{5.16}$$

Following the similar manner, the viscosity matrix $\mathbf{C}(\boldsymbol{\theta}, \dot{\boldsymbol{\theta}})$ can be affinely decomposed as follows:

$$\mathbf{C}(\boldsymbol{\theta}, \dot{\boldsymbol{\theta}}) = \mathbf{C}_0 + \sin\theta_e \dot{\theta}_s \mathbf{C}_1 + \sin\theta_e \dot{\theta}_e \mathbf{C}_2, \tag{5.17}$$

where

$$\mathbf{C}_0 = \mathbf{0}, \quad \mathbf{C}_1 = m_2 l_1 \bar{l}_2 \begin{bmatrix} 0 & -1 \\ 1 & 0 \end{bmatrix}, \quad \mathbf{C}_2 = m_2 l_1 \bar{l}_2 \begin{bmatrix} -1 & -1 \\ 0 & 0 \end{bmatrix}. \tag{5.18}$$

Thus, the arm dynamics can be expressed as:

$$\mathbf{H}(\boldsymbol{\theta})\ddot{\boldsymbol{\theta}} = -\mathbf{C}(\boldsymbol{\theta}, \dot{\boldsymbol{\theta}})\dot{\boldsymbol{\theta}} + \mathbf{K}\mathbf{u} \tag{5.19}$$

$$(\mathbf{H}_0 + \cos\theta_e \mathbf{H}_1)\ddot{\boldsymbol{\theta}} = -\left(\mathbf{C}_0 + \sin\theta_e \dot{\theta}_s \mathbf{C}_1 + \sin\theta_e \dot{\theta}_e \mathbf{C}_2\right)\dot{\boldsymbol{\theta}} + \mathbf{K}\mathbf{u} \tag{5.20}$$

$$\begin{aligned} \ddot{\boldsymbol{\theta}} = &-(\mathbf{H}_0 + \cos\theta_e \mathbf{H}_1)^{-1}\left(\mathbf{C}_0 + \sin\theta_e \dot{\theta}_s \mathbf{C}_1 + \sin\theta_e \dot{\theta}_e \mathbf{C}_2\right)\dot{\boldsymbol{\theta}} \\ &+ (\mathbf{H}_0 + \cos\theta_e \mathbf{H}_1)^{-1}\mathbf{K}\mathbf{u}, \end{aligned} \tag{5.21}$$

or

$$\underbrace{\begin{bmatrix} \ddot{\boldsymbol{\theta}} \\ \dot{\boldsymbol{\theta}} \end{bmatrix}}_{\dot{\boldsymbol{\Theta}}} = \underbrace{\begin{bmatrix} -\left(\mathbf{H}_0 + \cos\theta_e \mathbf{H}_1\right)^{-1}\left(\mathbf{C}_0 + \sin\theta_e\dot{\theta}_s\mathbf{C}_1 + \sin\theta_e\dot{\theta}_e\mathbf{C}_2\right) & \mathbf{0} \\ \mathbf{I} & \mathbf{0} \end{bmatrix}}_{\mathbf{A}_p(\boldsymbol{\rho})} \underbrace{\begin{bmatrix} \dot{\boldsymbol{\theta}} \\ \boldsymbol{\theta} \end{bmatrix}}_{\boldsymbol{\Theta}}$$

$$+ \underbrace{\begin{bmatrix} \left(\mathbf{H}_0 + \cos\theta_e \mathbf{H}_1\right)^{-1}\mathbf{K} \\ \mathbf{0} \end{bmatrix}}_{\mathbf{B}_p(\boldsymbol{\rho})} \mathbf{u} \tag{5.22}$$

$$\boldsymbol{\theta} = \underbrace{\begin{bmatrix} \mathbf{0} & \mathbf{I} \end{bmatrix}}_{\mathbf{C}_p} \boldsymbol{\Theta}. \tag{5.23}$$

The input to the EC filter, $\mathbf{u}_{EC}$ is related to the output, $\mathbf{u}$ as in the following transfer function

$$\mathbf{U} = \frac{\kappa^2}{(s+\kappa)^2} \begin{bmatrix} 1 & 0 \\ 0 & 1 \end{bmatrix} \mathbf{U}_{EC},$$

where $\mathbf{U}$ and $\mathbf{U}_{EC}$ are the Laplace transforms of $\mathbf{u}$ and $\mathbf{u}_{EC}$ respectively. Its relation in the state space form is given by:

$$\begin{aligned} \dot{\boldsymbol{\zeta}} &= \mathbf{A}_{EC}\boldsymbol{\zeta} + \mathbf{B}_{EC}\mathbf{u}_{EC} \\ \mathbf{u} &= \mathbf{C}_{EC}\boldsymbol{\zeta}. \end{aligned}$$

Thus the augmented parameterized plant from the input of the EC filter to the joint angles is

$$\underbrace{\begin{bmatrix} \dot{\boldsymbol{\Theta}} \\ \dot{\boldsymbol{\zeta}} \end{bmatrix}}_{\dot{\boldsymbol{\zeta}}_a} = \underbrace{\begin{bmatrix} \mathbf{A}_P(\boldsymbol{\rho}) & \mathbf{B}_P(\boldsymbol{\rho})\mathbf{C}_{EC} \\ \mathbf{0} & \mathbf{A}_{EC} \end{bmatrix}}_{\mathbf{A}_a(\boldsymbol{\rho})} \underbrace{\begin{bmatrix} \boldsymbol{\Theta} \\ \boldsymbol{\zeta} \end{bmatrix}}_{\boldsymbol{\zeta}_a} + \underbrace{\begin{bmatrix} \mathbf{0} \\ \mathbf{B}_{EC} \end{bmatrix}}_{\mathbf{B}_a} \mathbf{u} \tag{5.24}$$

$$\boldsymbol{\theta} = \underbrace{\begin{bmatrix} \mathbf{C}_p & \mathbf{0} \end{bmatrix}}_{\mathbf{C}_a} \underbrace{\begin{bmatrix} \boldsymbol{\Theta} \\ \boldsymbol{\zeta} \end{bmatrix}}_{\boldsymbol{\zeta}_a}. \tag{5.25}$$

Then, the augmented system has parameter dependence only on $\mathbf{A}_a(\boldsymbol{\rho})$.

In this chapter, only the configuration dependency, i.e., the effect of the elbow angle, θ_e through the inertial matrix $\mathbf{H}(\boldsymbol{\theta})$ is examined. This is because of the following reasons. First, including angular velocity terms requires exponential addition of LMI's to be solved and implementation of corresponding controllers. As there are two parameters in the viscosity matrix in Eqn 5.17, i.e., $\sin\theta_e\dot{\theta}_s$ and $\sin\theta_e\dot{\theta}_e$, total increase of the number of the scheduling parameters would be 2×2 where additional 2 comes from the inversion of the inertial matrix. Thus, the number of additional LMI's to be solved will be $2^{2+4}-2^2=60$. Secondly, the viscosity matrix contains terms with joint velocities, $\sin\theta_e\dot{\theta}_s$ and $\sin\theta_e\dot{\theta}_e$. Thus, the size of workspace is not sufficient to estimate the bounds of the scheduling parameters unless wide variety of movements with varying velocity in the workspace is performed. Therefore, in the case under the consideration, i.e., $\dot{\theta}_e=\dot{\theta}_s=0$, there is effectively only one parameter, θ_e characterizing the scheduling variables. Thus, $\mathbf{A}_p(\boldsymbol{\rho})$ is now a constant matrix as $\mathbf{C}_0=\mathbf{0}$ and at equilibrium $\dot{\theta}_s=\dot{\theta}_e=0$, i.e.,

$$\mathbf{A}_p(\boldsymbol{\rho})=\begin{bmatrix}\mathbf{0} & \mathbf{0}\\ \mathbf{I} & \mathbf{0}\end{bmatrix}. \tag{5.26}$$

Yet, $\mathbf{H}(\boldsymbol{\theta})^{-1}$ in $\mathbf{B}_p(\boldsymbol{\rho})$ contains two parameters both of which are functions of θ_e:

$$\mathbf{H}(\boldsymbol{\theta})^{-1}=\rho_1(\theta_e)\begin{bmatrix}h_2 & -h_2\\ -h_2 & h_1+h_2+m_2l_1^2\end{bmatrix}+\rho_2(\theta_e)\begin{bmatrix}0 & -m_2l_1\bar{l}_2\\ -m_2l_1\bar{l}_2 & 2m_2l_1\bar{l}_2\end{bmatrix}$$

where

$$\begin{aligned}\rho_1(\theta_e) &= \frac{1}{h_1h_2+h_2m_2l_1^2-(m_2l_1\bar{l}_2\cos\theta_e)^2},\\ \rho_2(\theta_e) &= \frac{\cos\theta_e}{h_1h_2+h_2m_2l_1^2-(m_2l_1\bar{l}_2\cos\theta_e)^2}.\end{aligned}$$

The LPV controller that depends on ρ_1 and ρ_2 are denoted as LPV2. Note that this formulation does not account for the rate variation of ρ_1 and ρ_2 directly in addition to excluding

the joint velocities themselves. Therefore, the arm dynamics used here is still a subset of the arm dynamics which only contains the inertial effect.

Variation of the denominators in Eq's (5.27,5.27), or the determinant of the inertia matrix $\mathbf{H}$ is relatively small given all the physical parameters used as well as the fact that $|\cos\theta_e| \leq 1$ for all possible values of θ_e. Thus, empirically we can approximate the determinant as a constant by evaluating it at the center of the workspace. Then, the $\mathbf{H}(\boldsymbol{\theta})^{-1}$ can be seen as

$$\begin{aligned}\mathbf{H}(\boldsymbol{\theta})^{-1} \approx & \frac{1}{h_1h_2 + h_2m_2l_1^2 - (m_2l_1\bar{l}_2\cos\theta_e^a)^2}\begin{bmatrix} h_2 & -h_2 \\ -h_2 & h_1+h_2+m_2l_1^2 \end{bmatrix} \\ & + \frac{\rho_3(\theta_e)}{h_1h_2 + h_2m_2l_1^2 - (m_2l_1\bar{l}_2\cos\theta_e^a)^2}\begin{bmatrix} 0 & -m_2l_1\bar{l}_2 \\ -m_2l_1\bar{l}_2 & 2m_2l_1\bar{l}_2 \end{bmatrix}, \end{aligned} \tag{5.27}$$

where

$$\rho_3(\theta_e) = \cos\theta_e,$$

and θ_e^a is the elbow angle corresponding to the configuration where the hand is at the center of the workspace. Then, using this approximated inverse of the inertia matrix, an LPV controller that depends only on one parameter, ρ_3 is designed and is denoted as LPV1.

In order to use a polytope based LPV synthesis, we need to set, or find, the lower and upper bounds for all the scheduling parameters, ρ_i to define the vertices for the design process. To find the bounds on ρ_i, the inverse kinematic relation between the hand location in Cartesian coordinate (x_h, y_h) and the joint angles (θ_s, θ_e) and the size of the Cartesian workspace are used as follows:

$$\begin{aligned} \underline{\rho}_i &= \min_{\theta_e\in[\underline{\theta}_e,\bar{\theta}_e]} \rho_i, \\ \overline{\rho}_i &= \max_{\theta_e\in[\underline{\theta}_e,\bar{\theta}_e]} \rho_i, \\ \underline{\rho}_i &\leq \rho_i(t) \leq \overline{\rho}_i \quad \forall i \end{aligned}$$

where $\underline{\theta}_e$ and $\overline{\theta}_e$ are the minimum and the maximum of the elbow joint angle computed from

the size of the workspace through the inverse kinematics.

Low frequency tracking performance can be emphasized with a choice of the weighting $\mathbf{W}_1$ to be a lowpass filter. In this study, a parameter independent frequency weighting matrix shown below is used:

$$\mathbf{W}_1(s) = \begin{bmatrix} \frac{50}{(s+5)^2} & 0 \\ 0 & \frac{50}{(s+5)^2} \end{bmatrix}.$$

The weighting filter for the complementary sensitivity function, $\mathbf{W}_2(s)$ is set to be unity.

5.4 Simulation method

The arm configuration is shown in Fig. 5-6. The workspace is a 40 cm $\times$ 40 cm square box and is enclosed by the dashed-box. The two-joint arm is characterized by the two joint angles θ_s and θ_e, the shoulder and elbow angles respectively. The location of the hand is denoted by the purple circle with (x_h, y_h). First to see the effect of the LPV controllers vs. one $\mathcal{H}_\infty$ controller over the workspace, tracking phase of the circular tracking similar to that shown in Fig. 5-1 is performed. Second, a series of double step task is performed. The motivation to perform a series of double step task is to see how LPV controllers handle directional changes by looking at one directional change during a movement as opposed to a series of directional changes in a continuous circular movement.

To implement a sudden direction change during a point-to-point movement, a set of double step tasks is employed. Additional points are included in the workspace. The center of the workspace is denoted by the red circle with (x_c, y_c). The center also acts as the first target of the task described below. The four green circles are possible starting and termination points of the task. Each green circle is denoted labeled with north (N), west(W), south (S), and east (E), respectively. The plant parameters as well as the location of the center of the workspace used in this section are shown in Appendix A.2. In each set, starting position is one of the four green targets. Then, initially the hand is driven to the center

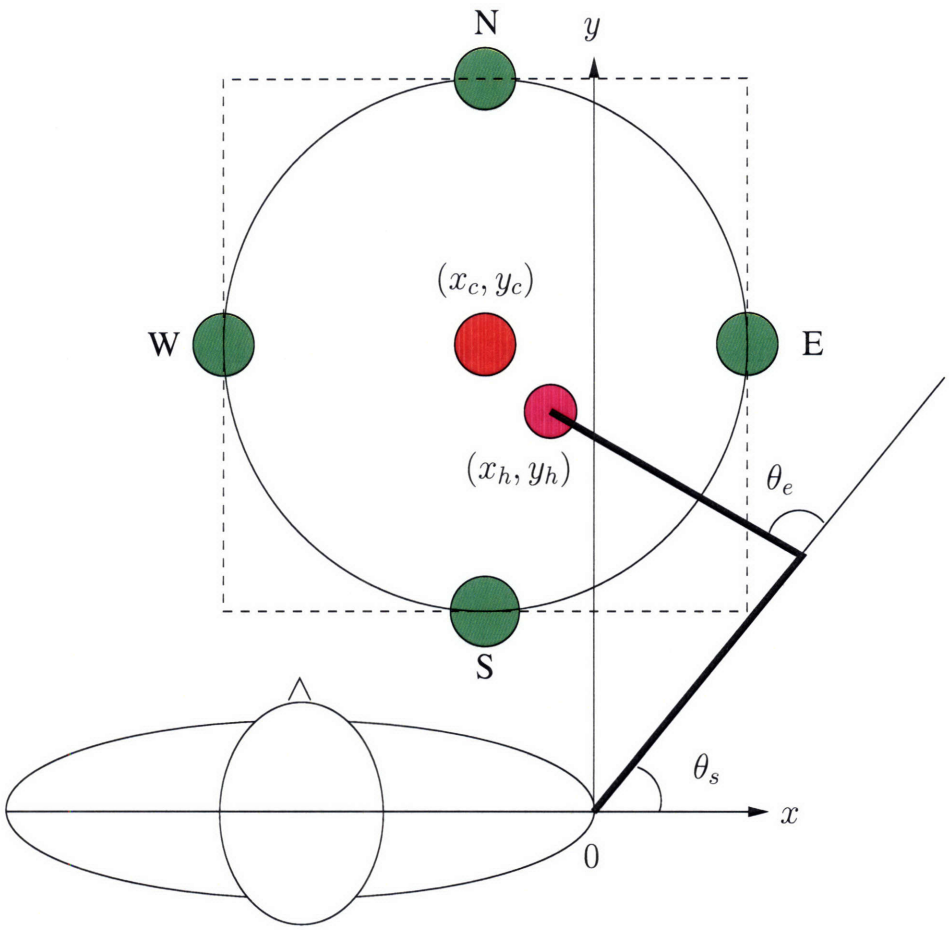

Figure 5-6: The arm configuration for the simulation.

target by a minimum jerk command with a duration of 350 ms. During or at the end of the initial movement, a second segment of the movement aiming to a fixed target out of the three green targets, excluding the starting point out of the four, is sent to the arm plant. For example, one possible sequence is from N to center to W. The second segment of the movement is also characterized by the minimum jerk profile with a duration of 350 ms and is superimposed to the first segment. The timing of the initiation of the second movement are 50, 100, 150, 200, 250, 300, and 350 ms from the onset of the first segment. Thus, seven simulations are performed in each set. Total of 12 sets, 4 starting positions and 3 possible second targets for each starting position, are performed.

5.5 Simulation results

Two LPV controllers, LPV1 and LPV2, and an $\mathcal{H}_\infty$ controller for the simplified two-joint arm plant were designed. The single $\mathcal{H}_\infty$ controller was designed based on the linearized two-link arm plant around (x_c, y_c). The order, based on the number of the states, is 12 for both the single $\mathcal{H}_\infty$ controller and for each controller from the LPV syntheses at each vertex as the arm plant itself has 4 states, the EC activation filter 4, and the weighing filter on the error 4. The simulation was implemented in Simulink^{TM}. `ode14x` was chosen as the integration scheme for numerical stability.

Achievable performance that is measured in terms of the spectral radius γ, as in Eqn 5.7, is summarized in Table 5.1. For all designs, the achievable values of γ are more than unity, i.e., the objectives are not met. Note that weighting matrices for all the cases were the same so that fine loopshaping was not performed.

	single $\mathcal{H}_\infty$	LPV1	LPV2
γ	1.0140	1.0184	1.0211

Table 5.1: Achievable performance of the controllers.

5.5.1 Circular tracking performance

First, in order to compare the overall tracking performance of the single $\mathcal{H}_\infty$ controller and LPV 2 controller, the circular tracking task similar to that in Fig. 5-1 is performed using the set of parameters for a human arm used for the rest of the chapter. A set of simulation results for four different launching directions and the target angular speed of 150 deg/s is shown in Fig. 5-7. First, notice that both controllers do not achieve high tracking performance in the upper right quadrant. This may be due to the fact that no viscosity terms are considered in the controller design. However, for the rest of the circle, regardless of the launch angle, the responses from LPV2 yield smaller deviation from the reference circle. In particular, along the path from 7 o'clock to 10 o'clock the responses of $\mathcal{H}_\infty$ are always significantly inside of the reference circle. Without any afferent and efferent delays as well as nonlinear muscles,

a single $\mathcal{H}_\infty$ performs fairly well for this tracking task. However, there is some systematic difference in tracking performance depending on the location in the workspace, which implies that state dependent controller such as LPV2 does appear to improve tracking performance over a large workspace. Thus, for the rest of the chapter, we would like to concentrate on how there is a difference between a single $\mathcal{H}_\infty$ controller and LPV controllers in terms of how a rapid and sharp direction change can be handled.

5.5.2 Single $\mathcal{H}_\infty$ controller

For comparison, an $\mathcal{H}_\infty$ controller (L in the figures) with the same frequency weighing matrix $\mathbf{W}_1$ was designed for the arm plant linearized about the center of the workspace. First, in order to see the effect on the nonlinearity in the plant, the same controller was applied to both the linearized plant (L arm in the figures) and the nonlinear plant (NL arm in the figures). The first example in Fig. 5-8 shows a comparison between a vertical movement and a horizontal movement. For the vertical movement, there are almost no difference in responses from the linear and nonlinear plants. In both cases, the paths are fairly straight. For the horizontal movement, in comparison, there are two notable differences. First, the response from the linear plant converges to the final target, while that from the nonlinear plant shows some offset at the end of the movement. Second, the response from the linear plant exhibits a bow-like path as well as slightly lower speed around the maximum peak, while that from the nonlinear plant an S-like path with higher speed.

The second example in Fig. 5-9 shows a comparison between similar curved paths, but the movement directions are reversed. When the target sequence is N-C-E, the responses from both the linear and the nonlinear plants are very similar, while when the target sequence is E-C-N, the path from the nonlinear plant diverges more to the right and has more significant "terminal correction" seen in the path.

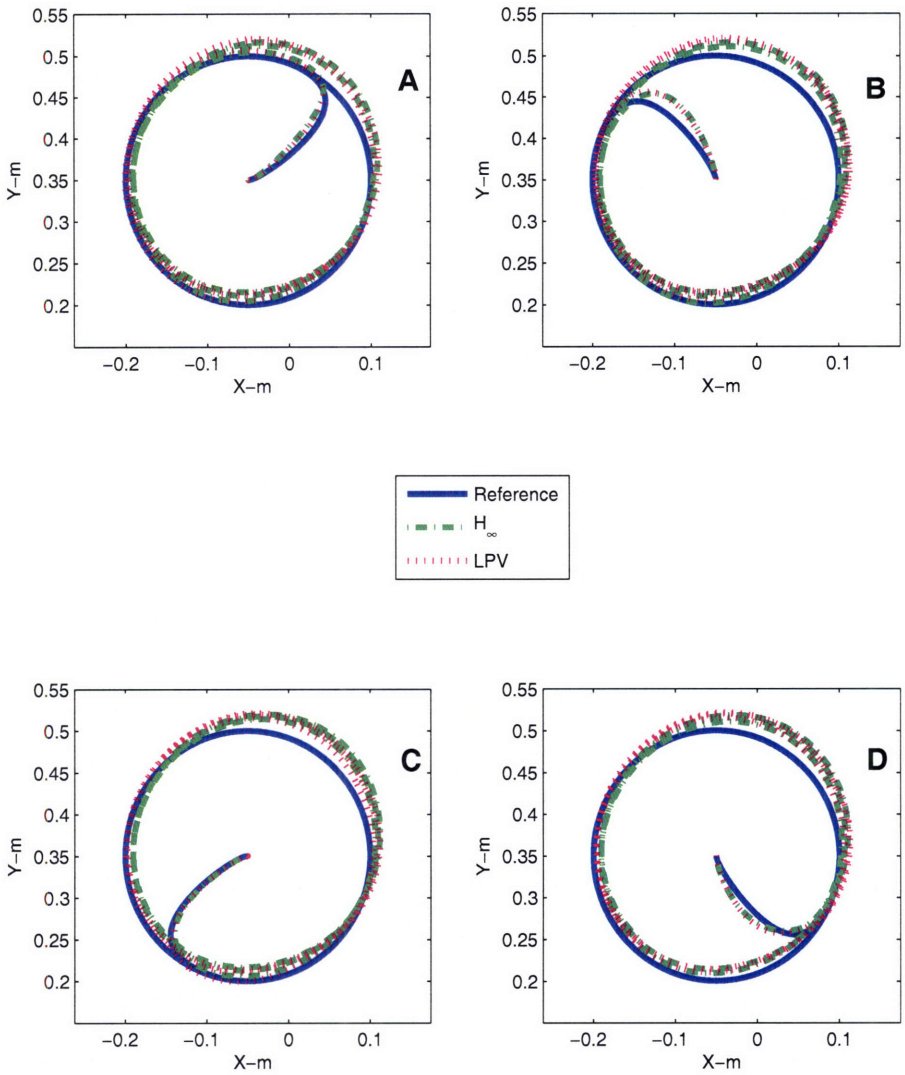

Figure 5-7: LPV2 and $\mathcal{H}_\infty$ controller models simulated hand motion for the tracking speed at 150 deg/s. In all four figures, the solid blue lines show the Cartesian reference hand position, the green dash-dot lines the responses of $\mathcal{H}_\infty$ controller system, and the magenta dotted lines the responses of LPV2 controller system.A through D represent different launch angles, 0, 90, 180, and 270 respectively.

5.5.3 LPV controllers

First, the simulation results of the LPV2 controller with the nonlinear plant are presented in Fig. 5-10. For comparison, the results of the $\mathcal{H}_\infty$ (L) are presented. From the common starting point of S, three sets of hand speeds and paths are presented. Peak speeds for

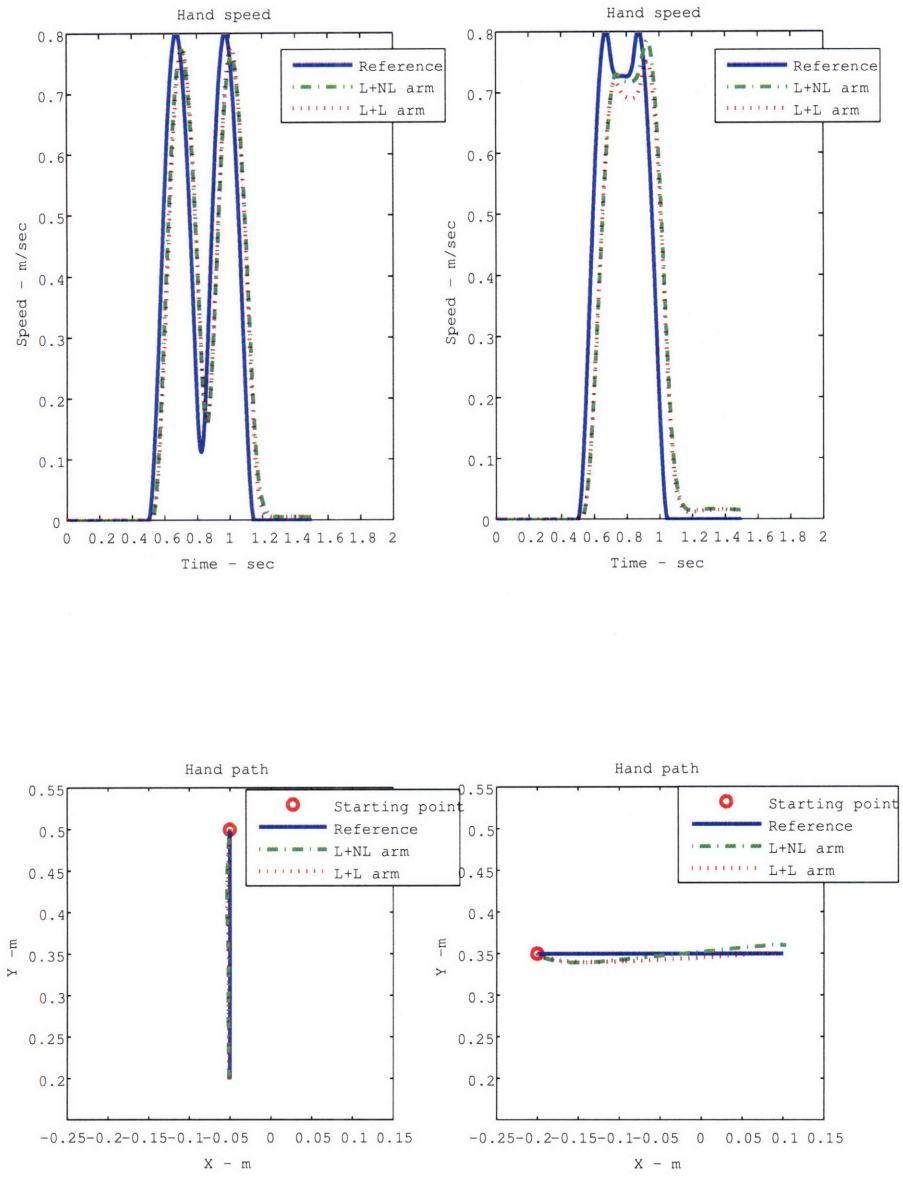

Figure 5-8: A simulation result on the $\mathcal{H}_\infty$ controller with the nonlinear plant and the linearized plant about the center of the workspace. Upper row: Hand Speeds. Lower row: Hand paths. Left column: Target sequence N-C-E and second movement initiated at 300 ms after the first. Right column: Target sequence E-C-N and second movement at 200 ms.

LPV2 tend to be higher than those for the single controller response. The paths for S-C-E and S-C-N do not differ much between the two controller types, but there is a noticeable difference in the paths for S-C-W. Among the simulations performed, the LPV2 controllers have slightly inferior performance to the linear controller in the segment between W and C.

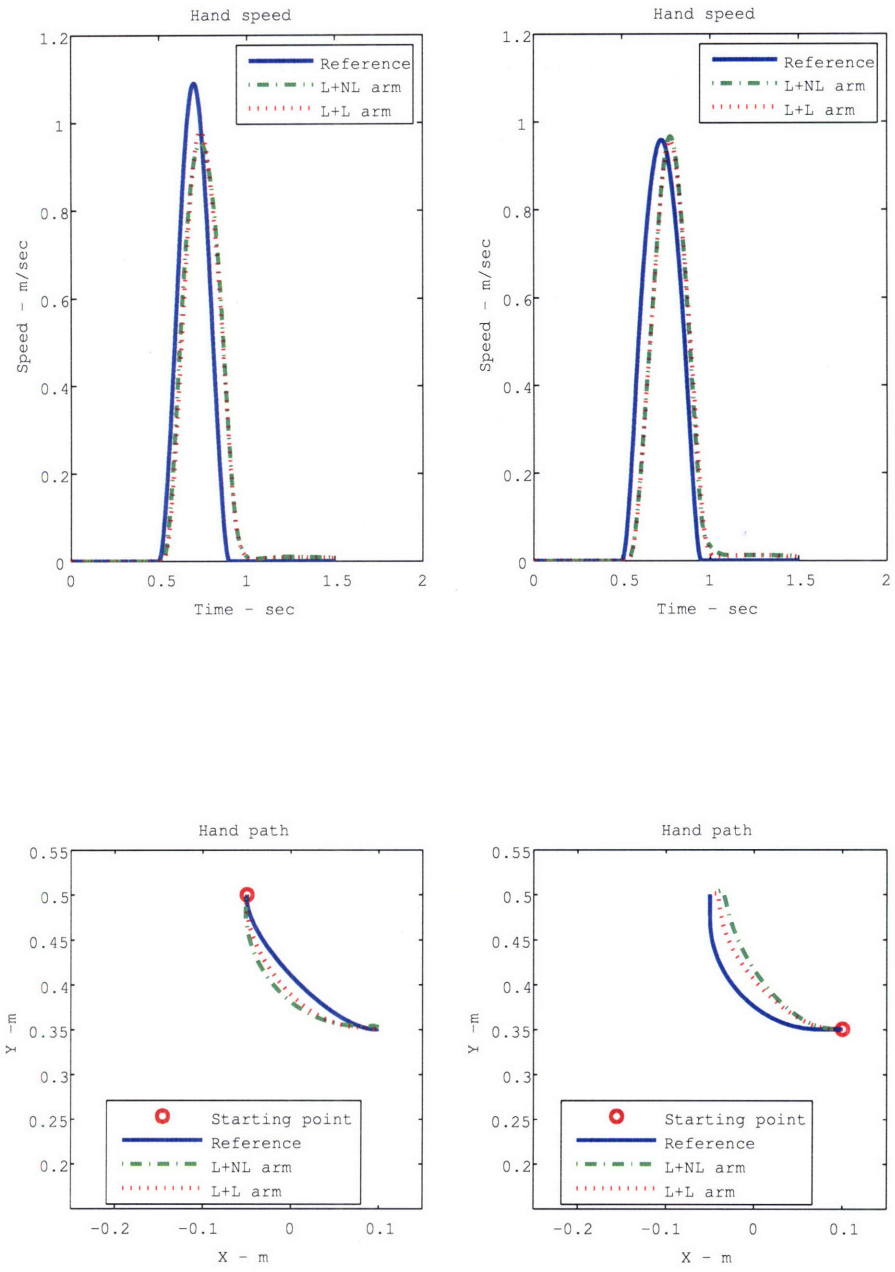

Figure 5-9: A simulation result on the $\mathcal{H}_\infty$ controller with the nonlinear plant and the linearized plant about the center of the workspace. Upper row: Hand Speeds. Lower row: Hand paths. Left column: Target sequence N-C-S and second movement initiated at 300 ms after the first. Right column: Target sequence W-C-E and second movement at 200 ms.

During the simulations for these three particular movements, the temporal variations of the scheduling variables ρ_1 and ρ_2 as well as the corresponding controller weights α_i,

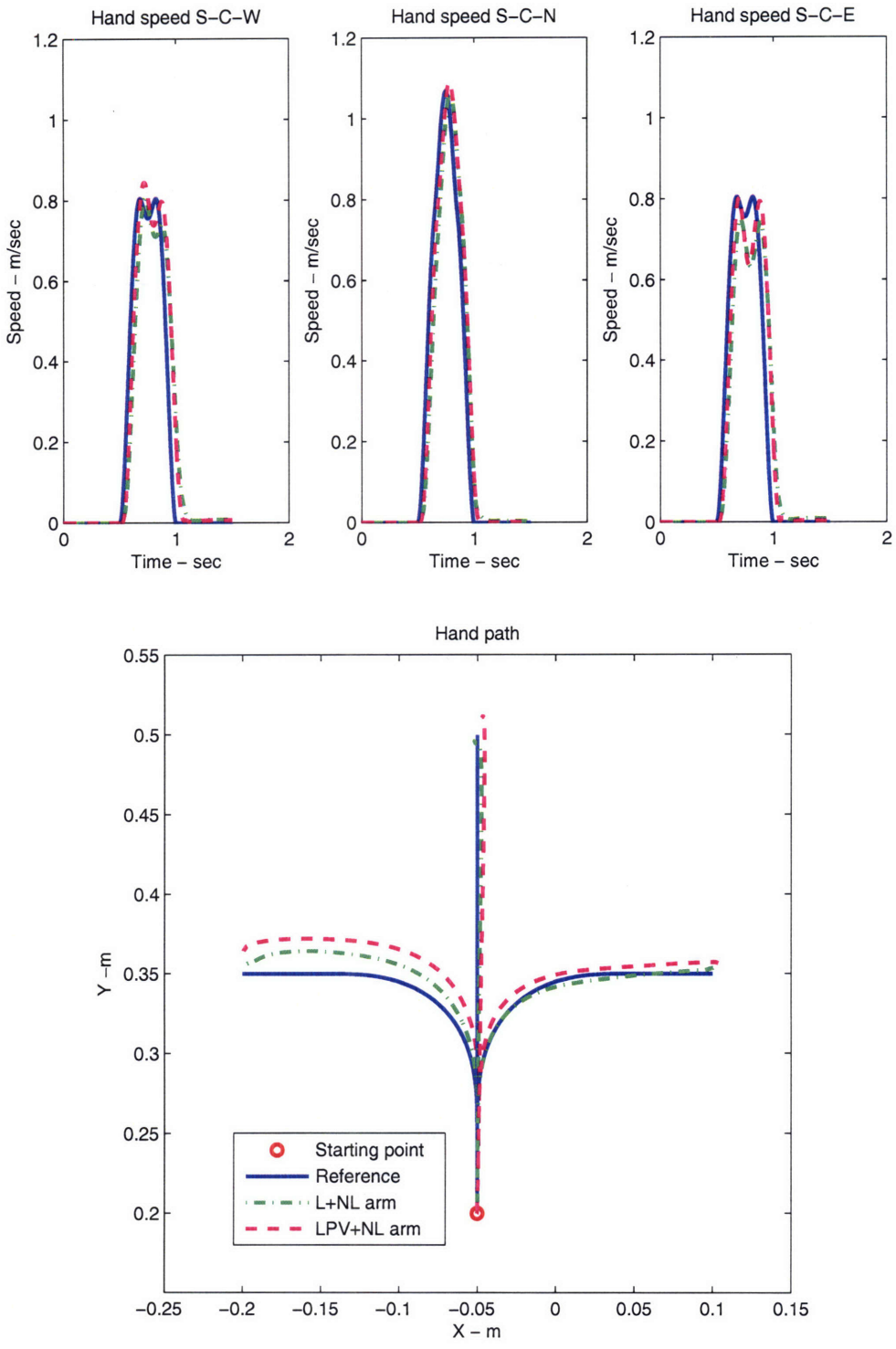

Figure 5-10: Simulation results on LPV2 controller and $\mathcal{H}_\infty$ controller. The second segment is initiated at 150 ms after the first is initiated.

$i = 1, 2, 3, 4$ for LPV2 are shown in Fig. 5-11. Across all three directions for the second segment, the variation of ρ_1 is much smaller than that of α_2. In fact, this is true for the entire workspace. Thus, the variation of ρ_1 may not affect the limb dynamics significantly.

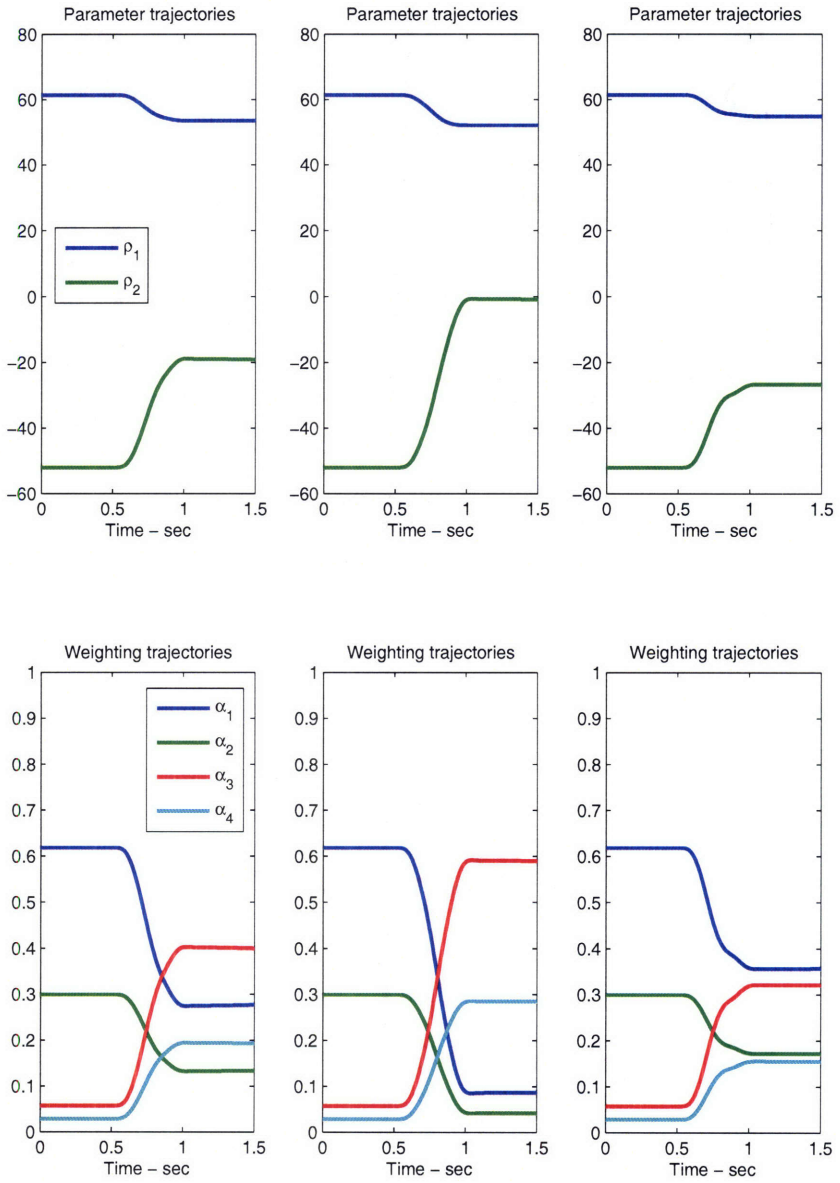

Figure 5-11: Trajectories of scheduling parameters ρ_1 and ρ_2 and of the weights α_i, $i = 1, 2, 3, 4$ for the LPV2 controller

To see the effect of each scheduling variable, the singular values of the arm dynamics at each vertex are examined. As it can be seen from Eq. (5.26), all four eigenvalues of the

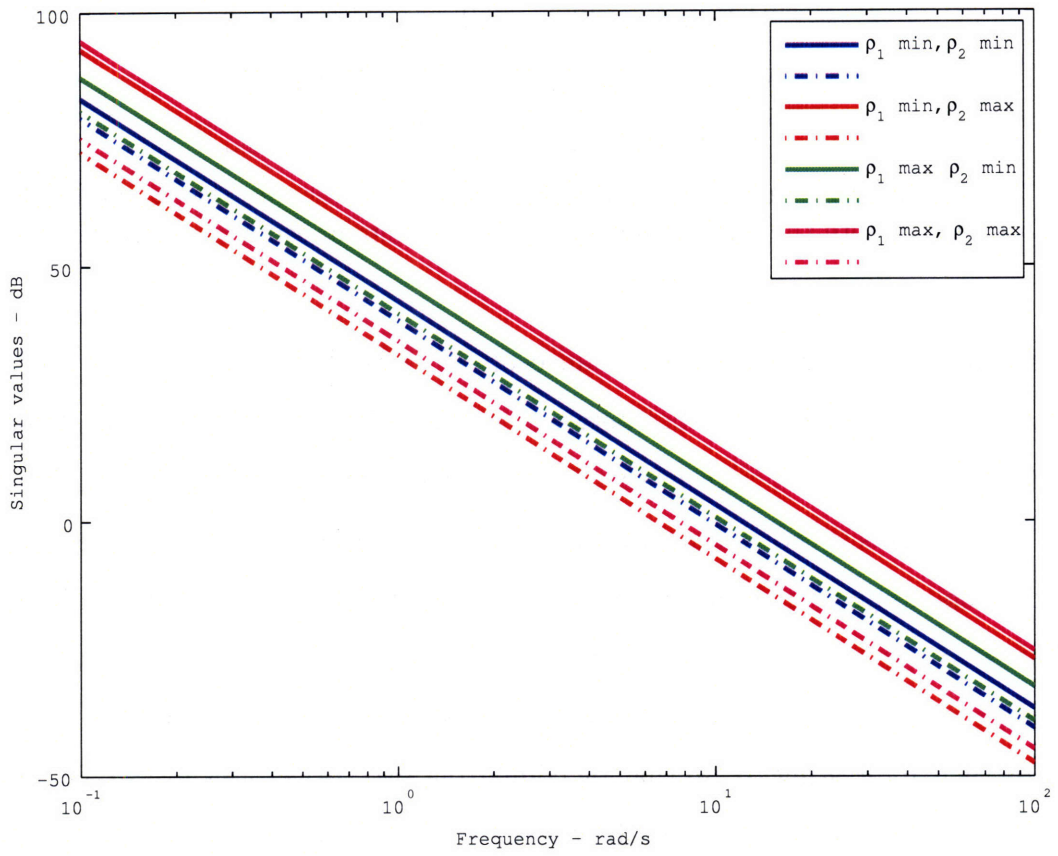

Figure 5-12: Singular values of the frequency responses of arm dynamics evaluated at each vertex. Solid lines denote the largest singular values, and the Dashed-dotted lines the smallest singular values. A pair of lines for each color denotes the same scheduling variable values.

arm dynamics without the viscosity term are zero. Also, it is easy to check that there is no zeros in the arm dynamics. Thus, the arm dynamics evaluated at each vertex is simply a cascade of integrators with different gains. In order to see the effect of scheduling variables on variations on singular values, it suffices to check the singular values at a frequency. Table 5.2 below shows the variations of the largest and the smallest singular values, $\overline{\sigma}$ and $\underline{\sigma}$ respectively, against the extrema of the scheduling variables. While maintaining $\overline{\rho}_2$ or $\underline{\rho}_2$, the singular values with different values of ρ_1 do not change relatively much. Thus, the empirical scheduling variable reduction outlined in 5.3 appears to be reasonable.

An example of the performance of parameter-reduced LPV controller, LPV1, is shown in Fig. 5-13. The speed profiles as well as paths are slightly different between LPV1 and

Varied	ρ_1		ρ_2	
Fixed	$\overline{\rho}_2$	$\underline{\rho}_2$	$\overline{\rho}_1$	$\underline{\rho}_1$
$\Delta\overline{\sigma}$	0.0173	0.0485	0.0746	0.1040
$\Delta\underline{\sigma}$	0.0173	0.0486	0.0747	0.1041

Table 5.2: Variations in the singular values of the arm plant as the scheduling variables change. $\overline{\sigma}$ and $\underline{\sigma}$ denote the largest and the smallest singular values respectively.

LPV2 responses. The tracking performance of LPV1 is slightly worse than LPV2. The overall difference is smaller than that between responses from LPV2 and $\mathcal{H}_\infty$. However, one significant difference can be seen in the speed profiles where the those from LPV1 tend to decrease slower. This speed characteristics is fairly uniform in all the LPV1 responses.

The corresponding profiles of the scheduling variable and weights are shown in Fig. 5-14. Note that $\rho_3 = \cos\theta_e$. In the scheduling parameter profile for the S-C-W path, it can be clearly seen that the convergence of the parameter is fairly slow (between 1 and 1.5 seconds). In addition, it is interesting to see that by comparing two trajectories for S-C-W and S-C-E the variation of the elbow angle for those two trajectories are more similar than that for S-C-N, although the movement directions are totally opposite for the second segment of the movements.

5.6 Discussions

Two LPV controllers were designed in this study. For comparison, one $\mathcal{H}_\infty$ controller based on the center of the workspace was designed. All three controllers are designed based on a simple two link arm model that does not include the viscosity term and shared the same weighting matrix applied to the sensitivity transfer function. Based on this, the $\mathcal{H}_\infty$ controller achieved the smallest γ. The resultant controllers applied to the nonlinear arm model showed similar responses for the vertically straight paths and the movements performed in the down-right quadrant. However, all the other types of the movements showed some difference in curvature and terminal error, in particular the slow convergence to the final target using the LPV1 controller. To achieve higher performance, parameter dependent weighting

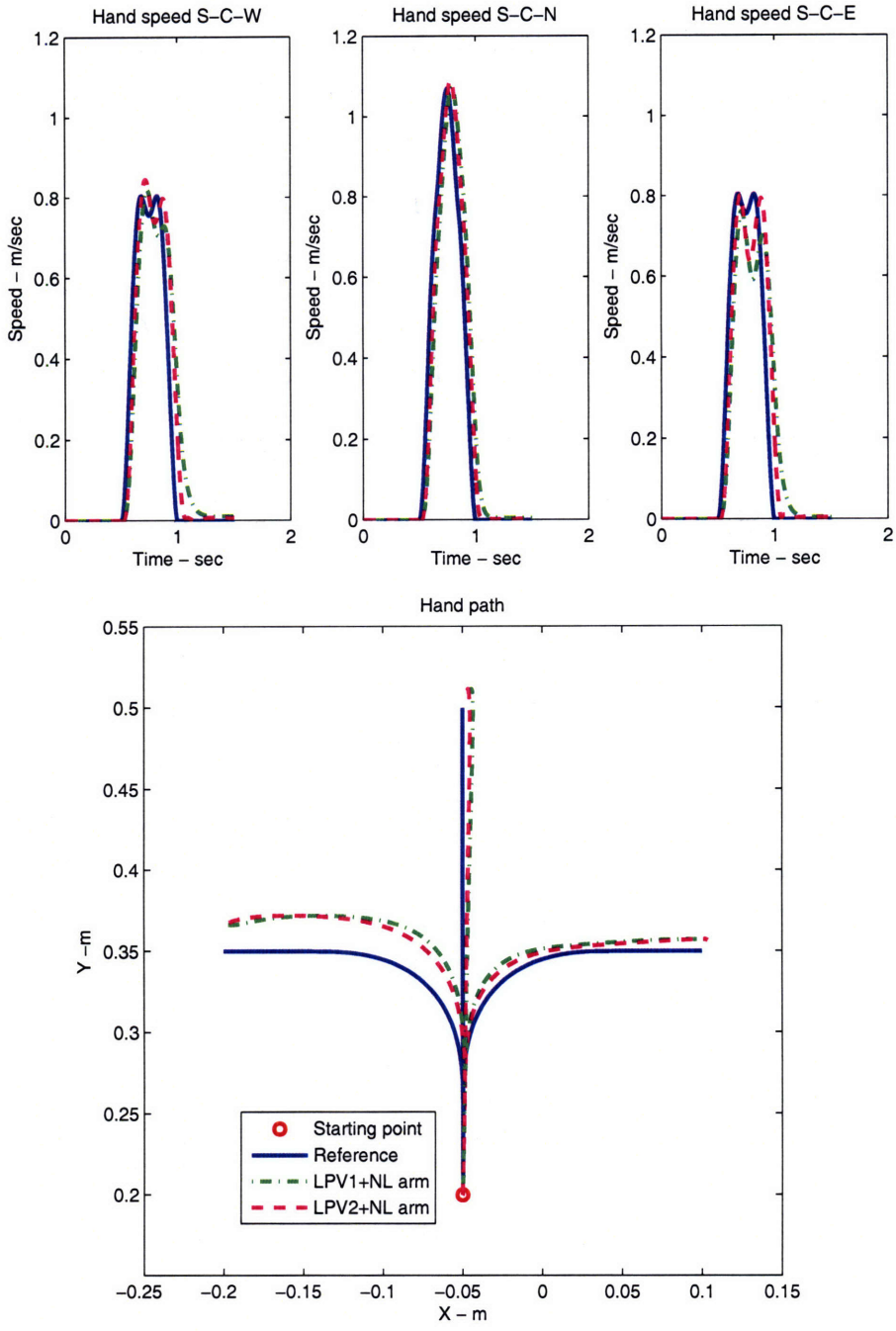

Figure 5-13: Simulation results on LPV1 controller and LPV2 controller. The reference commands are the same as in Fig. 5-10

could have been used for better loop shaping as each plant used in the control synthesis has a fairly different dynamics. This idea may be biologically feasible and is discussed below. In

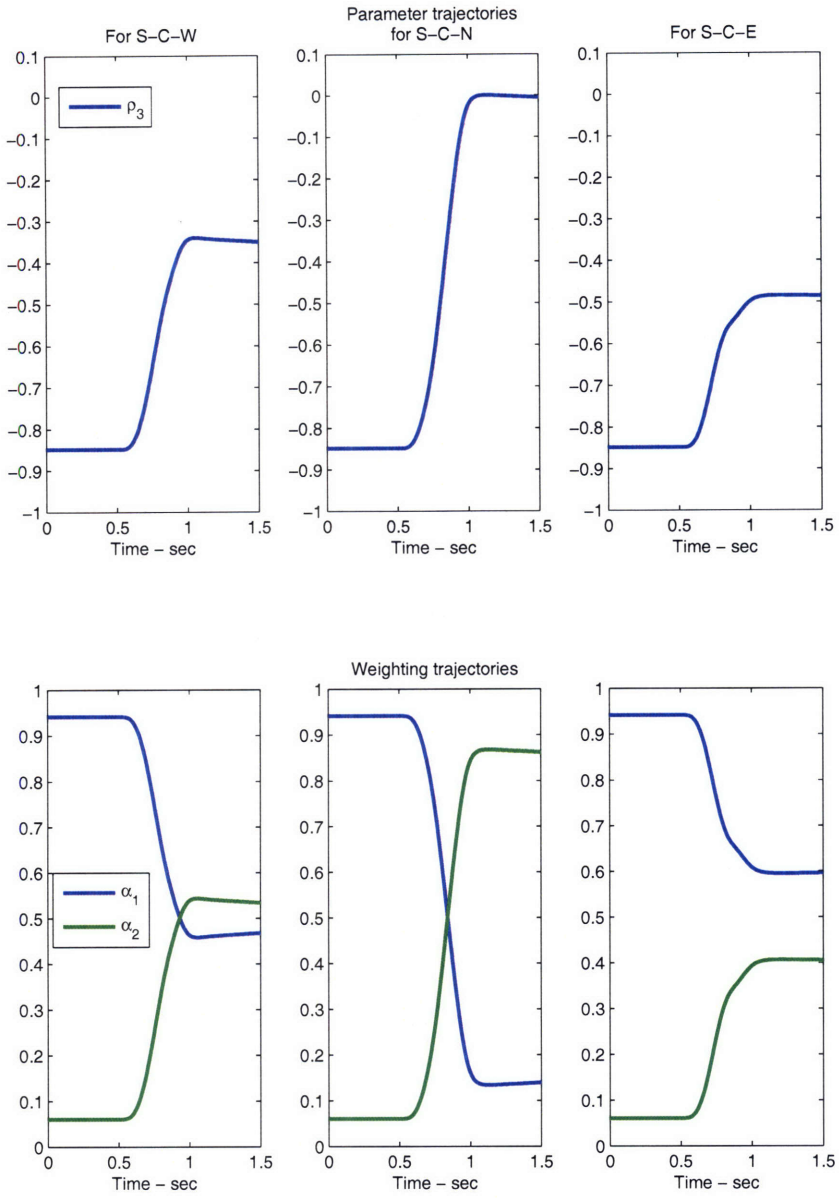

Figure 5-14: Trajectories of scheduling parameters ρ_3 and of the weights α_1 and α_2 for the LPV1 controller

addition, there was not explicit scheduling based on the velocity. Thus, building a quasi-LPV system by including velocity terms explicitly would have improved the overall performance of the LPV controllers. However, inclusion of velocity terms would increase the number of LMI's to be solved exponentially as discussed below.

5.6.1 Comparison of LPV with other control models

The ability to learn and retain the properties of several different environments has been offered as evidence of a modular structure to motor learning (Ghahramani and Wolpert 1997; Wolpert and Kawato 1998; Haruno et al. 2001; Doya et al. 2002). As an example, Ghahramani and Wolpert (1997) examined adaptation to opposite visual perturbations that were applied during movements from two different starting locations. They presented evidence consistent with the idea that subjects that learned the two mappings generalized to intermediate starting positions by an interpolation process. According to the authors the motor system uses two distinct visuomotor "expert modules" and interpolates to intermediate starting locations by using a weighted average of the two experts outputs. By this account, the configuration of the limb stands as a contextual cue that indicates which of the expert modules should intervene. Thus, in the sense that LPV system is similar to, and could conceivably be used to formally represent a set of "expert modules" each of whichs corresponds to a local controller characterized by a set of extrema of scheduling variables at a vertex of the box of $\mathbb{R}^n$ where n is the number of the scheduling variables. Thus, the local controllers are continuously recruited based on the scheduling parameters.

Narendra et al. (1995) suggested a control scheme with multiple models where there are multiple models to approximate the input-output relation of a plant to be controlled in the context of system identification. There are N models to be identified, $M_1, \cdot, M_N$. Then, corresponding to a model M_j there exists a parameterized controller C_j such that M_j together with C_j in the feedback path would behave like the reference model, or alternatively achieve the desired control design objectives. The estimation error is measured for each model such and defined by $e_j = y - y_j$ where y is the output of the true model and y_j is the output of M_j. The output of each controller C_j is used to control the plant. Then, the design problem is to choose the models M_j and the controllers C_j together with the rules for switching between the controllers so that overall system is stable and achieves improved performance. Based on a switching criterion (for potential choices, see Narendra et al. (2003)), the controller corresponding to have the smallest error index is used at that instant. Mathematically it is

proven that any of the switching criterion in Narendra et al. (2003) ensure the closed loop stability. However, at the same time the parameters in each model M_j and the corresponding controller C_j are adapted directly or indirectly (Narendra et al. 2003). Thus, switching is rapid but not sufficiently accurate while tuning or adaptation is relative slow but is desirable for improving the performance of the overall closed loop system.

In order to use multiple models simultaneously, an extended approach has been taken to be more relevant to neural circuitry responsible for movements. A series of studies by Kawato and his collaborators suggests (Wada et al. 2003; Imamizu et al. 2004; Haruno et al. 2001) that an extended version of a set of paired feedforward internal models and corresponding inverse internal models, MOSAIC (modular selection and identification for control) model has been identified in cerebellum to account for context dependent activation, through fMRI studies. They argue that this observed differential activation in cerebellum is a proof that multiple internal models are implemented in cerebellum.

There are some similarities and differences between MOSAIC model and LPV. First similarity is that both of them consist of local controllers each of which is responsible for the corresponding local dynamics or tasks to be compensated for. Second similarity is the interpolation scheme of local controllers. Both models use simple linear interpolation of local controllers. Third similarity is that both of them have potential to account for afferent delays as well as feedforward command delay, although such potentials had not been investigated in this chapter. As a component of MOSAIC is a pair of feedforward internal model and inverse internal model, MOSAIC is, in principle, capable of accounting for both types of delays. For LPV, there are some ongoing research to develop LPV syntheses to account for both types of delays (Fen and Grigoriadis 1997; Yuan et al. 2005).

However, there are some critical differences. First, each controller for MOSAIC model consists of a pair of a feedforward internal model and a corresponding inverse internal model, while each local controller for LPV is an LTI system. It is not clear at this point whether the input-output relation of a pair for MOSAIC is similar to a local controller for LPV. Second, as an optimal control synthesis, LPV comes with a closed-loop stability guarantee

and a performance and robustness guarantee with appropriate weighting filters when the corresponding LMI's have a feasible solution. On the other hand, MOSAIC does not have any guarantee and requires some preliminary inverse model designs which may or may not be carried out easily. Third clear difference between MOSAIC model and LPV formulation shown here is the level of the implementation. It is highly possible for the MOSAIC model to be extended, or to be granulated to be more biologically accurate as claimed in Imamizu et al. (2004) that each local controller may corresponds to a microzone in cerebellum. However, it is not clear what processes or computations are performed in the activated areas or a set of modules identified in the fMRI study in relation to MOSAIC formulation. Last clear difference is that each local controller in LPV formulation is designed about a point in the state space of the plant, while Imamizu et al. (2004) claims that each module of MOSAIC model does not correspond to different kinematics or errors, but only corresponds to a task or an external environment to compensate for. A recent study by (Milner and Hinder 2006) showed that during adaptation against force fields, only position information but not force information is used. The authors concluded that the CNS uses only position error for updating the inverse internal model of the environment dynamics and modifying feedforward commands. This result appears to favor LPV to MOSAIC. In addition, even when the plant becomes more complex, LPV offers a systematic approach to design a set of controllers with closed-loop stability guaranteed and yield a guaranteed bound γ as in Eqn 5.7. Furthermore, with availability of such a systematic synthesis, LPV could predict how many controllers or corresponding neural modules would be required to perform the task successfully. Therefore, it is worthwhile to pursue LPV gainscheduling approach to characterize limb movements.

5.6.2 Feasibility/rationale of LPV/gainscheduling models for cerebrocerebellar limb control system

As shown in Chapter 3, it may be argued that simple spike activity of each Purkinje cell is modulated by a linear combination of both joint angels, θ_s, θ_e and velocities, $\dot{\theta}_s, \dot{\theta}_e$. In addition, it has been shown in primary motor and premotor cortices that both individual

cells and populations of cells reflect changes to the location of the limb and velocity (Sergio and Kalaska 1998). However,, assuming that these signals are in fact used to schedule the control, it cannot be asserted clearly whether the scheduling variables are a linear feedforward, feedback, or mixed. RICSS formulation implies that there is a descending signal from area 3a and primary motor cortex that chooses particular sets of mossy fibers (sigMF in the RICSS model) and correspondingly Purkinje cells to process control signals, and those Purkinje cells are further modulated by the state information of the limb (selMF in the RICSS model). Therefore, it is more likely to have scheduling signals which are both feedback and feedforward.

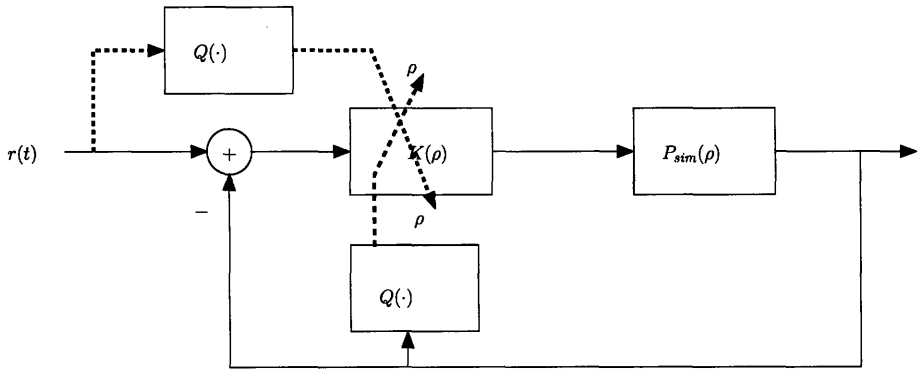

Figure 5-15: Control system gainscheduled by both feedforward and feedback signals.

Fig. 5-16 shows a set of examples of feedforward or feedback driven LPV2 systems. Here, feedforward means that the scheduling variables are computed based on the reference command, and feedback means that the scheduling variables are computed based on the output of the plant. The difference in their performance is almost negligible. This result is expected given that there is no afferent or feedback delay present in the system. Although there is no pure delay in the system, there are some delay effects seen in the scheduling variables (top row in Fig. 5-16). In addition, this slight difference yield different weighting of local controllers even at the termination of the movement.

In order to investigate the issue of feedback vs. feedforward, delays, as shown in Fig. 5-5, need to be included in the controller synthesis. An attempt was made to design an optimal controller by including various degrees of Pade approximations of a feedback delay of 10 ms or

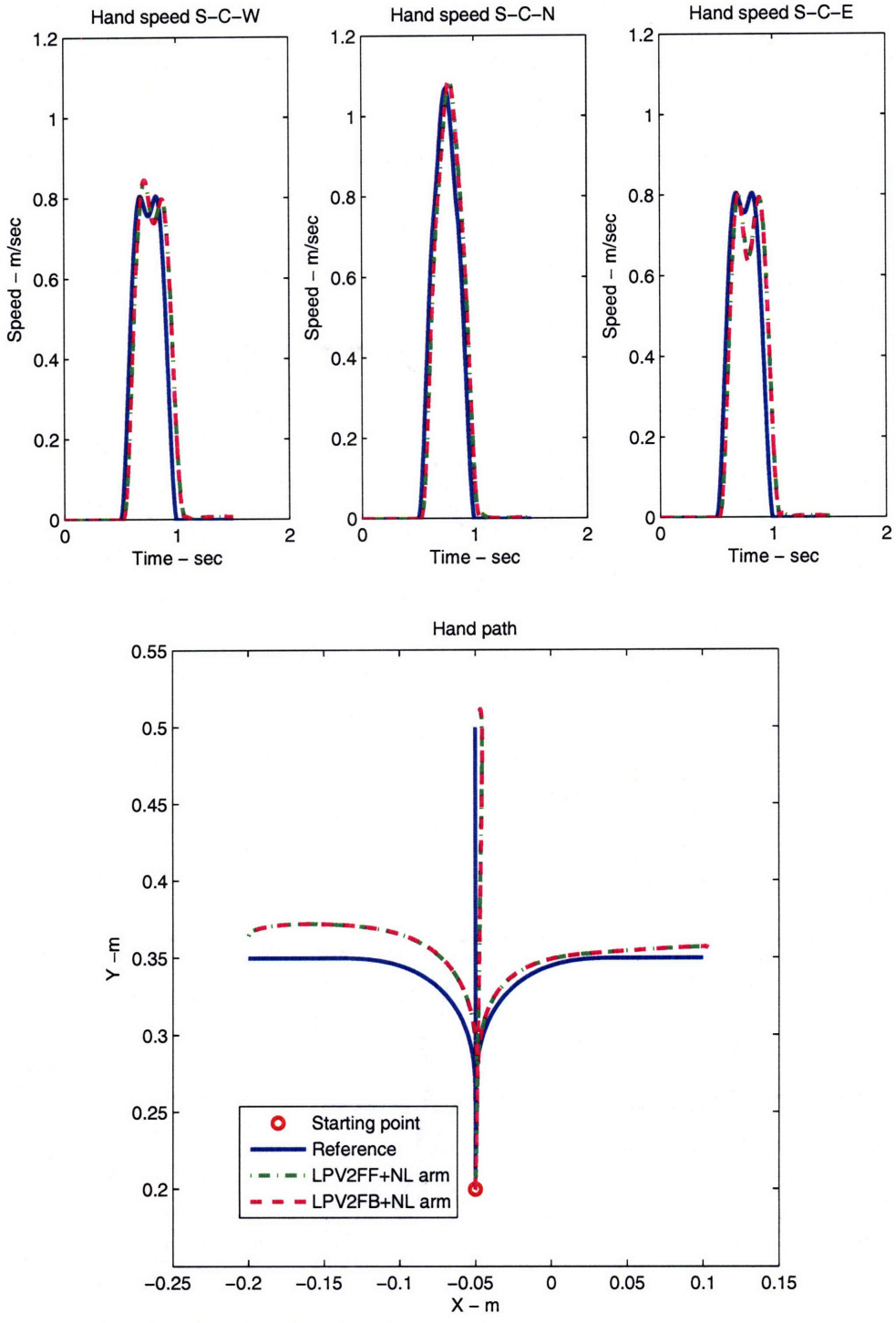

Figure 5-16: Simulation results of hand speeds and hand paths for LPV2 system with feed-forward and feedback scheduling. The reference commands are the same as in Fig. 5-10.

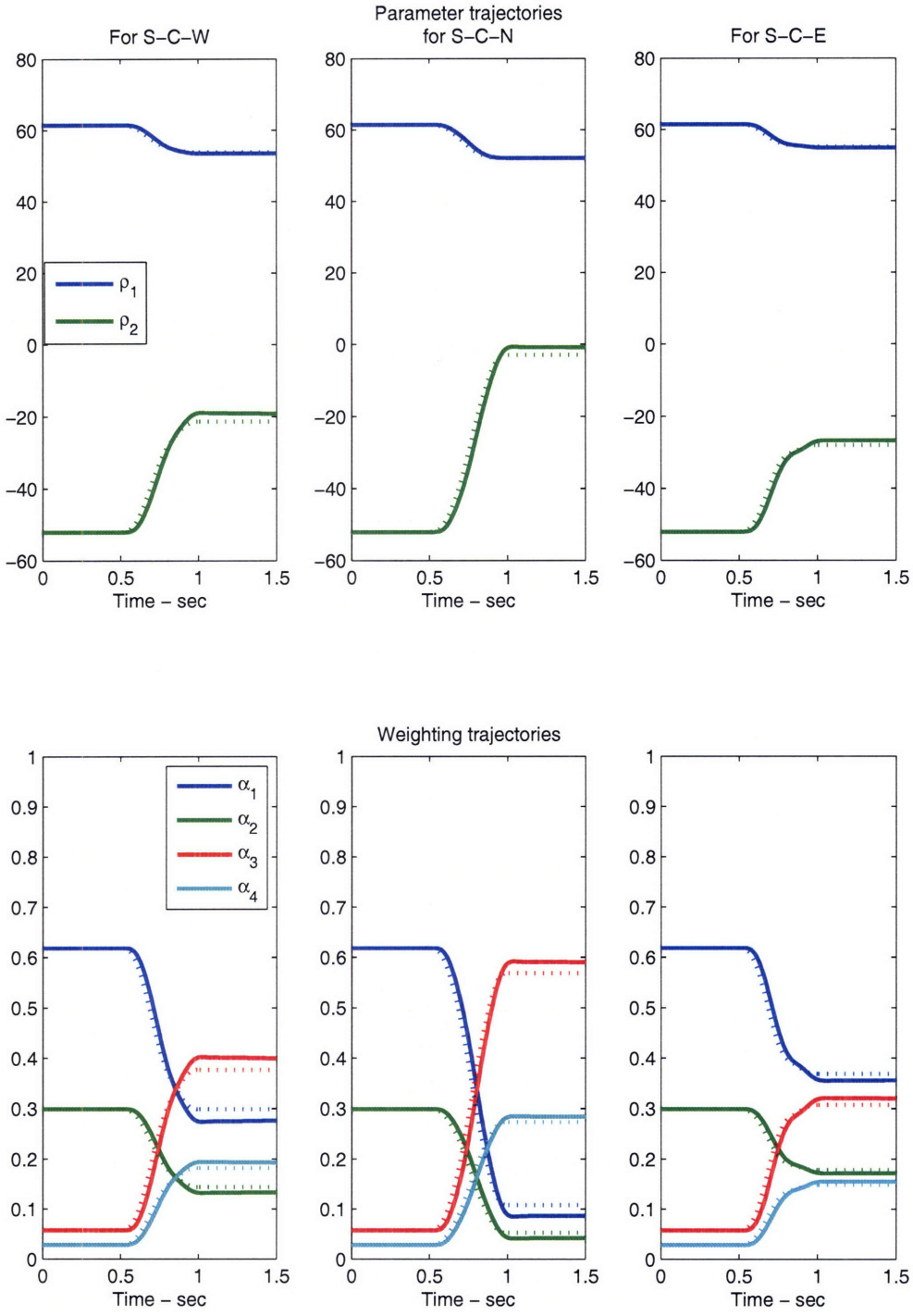

Figure 5-17: Simulation results of the scheduling parameters and the corresponding weights for LPV2 system with feedforward and feedback scheduling. Solid:Feedback, Dashed:Feedforward.

longer in both single $\mathcal{H}_\infty$ or LPV syntheses. However, no controllers with reasonable performance were obtained, or the syntheses could not yield a feasible solution to the corresponding LMI problem, especially with higher orders of Pade approximation. In fact, development of optimal gainscheduling controller syntheses with presence of delay components is an active area of research (Fen and Grigoriadis 1997; Wang and Wang 2004). Therefore, more recently developed LPV syntheses accounting for delays should be implemented and tested.

5.6.3 Reduction of the number of scheduling variables

Although the design procedure appears to be fairly simple and to have efficient computational tools, a practical limitation of LPV formulation is that the number of the controllers to be designed, or the number of LMI's to be solved correspondingly, increases exponentially as a function of the number of the scheduling variables. In addition, in order to secure the scheduling parameter space to be large enough to cover all possible operation range, the issue of the conservatism arises. In the formulation above, the original linearized arm plant has the elbow joint angle θ_e being the only scheduling variable, but because of the inversion of the inertia matrix $\mathbf{H}(\theta_e)$, the resultant plant was characterized to have two scheduling variables both of which were functions of θ_e alone.

The actual variations of smaller varying parameter in corresponding to the LPV controller designed, LPV1, in the range specified was approximately 5%. Thus, the resultant LPV synthesis required only one pair of vertices. Thus, in our formulation, the resultant LPV plants could contain only up to two scheduling variables that are purely based on the geometric configuration of the limb. Thus, deriving the bounds on those scheduling parameter should be an easy task once the size of the workspace was determined. However, these plants are clearly over-simplification of the original two-link dynamics which contains velocity, or viscosity, terms as well as nonlinear muscle dynamics. As the RICSS model as well as many other neural recording studies from variety of motor areas suggest that speed or velocity is encoded in the brain. In addition, it has been shown that viscosity terms in the limb dynamics indeed affects the movement performance. Therefore, the plant on which

a controller design is based should include the velocity terms to be more realistic. With the inclusion of the viscosity matrix in the arm dynamics described by Eq. (5.1), the number of the scheduling variables becomes 8 and requires $2^8 - 1 = 255$ LMI's to be simultaneously solved. There is a scientific question as to whether this number is realistic or not in terms of the actual number of individual or ensembles of neurons participating in real time computation of the movement and how those ensembles emerge. However in order to perform a functional characterization using an engineering model, it is desired to reduce the number of the controllers or corresponding neural ensembles.

Kwiatkowski and Werner (2005) investigated this problem based on a pseudo-LPV model of the two-link robotic arm plant as considered here. Their original plant that contains 10 scheduling parameters results in $2^{11} - 1 = 2049$ LMI's to be simultaneously solved. In order to reduce the scheduling parameters, they took the following steps:

(i) Generating typical operating trajectories for the plant by measurement or simulation. These trajectories should roughly span the expected range of operation of the controlled plant and generate typical scheduling parameters' trajectories. It is noted, clearly, that this approach is only useful for a given operating range tested.

(ii) Applying Principal Component Analysis (PCA) to determine a set of fewer principal components that can be used to approximate the data.

(iii) Applying the same PCA reduction to the scheduling parameters of an LPV model to obtain an approximated LPV model with fewer scheduling parameters.

With this method, the authors successfully reduced the scheduling parameters by 7 to 3 while maintaining the performance. This type of empirical reduction methods can potentially cause conservatism as the design procedure does not fully account for the plant dynamics and associated uncertainty. However, this approach may have some biological and behavioral relevance in terms of organization of motor systems as well as learning as opposed to more iterative algebraic approaches used to solve LMI's for example.

As it has been shown at the level of EMG limb kinematics in frog's hindlimb movement

(d'Avella et al. 2003), human walking (Jo 2006), and DSCT neurons (Bosco and Poppele 2003), there appears to be a behaviorally relevant basis functions, or synergies, that can be combined to produce a wide variety of natural movements. Also, in connection to the RICSS formulation, the sensory feedback information through $selMF$ may potentially approximate the scheduling variables to recruit Purkinje cells that are responsible for a particular range in the state space. As suggested by Hawkes and Eisenman (1997), if the number of the microzones each of which is responsible for controlling a corresponding local region in a state space, then adjusting the local controllers might be performed locally in space and slowly in time while changing weight of those local controllers, hence the net output being the sums of all the microzone modules, to achieve global performance objective can be fairly dramatic.

5.6.4 Cerebellum as a gain-scheduled controller

Although the model by Schweighofer et al. (1998b) included reasonably detailed anatomy and physiology of cerebrocerebellar systems and successfully reproduced slow movements, the model suffered from its slow learning rate for fast movements. Hence, the authors argued that there should be an internal model. However, the slow learning rate may be attributed to the structure of learning. It seems that all synaptic elements are adapted while the system is learning the multiple paths. Furthermore, no a priori information as to where the limb is moving is given to the system. Thus, it is likely that the adaptive elements in the system are not partitioned accordingly to account for particular commands or particular states of the limb dynamics. If such a partition scheme exists or the system chooses subsets of adaptive gains based on the dynamic or kinematic demands of the task, then the number of the adaptive elements can potentially reduce significantly thence to increase the adaptation speed.

Another anatomical and physiological neural network cerebellar model by Kettner et al. (1997) faced the same issues. One difference this model posses is the implementation of mossy fibers each of which is tuned for a specific preferences in position or velocity as in selMF and their errors similar to sigMF in the RIPID model. However, the activity of the corresponding

parallel fibers (PFs) is assigned either 0 or 1 through the Golgi-granule interaction and lasts for a very brief period, in the order $\sim$ 10 ms (Fig. 4 in Kettner et al. (1997)). Thus, each Purkinje cell (PC) which is responsible for either a horizontal or vertical movement direction receives 6000 PF inputs to drive the continuous eye movement. This convergence of the PFs to a PC seems biologically feasible, but there are two potential problems. First, a temporal window within which each PF participates in the generation of motor command is very short. Second, the learning mechanism adjusts each PF synaptic weight based on a eligibility trace (a response induced by an activation of a PF) as well as the climbing fiber activity characterized by the inner product of a PC's preferred direction and the velocity error. Since each Golgi cell in the model received five randomly chosen mossy fiber inputs, the adaptation of each PF synaptic weight occurs almost independently. Therefore, if there is a more systematic grouping of signals at Golgi or PF level, then adaptation speed may be reduced significantly.

The LPV formulation shown here does not imply any adaptive scheme, but it specifically addresses the issue on how a partition of controllers can be achieved by having a set of controllers each of which is specifically accounting for a local state of the limb dynamics.

Fuzzy, or neurofuzzy, control seems promising not only to reduce the number of the scheduling variables, but also to adaptively find, or define, a set of ranges for which each controller is responsible and how to interpolate them to ensure the performance in a systematic manner(Espinoza et al. 2004; Tanaka and Wang 2001). In fact, the LPV formulation can be classified into a class of fuzzy control (Tanaka and Wang 2001). Furthermore, a recent development in modular and reconfigurable robotics suggests hierarchical neurofuzzy control systems be able to adapt both skill control, i.e., task and planning, as suggested in (Haruno et al. 2001; Imamizu et al. 2004), and low level execution control, as shown by the LPV scheme (Melek and Goldenberg 2003). Analogy and difference between such engineered control systems and CNS need to be further explored. In particular, it is yet unclear as to how each controller is composed of groups of neurons or is related to anatomical segregation such as cortical minicolumns or cerebellar microzones. This issue of actual neural implementation

of a specific controller scheme needs further investigation.

Chapter 6

Human double step experiment

6.1 Introduction

In Chapter 5, an LPV formulation was carried out to synthesize a set of controllers for the two-link arm model with linear muscles. The eventual goal is to determine whether the RIPID model can be extended to cover a larger workspace by controlling faster movements that have changes in movement direction. Since there is as yet no straightforward method to design gains for the RIPID model, a test was performed using the LPV controller which shares a similar structure as that of the RICSS. In particular, both enable state-dependent selection of gains. Behaviorally we will seek to model sequentially cued point-to-point movements.

In this case, the simplest hypothesis is that simple superposition of sequential point-to-point targeting commands can be used as input and that the curvature of the hand path following these commands is accounted for largely by the dynamics of the control (hence by the cerebrocerebellar system), and not by the central kinematic plan. In addition, the monkey, as observed (Roitman et al. 2004), stopped chasing the moving target cursor once the target cursor disappeared. Thus, it is not unreasonable to assume that the monkey was chasing a target to reach in a neighborhood of the moving target cursor. Therefore, it is hypothesized that a circular tracking motion by the monkey can be approximated in human by sequential point-to-point movements. In this chapter, the LPV models developed

in Chapter 5 were adopted to fit the data of the human experiment in which the subjects performed double step, or two sequential point-to-point movement tasks.

6.2 Methods

6.2.1 Behavioral task

The experimental protocol was approved by Committee on the Use of Humans as Experimental Subjects (COUHES) at MIT. None of the participants was aware of the tested hypotheses or had reported any prior history of neurological disorders. Four right-handed subjects (B11, B12, R12, Y11), two males and two females (22$\sim$34 years old), volunteered to participate in the study.

Each subject sat on a chair and his/her body was stabilized by a back support as well as four-point seat belt such that the upper body motion, particularly in sagittal plane, was minimized to achieve two degrees of freedom arm motion in a horizontal plane as much as possible. Each subject held a handle of the InMotion2^{TM} two-link manipulundum to control the location of the yellow cursor shown on the monitor which is mounted on the top motor of the manipulundum. Further, to minimize wrist movements, a plastic sleeve that restricted the arm motion to two degree of freedom was attached to the handle so that subjects could rest their forelimb on the sleeve.

Each subject had practice trials to get accustomed to the apparatus, for 40 $\sim$ 120 trials, until s/he felt comfortable with moving the manipulundum. Then, there were four blocks of trials where within each block the starting point, either North (N) or South (S), and the final target, either on the Right (R) or the Left (L) side, all relative to the center (C), remained fixed for 140 trials. Both starting targets, N and S, are located 15 cm vertically away from the C respectively.

An example of an action sequence in each trial is shown in Fig. 6-1 and is explained here for the case where the starting point is in S and the group of second targets is on the L side. Each trial was initiated by a subject moving the small yellow cursor (1 cm diameter)

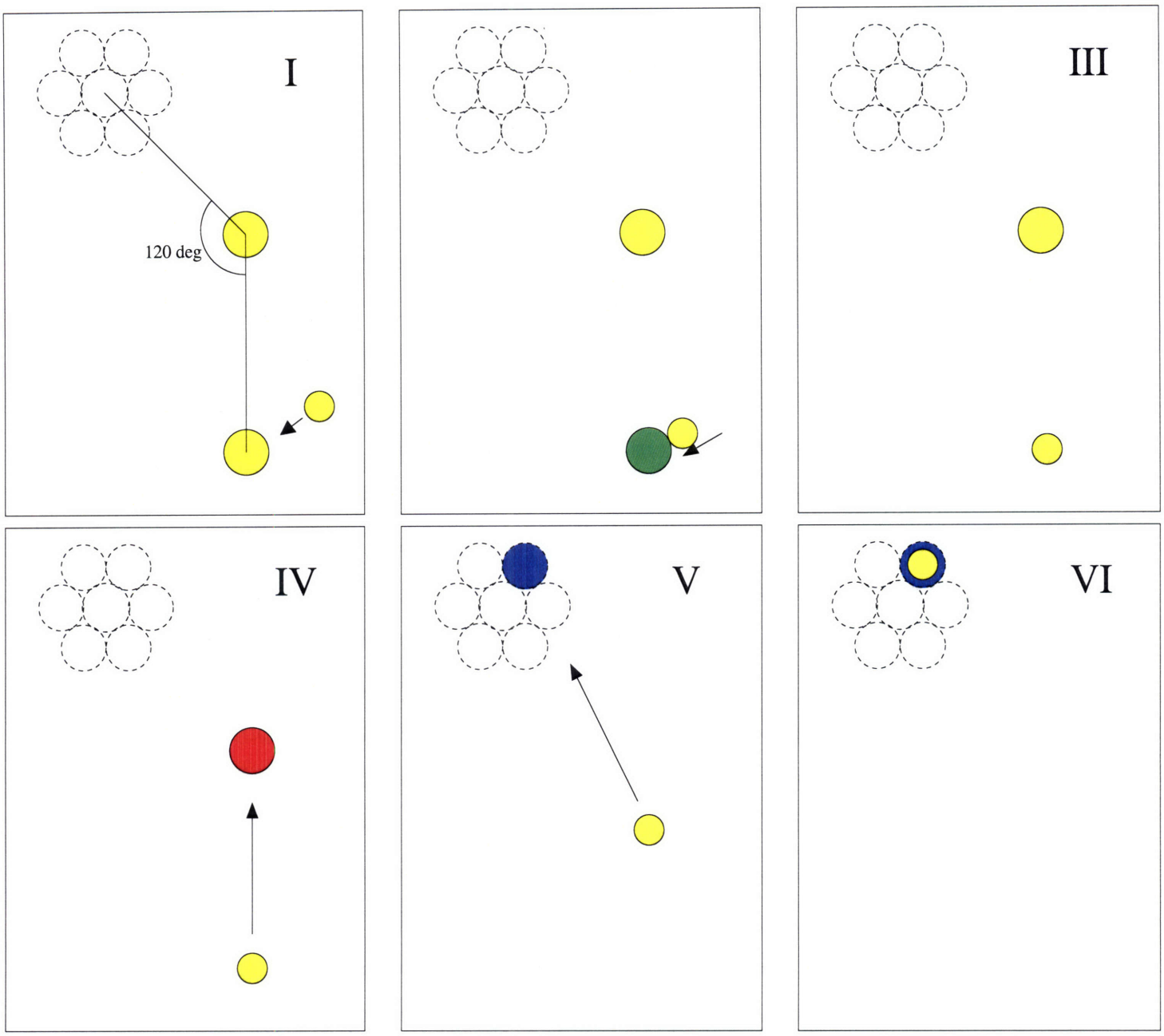

Figure 6-1: Human double-step reaching protocol.

corresponding to the hand location to a large yellow circle (2 cm diameter) which was one of the two start locations, N or S (Fig. 6-1-I). Once the small yellow cursor touched the starting point, trial initiation was indicated by change in the color of the large circle from yellow to green (Fig. 6-1-II). The subject was instructed to hold the cursor in the green circle for 1 $\sim$ 1.5 seconds until the circle disappears (Fig. 6-1-III), and the first target (2

cm diameter) which was always at C of the workspace changed its color to red to cue the subject to reach to C at a reasonably fast speed (Fig. 6-1-IV). The second target (2 cm diameter) which was always blue appeared on the screen after some random time ranging from 100 ms to 400 ms after the first cue (Fig. 6-1-V). On any given trial within a block, the second target was randomly chosen from the seven possible targets which were denoted as dashed circles in Fig. 6-1 such that the number of trials to each possible target was equal to 20. The distance between the center of the cluster and the first target is 15 cm and the angle made by the start-first-second targets is 120 deg (Fig. 6-1-I) such that those three points are on a circle whose radius is 15 cm. This particular clustering of the possible second targets was chosen for 3 reasons: 1) In order to see if the trajectory variability is due to the effect of imprecision to aim a virtual point in a target circle to mimic the circular tracking movements, the possible second targets had to be close enough so that the subjects would not notice if they were aiming at a different target in each trial. 2) The targets did not overlap each other so that it was easy to check if the subjects were reaching to the final targets accurately. 3) The ratio between the radius (15 cm here) and the maximum range of possible second target ($2 \times 3 = 6$cm here) is close, but higher than that of the monkey's circular tracking task, 5 cm radius and 2.5 cm target. The same ratio as that of the monkey experiment was used in a set of experiments before finalizing the design of the task, but human subjects (different volunteers from those whose data are used in this study) noticed that they were moving to different targets most of the trials. The current ratio chosen (15 cm radius and 6 cm target) was the closest ratio to that of the monkey's experiment, but was that none of the subjects would notice s/he was was moving to a different target in each trial. Once the subject successfully reached and stopped at the second target, s/he was instructed to stay in the blue target for a second (Fig. 6-1-VI). Subjects controlled the time between trials on their will to reduce the effect on fatigue.

Before each experiment, a subject was told to try not to look at his/her arm and hand location during movements, but to look at the monitor. It was observed by the experimenter and reported by the subjects after the experiments that subjects rarely looked at their limbs

in order to guide their hands to targets.

6.2.2 Data acquisition

In each trial, the location of the handle corresponding to the hand location of a subject was recorded at 200 Hz in workspace coordinate, and the timings of the first and the second cues were recorded by the two-link manipulundum and data acquisition system. Then, the hand position data was bidirectionally lowpass filtered by a 6th order Butterworth filter with a cutoff frequency of 6 Hz, and was numerically differentiated to obtain hand velocity signals. As discussed in Chapter 4, the 6 Hz filter was used because it kept the majority of the large speed pulses were kept while attenuating high frequency noise effectively.

6.2.3 Data analysis

Kinematic data, hand position and velocity, from each trial was fit with two minimum jerk profiles in series as done in Flash and Henis (1991) to perform kinematic fitting and to estimate reaction times to two consecutive targets.

The minimum jerk position profile in the x component can be defined as follows.

$$\tau_i = \begin{cases} 1, & \text{if } t \geq T_{0i} + T_i \\ \dfrac{t - T_{oi}}{T_i}, & \text{else} \\ 0, & \text{if } t \leq T_{0i} \end{cases} \qquad i = 1, 2 \tag{6.1}$$

$$x_1(t) = x_I + \Delta x_1 \left(10\tau_1^3 - 15\tau_1^4 + 6\tau_1^5\right) \tag{6.2}$$

$$x_2(t) = \Delta x_2 \left(10\tau_2^3 - 15\tau_2^4 + 6\tau_2^5\right) \tag{6.3}$$

$$x(t) = x_1(t) + x_2(t), \tag{6.4}$$

where τ_i is the time normalized by the temporal shift T_{0i} and the temporal scaling T_i, x_I is the initial position of the hand, Δx_i is the distance between the initial and final positions of each segment, $x_1(t)$ and $x_2(t)$ are the x component of the hand position profile in the first and

the second segment respectively , and $x(t)$ is the overall x component of the hand position profile throughout both segments. The value of x_I is given as the value of the x component of the actual hand location when the first cue is sent. Thus, there are six parameters to be determined: Δx_1, 'Δx_2, T_{0i}, and T_i for $i = 1, 2$ in the x component. In the same way, y_I can be defined, and by finding Δy_1 and Δy_2 with the same T_{0i} and T_i for $i = 1, 2$, the y position profile can be defined as well. Therefore, the whole trajectory is kinematically characterized by 8 parameters. The minimum jerk velocity profile is defined as a time derivative of the minimum jerk position profile defined above.

Genetic algorithm command in MATLAB, `ga`, was used to find a set of eight coefficients by first fitting a hand velocity in horizontal and vertical directions independently to obtain a reasonable set of initial conditions for a subsequent optimization on position profiles. The genetic algorithm was chosen over other nonlinear optimization routines as the genetic algorithm was capable to take a set of initial conditions from predefined ranges for each parameter as opposed to one initial condition so that the algorithm tests a series of different initial conditions and tried to modify the initial conditions such that subsequent set of optimizations tended to perform better than the previous stage. Furthermore, the ranges of initial conditions were automatically changed slightly to extend a search space. The range for each parameter was set manually by fitting several trajectories reasonably well. In order to increase the performance of data fit, each hand speed profile was truncated at the first local minima, t_{tr}, after the hand speed becomes less than 0.1 m/sec. Then, both position and velocity profiles were fit simultaneously by minimizing the squared error between the data and the fit. The terminal condition for the first round was that a number of genetic mutations, mixing a set of initial conditions to yield a better set of initial conditions, reached 100. In the second round of the minimization, the terminal set of parameters from the first round was used as an initial condition with the same range for each parameter as in the first round minimization. An equality constraint was added such that the end point of the fit data characterized by the vector $(\Delta x_1 + \Delta x_2, \Delta y_1 + \Delta y_2)$ was equal to the vector $(x_F - x_I, y_F - y_I)$ where (x_F, y_F) corresponded to the location of the hand at $t = t_{tr}$. The

termination condition was that the error normalized by the sum of squares of both position and velocity profile became less than 5%. The final fit was compared with the data visually to make sure that the fit was reasonable.

After the kinematic fit by the genetic algorithm to obtain the movement distance and duration for each movement segment, a simple reaction time analysis was performed. Reaction time (RT) to the cues was defined to be

$$\begin{aligned} RT_i &= \text{Initiation time of minimum jerk hand speed profile for i-th movement segment} \\ &\quad - \text{i-th Cue time}\ , \quad i = 1, 2. \end{aligned} \tag{6.5}$$

Next, the kinematic data was fit with the output of one of the LPV models, LPV2, developed in Chapter 5. For this purpose, the arm's geometric configuration parameters as well as a body weight for estimating the weight and inertia of each upper limb segment were acquired from each subject after the whole experiment. Then, kinematically well fit data with the minimum jerk profile being reference trajectories to the LPV model were chosen to be fit with the LPV model. Again, the genetic algorithm command, `ga` was used to find the eight parameters for the two sequential minimum jerk profiles with the initiation parameters being the parameter values found in the kinematic fit. There were no equality constraints posed this time for componentwise sums in x and y directions of the distance parameters to match the end point of the movement since the output of the LPV2 system would not need to have the zero error at the terminal point, as seen in some examples from Chapter 5. For the LPV fit analysis, only qualitative assessments will be made.

6.3 Results

6.3.1 General description of kinematics

Data recorded from the four subjects were used in this study. Each data set consisted of 560 trials total, 140 trials for each of the combinations of the starting point (N,S) and final

targets (L,R) described in Section 6.2.1. Although the distance between possible second targets is fairly significant relative to the distances between the center target and possible second targets, none of the subjects noticed that s/he was aiming to a different second target at each trial. Nevertheless, the subjects successfully made initial straight movements to the first target and reacted to the cue to reach to a second target. Figs. 6-2 and 6-3 show a pair of examples of hand movement trajectories and their corresponding hand speed profiles of one subject, B11. An example in Fig. 6-2 shows a hand path with smooth transition from the first segment to the second segment of the movement. The hand speed has only one clear peak before the hand reaches to the second target. On the other hand, another example in Fig. 6-3 shows a hand path which appears to have two relatively straight paths connected around the first target and a hand speed profile with two distinct peaks each of which corresponds to each segment of the movement. Furthermore, the widths and heights of the speed peaks appear to be fairly different.

However, during many trials all subjects showed a "hook" at the end of the movements to attempt to eliminate the error to arrive at the second target accurately. An example of this is shown in Fig. 6-4.

It is noteworthy that three subjects, B11, Y11, and R12 reported that one particular set of movements, N to C to L (NL) was "difficult" compared to the other sequences. One subject, B12, reported that a set of movements, S to C to R (SR), in particular, the second segment was difficult to "learn" to make coordinated movements.

Furthermore, all four subjects reported, during or after the entire experiment, that it was difficult to maintain her/his attention level to react to the cues as quickly as s/he wished because of the repetitive nature of the tasks. In addition, all subjected reported that they occasionally made their "own" movements in which they neglected or did not react to the second cue as quickly as possible so that they could make "smooth" transitions and ensure high accuracy in the terminal error.

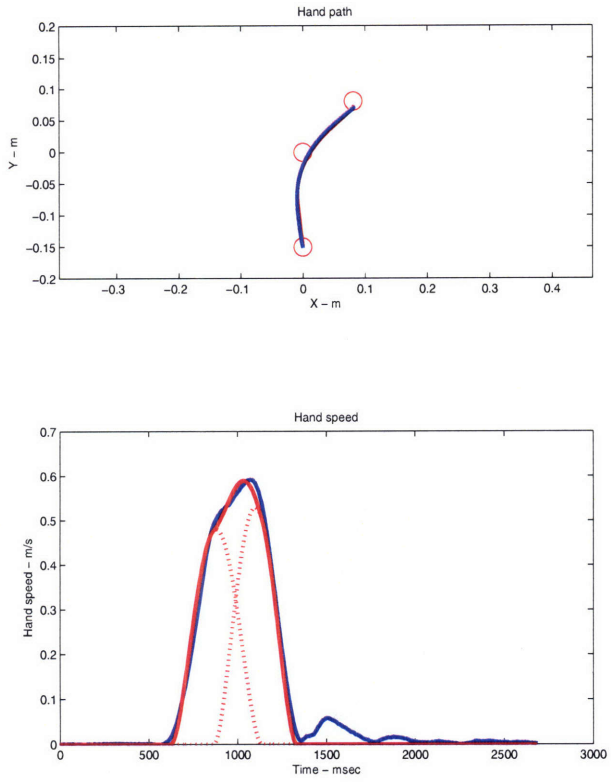

Figure 6-2: An example of hand path and speed for a movement from S to C to R. Only one distinct speed peak is prominent. Red circles:Initial and target locations, Solid blue:Data, Solid red:Overall fit, Dashed red:Individual segment fits

6.3.2 Kinematic Data Fit

Hand position as well as hand velocity data were fit kinematically using two sequentially added minimum jerk profiles as in Eq's (6.1 $\sim$ 6.4). The subjects exhibited various patterns of trajectories, but in general in terms of quality of fit there were four, but not mutually exclusive classes of trajectories: a) Those fit well by two minimum jerk trajectories, b) those with a terminal "hook", c) those with a premature and abortive turn, and d) those with speed profiles that were clearly not consistent with a minimum jerk trajectory.

a) Examples of good fits are shown in Figs. 6-2 and 6-3 which reproduce both hand paths and speeds faithfully. Both examples show hand speeds that attenuate well once the hand reaches to the second target.

b) Many trials had a "hook" at the end of the movement. Those movements did not have

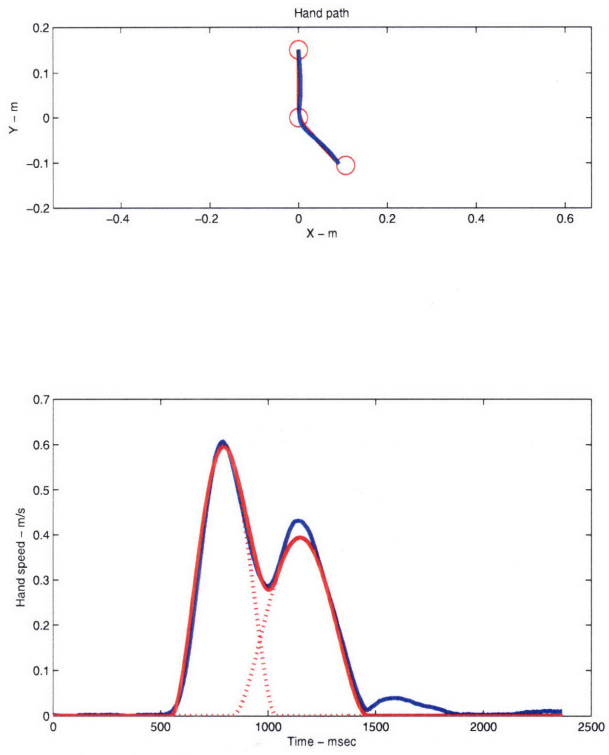

Figure 6-3: Another example of hand path and speed for a movement from N to C to R. There are two distinct speed peaks. Line types are the same as in Fig. 6-2

nice kinematic fits. An example of such a case is shown in Fig. 6-4. The first segment is fit reasonably well both in path and hand speed, while the second segment is not especially in the path. c) Subjects made a transition from the first segment to the second too abruptly. As a result, although the hand speed appear to be reasonable, the corresponding hand path has a change in convexity as shown in Fig. 6-5, and occasionally even a swerve.

d) Either initiation or termination of the movement was extremely slow so that the optimization resulted in faulty a movement initiation or movement duration. This can be seen also in Fig. 6-5 where the hand speed decreases very slowly as the hand approaches to the final target so that the duration of the second segment is not well approximated by a minimum jerk speed profile.

Therefore, every fit was inspected visually to see if the fit was reasonable. If the fit was reasonable, then it was retained for further analysis. The number of trials used for the rest

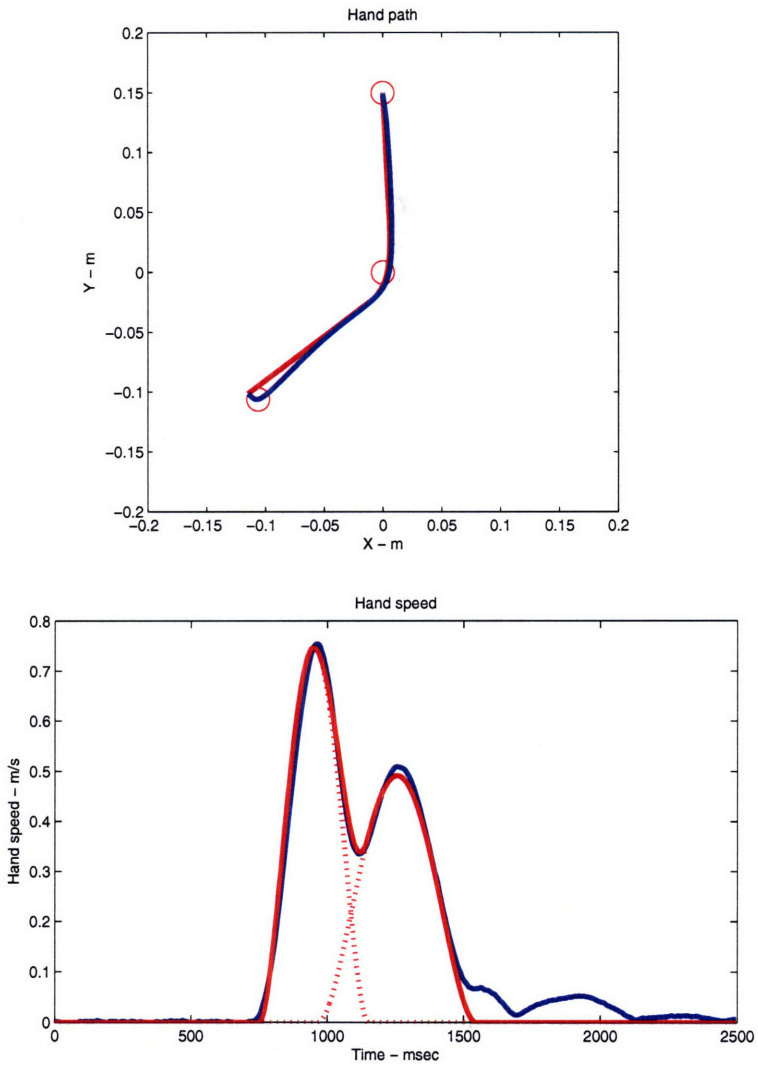

Figure 6-4: An example of hand kinematics with a terminal hook and corresponding fit for a movement from N to C to L. Line types are the same as in Fig. 6-2

of the analysis in this study is summarized in Table 6.1.

Subject \ Task	NL	NR	SL	SR	Total
B11	35	32	21	46	134
B12	24	15	9	33	81
R12	31	20	21	28	100
Y11	12	25	34	47	118

Table 6.1: Number of trials used in the kinematic and reaction time analyses.

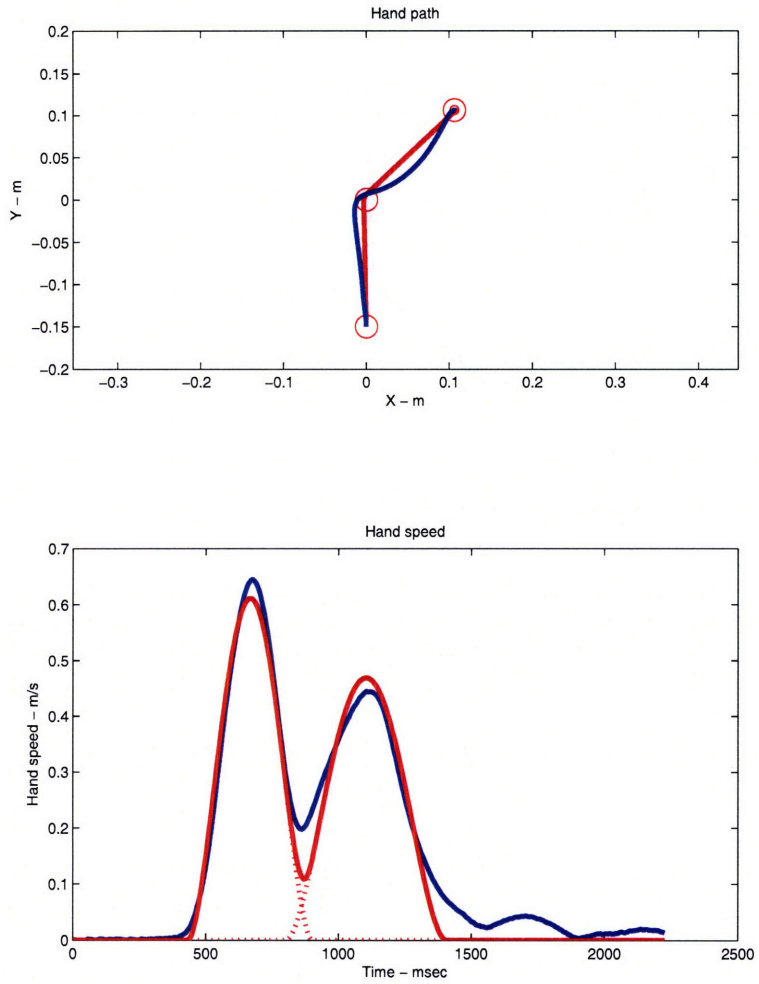

Figure 6-5: An example of hand kinematics with convexity change and corresponding fit for a movement from S to C to R. Line types are the same as in Fig. 6-2

The number of trials whose data was fit badly in a particular movement directions does not appear to reflect how the subjects felt about the difficulty of the tasks.

Movement distance analysis

From the qualified kinematic fit, the movement distances characterized by Δx_i and Δy_i, $i = 1, 2$ were collected. The statistical summary of those parameters are shown in Table 6.2.

In this study, the first segments of all movements performed were either N to C or S to C so that $\Delta x_1 = 0$ and $\Delta y_1 = \pm 15$ cm. Note that the first target location, C, was always the

Subject \ Task		NL	NR	SL	SR
B11	Δx_1	0.62 ± 0.82	-0.02 ± 0.72	0.32 ± 0.87	0.19 ± 0.90
	Δy_1	-15.20 ± 0.75	-15.57 ± 0.81	15.76 ± 0.37	15.33 ± 0.86
	Δx_2	-11.31 ± 1.21	10.82 ± 1.21	-11.02 ± 1.04	11.32 ± 1.25
	Δy_2	-10.21 ± 1.20	-10.28 ± 1.15	10.34 ± 0.93	10.15 ± 1.25
B12	Δx_1	0.58 ± 1.68	0.02 ± 1.27	-0.80 ± 1.53	-2.12 ± 0.82
	Δy_1	-14.88 ± 1.41	-14.95 ± 1.59	15.01 ± 1.69	15.39 ± 1.01
	Δx_2	-11.54 ± 1.63	10.26 ± 1.87	-9.86 ± 1.02	13.01 ± 1.78
	Δy_2	-12.01 ± 1.98	-10.68 ± 1.73	10.18 ± 1.82	10.89 ± 1.71
R12	Δx_1	0.70 ± 1.51	0.30 ± 0.90	-0.45 ± 1.13	-1.48 ± 0.99
	Δy_1	-14.41 ± 1.52	-14.69 ± 1.32	14.52 ± 1.64	15.50 ± 0.76
	Δx_2	-13.51 ± 1.68	10.56 ± 1.54	-11.29 ± 1.91	13.07 ± 1.49
	Δy_2	-12.17 ± 0.70	-10.75 ± 1.56	12.45 ± 2.10	11.06 ± 1.65
Y11	Δx_1	-0.57 ± 1.47	0.14 ± 0.87	-0.54 ± 1.31	-0.05 ± 1.25
	Δy_1	-15.29 ± 0.89	-14.88 ± 1.23	14.41 ± 1.92	15.06 ± 1.23
	Δx_2	-10.30 ± 1.21	9.95 ± 1.23	-10.09 ± 1.11	11.30 ± 1.63
	Δy_2	-10.10 ± 0.80	-10.78 ± 2.01	12.21 ± 0.60	11.72 ± 1.94

Table 6.2: Summary of the distance parameters in Eq's 6.1 $\sim$ 6.4 characterizing the hand position and velocity profiles in each type of paths in each subject. Each of the data entry takes the form of mean $\pm$ std. Units are in cm.

same and therefore deterministic. The mean offset of Δx_1 was fairly small except for the SR task by the subjects B12 and R12. R12 reported that the SR task was difficult to "learn" to make movements with coordinated elbow and shoulder movements. This large offset might possibly be a reflection of a subject strategy to mainly use the shoulder movement first to bring the hand to further left than necessary, so that the second segment was mostly driven by the elbow movement to the final target.

The second segments of all movements performed were from C to L or R so that if the second segment started from C to one of the targets in L or R the following should hold on average: $\Delta x_2 = \pm 15/\sqrt{2} = \pm 10.61$ and $\Delta y_2 = \pm 15/\sqrt{2} = \pm 10.61$ where the sign was determined for a specific movement direction. For a given trial, the second target was randomly but equally likely chosen from the seven possible targets within a cluster of targets that were known to a subject prior to his/her making the first segment of each movement. However, as seen in Table 6.1, not the same number for each of the seven possible targets

was used for the analysis so that there should be some bias in the statistics shown in Table 6.2. Nonetheless, the combination of the statistics from the first and second segments would indicate how a subject might have employed a biased movement strategy with a shifted first target location.

Movement time analysis

First, the summary of movement duration distributions in terms of their means $\pm$ std's for each subject for each movement direction is shown in Fig. 6-6. There was no active constraints on the movement durations. Through a practice session, each subject found a range of velocity and corresponding movement durations in which s/he could perform the task comfortably.

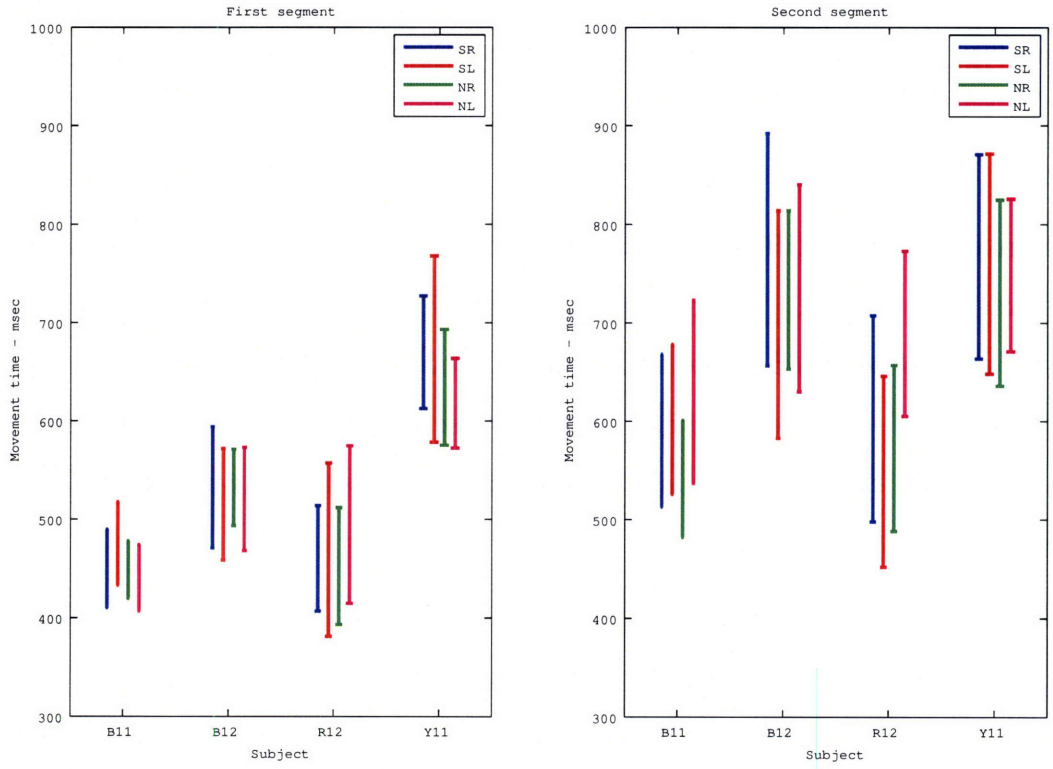

Figure 6-6: Summary of movement durations.

It can be seen that the durations for the first segment are consistently shorter (pairwise t-test, $\alpha = 0.05$) and have less variance than those for the second segment (two-sample

F-test, $\alpha = 0.05$). Although the degrees are not the same, subjects B11 and R12 made movements of shorter durations than B12 and Y11 did (B11 against B12 and Y11, and R12 against B12 and Y11, pairwise t-test, $\alpha = 0.05$) while each subject traveled for roughly the same distance in each trial. For subject B12, the SR direction which was reported as the most difficult direction to learn indeed has the longest duration (pairwise t-test, $\alpha = 0.05$) and the highest variance (two-sample F-test, $\alpha = 0.05$, except for SR against SL) for both segments. However, for the rest of the subjects, the same can't be said for the NL direction which was claimed be the most difficult direction to move by the rest of the subjects . Thus, the directional difficulty felt by the subjects does not seem to be explicitly reflected in longer movement durations and wider variance in durations.

The summary of reaction time distributions in terms of their means $\pm$ std's for each subject for each movement direction is shown in Fig. 6-7. Across all subjects and all movement directions, the reaction times to the first target are mostly positive except for a small number of trails by the subject Y11 (5 trials (4.2 %)) and have smaller variances than those for the second segment (two-sample F-test, $\alpha = 0.05$). The reaction times to the second target are, on average, much shorter than those to the first target (pairwise t-test, $\alpha = 0.05$), and sometimes even negative as shown in Fig. 6-8. Both hand path and speed fits are extremely well, but RT_2 for this particular trial is -152 ms. The exact sources of this negative reaction time are unknown. One potential source is that data fitting method used in the current study as the minimum jerk profile was used as the template. The minimum jerk velocity profile is symmetric, but as reported previously (Milner 1992), an empirical velocity profile tends to be asymmetric and to have a longer tail. Thus, such an asymmetric profile enables the second profile to start later. Another, yet more likely, source is that subjects reportedly made their own movements, i.e., subjects ignored the cue for the second target. Thus, at some trials the subjects guessed when to turn toward the second target area before the cue for the second target appeared. This could have been the case for many of the trials with negative reaction times.

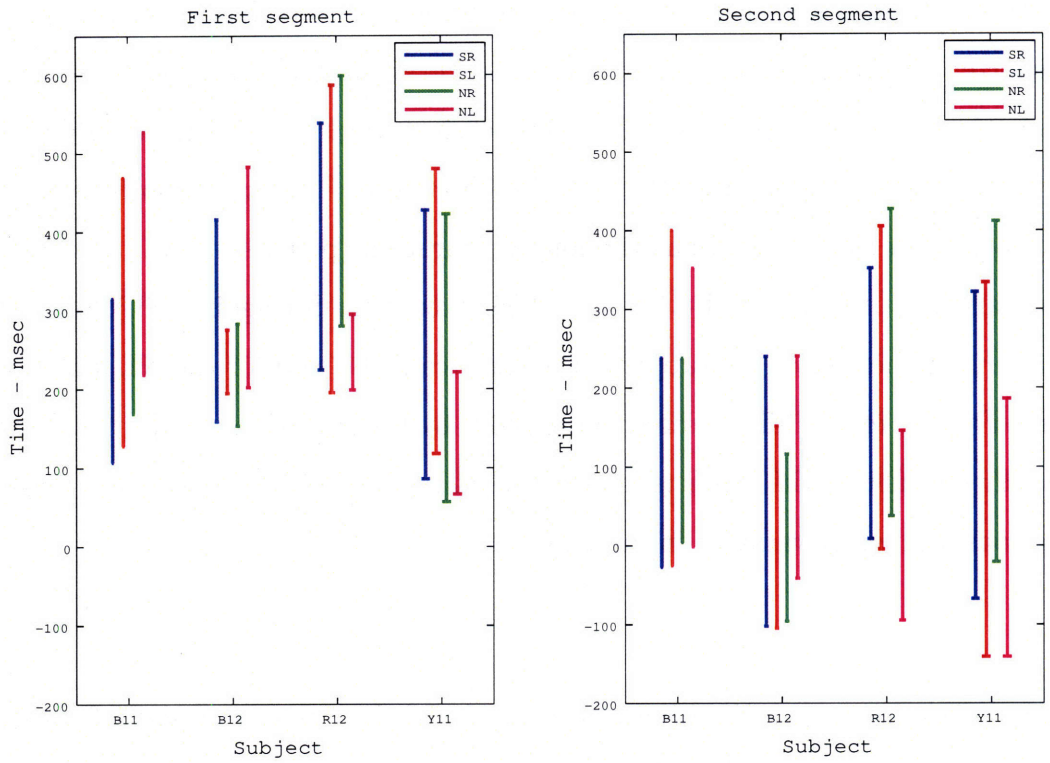

Figure 6-7: Summary of reaction times.

6.3.3 LPV model fit

As shown in Chapter 5, LPV2, an LPV model with two scheduling parameters was developed for a two-link arm model. Given the physical measurements from each subject, sets of necessary parameters were used or estimated to characterize his or her arm dynamics. However, the muscle stiffness used in the model remained the same for all the subjects. Based on those parameters and muscle stiffness, a set of LPV controller gains were designed as in Chapter 5. Then, a reference trajectory was estimated as outlined in Secion 6.2.3 to yield the best fit between the empirical hand position and velocity and those from the LPV model. From each subject, only five trials for the S-C-R task and another set of five trials for the S-C-L task, total of 10 trials were used to explore the quality of the fit.

Among the 40 trials used, `ga` algorithm converged for 39 trial data. Fig.6-9 shows an example of a data fit well by the LPV2 model. A minor curvature of the hand path in the first segment is not extremely accurately captured and there is a slight offset at the end point

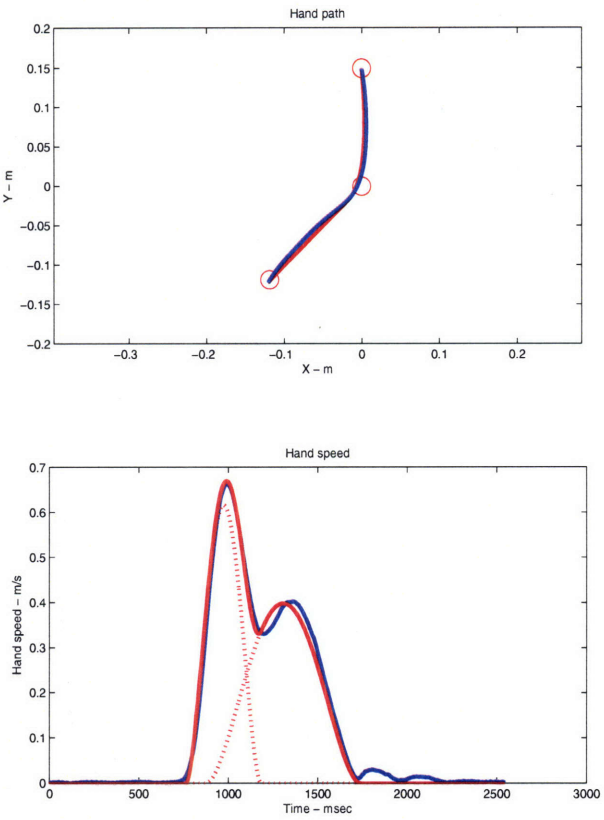

Figure 6-8: An example of kinematic fit resulted in negative reaction time to the second target for a movement from N to C to R. Line types are the same as in Fig. 6-2

of the movement exists, but the overall the hand path is fit by the LPV2 model well. The extrema of the hand speed slightly deviate from the data, but the LPV2 response faithfully captures the hand speed of this data whose second segment command starts roughly at the middle of the first movement segment.

The second example is shown in Fig. 6-10. The hand speed data has two well separated and distinct peaks and the LPV2 response reproduce the data very well. However, the hand path of the second segment shows almost constant offset till the end of the movement. This type of slight offset between the data and the LPV2 response in the second segment of the movements turned out to be fairly common, as seen for the following two examples as well, even thought the genetic algorithm used in this study was minimizing the error between the data and the LPV2 responses.

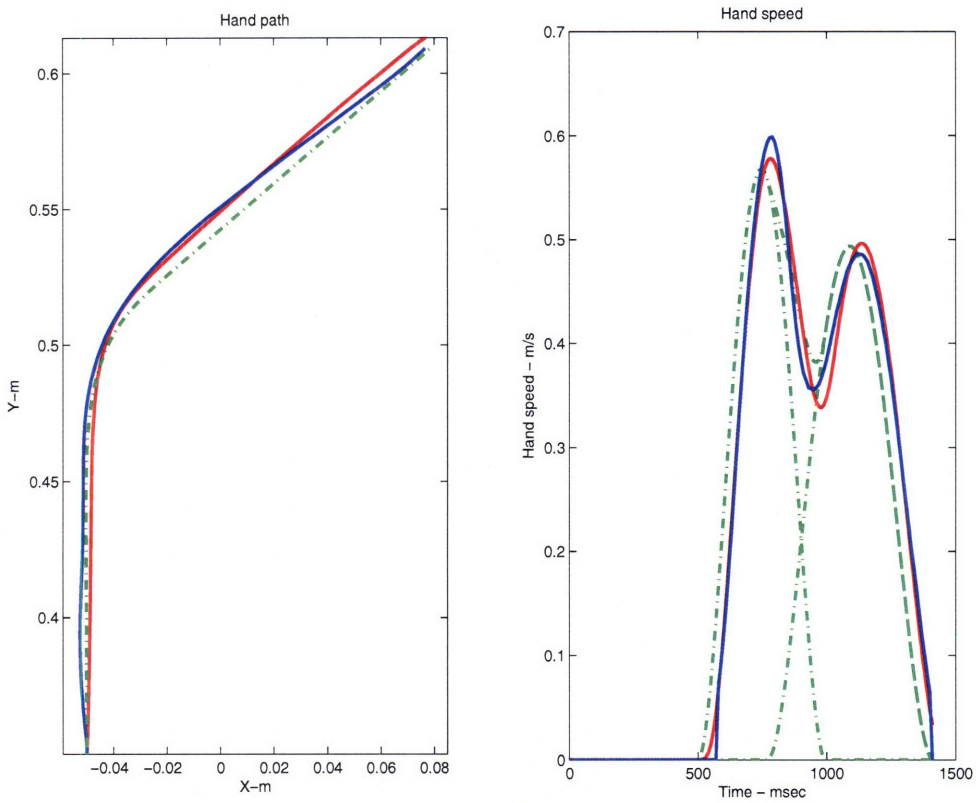

Figure 6-9: An example of kinematic fit of the data with response of the LPV2 system. Data from subject B11 performing S-C-R task. Experimental data (blue), LPV fit (red), and Reference command for the LPV system (green dashed). Left: Hand path. Right: Hand speed.

The first two examples show the case when the hand speed has distinct two peaks. Fig. 6-11 shows an example when the hand speed is unimodal. Overall, both the hand path and speed are fit well with the LPV2 system. The LPV2 response manages to trace the first segment of both the hand path and speed, however again, there is small deviation both in the path and speed.

Fig. 6-12 illustrates an example of a fit of the movement of the target sequence S-C-L to see if the LPV2 system can faithfully reproduce a direction that tracking performance was shown to be worse than S-C-N or S-C-E direction in Chapter 5, see in particular Fig. 5-10. Although there is a small difference between the data and the LPV2 response, both the hand path and speed are reproduced in S-C-L movements as well as in S-C-R movements.

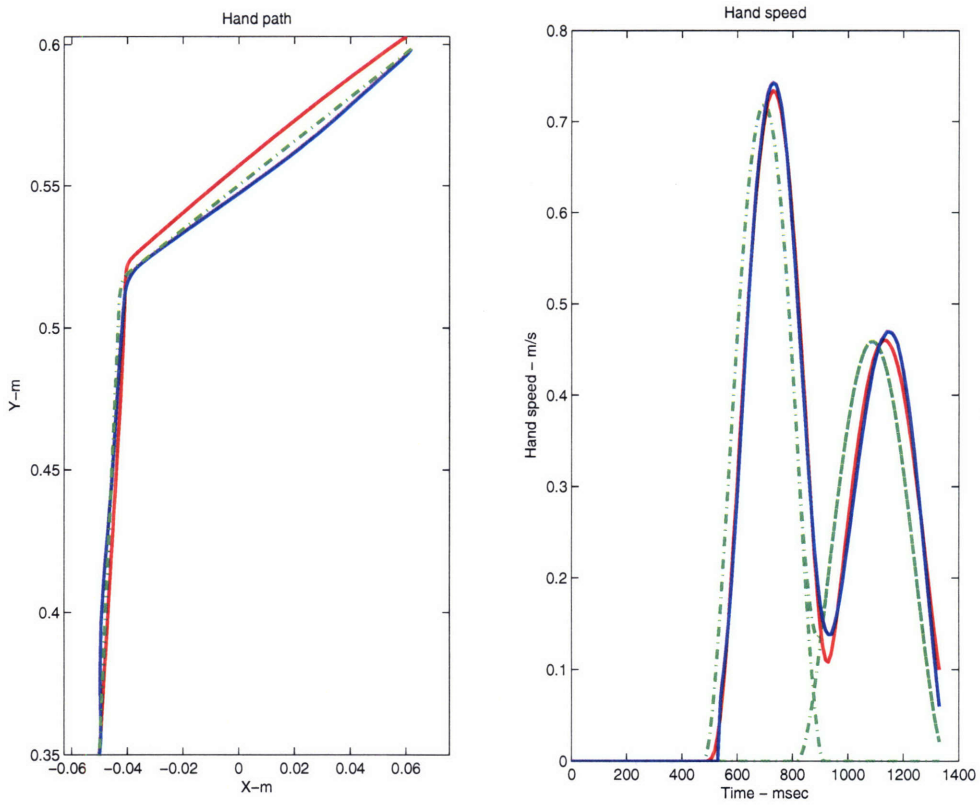

Figure 6-10: An example of kinematic fit of the data with response of the LPV2 system. Data from subject B12 performing S-C-R task. Line types follow Fig.6-9.

In addition, the small offset of the hand path in the second segment shown in Fig. 6-10 for S-C-R movements is present in many of the S-C-L movement as well.

6.4 Discussion

6.4.1 On movement variability

Despite simplicity of the task, or potentially because of the simple and repetitive nature of the task, there are multiple sources of movement variability. Although the task was simple, it is important to separate different sources of variability to how different components of motor planning and execution are implemented in the CNS (Vindras et al. 2005) so that the effect of the command in terms of its kinematics and the dynamic effects due to the

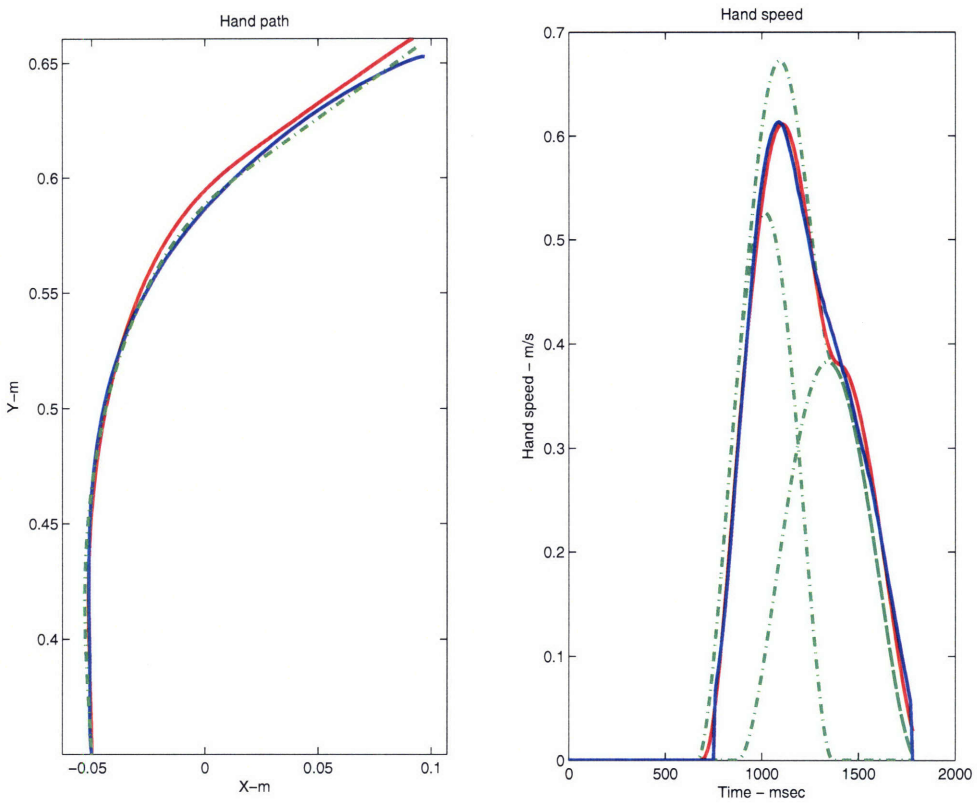

Figure 6-11: An example of kinematic fit of the data with response of the LPV2 system. Data from subject R12 performing S-C-R task. Line types follow Fig.6-9.

plant and the controller can be dissociated. Furthermore, it is desirable that the human task includes many of the same sources of variability as the primate experiment, but is constrained enough in terms of the probable reference command that you can have a chance to model the fundamental mechanism of making a turn.

First is the variability in paths and the distances estimated by the optimization procedure in each segment of the movement. There is a fairly large number of trials which were not used in the analysis in this study as they were not fit well by the sequential minimum jerk profiles. For example, the subjects overshot or miss-aimed the second target such that there was a correctional hook movement as shown in Fig. 6-4. Furthermore, depending on what strategy was employed by a subject, movement paths contained some biases such as the shown in Fig. 6-2 where the subject chose to make an initial movement towards slightly to left to make a smoother movement to turn right for the second segment. These classes of

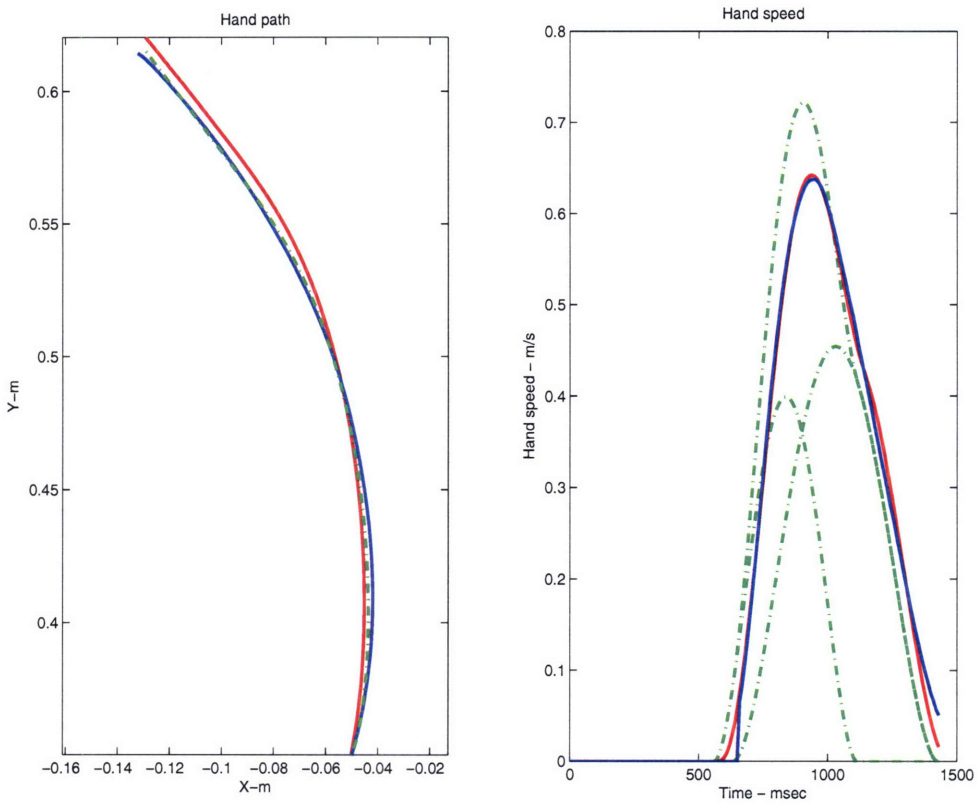

Figure 6-12: An example of kinematic fit of the data with response of the LPV2 system. Data from subject B12 performing S-C-L task. Line types follow Fig.6-9.

movement variability can probably be reduced with a tighter experimental control. Subjects could be asked to pay more attention to the location of the target or to abort a trial if the initial direction exceeds a certain threshold. It would be still important however that subjects remain relax while moving so that they would not change their limb stiffness significantly from the value assumed by the model.

Second is the variability of the movement durations for each segment. There was no duration constraint in the current study so that the movement durations were determined completely by the subjects. However, the subjects were told to make movements as fast as possible while maintaining the terminal accuracy as well as their comfort level, i.e., not causing noticeable cocontraction of muscles. Thus, a certain degree of duration variability is unavoidable and reflects a rough kinematic plan established by each subject. Furthermore, it has been suggested (Tanaka et al. 2006) that movement duration is a result of a trade-off

between speed (time optimality) and accuracy (acceptable endpoint scatter) and that such a formulation reproduced movement duration as a function of the ratio of target distance to target size known as Fitts's law. Thus, changing the target size in the current experiment would test the feasibility of the hypothesis suggested by Tanaka et al. (2006).

Third, the variability of the reaction time estimated using the kinematic fit of the hand speed with the minimum jerk profile was quite significant. Unlike other studies in which a double-step paradigm was employed, each subject knew the exact location of the first target and to which direction the second segment of a movement to be made before a trial started. It was reported (de Rugy and Sternad 2003) that initiation timing of a discrete movement during a periodic movement tended to be synchronized to a specific phase of a periodic singe joint elbow movement that the subjects were performing. This tendency was greater when the movements were self-paced than when the movements were of a reaction task. Although the subjects in our study did not perform any periodic movements, it may be possible that the CNS synchronizes multiple neural circuitries required to perform a task based on a phase of oscillatory activities that many brain areas exhibit. It has been observed Rubino et al. (2006) that during a preparation period of a point-to-point movement, many of simultaneously recorded neurons in motor cortical areas exhibit strong beta oscillation of local field potential (LFP) and evoked phase lock of beta oscillation across many motor cortical neurons to generate a cortical wave of tens of millisecond to a few hundred millisecond. Such waves were persistently generated during the instruction delay period and the beginning of movement initiation. Therefore, whether a movement is periodic or discrete, it appears that the brain utilizes phases of cortical oscillation. Thus, the movement initiation times estimated by the method in this study may include neural processing times of such synchronizing activities in the brain. To further investigate this issue, it would be interesting to record cortical oscillation through LFP, EEG or MEG while the subjects are performing the same reaction tasks.

Fourth, the resolution of choosing a virtual point to aim in the target circle may not be extremely accurate. In our experiment, all subjects indeed did not notice that they

targeted to a randomly chosen second target out of the seven possible ones. Thus it is possible that when a subject was to move to a second target from the first target, s/he knew approximately which direction and how far a movement needed to be, but the range of a virtual point to aim could lie within a circle containing all the seven possible second targets. However, once the virtual point was set from a smaller circle than the circle containing all the seven possible second targets, in this experiment such a small circle was explicitly presented to the subjects as one of the seven possible second targets, all the subjects could make a reasonably accurate movement to that point. Because in the primate experiments, the target cursor was relatively large (2.5 cm radius), the monkeys could move their hands to different locations within the target and still satisfy the experimental tracking requirement. That is, the endpoint locations of each catch-up movement to the target cursor were somewhat under constrained. As a result, individual segments of monkey movements were somewhat variable in duration and length. To provide an analogous situation for the human subjects, the second target was moved randomly to 7 locations within a region of diameter of 6 cm (Fig. 6-1 I $\sim$ VI). The ratio of region diameter to the average length of the last movement segment (C-R or C-L)was $15/6 = 2.5$ which approximates the ratio $5/2.5 = 2$ of the monkeys target cursor diameter to average movement length. We also verified that subjects did not notice that the randomly presented target cursors actually changed position by as much as 6 cm. Thus, some trajectory variability was induced that was comparable to that displayed by the monkeys, and the subjects did not have any sense that the task itself was varying. The induced variability presumably reduced over learning that might be associated with the static human task, and presumably helped keep the results comparable to the primate experiment. Thus, if the hypothesis that a circular tracking motion by the monkey can be approximated inhuman by sequential point-to-point movements holds, then some trajectory variability may be explained by the imprecision to aim a virtual point within the target circle.

Some, if not all, candidates for movement variability suggested above may well be coupled. Thus, even kinematically dissociating each component in the experiment and the

consequential data analysis can be fairly challenging.

6.4.2 Sequential command

In this experiment, a slightly randomized, in terms of the second target variability, static double step task was chosen because preliminary study (not shown) showed that human subjects used a predictable strategy for a predictable circular cursor tracking task as that of the monkey. Thus, in order to approximate a catch-up strategy employed by the monkey, a double step task was chosen. In the current formulation, the sequential command consisting of two minimum jerk templates was first used to perform kinematic fit to the data. The data analysis showed that some hand kinematics could be accounted for by having a vectorial superposition of two point-to-point movements each of which started and ended with zero velocity. This observation is consistent with previous studies (Flash et al. 1992; Rohrer et al. 2004; Vindras et al. 2005). The movement distances found to fit the minimum jerk profile appear to be reasonable, but some reaction times, especially for the second segment, turned out to be negative. One very likely cause for this negative reaction time is that subjects anticipated the second cue and started making a second movement by ignoring the second cue timing. Another, yet probably minor cause of this may be asymmetry of empirical velocity profile. It has been noted (Rohrer et al. 2004; Milner 1992) that a kinematic template to fit hand velocity can be asymmetric and be individually customized. Thus, short, but still positive, reaction times can be partially explained by this possible velocity profile asymmetry. As there was no record as to which trial a subject recognized that s/he did not follow the cue, it was impossible to pin down which trails belong to this category.

Even when the reaction times are reasonable, it is yet not clear how such a sequential command is generated physiologically. It was suggested that the generation of the reactive arm movement to the second target would be based on retinal errors between the first and the second targets (Boulinguez et al. 2001). In addition, the CNS appears to process the amplitude and the direction of a motion independently (Gordon et al. 1994; Vindras et al. 2005). A series of studies (Desmurget et al. 2003, 2004) suggest that the basal ganglia are

specifically involved in the planning of movement amplitude, but not in the movement direction. Thus, it is possible that the amplitude and the direction of a motion can be determined based on the location of the cue, but movement duration and/or speed is controlled by a different neural circuitry. Then, the high level command to the motor system may consist of a step function defining the target location and speed gain. In relation to the RIPID formulation, the reference command can be a step function and the speed gain can be a multiplicative gain of a cortical integrator in the motor cortex. This mechanism can yield a minimum-jerk-like velocity profile (Karameh and Massaquoi 2005). A similar approach has been used to generate a position command based on motion error signal (Bullock et al. 1999). The resultant kinematic profile of the model by Bullock et al. (1999) reproduced a velocity profile that is similar to what's seen in our experiment, i.e., it seems that it can be fit reasonably well by a sequence of minimum jerk profiles, but the velocity profile showed slight asymmetry. Thus, the minimum jerk command can account for the data to explain gross kinematic features well, but without implementing a more detailed neural mechanism such as BG-RIPID or the model by Bullock et al. (1999), some kinematic features such as asymmetry in the velocity profile may be difficult to explain.

6.4.3 LPV system to characterize a double-step movement

As shown in Figs 6-9 through 6-12, some kinematic data were fit reasonably well with the LPV2 model with a reference command consisting of two sequential minimum jerk profiles. A few sets of data that were not fit well by the minimum jerk profile are fit with the LPV2 responses, but the results are either consistent with fits by a sequence of minimum jerk profiles alone, or exhibiting some consistent trend of the fits by the LPV2 responses, such as hand path off set as shown in Figs 6-13 and responses, such as hand path off set as shown in Figs 6-14.

However, note that both examples have fairly accurate fits of the hand speeds. Although the errors in the each component of the hand trajectory and the hand velocity are equally weighted, generally the velocity components, hence correspondingly the hand speeds tended

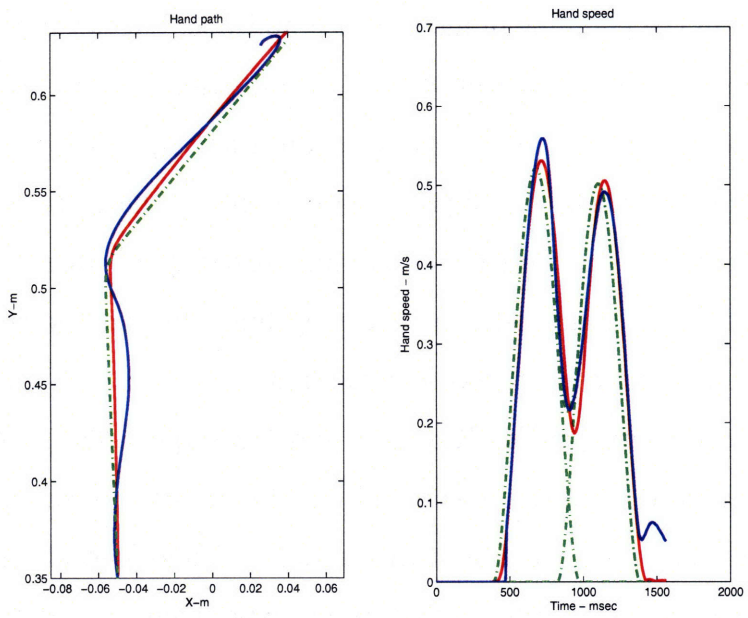

Figure 6-13: An example of kinematic fit of the data with response of the LPV2 system. Data from subject B12 performing S-C-L task. The data was not fit well purely kinematically by a sequence of the minimum jerk profiles. The hand path is fairly curved with varying convexity with terminal hook. Line types follow Fig.6-9.

to be fit better than the hand paths.

Unlike the purely kinematic fit procedure which placed a constraint to have a perfect match at the end point of the movements, the optimization routine used for the LPV fit could not include such a constraint. Furthermore, each data point in the trajectory or velocity data was treated equally. Thus a set of coefficients for a pair of minimum jerk reference command for the LPV system was chosen to minimize the mean squared error between the data and the fit. Therefore, we can't conclude with confidence that the characteristic deviation from the data seen in LPV2 fits, such as the path offset (see Fig. 6-10) and smoother hand speeds (see Fig. 6-11) may well be the result of a choice of uniform penalty in the optimization routine over the hand path and hand speed, or over each point in the data.

Although there was significant performance difference of the LPV models based on the directions of the movements as shown in Fig. 5-10, the LPV2 responses fit a set of data reasonably well for both S-C-L and S-C-R movements. There are two potential reasons.

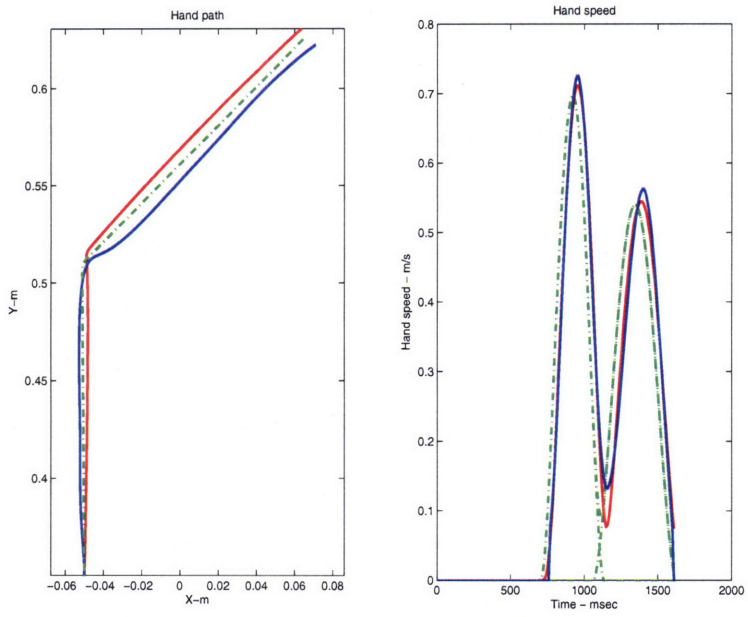

Figure 6-14: Another example of kinematic fit of the data with response of the LPV2 system. Data from subject R12 performing S-C-L task. The data was not fit well purely kinematically by a sequence of the minimum jerk profiles. The hand path makes almost a right turn. Line types follow Fig.6-9.

First, the durations of the movements in the experiment were usually longer, and thence the movements were slower. The peak hand speeds of the LPV simulations in Chap 5 are above 0.8 m/s for most of the cases, sometimes even around 1.0 m/s, while in the experiments most of the data that resulted in reasonable purely kinematic fit did not have such high peak speeds, usually less than 0.7 m/s. Second, the second target arrangements are different between the LPV simulations and the experiment. The LPV simulations had sharper turns to make with faster speeds as above. Thus, the whole tasks were dynamically more demanding than those that subjects ended up performing to result in reasonably fittable data. Based on this argument, a single $\mathcal{H}_\infty$ controller might yield a response that fits the experimental data well. Fig. 6-15 shows an performance comparison between $\mathcal{H}_\infty$ and LPV2 responses. During the first segment of the movement, the responses from both systems do not differ much either in the hand path or speed, but in the second segment it appears that the initiation of the second segment was not on time and the direction of the second segment was slightly off to

the left. Furthermore, the end point error of $\mathcal{H}_\infty$ controller is much larger than that of the LPV2. This is one of a few data set that show significantly inferior performance by the $\mathcal{H}_\infty$ controller to that by the LPV2 controller. Other data sets were fit comparably well by both the $\mathcal{H}_\infty$ controller and the LPV2 controller, usually slightly better by the LPV 2 controller. Thus, despite these examples one cannot conclude that the actual experimental data could be reproduced better with LPV2 system than a single $\mathcal{H}_\infty$ controller system. However, they may indicate that the actual data can always be fit better with LPV2 systems especially given the variability in kinematic data and the speed of the tasks that subjects performed. In order to critically test if a LPV, or gainscheduling system is better than a single $\mathcal{H}_\infty$, or even a gainscheduling is necessary to explain behavioral data, more data with faster speeds would be required. Furthermore, in order to avoid ambiguity of the effects between the responses of dynamical systems and those of optimization procedures to minimize the difference between the simulation responses and the experimental data, a better method of combining dynamical controller design and data fitting need to be developed without setting an extremely fine grid in both command and controller parameter spaces and searching those spaces exhaustibly. A new development in fuzzy control Espinoza et al. (2004) may be used to fit a data better while both a set of controllers and a command can be modified.

The LPV modeling suggests that physiological control might be implemented by scheduling of linear controllers that are selected in a feedforward manner based on movement plan. In this regard, it is of interest that based on the simultaneous recording of multiple single neurons in M1 by Hatsopoulos et al. (2003), the correlated spike activities between pairs of neurons differed when these sequences were planned as a whole as opposed to when they were planned one segment at a time. This observation held even when the firing rates of these neurons did not distinguish between the two conditions. One possible interpretation of this result would be that based on the kinematic plan a set of neurons, at least partially, in M1 is recruited in a feedforward manner. In our study, all subjects knew the template of the task so that they just needed to react to the target cues to carry out a whole sequence. Furthermore, in our experiment the accuracy constraint was posed preferably more heavily toward

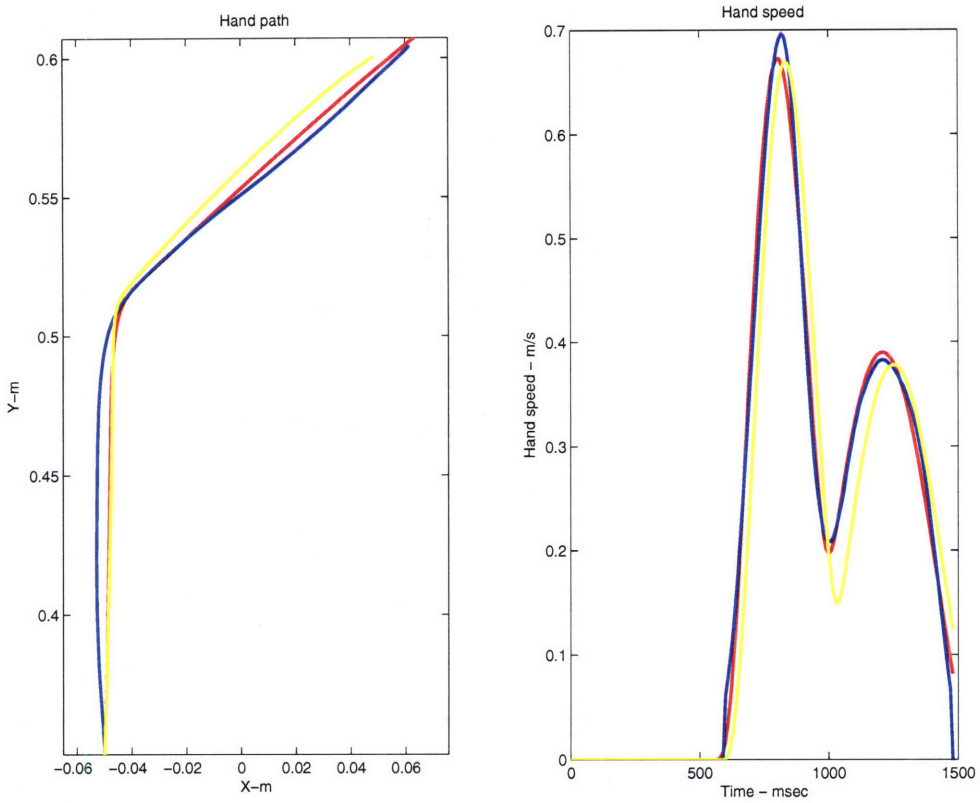

Figure 6-15: Difference between the single $\mathcal{H}_\infty$ controller response and the LPV2 response. Data from subject RB11 performing S-C-L task. Experimental data (blue), LPV fit (red), and $\mathcal{H}_\infty$ fit (yellow). Left: Hand path. Right: Hand speed.

the second target as most of the time the subjects needed not to stop at the first target. Thus, it is interesting to note from Hatsopoulos et al. (2003) that the correlation between two neurons in M1 which had statistically indistinguishable firing rates before and during a movement was strengthened when the directional preferences of the neurons matched the direction of final segment of the sequence. This may imply that there is a predetermined sequence to recruit a set of neurons prior to a movement, and potentially corresponding controllers in cerebellum that have connections to a particular group of neurons in M1 as suggested by (Kelly and Strick 2003) , based on a trajectory plan, there is at least another set of neurons that is responsible for the termination phase of the movement. Thus, in addition to spinocerebellar selector mechanism based on afferent state information suggested by the RIPID/RICSS, there may be a feedforward controller recruitment mechanism based on a

trajectory plan. Such feedforward recruitment may be useful not to recruit more than necessary number of neurons. An engineering model implementing a similar two-phase coarse scheduling is suggested by Massaquoi (2006a).

Finally, the LPV model with a sequence of minimum jerk command is yet a simplification made from the RIPID/RICSS so that a set of local controllers can be designed systematically once a set of plant parameters are known. It is shown here that the LPV model with a sequence of minimum jerk commands could account for the human experiment data reasonably well when a curvature of the hand path is relatively smooth. In order to make the model more biologically realistic, the minimum jerk-like reference signals for the LPV controllers could be generated by a sequence of step inputs to a RIPID model equipped with nonlinear integration (Karameh and Massaquoi 2005). In addition, as RICSS suggested that afferent feedback of velocity may be a component of selector or scheduling variable. Thus, in order to be more faithful to the RIPID/RICSS formulation, velocity should be included in the synthesis of LPV model to further test the validity of gain scheduling in a more theoretically tractable way.

Chapter 7

Conclusions and future extensions

7.1 Conclusions

This thesis demonstrates that a currently proposed recurrent integrator PID (RIPID) cerebellar limb control model (Massaquoi 2006a) is consistent with average neural activity recorded in a monkey by developing the Recurrent Integrator-based Cerebellar Simple Spike (RICSS) model. The RICSS formulation is consistent with known or plausible cerebrocerebellar and spinocerebellar neurocircuitry, including hypothetical classification of mossy fiber signals. The RICSS model accounts well for variety of cerebellar simple spike activity recorded from the monkey and outperforms any other existing models. The RIPID model is extended to include a simplified cortico-basal ganglionic loop to capture statistical characterization of intermittency observed in individual trials of the monkey. A natural way to enable the RIPID model to be effective throughout a larger workspace or more dynamically demanding tasks is to schedule its control gains according to local state information. There appears to be a neuroanatomically plausible mechanism to perform such a control scheme. Analytically, a linear parameter varying (LPV) formulation, which shares a similar structure to that suggested by the RICSS model, is used to check its feasibility. The LPV system reproduced some kinematic features of the data of the human subjects performing double step tasks which requires rapid change in movement directions.

7.1.1 RIPID and RICSS models

The basic structure of the RICSS arose from neurophysiological and neuroanatomical considerations. Ongoing studies of the cerebellar cortex reveal increasing complexities in its circuitry and corresponding functional roles of each cell type (e.g., Simpson et al. (2005)). In addition, multimodal nature of the inputs to the cerebellar cortex, such as visual-vestibular interaction (Buttner et al. 2003) has been observed. Thus, actual computation performed in the cerebellar cortex is most likely fairly convoluted. However, the central implication of the RICSS model is that the average PC simple spike activity patterns in a behaving monkey can be described by a relatively simple model. However, two principal features in the RICSS model were developed more empirically as follows. The first is the dependence of cortical background firing rate on the square-root of movement speed. The precise origin of cortical background activity is unknown. However, it is noteworthy that some models of muscle spindle function (Hasan 1983; Houk et al. 1981) have used a similar subunity exponent for the velocity dependence of stretch responses that include a static bias offset. The second empirically useful proposition is the simple multiplicative action of the hypothetical selector PFs through lateral inhibition (Grossberg and Kuperstein 1989). It is conceivable that therefore Eq. (3.3) represents an undue oversimplification. Especially given the large number of selPFs and interneurons that potentially influence a given PC, it is arguable that the model should have greater complexity. Although the incorporation of these elements could improve the fit, it would not alter the overall implications of the model. The fact that the current model is effective in describing the SS activity of most PCs, may indicate that it includes a good functional description of selPF activity notwithstanding its relative simplicity.

The RICSS appears to provide an explanation for the effectiveness of the UPVSc model (Roitman et al. 2004) in a manner that is consistent with known or plausible cerebrocerebellar and spinocerebellar neurocircuitry as well as physical control of a primate limb using long-loop servo control. In particular, the activity might be based upon processing of the filtered error-like signal proposed by the RIPID cerebrocerebellar control model (Massaquoi 2006a).

Moreover, the nonlinearity that appears to be fundamentally important derives in part from the multiplicative interaction between error-like signal transmitted by signal parallel fibers, and in part from state feedback information carried hypothetically by selector parallel fibers to control the effectiveness of the inhibition action through inhibitory cerebellar interneurons. This feature is consistent with the hypothesized mechanism of cerebellar gainscheduling that is posited to enable the cerebellum to adjust its feedback control according to body motion and configuration (Jo and Massaquoi 2004). Taken together, the findings herein support the validity of the RIPID control model.

Unfortunately, because the net cerebellar control signal is presumably related to the output of the entire PC population as well as direct transnuclear signals from precerebellar nuclei to deep cerebellar neurons, which are unknown to us, we cannot directly relate the PC signals seen here to the motor command to the arm. In addition, the RIPID control model also suggests that other extra-cerebellar pathways contribute significantly to arm control which further reduces the likelihood of interpreting limb control directly in terms of the recorded PC activity. Yet, although the RIPID and RICSS models contain a number of free parameters, their structures are specific and explicit. They therefore constrain internal signal behavior and afford specific, quantitative predictions for future studies.

The regression findings do not exclude other models that have been proposed for cerebellar function. However, taken together with other accumulating evidence, the results highlight contrast to alternative formulations. The observed behavior that most units responded to passive manipulation argues strongly for the presence of feedback signals in PC firing activity, as used by the RICSS model, and against purely feedforward cerebellar control models (Contreras-Vidal et al. 1997; Kawato et al. 1987). The nonlinearity in the relationship between kinematics and cerebellar signals confirmed here had not been emphasized before the UPVSc model, although purely linear formulations such as in Pellionisz and Llinas (1982) and Gomi et al. (1998), do not appear to consider linearity as a fundamental requirement. Other proposals (Kawato 1999; Kettner et al. 1997; Schweighofer et al. 1998b) are already sufficiently general to be potentially consistent with PC data used here. However, these

models have not yet been explicitly reconciled with cerebrocerebellar circuitry and cerebellar signals recorded during arm movements.

7.1.2 Intermittency

Segmentation, or irregularity, of apparently continuous movements was first observed by Woodworth (1899) more than a century ago. There is still a debate as to what constitutes a "unit" movement in the segmented kinematics (Roitman et al. 2004; Milner 1992; Flash and Henis 1991; Novak et al. 2002), or its existence itself (Sternad and Schaal 1999), submovements, which have been identified by non-smooth speed profiles with local minima and maxima, have been described in many types of movements. Based on the simple template-free submovement decomposition applied to a fairly large dataset, analysis of the speed pulses revealed three properties of the submovements. The first property, which may be limited to tracking for a long duration, is the substantial invariance of the duration distributions across the target speeds during the tracking phase. This observation was confirmed in a human study by Pasalar et al. (2005). Therefore, the observation many imply that there may exist a neural structure that is involved in generation of motor command irrelevant to the speeds of the targets during the tracking phase. The second property is the affine relation between the amplitude and the duration of speed pulses at a fixed target speed. Since the target speed and the average speed of tracking are nearly identical, this affine relation also holds true at a given tracking speed. The third property is the affine relation between the scaling factor a_1 and the target speed in the tracking phase. Roitman et al. (2004) found a slightly different result that this third property held for both the intercept and tracking phases. However, given that the exact intercept mechanism is not yet unknown and that the definition of the intercept phase used in this study may include the transition from the intercept to the tracking phase and furthermore the tracking phase itself. Nevertheless, all three properties hold in the tracking phase.

Kinematically, it has been hypothesized that a series of stereotypical velocity templates are used to make one composite movement (Flash and Henis 1991; Milner 1992). Stereotypy

is an appealing concept in that it reduces the control problem to manipulating scaled versions of a single prototype velocity template. This concept of stereotypy was supported by the first set of kinematic analysis on individual trials of the monkey. Based on this mechanism, in order to achieve a faster movement, the amplitudes of pulses increase as prescribed by the affine relation between a_1 and the target speeds, while the duration distribution remains the roughly constant regardless of the speeds.

In order to explain the intermittency observed in individual trials, the RIPID formulation was extended to the BG-RIPID by including a cortico-basal ganglia loop which was considered to function as a context dependent switching controller (Mao 2005; Mao and Massaquoi 2005; Massaquoi 2006b). In this model, an adjusted error signals are generated potentially in areas 4 and 5. Each error signal is compared against a threshold value in each corresponding BG module. If the magnitude of the error signals are smaller than the threshold values, then BG modules inhibit the activities of corresponding thalamic nucleus VLo so that the VLo don't output any error signals to be integrated to generate the motor command to be sent to the motor cortex.

The model was reduced to one dimension to hypothetically reproduce the two dimensional circular tracking task of the monkey into an angular tracking task in one dimension. Thus, it is not possible to test if the submovement initiation mechanism takes into DE account.

This simple model which takes a continuous command signal which is slightly leading the visual target managed to reproduce at least two features observed in the monkey data, substantially invariant duration distributions across the speed and relation between the amplitudes and the durations of the pulses. It is yet unclear as to how this model can be extended into a higher dimension, the model suggests that the cortico-basal ganglia loop structure proposed by (Mao 2005) may be responsible for intermittency in individual movements.

Roitman et al. (2004) suggested, based on the cross correlation of various error signals and the speed profiles, that two types of errors may trigger a submovement. The first type is the directional error (DE), which is the difference between the present direction and the

desired direction of the motion. The second type is modified speed error (MSE) which is defined to be a linear sum of the difference between the present and desired position and the difference between the present and desired velocity multiplied by a time constant, τ. In both error signals, τ represents the interval for which the simple linear prediction about the target behavior is made by the control system (Engel and Soechting 2000). This kinematic error based mechanism may potentially function in a similar way to the BG-RIPID model. In fact the BG-RIPID model the integrator doesn't get turned on again unless the error gets larger than a threshold. One possible difference in the models is that MSE based model may cause the motor command generation mechanism to have to wait until the error is fairly large before initiating a submovement. The BG-RIPID would start rapidly then turn off when caught up. This possible difference would have to be explored. The other, yet critical, difference is that Roitman et al. (2004) does not explain how a scaling of the template is performed while the BG-RIPID model does not require the template but performs scaling automatically given the speed difference in the reference command. Further study similarity and difference between these two types models should be explored.

7.1.3 Gainscheduling

The RIPID model received a strong support to account for the average kinematics of low-speed movements in a small workspace while internal signal integrity was verified with the RICSS model. Then, the RIPID formulation was extended to account for individual trials which contained kinematic variability manifested in intermittency. The last attempt in this thesis to extend the RIPID model was to account for faster movements in a larger workspace with sudden directional changes.

The RICSS model suggested a particular multiplicative relation between the error-like signal and state information at the PCs. This mechanism was realized in a well known gainscheduling control scheme of linear parameter varying (LPV) systems. To test the feasibility of such a formulation, the double step reaction task was performed to human subjects. The LPV model accounted decently well for some of the human data. Thus, there

is a potential to extend the RIPID formulation into a gainscheduled version.

Because of the nature of the data fit procedure, detailed performance analysis was not performed. Furthermore, there were significant amount of simplifications made in the formulation. First, the nonlinearity due to viscosity terms was not included due to the resultant computational burden to synthesize a set of controllers. Second, signal delays, both afferent and efferent directions, were not included in the formulation. Third, the muscle model was completely linear to allow a straightforward application of the LPV synthesis. Therefore, the LPV model alone should not be able to account for many details observed in the human data. Furthermore, variability such as attention even within a given subject could not be modeled. Therefore, the result presented here is a first step to check the feasibility of the LPV model as an abstraction of RIPID/RICSS model. In addition, a theoretically tractable formulation such as LPV allows to test specific hypothesis. A hypothesis is that higher cortical areas modulate broadly based on the intention and decision made to pre-recruit populations of cells in motor and sensorimotor cortical areas, then more fine modulations at the cerebellar level based on the actual states are performed to selectively modulate cerebral and cerebellar modules which are specialized for a particular part of state space, whether it is represented in terms of work space, error space, or combined as suggested by the RICSS model. Further theoretical development to test this hypothesis, such as inclusion of delays in the synthesis procedure, needs to be made.

7.2 Possible extensions

7.2.1 Further extensions of RIPID

One feature in the RIPID model that has not been explicitly tested is its ability to track force levels. Although there have been physiological studies to suggest that some brain areas are related to force control (Hore and Flament 1986; Sergio and Kalaska 1997, 1998; Nowak et al. 2002), it is not yet clear as to how each area is connected to convey the force information data. A few anatomically and physiologically feasible models have been suggested to handle

both kinematic tracking under force loading (Contreras-Vidal et al. 1997; Bullock et al. 1998).

7.2.2 Adaptive RIPID/RICSS

Another major feature missing in the RIPID model as a cerebrocerebellar model is its capability of adaptation. Schweighofer et al. (1998a,b) suggested a model which included the motor cortex, the spinal cord, and the intermediate cerebellum. The model emphasized the importance of the cerebellum as a compensator for the interaction torques across different joints. By including the inferior olive as a "teaching" signal, the model learned, through long term depression (LTD), the part of inverse dynamics of interaction torques to achieve a reasonable tracking performance (yet see Fig. 2 in (Schweighofer et al. 1998b)). Contreras-Vidal et al. (1997) proposed an arm movement control model that illustrated how a central pattern generator in cerebral cortex and basal ganglia, a neuromuscular force controller in spinal cord, and cerebellum cooperate to reduce motor variability. This model not only included LTD as many other cerebellar learning models, but also long term potentiation (LTP) in response to uncorrelated parallel fiber signals. This LTP mechanism enables previously weakened synapses to recover. Such a rebound mechanism has been recently proposed at the neuroreceptor level (kakegawa and Yuzaki 2005). The two adaptive cerebellar models are anatomically and physiologically reasonable, but their learning algorithms only incorporate the global kinematic error.

Schaal and Atkeson (1998) suggested a incremental learning algorithm for regression problems that models data by means of spatially localized linear models. The size and shape of the receptive field of each locally linear model, as well as the parameters of the locally linear model itself, are learned without the need for competition or any other kind of communication by minimizing a weighted local cross-validation error.

This algorithm was evaluated to learn the inverse dynamics of two joint arm by having a local approximation of the state space map. The algorithm required a fair amount of training points (45000 points) sampled at a high frequency (100 Hz), but the system managed to learn

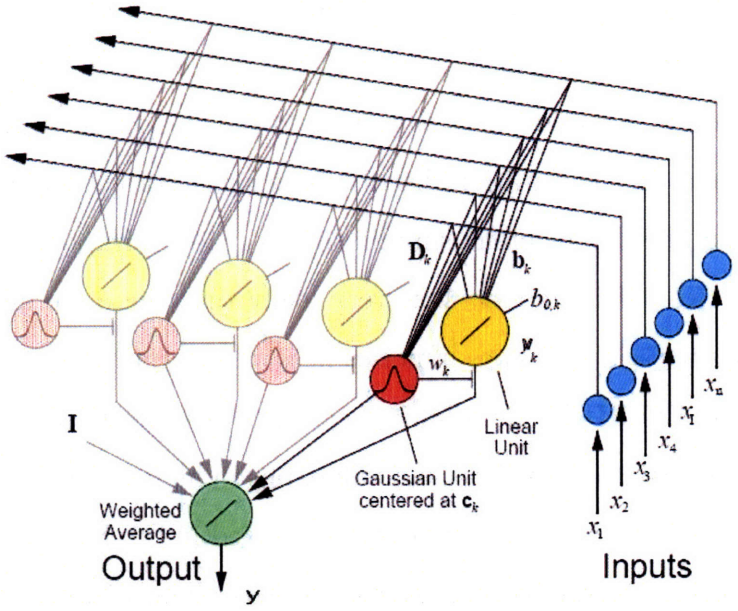

Figure 7-1: A network illustration of receptive field-weighted regression. Adapted from Figure 3 in Schaal and Atkeson (1998).

the map. This approach was extended to design a feedback linearizing controllers based on the learned inverse dynamics of the arm and successfully trace a figure eight (Nakanishi et al. 2005).

The biological feasibility of the model by Schaal and Atkeson (1998) as well as its idea of feedback linearization of the plant are speculative, and the robustness of the resultant controllers against parameter variations as well as disturbance has never been tested. However, an appealing feature of this algorithm is its structural similarity to cerebellar circuitry, in particular the RICSS formulation. Thus, in order to extend the RIPID/RICSS formulation to be adaptable, it would be natural to develop an algorithm that uses local sensory information to update corresponding local controllers.

7.2.3 Classification of submovements

In Chapter 4 two affine relations in intermittency were shown: The first was between the durations and amplitudes of the submovements and the second was between the slopes of

the first relation and the target speeds in the tracking phase. The BG-RIPID model preliminarily showed its ability to explain those two affine relations. However, the model did not quite show the invariant duration distributions across the speeds. In addition, the model showed multiple modes in the duration distributions as the target speed increases. Such an imperfect feature may be due to many simplifications made. First of all, there was only one noise source in the BG-RIPID model. It is very likely that there are multiple noise sources present at different sites and the types of noises need not be multiplicative. Second, the simulation results of the BG-RIPID were limited to one dimensional case. In one dimensional case, it was relatively easy to set a threshold value, but in higher dimensional case even when all error signals were completely independently processed in the BG and thalamus, setting a set of threshold values to reproduce realistic movements along with the empirically observed statistical features may not be an easy task, or may not even be realistic. Furthermore, the BG-RIPID along with the RIPID models only consider proprioceptive loops, but not a visual loop which possesses a more significant delay time. Thus, it is highly likely that the CNS has multiple loops that share a similar structure to that of the BG-RIPID, but each loop may contain a different delay time and threshold values. Related to this aspect, any high level cognitive error correction mechanism which intentionally modifies the intended path/trajecotry may produce apparent segmentations. Thus, it may be useful to further study the data statistically, in particular, it would be interesting to perform hierarchical structure analysis, such as hierarchical mixture of Gaussians to investigate statistical dependency on the durations of Gaussians. If such a hierarchical structure exists, then it would guide us to suggest corresponding anatomical structures.

7.2.4 Application to neuroprostheses

A recent and rapid development of the brain machine interface (BMI) to hope assisting disabled patients by translating neural activity from the brain into control signals for prosthetic devices has been impressive (Donoghue 2002; Shenoy et al. 2003; Santhanam et al. 2006; Hochberg et al. 2006). Multiple neurons are recorded simultaneously using a multiple

electrode array usually from one brain region. However, in order to harvest enough detail of the motor plan to accurately reconstruct/estimate the desired movement in real time, it would be necessary to record neurons with tens to hundreds of electrodes implanted in several key cortical areas.

Therefore numerous channels for neural signals need to be amplified, filtered, and digitized for subsequent processing, and much of this circuitry may eventually be integrated with or near the recording electrodes which imposes computational power available for real-time processing of neural signals.

In order for the RIPID/RICSS formulation to be considered as a part of the algorithm for BMI, more feasibility check needs to be performed on the RIPID/RICSS model. It is known that the bulk of cerebrocerebellar control involves both forward command and sensory feedback information inextricably combined. it predicts that forward commands may be fairly simple or crude and still be highly effective because refinement will occur due to feedback. This would imply in turn that cerebral cortical command generation circuitry may be simpler than might otherwise be surmised. The view also predicts that fundamentally most motor cortical and cerebellar signals recorded in intact animals will not be entirely representative of the signals recorded in deafferented animals. If true, this fact could be relevant to optimizing the design of decoding algorithms for neuroprostheses when afferent pathways have been compromised. Conceivably, if the role of sensory input is correctly understood, appropriate adjustments can be made to signals recorded in their absence. Furthermore, the current BMI and corresponding estimation technology have not even attempted to account for dynamic interactions of the limb movements for which cerebellum is known to compensate. Thus, the inclusion of the cerebellar modules in the BMI algorithm would be crucial to produce a smoother and more natural movements in the future.

Appendix A

Tables

A.1 The two-link arm plant dynamics and muscle model parameters used in Chapter 3

The arm dynamics and the muscle models are presented in Eqs. (1)(2). The two tables below summarize the arm parameters used for this study.

Table A.1: Arm plant parameters used in Chapter 3 - m_i is mass, l_i is limb segment length, $\bar{l}_i$ is distance to segment center of mass from joint, and h_i is moment of inertia for i-th link

i = 1,2	m_i (kg)	l_i (cm)	$\bar{l}_i$ (cm)	h_i (kg m^2)
Link 1	0.36	14.1	6.20	0.0024
Link 2	0.36	14.1	6.20	0.0024

Table A.2: Moment arms - See the notation inKatayama and Kawato (1993)

	a_1,a_2	a_3, a_4	a_5,a_6	a_7, a_8
Moment arm (cm)	1.6	1.0	1.1	1.4

The moment arm matrix is given by

$$\mathbf{A} = \begin{bmatrix} a_1 & -a_2 & 0 & 0 & a_5 & -a_6 \\ 0 & 0 & a_3 & -a_4 & a_7 & -a_8 \end{bmatrix}.$$

All the diagonal elements of $\mathbf{K}_m$ are 400 N/m and of $\mathbf{B}_m$ are 40 Ns/m, respectively. All the off-diagonal elements for both $\mathbf{K}_m$ and $\mathbf{B}_m$ are zero.

The two link arm dynamics is given by Eq. (3.1):

$$\boldsymbol{\tau} = \mathbf{H}(\boldsymbol{\theta})\ddot{\boldsymbol{\theta}} + \mathbf{C}(\boldsymbol{\theta}, \dot{\boldsymbol{\theta}})\dot{\boldsymbol{\theta}}, \tag{A.1}$$

where

$$\begin{aligned}
\mathbf{H}(\boldsymbol{\theta}) &= \begin{bmatrix} h_{11}(\theta_e) & h_{12}(\theta_e) \\ h_{21}(\theta_e) & h_{22} \end{bmatrix}, \qquad (A.2)\\
h_{11}(\theta_e) &= h_1 + h_2 + m_2(l_1^2 + 2l_1\bar{l}_2\cos(\theta_e)),\\
h_{21}(\theta_e) &= h_{12} = h_2 + m_2 l_1 \bar{l}_2 \cos(\theta_e),\\
h_{22}(\theta_e) &= h_2,\\
\mathbf{C}(\boldsymbol{\theta}, \dot{\boldsymbol{\theta}}) &= m_2 l_1 \bar{l}_2 \sin(\theta_e) \begin{bmatrix} -\dot{\theta}_e & -(\dot{\theta}_e + \dot{\theta}_s) \\ \dot{\theta}_s & 0 \end{bmatrix}. \qquad (A.3)
\end{aligned}$$

B. Parameter values used in the RIPID simulation

$$\begin{aligned}
\mathbf{I}_1 &= \begin{bmatrix} 0 & 0 \\ 0 & 0 \end{bmatrix}, \mathbf{I}_2 = \begin{bmatrix} 400 & 0 \\ 0 & 400 \end{bmatrix}, \mathbf{I}_3 = \begin{bmatrix} 350 & 0 \\ 0 & 350 \end{bmatrix},\\
\mathbf{I}_a &= \begin{bmatrix} 1.3 & 0 \\ 0 & 1.3 \end{bmatrix}, \mathbf{F}_2 = \begin{bmatrix} 0.4 & 0 \\ 0 & 0.4 \end{bmatrix}, \mathbf{F}_3 = \begin{bmatrix} 0.6 & 0 \\ 0 & 0.6 \end{bmatrix},\\
\mathbf{G}_b &= \begin{bmatrix} 1.2 & 0 \\ 0 & 1.2 \end{bmatrix}, \mathbf{G}_k = \begin{bmatrix} 0.7 & 0 \\ 0 & 0.7 \end{bmatrix}, \mathbf{MC} = \begin{bmatrix} 1 & 0 \\ 0 & 1 \end{bmatrix}.
\end{aligned}$$

For simplicity, the following two delays are set to be the same value: $t_{eff} = t_{aff} = 25$ ms .

A.2 The two-link arm plant dynamics parameters used in Chapter 5

Table A.3: Arm plant parameters used in Chapter 5- m_i is mass, l_i is limb segment length, $\bar{l}_i$ is distance to segment center of mass from joint, and h_i is moment of inertia for i-th link

i = 1,2	m_i (kg)	l_i (cm)	$\bar{l}_i$ (cm)	h_i (kg m^2)
Link 1	0.90	34.0	12.0	0.065
Link 2	1.1	35.0	17.0	0.10

The location of the center of the workspace relative the location of the shoulder is $(x_c, y_c) = (-0.05, 0.35)$ in m.

Bibliography

R. Ajemian, D. Bullock, and S. Grossberg. A model of movement coordinates in the motor cortex: Posture-dependent changes in the gain and direction of single cell tuning curves. *Cereb. Cortex*, 11(12):1124–1135, 2001.

J. Albus. A theory of cerebellar function. *Mathematical Biosciences*, 10:25–61, 1971.

G. Allen and N. Tsukahara. Cerebrocerebellar communication systems. *Physiol Rev*, 54(4): 957–1006, Oct 1974.

B. Amirikian and A. P. Georgopoulos. Modular organization of directionally tuned cells in the motor cortex: Is there a short-range order? *PNAS*, 100(21):12474–12479, 2003.

P. Apkarian and P. Gahinet. A convex characterization of gain scheduled $\mathcal{H}_\infty$ controllers. *IEEE Trans. Aut. Contr.*, 40(5):853–863, 1995.

P. Apkarian, P. Gahinet, and G. Becker. Self-scheduled $\mathcal{H}_\infty$ control of linear parameter-varying systems: a design example. *Automatica*, 31(9):1251–1261, Sep 1995.

C. Asanuma, W. Thach, and E. Jones. Distribution of cerebellar terminations and their relation to other afferent terminations in the ventral lateral thalamic region of the monkey. *Brain Res*, 286(3):237–65, May 1983.

H. Asanuma and I. Rosen. Topographical organization of cortical efferent zones projecting to distal forelimb muscles in the monkey. *Exp Brain Res*, 14(3):243–56, 1972.

O. Ayaso, M. Dahleh, and S. G. Massaquoi. Coarse gain recurrent integrator model for sensorimotor cortical command generation. volume 3 of *Proceedings of the American Control Conference*, pages 1736–41, Anchorage, Alaska, 2002.

J. S. Barlow. *The cerebellum and adaptive control.* Cambridge university press, 2002.

A. Barto, A. Fagg, N. Sitkoff, and J. Houk. A cerebellar model of timing and prediction in the control of reaching. *Neural Comput.*, 11(3):565–94, 1999.

A. J. Bastian, T. A. Martin, J. G. Keating, and W. T. Thach. Cerebellar ataxia: abnormal control of interaction torques across multiple joints. *J Neurophysiol*, 76(1):492–509, 1996.

E. Bauswein, F. Kolb, B. Leimbeck, and F. Rubia. Simple and complex spike activity of cerebellar purkinje cells during active and passive movements in the awake monkey. *J Physiol*, 339:379–94, Jun 1983.

E. Bauswein, F. Kolb, and F. Rubia. Cerebellar feedback signals of a passive hand movement in the awake monkey. *Pflugers Arch*, 402(3):292–9, Nov 1984.

N. Bhushan and R. Shadmehr. Computational nature of human adaptive control during learning of reaching movements in force fields. *Biol Cybern*, 81(1):39–60, 1999.

E. Bizzi, N. Accornero, W. Chapple, and N. Hogan. Posture control and trajectory formation during arm movement. *J Neurosci*, 4(11):2738–44, Nov 1984.

G. Bosco and R. Poppele. Modulation of dorsal spinocerebellar responses to limb movement. ii. effect of sensory input. *J. Neurophysiology*, 90(5):3372–83, 2003.

G. Bosco and R. E. Poppele. Proprioception From a Spinocerebellar Perspective. *Physiol. Rev.*, 81(2):539–568, 2001.

P. Boulinguez, J. Blouin, and V. Nougier. The gap effect for eye and hand movements in double-step pointing. *Exp Brain Res.*, 138(3):352–8, Jun 2001.

J. Bower. *Is the cerebellum sensory for motor's sake, or motor for sensory's sake: the view from the whiskers of a rat?*, volume 114 of *Prog Brain Res.*, pages 463–96. Elsevier, 1997.

J. M. Bower. The organization of cerebellar cortical circuitry revisited: Implications for function. *Ann NY Acad Sci*, 978(1):135–155, 2002.

J. M. Bower and D. C. Woolston. Congruence of spatial organization of tactile projections to granule cell and Purkinje cell layers of cerebellar hemispheres of the albino rat: vertical organization of cerebellar cortex. *J Neurophysiol*, 49(3):745–766, 1983.

S. Boyd, L. E. Ghaoui, E. Feron, and V. Balakrishnan. *Linear Matrix Inequalities in System and Control Theory*, volume 15 of *Studies in Applied Mathematics*. SIAM, 1994.

V. B. Brooks. *The neural basis of motor control*. Oxford University Press, 1986.

J. Brown, D. Bullock, and S. Grossberg. How laminar frontal cortex and basal ganglia circuits interact to control planned and reactive saccades. *Neural Netw.*, 17(4):417–510, May 2004.

L. Brown, J. Schneider, and T. Lidsky. Sensory and cognitive functions of the basal ganglia. *Curr Opin Neurobiol.*, 7(2):157–63, Apr 1997.

D. Bullock, P. Cisek, and S. Grossberg. Cortical networks for control of voluntary arm movements under variable force conditions. *Cereb Cortex.*, 8(1):48–62, Jan-Feb 1998.

D. Bullock, R. Bongers, M. Lankhorst, and P. Beek. A vector-integration-to-endpoint model for performance of viapoint movements. *Neural Netw.*, 12(1):1–29, Jan 1999.

U. Buttner, S. Glasauer, L. Glonti, Y. Guan, E. Kipiani, J. Kleine, C. Siebold, T. Tchelidze, and A. Wilden. Multimodal signal integration in vestibular neurons of the primate fastigial nucleus. *Ann N Y Acad Sci.*, 1004:241–51, Oct 2003.

R. Caminiti, P. Johnson, and A. Urbano. Making arm movements within different parts of space: dynamic aspects in the primate motor cortex. *J Neurosci.*, 10(7):2039–58, Jul 1990.

J. H. K. Carolyn W.-H. Wu. Somatosensory cortex of prosimian galagos: Physiological recording, cytoarchitecture, and corticocortical connections of anterior parietal cortex and cortex of the lateral sulcus. *The Journal of Comparative Neurology*, 457(3):263–292, 2003.

D. Cohen and Y. Yarom. Cerebellar on-beam and lateral inhibition: Two functionally distinct circuits. *J Neurophysiol*, 83(4):1932–1940, 2000.

J. Coltz, M. Johnson, and T. Ebner. Cerebellar purkinje cell simple spike discharge encodes movement velocity in primates during visuomotor arm tracking. *J Neurosci*, 19(5):1782–803, Mar 1999.

J. Contreras-Vidal, S. Grossberg, and D. Bullock. A neural model of cerebellar learning for arm movement control: cortico-spino-cerebellar dynamics. *Learn Mem.*, 3(6):475–502, Mar-Apr 1997.

K. J. W. Craik. Theory of the human operator in control systems. i, the operator as an engineering system. *Br. J. Psychol.*, 38:56–61, 1947.

M. Crutcher, G. Russo, S. Ye, and D. Backus. Target-, limb-, and context-dependent neural activity in the cingulate and supplementary motor areas of the monkey. *Exp Brain Res.*, 158(3):278–88, Oct 2004.

A. d'Avella, P. Saltiel, and E. Bizzi. Combinations of muscle synergies in the construction of a natural motor behavior. *Nat Neurosci*, 6(3):300–8, Mar 2003.

A. de Rugy and D. Sternad. Interaction between discrete and rhythmic movements: reaction time and phase of discrete movement initiation during oscillatory movements. *Brain Res*, 994(2):160–74, Dec 2003.

M. Desmurget, C. Epstein, R. Turner, C. Prablanc, G. Alexander, and S. Grafton. Role of the posterior parietal cortex in updating reaching movements to a visual target. *Nat Neurosci.*, 2(6):563–7, Jun 1999.

M. Desmurget, S. Grafton, P. Vindras, H. Grea, and R. Turner. Basal ganglia network mediates the control of movement amplitude. *Exp Brain Res.*, 153(2):197–209, Nov 2003.

M. Desmurget, S. Grafton, P. Vindras, H. Grea, and R. Turner. The basal ganglia network mediates the planning of movement amplitude. *Eur J Neurosci.*, 19(10):2871–80, May 2004.

L. Dipirtro, N. Hogan, H. I. Krebs, and B. Volpe. Submovements underline voluntary human arm movements: Evidence from emg. In *Annual meeting.* Society for Neuroscience, 2005.

J. Doeringer and N. Hogan. Intermittency in preplanned elbow movements persists in the absence of visual feedback. *J Neurophysiol.*, 80(4):1787–99, 1998.

J. Donoghue. Connecting cortex to machines: Recent advances in brain interfaces. *Nat Neurosci*, 5(Supp 1):1085–8, Nov 2002.

J. Donoghue, S. Leibovic, and J. Sanes. Organization of the forelimb area in squirrel monkey motor cortex: representation of digit, wrist, and elbow muscles. *Exp Brain Res.*, 89(1): 1–19, 1992.

K. Doya, K. Samejima, K.-i. Katagiri, and M. Kawato. Multiple model-based reinforcement learning. *Neural Comput*, 14(6):1347–69, Jul 2002.

R. P. Dum and P. Strick. *Motor cortex in voluntary movements. A Distributed system for distributed functions*, chapter Motor areas in the frontal lobe: The anatomical substrate for the central control of movement, pages 3–48. CRC Press, 2005.

R. Dunbar, G. Chen, W. Gao, K. Reinert, R. Feddersen, and T. Ebner. Imaging parallel fiber and climbing fiber responses and their short-term interactions in the mouse cerebellar cortex in vivo. *Neuroscience*, 126(1):213–27, 2004.

C. Ekerot. personal communication, 2005.

K. Engel and J. Soechting. Manual tracking in two dimensions. *J Neurophysiol.*, 83(6): 3483–96, Jun 2000.

J. Espinoza, J. Vandewalle, and V. Wertz. *Fuzzy Logic, Identification and Predictive Control.* Advances in industrial control. Springer, 2004.

W. Fen and K. Grigoriadis. Lpv systems with parameter-varying time delays. In *Proceedings of the 36th IEEE Conference on Decision and Control*, volume 2, pages 966 – 71. IEEE, 1997.

S. Ferraina and L. Bianchi. Posterior parietal cortex: functional properties of neurons in area 5 during an instructed-delay reaching task within different parts of space. *Exp Brain Res.*, 99(1):175–8, 1994.

T. Flash. The control of hand equilibrium trajectories in multi-joint arm movements. *Biol Cybern*, 57(4-5):257–74, 1987.

T. Flash and E. Henis. Arm trajectory modifications during reaching towards visual targets. *Journal of Cognitive Neuroscience*, 3(3):221–230, 1991.

T. Flash, R. Inzelberg, E. Schechtman, and A. Korczyn. Kinematic analysis of upper limb trajectories in parkinson's disease. *Exp Neurol*, 118(2):215–26, 1992.

P. A. Fortier, J. F. Kalaska, and A. M. Smith. Cerebellar neuronal activity related to whole-arm reaching movements in the monkey. *J Neurophysiol*, 62(1):198–211, 1989.

Q. Fu, J. Suqrez, and T. Ebner. Neuronal specification of direction and distance during reaching movements in the superior precentral premotor area and primary motor cortex of monkeys. *J Neurophysiol*, 70(5):2097–116, Nov 1993.

Q. Fu, D. Flament, J. Coltz, and T. Ebner. Relationship of cerebellar purkinje cell simple spike discharge to movement kinematics in the monkey. *J Neurophysiol*, 78(1):478–91, July 1997.

A. Georgopoulos, J. Kalaska, R. Caminiti, and J. Massey. On the relations between the direction of two-dimensional arm movements and cell discharge in primate motor cortex. *J. Neurosci.*, 2(11):1527–1537, 1982a.

A. Georgopoulos, R. Kettner, A. Schwartz, and A. Georgopoulos. Primate motor cortex and free arm movements to visual targets in three-dimensional space. ii. coding of the direction of movement by a neuronal population. *J Neurosci.*, 8(8):2928–37, Aug 1988.

A. P. Georgopoulos, J. F. Kalaska, R. Caminiti, and J. T. Massey. On the relations between the direction of two-dimensional arm movements and cell discharge in primate motor cortex. *J Neurosci*, 2(11):1527–1537, 1982b.

Z. Ghahramani and D. Wolpert. Modular decomposition in visuomotor learning. *Nature*, 386(6623):392–5, Mar 1997.

R. Gilbert and W. Thach. Purkinje cell activity during motor learning. *Brain Res.*, 128(2): 309–28, Jun 1977.

H. Gomi and M. Kawato. Adaptive feedback control models of the vestibulocerebellum and spinocerebellum. *Biol Cybern.*, 68(2):105–14, 1992a.

H. Gomi and M. Kawato. Adaptive feedback control models of the vestibulocerebellum and spinocerebellum. *Bilo Cybern*, 68(2):105–14, 1992b.

H. Gomi, M. Shidara, A. Takemura, Y. Inoue, K. Kawano, and M. Kawato. Temporal firing patterns of purkinje cells in the cerebellar ventral paraflocculus during ocular following responses in monkeys I. Simple spikes. *J Neurophysiol*, 80(2):818–831, 1998.

J. Gordon, M. Ghilardi, and C. Ghez. Accuracy of planar reaching movements. i. independence of direction and extent variability. *Exp Brain Res.*, 99(1):97–111, 1994.

C. Gravel, N. Leclerc, J. Rafrafi, R. Sasseville, L. Thivierge, and R. Hawkes. Monoclonal antibodies reveal the global organization of the cerebellar cortex. *J Neurosci Methods.*, 21 (2-4):145–57, Oct 1987.

M. Graziano. Is reaching eye-centered, body-centered, hand-centered, or a combination? *Rev Neurosci*, 12(2):175–85, 2001.

M. Graziano, C. Tayloer, and T. Moore. Complex movements evoked by microstimulation of precentral cortex. *Neuron*, 34(5):841–51, May 2002.

M. Graziano, T. Aflalo, and D. Cooke. Arm movements evoked by electrical stimulation in the motor cortex of monkeys. *J Neurophysiol.*, 94(6):4209–23, Dec 2005.

S. Grossberg and M. Kuperstein. *Neural dynamics of adaptive sensory-motor control.* Neural networks, research and applications. Pergamon Press, New York, expanded edition, 1989.

C. M. Harris and D. M. Wolpert. Signal-dependent noise determines motor planning. *Nature*, 394:780–784, Aug 1998.

B. Hartman and P. Fitts. Relation of stimulus and response amplitude to tracking performance. *J Exp Psychol.*, 49(2):82–92, Feb 1955.

M. Haruno, D. Wolpert, and M. Kawato. Mosaic model for sensorimotor learning and control. *Neural Comput.*, 13(10):2201–20, Oct 2001.

Z. Hasan. A model of spindle afferent response to muscle stretch. *J Neurophysiol*, 49(4): 989–1006, 1983.

N. G. Hatsopoulos, L. Paninski, and J. P. Donoghue. Sequential movement representations based on correlated neuronal activity. *Exp Brain Res*, 149(4):478–486, Apr 2003.

R. Hawkes and L. M. Eisenman. Stripes and zones: the origins of regionalization of the adult cerebellum. *Perspect Dev Neurobiol.*, 5(1):95–105, 1997.

R. Hawkes and N. Leclerc. Antigenic map of the rat cerebellar cortex: the distribution of parasagittal bands as revealed by monoclonal anti-purkinje cell antibody mabq113. *J Comp Neurol.*, 256(1):29–41, Feb 1987.

L. Hochberg, M. Serruya, G. Friehs, J. Mukand, M. Saleh, A. Caplan, A. Branner, D. Chen, R. Penn, and J. Donoghue. Neuronal ensemble control of prosthetic devices by a human with tetraplegia. *Nature*, 442(7099):164–71, Jul 2006.

S. Hocherman and J. Aharon-Peretz. Two-dimensional tracing and tracking in patients with parkinson's disease. *Neurology*, 44(1):111–6, Jan 1994.

N. Hogan. The mechanics of multi-joint posture and movement control. *Biol Cybern*, 52(5): 315–31, 1985.

G. Holmes. The cerebellum of main. *Brain*, 62:1–30, 1939.

F. B. Horak and H. C. Diener. Cerebellar control of postural scaling and central set in stance. *J Neurophysiol*, 72(2):479–493, 1994.

J. Hore and D. Flament. Evidence that a disordered servo-like mechanism contributes to tremor in movements during cerebellar dysfunction. *J Neurophysiol.*, 56(1):123–36, Jul 1986.

J. Hore, J. Preston, and P. Cheney. Responses of cortical neurons (areas 3a and 4) to ramp stretch of hindlimb muscles in the baboon. *J Neurophysiol.*, 39(3):484–500, May 1976.

E. Hoshi and J. Tanji. Area-selective neuronal activity in the dorsolateral prefrontal cortex for information retrieval and action planning. *J Neurophysiol*, 91(6):2707–2722, 2004a.

E. Hoshi and J. Tanji. Differential roles of neuronal activity in the supplementary and pre-supplementary motor areas: From information retrieval to motor planning and execution. *J Neurophysiol*, 92(6):3482–3499, 2004b.

E. Hoshi and J. Tanji. Differential involvement of neurons in the dorsal and ventral premotor cortex during processing of visual signals for action planning. *J Neurophysiol.*, 95(6):3596–616, Jun 2006.

J. Houk and S. Wise. Distributed modular architectures linking basal ganglia, cerebellum, and cerebral cortex: their role in planning and controlling action. *Cereb Cortex.*, 5(2): 95–110, Mar-Apr 1995a.

J. Houk and S. Wise. Distributed modular architectures linking basal ganglia, cerebellum, and cerebral cortex: their role in planning and controlling action. *Cereb Cortex*, 5(2): 95–110, Mar-Apr 1995b.

J. C. Houk, W. Z. Rymer, and P. E. Crago. Dependence of dynamic response of spindle receptors on muscle length and velocity. *J Neurophysiol*, 46(1):143–166, 1981.

K. Huffman and L. Krubitzer. Thalamo-cortical connections of areas 3a and m1 in marmoset monkeys. *J Comp Neurol.*, 435(3):291–310, Jul 2001a.

K. Huffman and L. Krubitzer. Area 3a: Topographic organization and cortical connections in marmoset monkeys. *Cereb Cortex*, 11(9):849–867, Sep 2001b.

K. Hunt, M. Munih, N. Donaldson, and F. Barr. Optimal control of ankle joint moment: toward unsupported standing in paraplegia. *Automatic Control, IEEE Transactions on*, 43(6):819–32, Jun 1998.

H. Imamizu, T. Kuroda, T. Yoshioka, and M. Kawato. Functional magnetic resonance imaging examination of two modular architectures for switching multiple internal models. *J Neurosci.*, 24(5):1173–81, Feb 2004.

M. Inase, H. Tokuno, A. Nambu, T. Akazawa, and M. Takada. Corticostriatal and cortico-subthalamic input zones from the presupplementary motor area in the macaque monkey: comparison with the input zones from the supplementary motor area. *Brain Research*, 833 (2):191–201, Jul 1999.

M. Ito. Historical Review of the Significance of the Cerebellum and the Role of Purkinje Cells in Motor Learning. *Ann NY Acad Sci*, 978(1):273–288, 2002.

M. Ito. *The cerebellum and neural control.* Raven Press, 1984.

S. Jo. *Hierarchical neural control of human sagittal balance and bipedal walking.* Ph.d, MIT, Cambridge, MA, 2006.

S. Jo and S. G. Massaquoi. A model of cerebellum stabilized and scheduled hybrid long-loop control of upright balance. *Biol Cybern*, 91(3):188–202, September 2004.

M. Johnson, J. Coltz, M. Hagen, and T. Ebner. Visuomotor processing as reflected in the directional discharge of premotor and primary motor cortex neurons. *J Neurophysiol*, 81 (2):875–94, Feb 1999.

H. Kajiwara, P. Apkarian, and P. Gahinet. Lpv techniques for control of an inverted pendulum. *Control Systems Magazine, IEEE*, 19(1):44–54, Feb 1999.

W. kakegawa and M. Yuzaki. A mechanism underlying ampa receptor trafficking during cerebellar long-term potentiation. *PNAS*, 102(49):17846–51, Dec 2005.

S. Kakei, J. Yagi, T. Wannier, J. Na, and Y. Shinoda. Cerebellar and cerebral inputs to corticocortical and corticofugal neurons in areas 5 and 7 in the cat. *J Neurophysiol*, 74(1): 400–412, 1995.

J. Kalaska, D. Cohen, M. Prud'homme, and M. Hyde. Parietal area 5 neuronal activity encodes movement kinematics, not movement dynamics. *Exp Brain Res.*, 80(2):351–64, 1990.

J. F. Kalaska, S. H. Scott, P. Cisek, and L. E. Sergio. Cortical control of reaching movementscurr opin neurobiol. *Curr Opin Neurobiol.*, 7(6):849–59, Dec 1997.

E. R. Kandel, J. H. Schwartz, and T. M. Jessell, editors. *Principles of neural science.* McGraw-Hill, 4th edition, 2000.

T. Kaneko, M. A. Caria, and H. Asanuma. Information processing within the motor cortex. i. responses of morphologically identified motor cortical cells to stimulation of the somatosensory cortex. *The journal of comparative neurology*, 345(2):161–171, Jul 1994.

F. Karameh and S. Massaquoi. A model of nonlinear motor cortical integration and its relation to movement speed profile control. In *IEEE-EMBS 27th Annual International Conference of the Engineering in Medicine and Biology Society*, pages 4331– 4336, 2005.

A. Karniel. Three creatures named 'forward model'. *Neural Netw*, 15(3):305–7, Apr 2002.

M. Katayama and M. Kawato. Virtual trajectory and stiffness ellipse during multijoint arm movement predicted by neural inverse models. *Biol Cybern*, 69(5-6):353–62, 1993.

K. Kawato and H. Gomi. A computational model of four regions of the cerebellum based on feedback-error learning. *Biol Cybern*, 68(2):95–103, 1992a.

M. Kawato. Internal models for motor control and trajectory planning. *Curr Opin Neurobiol*, 9(6):718–27, Dec 1999.

M. Kawato and H. Gomi. A computational model of four regions of the cerebellum based on feedback-error learning. *Biol Cybern.*, 68(2):95–103, 1992b.

M. Kawato, K. Furukawa, and R. Suzuki. A hierarchical neural-network model for control and learning of voluntary movement. *Bilo Cybern*, 57(3):169–85, 1987.

J. Keifer and J. C. Houk. Motor function of the cerebellorubrospinal system. *Physiol. Rev.*, 74(3):509–542, 1994.

R. M. Kelly and P. L. Strick. Cerebellar loops with motor cortex and prefrontal cortex of a nonhuman primate. *J. Neurosci.*, 23(23):8432–8444, 2003.

R. Kettner, A. Schwartz, and A. Georgopoulos. Primate motor cortex and free arm movements to visual targets in three-dimensional space. iii. positional gradients and population coding of movement direction from various movement origins. *J Neurosci.*, 8(8):2938–47, Aug 1988.

R. E. Kettner, S. Mahamud, H.-C. Leung, N. Sitkoff, J. C. Houk, B. W. Peterson, and A. G. Barto. Prediction of complex two-dimensional trajectories by a cerebellar model of smooth pursuit eye movement. *J Neurophysiol*, 77(4):2115–2130, 1997.

H. I. Krebs, M. L. Aisen, B. T. Volpe, and N. Hogan. Quantization of continuous arm movements in humans with brain injury. *PNAS*, 96(8):4645–4649, 1999.

L. Krubitzer and J. H. Kaas. The organization and connections of somatosensory cortex in marmosets. *J Neurosci.*, 10(3):952–74, Mar 1990.

A. Kwiatkowski and H. Werner. Lpv control of a 2-dof robot using parameter reduction. CDC-ECC, pages 3369– 3374. IEEE, Dec 2005.

F. Lacquaniti, E. Guigon, L. Bianchi, S. Ferraina, and R. Caminiti. Representing spatial information for limb movement: Role of area 5 in the monkey. *Cereb. Cortex*, 5(5):391–409, 1995.

D. Lawrence and W. Rugh. Gain scheduling dynamic linear controllers for a nonlinear plant. *Automatica*, 31(3):381–390, 1995.

D. Lee, N. Port, and A. Georgopoulos. Manual interception of moving targets. ii. on-line control of overlapping submovements. *Exp. Brain Res.*, 116(3):421–33, 1997.

R. Levy, H. Friedman, L. Davachi, and P. Goldman-Rakic. Differential activation of the caudate nucleus in primates performing spatial and nonspatial working memory tasks. *J Neurosci.*, 17(10):3870–82, May 1997.

W. MacKay. Unit activity in the cerebellar nuclei related to arm reaching movements. *Brain Res.*, 442(2):240–54, Mar 1988.

W. A. MacKay and J. T. Murphy. Responses of interpositus neurons to passive muscle stretch. *J Neurophysiol*, 37(6):1410–1423, 1974.

G. Maimon and J. Assad. Parietal area 5 and the initiation of self-timed movements versus simple reactions. *J Neurosci.*, 26(9):2487–98, Mar 2006.

Z.-H. Mao. *Modeling the role of the basal ganglia in motor control and motor program.* Ph.d, MIT, 2005.

Z.-H. Mao and S. Massaquoi. A multi-input multi-output adaptive switching (mimoas) model of frontocortical and basal ganglionic interaction in procedural learning. Key Biscayne, FL, Apr 2005. Society for Neural Control of Movement.

B. Marconi, A. Genovesio, A. Battaglia-Mayer, S. Ferraina, S. Squatrito, M. Molinari, F. Lacquaniti, and R. Caminiti. Eye-hand coordination during reaching. i. anatomical relationships between parietal and frontal cortex. *Cereb Cortex*, 11(6):513–27, Jun 2001.

D. Marr. A theory of cerebellar cortex. *J Physiol.*, 202(2):437–70, Jun 1969.

M. Maschke, C. M. Gomez, T. J. Ebner, and J. Konczak. Hereditary Cerebellar Ataxia Progressively Impairs Force Adaptation During Goal-Directed Arm Movements. *J Neurophysiol*, 91(1):230–238, 2004.

S. G. Massaquoi. A ripid model of cerebro-cerebellar interaction in the stabilization of long-loop arm control ii: two-joint control. *Biol Cybern*, Submitted 2006a.

S. G. Massaquoi. A model of parkinsonian and cerebellar tremors and their reduction by lesions or stimulation at the thalamic vim nucleus. Key Biscayne, FL, May 2006b. Society for Neural Control of Movement.

S. G. Massaquoi and J. Slotine. The intermediate cerebellum may function as a wave-variable processor. *Neurosci Lett*, 215(1):60–4, Aug 1996.

J. Massey, J. Lurito, G. Pellizzer, and A. Georgopoulos. Three-dimensional drawings in isometric conditions: relation between geometry and kinematics. *Exp Brain Res*, 88(3): 685–90, 1992.

Y. Matsuzaka and J. Tanji. Changing directions of forthcoming arm movements: neuronal activity in the presupplementary and supplementary motor area of monkey cerebral cortex. *J Neurophysiol*, 76(4):2327–2342, 1996.

Y. Matsuzaka, H. Aizawa, and J. Tanji. A motor area rostral to the supplementary motor area (presupplementary motor area) in the monkey: neuronal activity during a learned motor task. *J Neurophysiol*, 68(3):653–662, 1992.

J. McIntyre and E. Bizzi. Servo hypotheses for the biological control. of movement. *J. Motor Behav.*, 25(3):193–202, Sep 1993.

W. Melek and A. Goldenberg. Neurofuzzy control of modular and reconfigurable robots. *Mechatronics, IEEE/ASME Transactions*, 8(3):381–389, Sep 2003.

D. Meyer, J. Smith, and C. Wright. Models for the speed and accuracy of aimed movements. *Psychol Rev*, 89(5):449–82, Sep 1982.

R. Miall and J. Jackson. Adaptation to visual feedback delays in manual tracking: evidence against the smith predictor model of human visually guided action. *Exp Brain Res.*, 172 (1):77–84, Jun 2006.

R. Miall, D. Weir, and J. Stein. Manual tracking of visual targets by trained monkeys. *Behav Brain Res*, 20(2):185–201, May 1986.

R. Miall, D. Weir, and J. Stein. Planning of movement parameters in a visuo-motor tracking task. *Behav Brain Res*, 27(1):1–8, Jan 1988.

R. Miall, D. Weir, and J. Stein. Intermittency in human manual tracking tasks. *J Mot Behav*, 25(1):53–63, Mar 1993a.

R. Miall, D. Weir, and J. Stein. Intermittency in human manual tracking tasks. *J Mot Behav*, 25(1):53–63, Mar 1993b.

R. Miall, D. Weir, D. Wolpert, and J. Stein. Is the cerebellum a smith predictor? *J Mot Behav*, 25(3):203–216, Sep 1993c.

D. Micci Barreca and F. H. Guenther. A modeling study of potential sources of curvature in human reaching movements. *J Mot Behav*, 33(4):387–400, Dec 2001.

T. Milner. A model for the generation of movements requiring endpoint precision. *Neuroscience*, 49(2):487–96, Jul 1992.

T. Milner and M. Hinder. Position information but not force information is used in adapting to changes in environmental dynamics. *J Neurophysiol.*, 96(2):526–34, Aug 2006.

T. Milner and M. Ijaz. The effect of accuracy constraints on three-dimensional movement kinematics. *Neuroscience*, 35(2):365–74, 1990.

V. B. Mountcastle. *Perceptual neuroscience: the cerebral cortex.* Harvard University Press, 1998.

J. Nakanishi, J. Farrell, and S. Schaal. Composite adaptive control with locally weighted statistical learning. *Neural Netw.*, 18(1):71–90, Jan 2005.

K. S. Narendra, J. Balakrishnan, and M. K. Ciliz. Adaptation and learning using multiple models, switching and tuning. *IEEE Control Systems Magazine*, 15(3):37–51, Jun 1995.

K. S. Narendra, O. Driollet, M. Feiler, and K. George. Adaptive control using multiple models, switching and tuning. *International Journal of Adaptive Control and Signal Processing*, 17(2):87–102, 2003.

F. Navas and L. Stark. Sampling or intermittency in the hand control system. *Biophys J*, 8 (2):252–302, 1968.

K. Novak, L. Miller, and J. Houk. Kinematic properties of rapid hand movements in a knob turning task. *Exp Brain Res*, 132(4):419–33, Jun 2000.

K. Novak, L. Miller, and J. Houk. The use of overlapping submovements in the control of rapid hand movements. *Exp Brain Res*, 144(3):351–64, Jun 2002.

D. Nowak, J. Hermsdorfer, C. Marquardt, and H. Fuchs. Grip and load force coupling during discrete vertical arm movements with a grasped object in cerebellar atrophy. *Exp Brain Res.*, 145(1):28–39, Jul 2002.

C. L. Ojakangas and T. J. Ebner. Purkinje cell complex and simple spike changes during a voluntary arm movement learning task in the monkey. *J Neurophysiol*, 68(6):2222–2236, 1992.

O. Oscarsson. Functional units of the cerebellum-sagittal zones and microzones. *Trends Neurosci*, 2:143–145, 1979.

S. Pasalar, A. Roitman, and T. Ebner. Effects of speeds and force fields on submovements during circular manual tracking in humans. *Exp Brain Res.*, 163(2):214–25, 2005.

M. Paulin. The role of the cerebellum in motor control and perception. *Brain Behav Evol*, 41(1):39–50, 1993.

A. Pellionisz and R. Llinas. Space-time representation in the brain. the cerebellum as a predictive space-time metric tensor. *Neuroscience*, 7(12):2949–70, 1982.

N. Picard and P. Strick. Motor areas of the medial wall: a review of their location and functional activation. *Cereb Cortex.*, 6(3):342–53, May-Jun 1996.

T. Pons and J. Kaas. Connections of area 2 of somatosensory cortex with the anterior pulvinar and subdivisions of the ventroposterior complex in macaque monkeys. *J Comp Neurol*, 240(1):16–36, 1985.

R. E. Poppele, G. Bosco, and A. M. Rankin. Independent representations of limb axis length and orientation in spinocerebellar response components. *J Neurophysiol*, 87(1):409–422, 2002.

J. Rathelot and P. L. Strick. Muscle representation in the macaque motor cortex: an anatomical perspective. *PNAS*, 103(21):8257–62, May 2006.

G. A. Reina, D. W. Moran, and A. B. Schwartz. On the relationship between joint angular velocity and motor cortical discharge during reaching. *J Neurophysiol*, 85(6):2576–2589, 2001.

B. Rohrer and N. Hogan. Avoiding spurious submovement decompositions: a globally optimal algorithm. *Biol Cybern*, 89(3):190–199, Sep 2003.

B. Rohrer and N. Hogan. Avoiding spurious submovement decompositions ii: A scattershot algorithm. *Biol Cybern.*, 94(5):409–14, May 2006.

B. Rohrer, S. Fasoli, H. Krebs, B. Volpe, W. Frontera, J. Stein, and N. Hogan. Submovements grow larger, fewer, and more blended during stroke recovery. *Motor Control.*, 8(4):472–83, Oct 2004.

A. V. Roitman, S. G. Massaquoi, K. Takahashi, and T. J. Ebner. Kinematic Analysis of Manual Tracking in Monkeys: Characterization of Movement Intermittencies During a Circular Tracking Task. *J Neurophysiol*, 91(2):901–911, 2004.

A. V. Roitman, S. Pasalar, M. T. V. Johnson, and T. J. Ebner. Position, direction of movement, and speed tuning of cerebellar purkinje cells during circular manual tracking in monkey. *Journal of Neuroscience*, 25(40):9244–9257, 2005.

D. Rubino, K. Robbins, and N. Hatsopoulos. Propagating waves mediate information transfer in the motor cortex. *Nat Neurosci*, 9(12):1549–57, Dec 2006.

J. Sanes and M. Schieber. Orderly somatotopy in primary motor cortex: does it exist? *Neuroimage.*, 16(6-1):968–74, Jun 2001.

F. Santamaria, D. Jaeger, E. De Schutter, and J. M. Bower. Modulatory effects of parallel fiber and molecular layer interneuron synaptic activity on purkinje cell responses to ascending segment input: a modeling study. *J Comput Neurosci*, 13(3):217–235, Nov-Dec 2002.

G. Santhanam, S. Ryu, B. Yu, A. Afshar, and K. Shenoy. A high-performance brain-computer interface. *Nature*, 442(7099):195–8, Jul 2006.

S. Schaal and C. Atkeson. Constructive incremental learning from only local information. *Neural Comput.*, 10(8):2047–84, Nov 1998.

H. Scherberger, M. Jarvis, and R. Andersen. Cortical local field potential encodes movement intentions in the posterior parietal cortex. *Neuron*, 46(2):347–54, Apr 2005.

M. H. Schieber. Constraints on somatotopic organization in the primary motor cortex. *J Neurophysiol*, 86(5):2125–2143, 2001.

A. B. Schwartz and D. W. Moran. Motor cortical activity during drawing movements: Population representation during lemniscate tracing. *J Neurophysiol*, 82(5):2705–2718, 1999.

N. Schweighofer, M. Arbib, and M. Kawato. Role of the cerebellum in reaching movements in humans. i. distributed inverse dynamics control. *Eur J Neurosci.*, 10(1):86–94, Jan 1998a.

N. Schweighofer, J. Spoelstra, M. Arbib, and M. Kawato. Role of the cerebellum in reaching movements in humans. ii. a neural model of the intermediate cerebellum. *Eur J Neurosci*, 10(1):95–105, Jan 1998b.

S. Scott, L. Sergio, and J. Kalaska. Reaching movements with similar hand paths but different arm orientations. ii. activity of individual cells in dorsal premotor cortex and parietal area 5. *J Neurophysiol.*, 78(5):2413–26, Nov 1997.

S. H. Scott and J. F. Kalaska. Reaching Movements With Similar Hand Paths But Different Arm Orientations. I.Activity of Individual Cells in Motor Cortex. *J Neurophysiol*, 77(2): 826–852, 1997.

L. Sergio and J. Kalaska. Systematic changes in directional tuning of motor cortex cell activity with hand location in the workspace during generation of static isometric forces in constant spatial directions. *J Neurophysiol.*, 78(2):1170–4, 1997.

L. Sergio and J. Kalaska. Changes in the temporal pattern of primary motor cortex activity in a directional isometric force versus limb movement task. *J Neurophysiol.*, 1998.

J. Shamma and M. Athans. Analysis of gain scheduled control for nonlinear plants. *Automatic Control, IEEE Transactions on*, 35(8):898–907, Aug 1990.

K. Shenoy, D. Meeker, S. Cao, S. Kureshi, B. Pesaran, C. Buneo, A. Batista, P. Mitra, J. Burdick, and R. Andersen. Neural prosthetic control signals from plan activity. *Neuroreport*, 14(4):591–6, Mar 2003.

M. Shidara, K. Kawano, H. Gomi, and M. Kawato. Inverse-dynamics model eye movement control by purkinje cells in the cerebellum. *Nature*, 365(6441):50–2, Sep 1993.

K. Shima and J. Tanji. Role for cingulate motor area cells in voluntary movement selection based on reward. *Science*, 282(5392):1335–8, Nov 1998.

Y. Shinoda, P. Zarzecki, and H. Asanuma. Spinal branching of pyramidal tract neurons in the monkey. *Experimental Brain Research*, 34(1):59–72, Jan 1979.

J. Simpson, H. Hulscher, E. Sabel-Goedknegt, and T. Ruigrok. Between in and out: linking morphology and physiology of cerebellar cortical interneurons. *Prog Brain Res.*, 148:329–40, 2005.

M. Smith, J. Brandt, and R. Shadmehr. Motor disorder in huntington's disease begins as a dysfunction in error feedback control. *Nature*, 403(6769):544–9, Feb 2000.

J. F. Soechting and M. Flanders. Sensorimotor representations for pointing to targets in three-dimensional space. *J Neurophysiol*, 62(2):582–594, 1989.

D. Sternad and S. Schaal. Segmentation of endpoint trajectories does not imply segmented control. *Exp Brain Res*, 124(1):118–136, Jan 1999.

P. Strick. Stimulating research on motor cortex. *Nat Neurosci.*, 5(8):714–5, Aug 2002.

H. Tanaka, J. W. Krakauer, and N. Qian. An optimization principle for determining movement duration. *J Neurophysiol*, 95(6):3875–3886, 2006.

K. Tanaka and H. O. Wang. *Fuzzy control systems design and analysis : a linear matrix inequality approach.* Wiley, 2001.

W. Thach. Timing of activity in cerebellar dentate nucleus and cerebral motor cortex during prompt volitional movement. *Brain Res.*, 88(2):233–41, May 1975.

E. Todorov and M. I. Jordan. Smoothness maximization along a predefined path accurately predicts the speed profiles of complex arm movements. *J Neurophysiol*, 80(2):696–714, 1998.

Y. Uno, M. Kawato, and R. Suzuki. Formation and control of optimal trajectory in human multijoint arm movement. minimum torque-change model. *Biol Cybern*, 61(2):89–101, 1989.

D. E. Vaillancourt, K. R. Thulborn, and D. M. Corcos. Neural basis for the processes that underlie visually guided and internally guided force control in humans. *J Neurophysiol*, 90(5):3330–3340, 2003.

D. E. Vaillancourt, M. A. Mayka, and D. M. Corcos. Intermittent visuomotor processing in the human cerebellum, parietal cortex, and premotor cortex. *J Neurophysiol*, 95(2): 922–931, 2006.

A. Vallbo and J. Wessberg. Organization of motor output in slow finger movements in man. *J Physiol.*, 469:673–91, 1993.

P. L. van Kan, A. R. Gibson, and J. C. Houk. Movement-related inputs to intermediate cerebellum of the monkey. *J Neurophysiol*, 69(1):74–94, 1993.

P. Vindras, M. Desmurget, and P. Viviani. Error parsing in visuomotor pointing reveals independent processing of amplitude and direction. *J Neurophysiol*, 94(2):1212–1224, 2005.

B. Vos, A. Volny-Luraghi, R. Maex, and E. De Schutter. Precise spike timing of tactile-evoked cerebellar golgi cell responses: a reflection of combined mossy fiber and parallel fiber activation? *Prog Brain Res.*, 124:95–106, 2000.

Y. Wada, Y. Kawabata, S. Kotosaka, K. Yamamoto, S. Kitazawa, and M. Kawato. Acquisition and contextual switching of multiple internal models for different viscous force fields. *Neurosci Res.*, 46(3):319–31, Jul 2003.

J.-L. Wang and C.-H. Wang. Delay-dependent $\mathcal{H}_\infty$ control for lpv systems with mixed time-varying delays. In *International Conference on Machine Learning and Cybernetics*, volume 1, pages 626 – 31. IEEE, Aug 2004.

Y. Wang, Y. Matsuzaka, K. Shima, and J. Tanji. Cingulate cortical cells projecting to monkey frontal eye field and primary motor cortex. *Neuroreport.*, 15(10):1559–63, Jul 2004.

D. Wolpert and M. Kawato. Multiple paired forward and inverse models for motor control. *Neural Netw*, 11(7-8):1317–1329, Oct 1998.

R. Woodworth. The accuracy of voluntary movements. *Psychol Rev Mono*, Suppl 3:1–114, 1899.

C. W. Wu, N. O. Bichot, and J. H. Kass. Converging evidence from microstimulation, architecture, and connections for multiple motor areas in the frontal and cingulate cortex of prosimian primates. *J Comp Neurol.*, 423(1):140–77, Jul 2000.

W. Wu and N. Hatsopoulos. Evidence against a single coordinate system representation in the motor cortex. *Exp Brain Res.*, 175(2):197–210, Nov 2006.

K. D. Wyatt and S. S.-H. Wang. Speed limits in the cerebellum: A comparative ultrastructural analysis of parallel fibers. volume 74.4. SfN, 2003.

W. Yuan, Y.-B. Duan, and J.-L. Wang. $\mathcal{H}_\infty$ model reduction for lpv systems with a state delay. In *Proceedings of international conference on machine learning and cybernetics*, volume 3, pages 1362–67. IEEE, Aug 2005.